UNIVERSITÀ degli STUDI di CATANIA

DOTTORATO DI RICERCA IN BIOTECNOLOGIE
UNIVERSITÀ DI CATANIA
Biometec

Department of Biomedical and Biotechnological Sciences

Ph.D. in Biotechnology

Curriculum in Pharmaceutical Biotechnology

XXXIII Cycle

CARLA BARBARACI

Sigma-HDACi hybrid ligands as potential therapeutic treatment for uveal melanoma: design, synthesis and biological evaluation

PhD Thesis

Tutor: *Prof. Agostino Marrazzo*

Coordinator: *Prof. Vito De Pinto*

ACADEMIC YEARS 2017/2020

Affiliation

Department of Drug and Health Sciences, University of Catania, Viale Andrea Doria 6, 95125 Catania, Italy – Professor Agostino Marrazzo.

Laboratorio de Sïntesis Asimétrica, Departamento de Quimica Organica, Facultad de Ciencias. Edificio D. Planta 3, Universidad de Zaragoza, Campus San Francisco, E-50009 Zaragoza, Aragon, Spain - Professor Pedro Merino (14/1/2019 – 24/7/2019).

Vera Salus Ricerca s.r.l, Via Penninazzo 11/A, 95029 Viagrande, Catania, Italy – Dr Claudia Leotta (1/12/2019 – 1/3/2020, 1/9/2020 – 1/12/2020)

Table of contents

Sommario

L'obiettivo principale di questa tesi di dottorato è stato quello di identificare nuove molecole di sintesi con efficacia terapeutica nei confronti del melanoma uveale, un tumore intraoculare tanto raro quanto aggressivo. Il lavoro è stato condotto presso il Dipartimento di Scienze del Farmaco e della Salute (Università degli Studi di Catania), presso il Departamento de Quimica Organica (Universidad de Zaragoza, España) e presso la Vera Salus s.r.l (Viagrande, Catania).

In particolare, il progetto persegue lo sviluppo di nuovi composti sintetici in grado sia di antagonizzare il recettore σ che di inibire alcune isoforme dell'enzima istone deacetilasi (HDAC), come potenziali target per il trattamento del melanoma uveale.

Come riportato in letteratura, i recettori σ sono presenti a livello uveale (iride e corpo ciliare) e, come abbiamo riportato in recenti studi preliminari, alcuni ligandi dual-target/dual-function (σ_1 e HDAC) mostrano sia proprietà antiangiogeniche che antiproliferative. Inoltre, il trattamento con opportuni ligandi σ induce apoptosi e autofagia nelle cellule umane di melanoma uveale. Allo stesso tempo, studi recenti hanno dimostrato che alcune mutazioni che disattivano l'istone H2A ubiquitina-idrolasi (BAP1) sono strettamente correlate alle forme metastatiche del melanoma uveale. Gli inibitori dell' HDAC, tra i quali acido valproico (VPA), LBH-589 e altri, sono in grado di invertire gli effetti della perdita di funzionalità del BAP1 inducendo la differenziazione dei melanociti, la cessazione del ciclo cellulare e l'inibizione della crescita tumorale. In particolare, VPA è attualmente in fase clinica II (NCT02068586) per il trattamento del melanoma uveale.

Sulla base di queste considerazioni, dopo un'attenta analisi iniziale riguardante la strategia multitarget basata sui diversi tipi strutturali di ligandi ad azione multipla, sono stati progettati diversi ligandi multipli. L'approccio dual-target/dual-function coinvolge la progettazione e la sintesi di nuove molecole in grado di avere un doppio effetto anti angiogenico ed antiproliferativo; agendo sia sui recettori σ, come nuovo bersaglio molecolare, che sull'HDAC come inibitori (l'uso di alcuni HDACi è già ampiamente convalidato come antitumorali).

Abstract

The main objective of this doctoral thesis was to identify new small molecules with therapeutic efficacy towards uveal melanoma, an intraocular tumor as rare as aggressive. The work was conducted at the Department of Drug and Health Sciences (University of Catania), at the Department of Organic Chemistry (University of Zaragoza, Spain) and at Vera Salus s.r.l (Viagrande, Catania)

In particular, the project envisages the development of new synthetic compounds capable of both antagonize the σ_1 receptor and to inhibit HDAC for the treatment of Uveal Melanoma.

As reported in the literature, σ receptors are present at the uveal level (iris and rabbit ciliary body) and, as we reported in recent preliminary studies, some dual-target/dual-function ligands (σ_1 and HDAC inhibitors) show both antiangiogenic and antiproliferative properties. Moreover, treatment with appropriate σ ligands induces apoptosis and autophagy in human uveal melanoma cells. At the same time, recent studies have shown that some mutations inactivating histone H2A ubiquitin-hydrolase (BAP1) are closely related to the metastatic forms of uveal melanoma. The HDAC inhibitors, as valproic acid (VPA), LBH-589 and others, are capable of reversing the effects of loss of functionality of BAP1 inducing melanocytic differentiation, cell cycle cessation and inhibition of tumour growth. Finally, VPA underwent phase II clinical trials (NCT02068586) for treatment of uveal melanoma.

On these grounds, after a careful initial analysis concerning the multitarget strategy and based on the different structural types of multiple-action ligands, several multi-ligands have been designed. The dual-target/dual-function approach involving the design and the synthesis of new molecules capable of having a double antiangiogenic and antiproliferative effect; acting on both σ receptors, as a new molecular target, that on HDAC as inhibitors (HDACi are already widely validated as anticancer).

Keywords and abbreviations

AD, Alzheimer disease

BAP1, breast cancer type 1 (BRCA1)–associated protein 1

B_iP, binding immunoglobulin protein

DTG, ditolylguanidine

EIF1AX, eukaryotic translation initiation factor 1A, X-linked

ER, endoplasmic reticulum

FRET, fluorescence resonance energy transfer

GNAQ, guanine nucleotide-binding protein Gq subunit alpha

GNA11, guanine nucleotide-binding protein Gq subunit alpha-11

GPCRs, G protein-coupled receptors

HAT, Histone acetyltransferase

HD, Huntington's disease

HDAC, histone deacetylase

HDLP, histone deacetylase-like protein

HP, haloperidol

HP-mII, haloperidol metabolite II

KO, knockout

MAM, mitochondrion-associated membrane

MDR, multidrug resistance

MDRP, multidrug resistance-associated protein family

MTDL, multitarget-directed ligand

PCP, phencyclidine

PD, Parkinson disease

PET, positron emission tomography

P-gp, P-glycoprotein

PGRMC1, progesterone receptor membrane component 1

SAHA, suberoylanilide hydroxamic acid

SF3B1, splicing factor 3B subunit 1

TMEM97, endoplasmic reticulum-resident transmembrane protein

TPX, trapoxin

TSA, tricostatin A

UM, uveal melanoma

VPA, valproic acid

WT, wild type

σ_1R, sigma-1 receptor

σ_2R, sigma-2 receptor

σR, sigma receptor

1. Introduction

1.1. Uveal Melanoma

Uveal melanoma is a rare malignant eye tumour, treatment of which is one of the unsatisfied needs in melanoma field. Uveal melanoma, with a low mean annual incidence of 5-10 cases per million, involve mainly the choroid (90%), ciliary body (6%) or iris (4%) – collectively referred to as uvea (Figure 1.1).[1] Among all cancers of the eye, 85% are primary tumours of this type occurred in individuals with a mean age of 60 years and the remaining 15% cases are non-Hodgkin lymphomas, retinoblastomas and medulloepitheliomas.[2] The uveal tract is beside the second most common location for melanoma (3-5%) after the skin.[3] Despite that, cutaneous and uveal melanomas are different in terms of biology, natural history and response to chemotherapies.

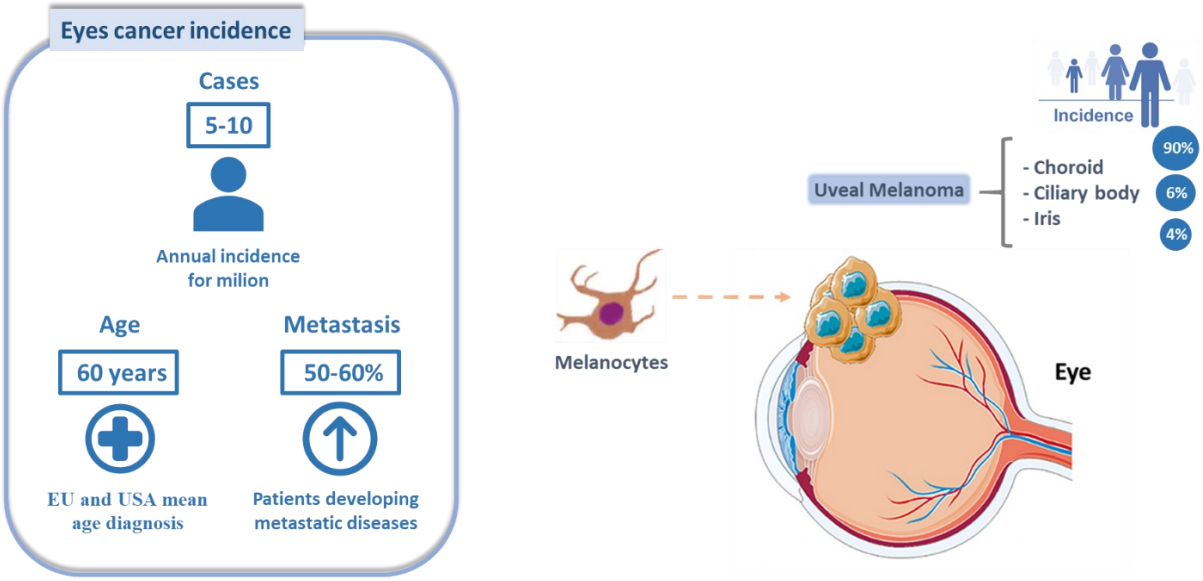

Figure 1.1. Eyes cancer incidence vs uveal melanoma incidence

The 5-year survival rate is 50 – 70% and about 50% of patients develop metastases within a median of 36 months.[4] Hepatic metastases occur in up to 90% of individuals, followed by metastases in lung and bones, with a median survival of 4 – 5 months after metastases and < 4% detectable at the time of diagnosis.[5] Many patients may present micro-metastasis clinically undetectable, therefore the

current tendency is to consider uveal melanoma as a systemic disease. Indeed, the considerable vascularity of those ocular tissues greatly influences the pathogenesis and clinical progression of uveal melanoma.[6] Lacking in an intraocular lymphatic system, uveal melanoma tends to spread via haematogenous route, supporting a relation between growth of intra-tumoral vessels and systemic diffusion. Recent studies have shown that different uveal melanoma cell lines produced copious amount of vascular endothelium growth factor (VEGF), involved in primary tumour neovascularisation, growth and metastatization.[7,8] In agreement with these concepts, the presence of fibrovascular loops and networks in UM was related to the microcirculation morphology, tumour progression and worse prognosis.[9]

The incidence of UM in males and females, as also right or left eye involvement, is similar with the median age at diagnosis of 62 years.[10] Among the risk factors predisposing for the development are included: age, sex, genetic or phenotypic - such as fair skin or light-coloured eyes - predisposition, the work environment and dermatological conditions (Figure 1.2).[11] The mean age of diagnosis also varies according to the geographical location. In Asia, it tends to affect younger individuals (45-55 years of age); while in Europe or in the USA, it usually presents at around the age of 60 years. It should be mentioned that uveal melanoma in young individuals has also been related to family history of choroid melanoma, syndrome dysplastic nevus, xeroderma pigmentosum and melanocytosis ocular congenital, with a mean onset age of 16 years and a better short-term prognosis owing to its lesser locoregional aggressiveness.[12]

Genetic analysis could be useful in predicting metastatic risk, in management and follow-up patients with this cancer. Several studies have identified the genes involved in development of uveal melanoma and highlighted as this neoplasm is characterized by a limited number of recurrent gene mutations. The most frequent chromosomal abnormalities in uveal melanoma are loss of chromosome 3 (monosomy 3) and gains of chromosome (8q) and 6 (6p).[13] Patients with chromosome 3 loss undergo the worst prognosis, whereas those with 6p gain have the best outcomes. Instead, amplification or gain of 8q has been shown to accelerate metastatic disease.[14]

Mutations in G-protein-α subunits GNAQ or GNA11 are observed in ≥ 80% of primary uveal melanomas and loss or inactivating BAP1 [breast cancer type 1 (BRCA1)–associated protein 1] mutations are found in approximately 50% of all cases, most frequently in metastatic disease. Mutations that are associated with a less aggressive behaviour are those in encoding splicing factor 3B subunit 1A (SF3B1) and encoding eukaryotic translation initiation factor 1A, X-linked (EIF1AX).[15-17]

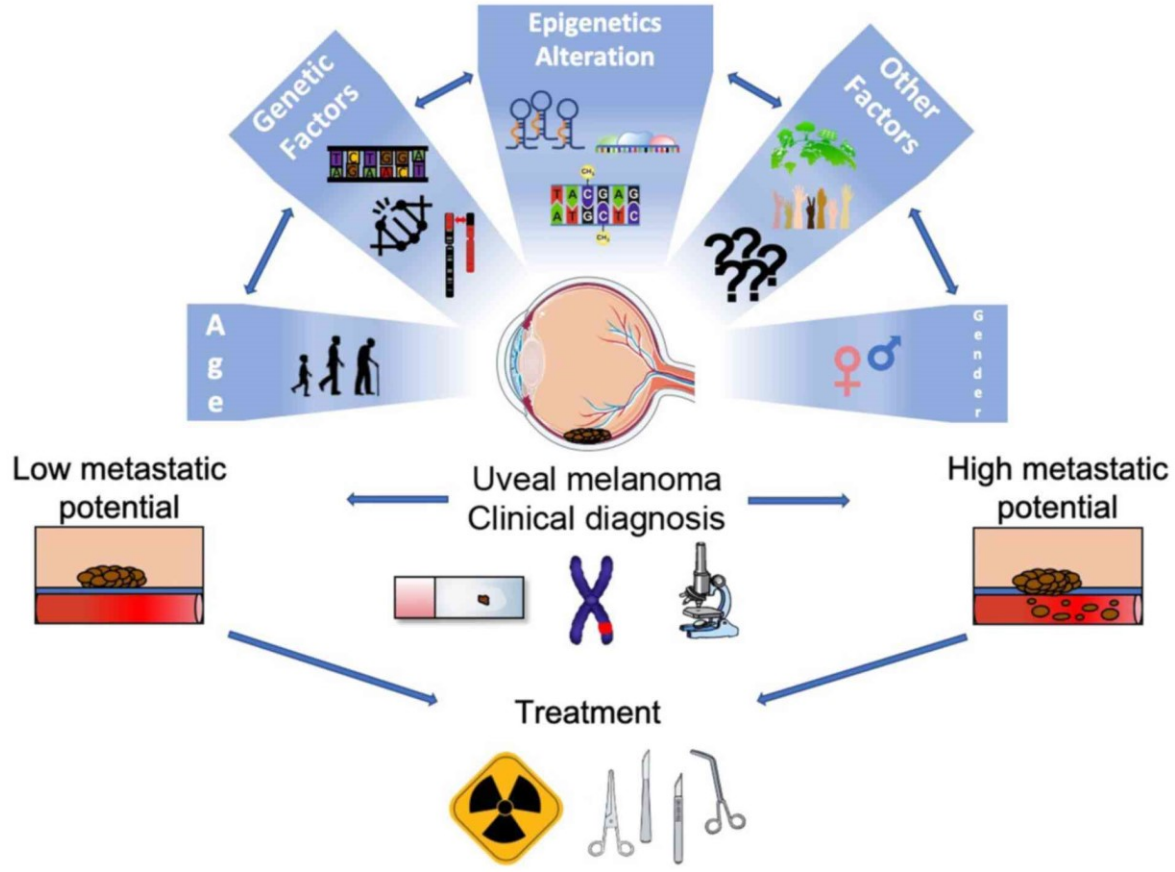

Figure 1.2. Schematic representation of the genetic and epigenetic alterations and risk factors involved in the development of uveal melanoma.[18]

The melanoma of the uvea appears classically as a brown or slate-grey cupoliform mass. cancer is pigmented in 55% of cases, not pigmented in 15% and mixed pigmented/not pigmented in 30%.[19] Clinical manifestations depend on the size and location of the tumour. Indeed, tumour detection in uveal melanoma may be difficult and tedious because of asymptomatic phase (ie, “lead-time bias”) until it reaches already a significant size.[20] Often, tumours are incidentally detected in an

ophthalmological exam (regular check-up or diabetic retinopathy screening) or through symptoms, such as vision loss, photopsia, myodesopsia or high intraocular pressure. When the tumour affects the macula, patients exhibit a gradual painless decline in visual acuity. If there is involvement of the iridocorneal angle, signs may be those of acute glaucoma, namely the loss of visual acuity, pain, photopsia and increased intraocular pressure. The involvement of the iris is usually asymptomatic and presents as a dark growing, invasive hyperpigmented lesion. If the ciliary body is involved, this can compromise the natural lens, causing its subluxation and impaired accommodation, thus interfering with the patient's vision. It should be noted that infrequently, intraocular progression can give rise to haemorrhage within the ocular cavity presenting as haemorrhage and exophthalmos.[12]

Despite intense research into the physiopathology, histology and molecular biology of uveal melanoma, there has been little improvement in its bleak prognosis. Patient management was thus focused on early detection and aggressive treatment.[21] Considerable advances have been made in the locoregional control of the disease through both conservative techniques, such as local radiation therapy using brachytherapy or, alternatively, charged-particle and proton-beam radiation, and more aggressive approaches like enucleation, which remains the only option for very large tumors.[15] The survival rate has remained stable over the past 30 years, and developments have therefore consisted mainly of more effective and less aggressive surgical techniques. Especially, considering the association between the prognosis and metastasis of uveal melanoma, immunotherapy could embody one of the main pillars of the treatment of this disseminated disease. Unlike cutaneous melanoma, uveal melanoma metastases generally do not respond to immune checkpoint inhibitors even if encouraging results with other immunotherapy strategies are emerging. Moreover, chemotherapy or targeted therapy are poorly effective for metastases from uveal melanoma and are usually fatal within 1 year of the onset of symptoms, with exception in patients with isolated liver metastases that are tractable with surgical resection. Systemic chemotherapy barely improves the overall prognosis of a patient and the response rate to conventional chemotherapy is < 1%. The hypothesis of anti-angiogenic therapies was also to treat uveal melanoma metastases, which requires new vessels to

grow and angiogenesis, but were previously considered poorly effective.[22] In this context, many questions remain unanswered but a recent study reports a potential benefit of adjuvant treatment with anti-VEGF therapy in metastatic UM.[23] Unsurprisingly, a clinical trial is currently underway using intravitreal injections of bevacizumab, an anti-angiogenic monoclonal antibody targeting all isoforms of VEGF-A.[24] In principle, though, pharmacological inhibition of proangiogenic pathways regulated by VEGF might represent effective therapeutic strategies to prevent UM metastatic disease.[25,26] However, there is still no standardized treatment available for the management of metastatic disease that has been able to improve the long-term survival of these patients.[1,12,27]

Table 1.1. Clinical trials for patients with advanced uveal melanoma in 2020

Agents	Phase	Clinical trial gov. ID
Adjuvants trials		
Sunitinib versus valproic acid[1]	II	NCT02068586
Ipilimumab and nivolumab	II	NCT03528408
PKC–MAPK pathway		
Intermittent selumetinib[2]	I	NCT02768766
IDE196[3]	I/II	NCT03947385
Epigenetic therapies		
Vorinostat[1]	II	NCT01587352
PLX2853[4]	I/II	NCT03297424
DNA damage repair targeting		
Neratinib[5]	II	NCT03207347
Immune checkpoint blockade		
Ipilimumab plus nivolumab[6] and immunoembolization	II	NCT03472586
Ipilimumab plus nivolumab and yttrium-90 radioembolization	0	NCT02913417
T cell redirection		
Tebentafusp (IMCgp100)[7]	II	NCT03070392

[1]HDAC inhibitors,· [2]MEK inhibitors, [3]IDEAYA Reports Darovasertib, [4]Bromodomain-containing protein 4 (BRD4) inhibitors, [5]Nerlynx®, PTKs inhibitors, [6]Yervoy® and Opdivo®, monoclonal antibody, [7]bispecific protein engineered to specifically target gp100, a lineage antigen expressed in melanocytes and melanoma.
Actively recruiting on January 2021; see www.clinicaltrials.gov for a real- time listing.

Multiple studies show how novel combinatorial strategies increase response rates, at once findings from ongoing clinical trials are promising (Table 1.1). Despite the great progress already made in clinical management, therapy requires new specific approaches and further investigations to identify

new therapeutic strategies leading to better results for patients.[28] For this purpose, a combination of different therapeutic approaches seems to open new paths in the clinical management of this pathology.

1.2. Multitarget approach

The drug discovery paradigm "one-molecule, one-target" remains, and probably will remain, a major breakthrough in the scientific world. In detail it lies in designing highly selective chemical entities to target a single biological entity, considered as a dominant player in certain diseases.[29] On the other hand, the attempt to improve the efficacy of drugs hitting only a single target challenges us to overcome the current paradigm in order to consider also developing agents capable to modulate multiple targets simultaneously (polypharmacology).[30] Indeed, polypharmacology is emerging as a new paradigm to develop small molecules for the treatment of multifactorial diseases in order to achieve desired physiological responses on certain targets.[31] Cancer and neurological disease were regulated by complex pathogenic mechanism and associated with many different symptoms. Therefore, drugs addressing a single target could be inadequate compared to multiple-ligand drugs with more than one pharmacological activity in developing new synthetic compounds for the treatment of these multi-factorial pathologies.[32,33] Multitarget approach could be realized as association of drugs (drug cocktail), combination of drugs (multicomponent drug) or a single drug with multiple ligands (multiple ligand). Compared to multicomponent drugs, whereby two or more agents are co-formulated in a single tablet, the multiple-ligand approach provide for a single chemical entity responsible for regulating multiple targets all at once.[34]

Many drugs already on the market act through interaction with multiple molecular targets, but the discovery of their multiple mechanism of action was accidental, also known as serendipity. Instead, premeditated design of compounds with a well-defined multitarget profile is now one of the new challenges in the field of pharmaceutical chemistry. A recent approach for the rational design of new drug candidates, also called multitarget-directed ligands (MTDL) strategy, has received more

attention by scientists who attending to develop a variety of hybrid compounds modulating multiple biological targets. In particular, this provide for combining different structural subunits, that allow the molecular recognition by more than one bioreceptor simultaneously, in a unique and single scaffold.[35] MTDL could be designed and classified as (Figure 1.3):

- linked ligands, in which the pharmacophore elements for each target are separated by a metabolically stable or cleavable linker group;
- fused ligands, in which the pharmacophore elements are strictly connected;
- merged ligands, in which the pharmacophore elements are overlapped, taking advantage from common structure of the starting ligands.

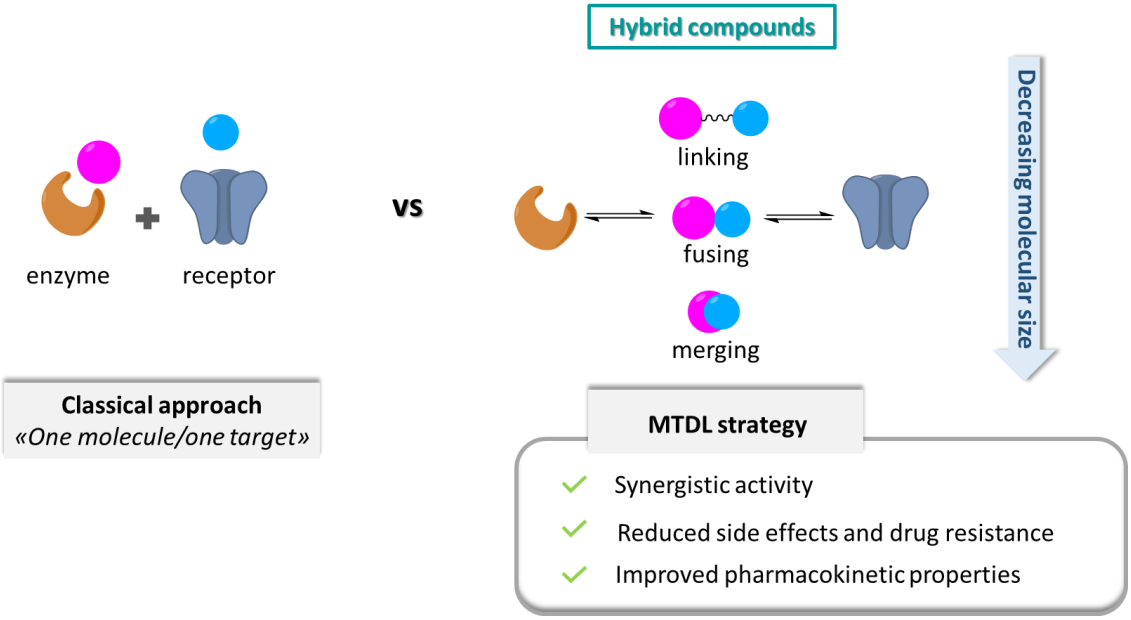

Figure 1.3. Shifting from classical approach to multitarget-directed ligands (MTDL) strategy: linked, fused and merged ligands.

The overlapping of the structural elements of the two selective ligands greatly affects the efficiency of the designed MTDL, in terms of binding energy. If there are few structural similarities between the starting ligands, the overlap is minimal and the multiple ligand obtained has a high molecular weight and a poor binding efficiency, because some regions only contribute to interaction with one of the two targets and are poorly tolerated by the other target. Alternatively, the design of multiple

ligands containing molecular fragments capable of interacting with both biological targets ensures low molecular weight of MTDL and good binding efficiency. In this case, the starting ligands are highly integrated in a single molecular structure.[34]

Clinical development of multi-ligands drugs present the advantages of reducing drug-drug interaction, therapeutic doses and therefore side effects, simplifying the pharmacokinetic profiles and improving therapeutic efficacy, patient compliance and tolerance. In addition, it show a lower risk of target-based drug resistance due to modulation of a few targets, single-target mutations or expression changes (Figure 3). Multidrug resistance (MDR) is a characteristic phenomenon of many cancer cells that have been exposed to cytotoxic agents. They manage to develop cross resistance to a varied range of structurally and functionally unrelated compounds. MDR is among the most important obstacles to overcome for successful cancer therapy.

1.3. Sigma Receptors

Sigma receptors (σRs) embody an enigmatic and unique class of chaperone proteins implicated in many pharmacological events that make them an attractive target proposed as potential therapeutic treatment for several diseases. Initially misclassified for opioid receptor due to their high affinity to (+)-benzomorphans and then incorrectly believed as the phencyclidine (PCP) binding site at the glutamate NMDA receptor, σRs have recently been reclassified as distinct receptors.[36]

In 1976 the existence of σRs was first postulated by Martin et *al*., studying the effects of (±)-N-allyl-normetazocine (± SKF 10,047) and related racemic benzomorphan in dogs which revealed the proposal of three distinct opioid receptor subtypes: μ, κ, and σ; but only in 1990, radioligand binding studies confirmed that σRs are orphan receptors.[37] According to their different binding profiles for [^{3}H](+)-pentazocine and [^{3}H]1,3-di-o-tolylguanidine (DTG), became possible the identification of two distinct binding sites, named Sigma-1 (σ_1) and Sigma-2 (σ_2) receptors, each which display a different molecule weights (25 and 18 − 21.5 kDa, respectively), tissue distribution and distinct

physiological and pharmacological properties. Moreover, the σ_2 subtype, differently from σ_1R, does not bind dextrorotatory benzomorphans and it exhibits high affinity for ditolylguanidine (DTG) and haloperidol.[38] The radioligand with high affinity and specificity for the σ_1 receptor [^{3}H](+)-pentazocine also allow to define the chemical structure responsible for high-affinity binding to the σ_1 receptor. The interactions with the binding site were generally due to an amine positively charged as basic core and two hydrophobic regions (Figure 1.4). The primary and secondary hydrophobic regions should be in the range of 6 - 10 Å and 2.5 - 3.9 Å respectively from the amine core, which is either a secondary or tertiary amine with only small substituents (e.g.CH_3) as third N substituent and either cyclic or acyclic nature. The primary hydrophobic pocket tolerates sterically demanding substituents, especially bulky aromatic groups; while the secondary hydrophobic pocket is probably relatively smaller and optimally accommodates three carbon chain or less lipophilic substituents.[39,40]

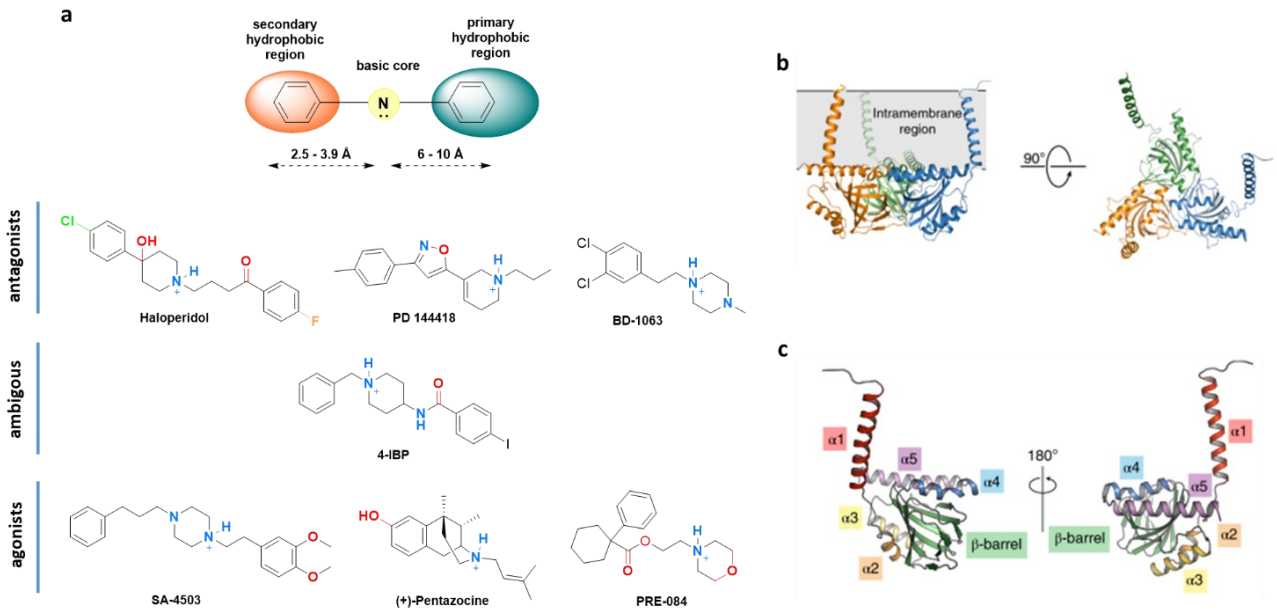

Figure 1.4. a) Representative σ receptor ligands, following the central σ_1 receptor pharmacophore. Adapted from Glennon *et al.* 2005.[39] b) The overall structure of the human σ_1 receptor (PDB 5HK1). c) The structure of a single σ_1 monomer, with the secondary structural elements labeled. Adapted from Schmidt *et al.* 2018.[41]

Since then, many potent and selective σ_1 receptor ligands fit with similar structural features the described general model.[39] Despite its endogenous ligands have not definitively been identified,

several endogenous molecules, such as neurosteroids and especially progesterone,[42] the hallucinogen *N*,*N*-dimethyltryptamine (DMT)[43] and sphingolipids,[44] are considered the most probable ones as they bind to σR regulating their activities. In addition, other steroids such as dehydroepiandrosterone sulfate (DHEAS), pregnenolone sulfate, testosterone and deoxycorticosterone showed lower affinity for σ_1 receptors than progesterone.[45] Noteworthy, in a recent study has been proposed choline as an endogenous agonist of σ_1R, promoting interaction of σ_1Rs with other signaling proteins.[46]

1.3.1. Sigma-1 receptor (σ_1R)

Sigma-1 receptor (σ_1R) is a mammalian transmembrane protein of 223 amino acids, encoded by a gene located on chromosome 9 in human[36,47] and resided mainly at the endoplasmic reticulum (ER) mitochondrion interface called MAM (mitochondrion-associated ER membrane).[48] Herein, σ_1R is associated to lipid microdomains (named "lipid rafts") and forms a complex with a chaperone called the binding immunoglobulin protein (BiP, also known as GRP78), which plays a critical role in protein folding and prevents the inactive state σ_1 receptor from translocation. In fact, activation of the σ_1R by small molecule agonists or by a decrease in ER calcium concentrations, due to stress conditions, cause the dissociation from BiP (Figure 1.5), leading to a σ_1R translocation to the ER, plasma and nucleus membranes or in other organelles where interact with client proteins and increase of its chaperone activity.[36,48-50] Indeed, different cellular functions are regulated by σ_1R binding through the modulation of a wide range of signaling pathways including protein kinases, transcription factors, G protein-coupled receptors (GPCRs), ion channels such as inositol triphosphate (IP3), voltage-gate K^+, Na^+, Ca^{2+} channels and NMDAR.[48,51-53]

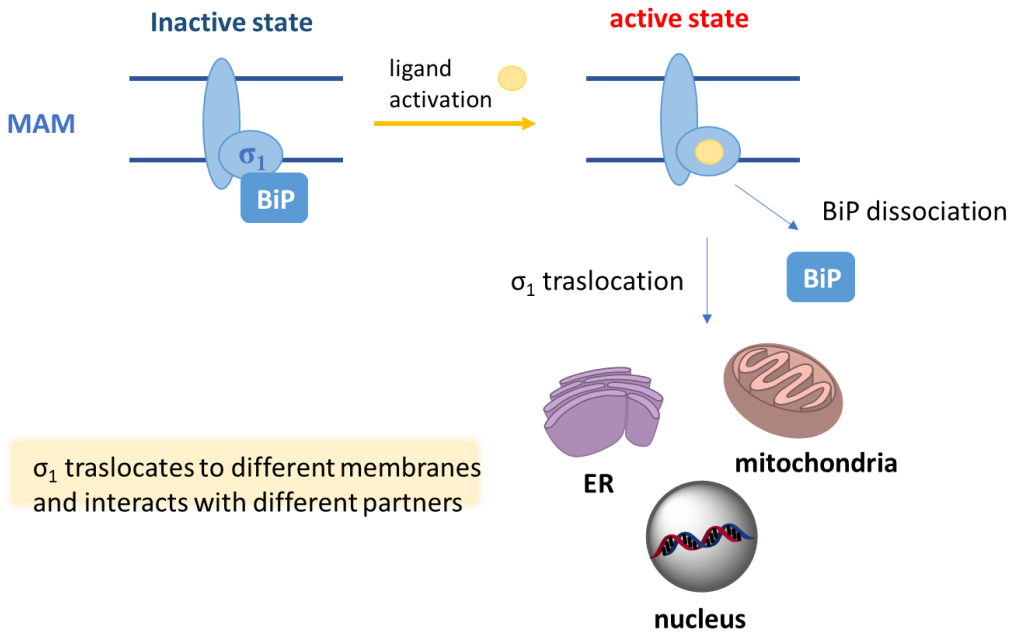

Figure 1.5. Protein interactions of σ_1R as a receptor chaperone in physiological and pathophysiological conditions.[54]

The cloning of the σ_1 receptor in the 1990s established that it is a revolutionary separate with no appreciable similarity to any other and lately the matter was definitively settled by its crystallization.[47,55-57] Schmidt et *al*. published for the first time the crystal structure of the human σ_1 receptor complexed with two chemically different ligands (a high-affinity antagonist PD144418 and either agonist or inverse agonist 4-IBP).[41] The receptor crystallized as a trimer and each protomer, including four α-helices each, exhibits a fold including a single transmembrane domain (located at its amino terminus and encompassing residues 8 to 32),[47] divergent from the main models of a two-pass transmembrane architecture (Figure 1.6A). The cytosolic domain of each of three promoters show β-barrel fold with the ligand-binding site buried at its center, which involves a charge–charge interaction with the highly conserved Glu172 residue and the basic nitrogen present in most σ_1R ligands (Figure 1.6B). This large, hydrophobic ligand-binding cavity shows remarkable plasticity in ligand recognition, while the rest of the ligand is free to fit into the large β-barrel-like binding pocket lined with hydrophobic residues.[41,58,59]

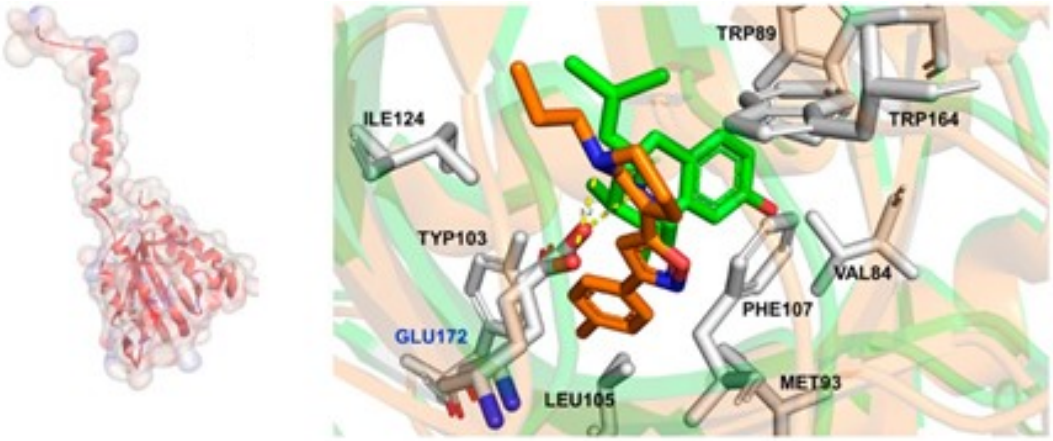

Figure 1.6. Overlays of the cocrystal structures of the σ_1 receptor bound to the antagonist PD144418 (PDB 5HK1, brown) and the agonist (+)pentazocine (PDB 6DK1, green). Residues are colored in gray. Adapted from Ye *et al.* 2020.[54]

This domain, including a β-barrel and two flanking α-helices, represents not only the ligand-binding site, but also the oligomerization interface. A cell-based study using fluorescence resonance energy transfer (FRET) method show that the σ_1 receptor interact with itself and form multiple oligomeric states that can be altered by ligands. Under non-liganded condition σ_1R form several different oligomeric states, instead binding with antagonist favoured higher order oligomers and binding with agonist enhanced the formation of small oligomers (Figure 1.7).[60,61] Even though the precise functional consequences of receptor oligomerization remain to be determined, the hypothesis is that σ_1R oligomerization states might affect its ability to bind client proteins. In particular, a recent correlation experiment showed that the σ_1R antagonist haloperidol, promoting the homomerization, reduced the σ_1R-BiP interaction, whereas σ_1R agonist PTZ, which assist the production of monomers, enhanced this interaction.[60] Recent studies have shown how agonists and antagonists occupy a different region of the binding pocket.[62] Antagonists adopt a more linear pose, with the primary hydrophobic region towards the space between helices α4 and α5, whereas primary hydrophobic site of agonists points towards helix α4. These small conformational changes would explain why agonists or antagonists may bias the receptor towards smaller or higher molecular weight states.

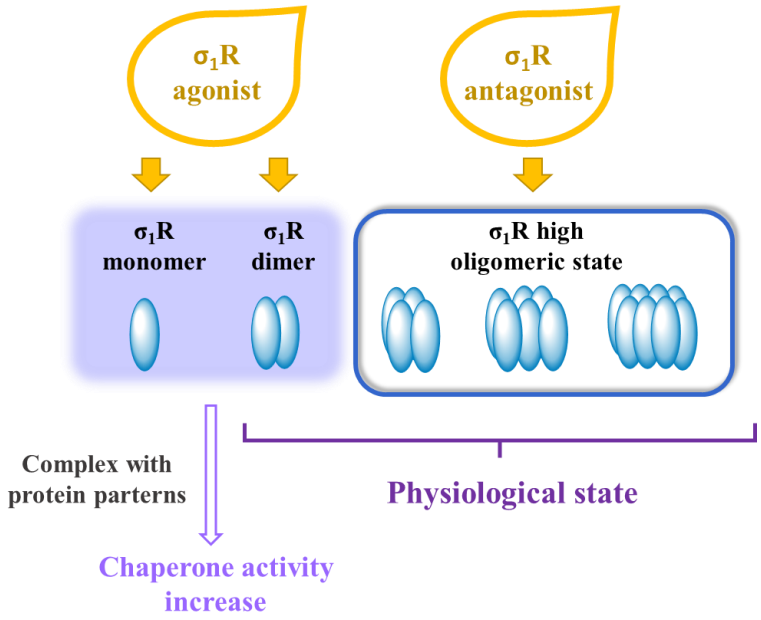

Figure 1.7. Representative change of the σ_1R oligomerization states caused by its ligands.

Based on their ability to simulate or not the genetic knockout (KO) of σ_1R in animal models σ_1R ligands have historically been classified respectively as agonists or antagonists.[63] Generally, antagonists are reported to have analgesic effects in both animals and humans and to enhance the opioid mediated analgesia,[64,65] while σ_1R receptor agonists are associated with cytoprotective effects, reversing the effects of antagonists.[66,67] Moreover, it has been assumed that σ_1 antagonist induce caspase-dependent apoptosis,[68] whereas agonists prevent caspase activation.[69] As a consequence, antagonists have antiproliferative and cytotoxic activity, whereas the agonists have anti-apoptotic and neuroprotective effect.[70]

1.3.2. Pharmacological aspect of σ_1R

The σ_1R is widespread across multiple peripheral tissues and nervous system. In the central nervous system (CNS), σ_1R is expressed in the hippocampus, cerebellum, basal ganglia, and spinal cord[71], as well as in peripheral nervous system on the level of the soma of peripheral sensory neurons and along the nerve in Schwann cells.[72,73] Unsurprisingly, the σ_1R has become an actively pursued drug target

for several CNS disorders, including, but not limited to, neurodegenerative diseases, pain, stroke, retinal degenerations, and depression.

Several studies have shown its involvement in cognition, memory and neuroprotection and neuroplasticity. Particularly, it was observed that σ_1 agonists or positive modulators can induce increased cognition, memory improvement, anti-amnesic effects in rat models affected by deficits in learning and that numerous σ ligands induce neuroprotection in mice model of Alzheimer's disease.[74,75] Disparate studies illustrated also that σ_1 agonists could lead the activation of endogenous defense and plasticity mechanisms in Parkinson disease (PD) models, attenuating the development of motor impairments and dopaminergic neuron death.[76,77] Moreover, several σ_1R mutations have recently been implicated in juvenile amyotrophic lateral sclerosis (ALS) and distal hereditary motor neuropathies.[78] So far, some selective σ_1 receptor ligands have been advanced into human phase II/III clinical trials for neurodegenerative pathologies: ANAVEX2-73, a σ_1 agonist, for Rett syndrome and early stage Alzheimer's disease (AD),[79] and also Pridopidine in a phase II study for Levodopa-induced dyskinesia and a phase III study for early stage Huntington's disease (HD).[80] Recent clinical trials support also the hypothesis of its involvement in modulation of nociception (Figure 1.8). S1RA, a σ_1 receptor antagonist, inhibited neuropathic pain, inflammatory hyperalgesia, activity-induced spinal sensitization, and paclitaxel-induced sensory-nerve mitochondrial abnormalities.[54] In particular, it showed a potential neuroprotective role in reducing acute oxaliplatin-induced peripheral neuropathy (OXAIPN).[81]

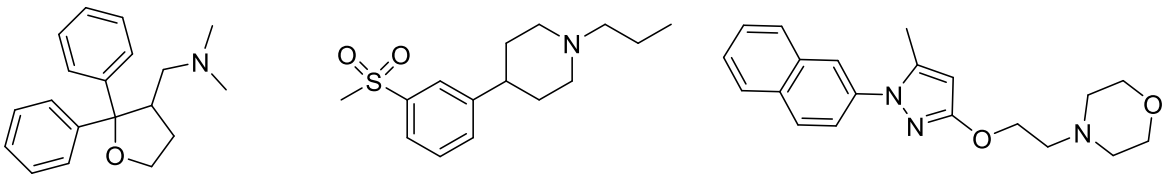

ANAVEX2-73
σ_1 agonist (IC_{50} = 0.86 μM)
Phase II/III – early AD

Pridopidine (ACR16)
σ_1 agonist (K_i = 81.7 nM)
Phase III – early HD

SIRA (E-52862)
σ_1 agonist (K_i = 81.7 nM)
Phase II - OXAIPN

Figure 1.8. Selective σ_1 receptor ligands in human clinical trials.

Effectively, in σ_1R knockout mice were observed attenuation of pain behaviors in different pain models and enhancement of morphine mechanical antinociception, which is consistent with the observation that σ_1R antagonists showed antinociception in pain models, including neuropathic, inflammatory, and visceral pain, and as adjuvants to opioid therapy. Animals treated with σ_1R antagonists showed no allodynia in both formalin- and capsaicin-induced nociception in σ_1R KO mice and in wild type (WT), confirmed by pharmacological treatments in σ_1R KO mice with traumatic nerve injury since mutant mice did not develop signs of either cold or mechanical allodynia.[82,83]

Interestingly, the σ_1R could be also a suitable target for the treatment of cancer, although its role in this context remains controversial. Binding experiment studies shown its involvement in cancer cell physiology and the overexpression in many human and rodent tumor cell lines including breast, lung, prostate, colon, melanoma, neuroblastoma and glioma.[84] As response to tumoral environmental conditions, it has been demonstrated that σ_1R may activate different adaptation mechanisms on the basis of the client protein in a given cancer cell type.[85] Indeed, many studies have explored its effect on the modulation of ion channel activity in the tumoral context and on the electrical plasticity of cancer cells associated with proliferation, cell death resistance, invasion, and angiogenesis. Recently, data show that small-molecule σ_1 modulators can be used to regulate PD-L1/PD-1 blockade strategies, regulating the tumor immune microenvironment.[86]

Notably, σ_1R plays a cytoprotective role which could be abolish by treatment with its antagonists, activating a proapoptotic response.[87] In particular, wide number of data had shown that treatment with σ_1 antagonists reduce anti-tumoral activity, cancer cells survival and induce cancer cells apoptosis.[88] Rimcazole, haloperidol and haloperidol metabolite II, as well as other σ_1R antagonists have shown to inhibit cell proliferation in breast, colorectal, melanoma and glioma cancer cell lines, but not in non-tumoral cells.[89] Even though the cytostatic and cytotoxic effects of ligands have long been demonstrated, the mechanisms by which tumor growth inhibition and cell death are induced are not yet fully elucidated.

1.3.3 Sigma-2 receptor (σ_2R)

Sigma-2 receptor (σ_2R) is an intracellular membrane protein, localized in "lipid rafts" in mitochondria, lysosomes, endoplasmic reticulum and plasmatic membrane and derived from a completely different gene than σ_1, as revealed from genetic knockout of the σ_1 receptor.

Although initial studies were encouraging, the association of sigma receptors with lipids and steroids and the ensuing proposal of the σ_2R as a part of the progesterone receptor membrane component 1 (PGRMC1) complex[90] was questioned by subsequent work in which σ_2R ligand binding didn't appear affected by the overexpression, siRNA knockdown or CRISPR-Cas9 knockout of PGRMC1.[91-93] The cloning of the σ_2R by Alon *et al.* solve the question and complete the molecular characterization of this class of receptor, opening the door to more studies exploring mechanisms of action. Using classical affinity purification approaches, the σ_2-binding site was isolated and designated as the endoplasmic reticulum (ER)-resident membrane protein TMEM97, also known as MAC30. With similar characteristics to the classical σ_2R binding site, TMEM97 showed appropriate affinity and selectivity for a range of prototypic σ_2 compounds, later confirmed through mutagenesis studies which established the importance of two aspartate residues (Asp29 and Asp56) in the binding pocket (Figure 1.9B). Structurally, the sequence of TMEM97/σ_2 predicts an integral membrane protein with an ER retention signal and four transmembrane domains with then N and C termini extending into the cytoplasm. The two aspartate residues important in binding are predicted to reside located in close proximity to one another and near its ER luminal surface (Figure 1.9A). Asp29 and Asp56 may play a similar role to the Asp126 and Glu172 for σ_1R in ligand binding to the σ_2 receptor.[94]

Several studies displayed also that TMEM97 gene is involved in cholesterol metabolism. Indeed, cholesterol-regulating signals, such as sterol depletion and sterol regulatory-element binding protein (SREBP) expression levels, affect TMEM97 expression.[95]

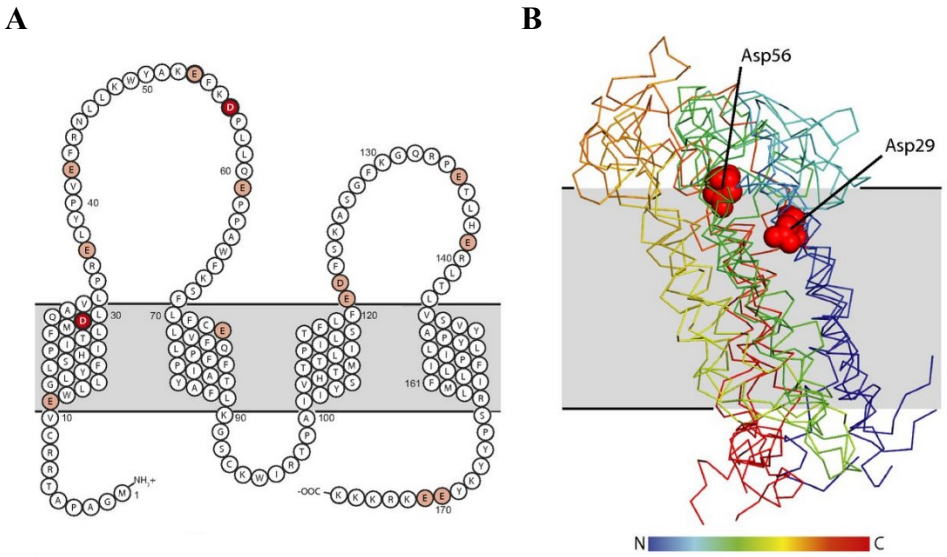

Figure 1.9. (A) Topology model of TMEM97/sigma2 receptor reproduced from Alon et al.[94] (B) Molecular models of TMEM97 generated by evolutionary coupling analysis.[96] The top four ranked models are presented as rainbow colored from the N terminus to the C terminus. The location of the membrane plane is shown in gray, Asp29 and Asp56 are shown as red spheres. For clarity a single representative residue pair is presented. Adapted from Alon *et al.* 2017.

Moreover, cholesterol trafficking processes, such as low density lipoprotein (LDL) uptake and cholesterol transport out of lysosome by interacting with and regulating Niemann-Pick C1 (NPC1) protein, were controlled at once by TMEM97.[95,97] In addition, either CRISPR/Cas9 knockout and siRNA knockdown of TMEM97 seemed to reduce cell proliferation, cell viability and migration/invasion in several kinds of cancer.[98,99] Moreover, even if several σ_2 ligands which exhibit different structures are able to induce cell death in cancer cells, it has been demonstrate that TMEM97 does not mediate σ_2 ligand cytotoxicity.[100]

The characterization of the TMEM97 crystal structure is important in the endeavour to understand σ_2R function. It is clear the existence of a binding pocket with established structure–activity relationships, even so there is no endogenous ligand and no indication of a structure corresponding to any established receptor class. Presumably, σ_2 ligand binding may lead to conformational changes as σ_1, that influence other associated protein systems. To date, several ligand have been characterized by binding ligand assays but the definition of σ_2/TMEM97 agonist and antagonist remains undefined.

Using the cell viability assay, σ_2 ligands have been categorized into agonists, partial agonists, and antagonists, determining their cytotoxicity as a percent relative to the cytotoxicity of siramesine (50 μM), commonly accepted σ_2 agonists.[101] During the years, some ligands with cytotoxic properties (σ_2 agonists) have given promising results in animal tumor models and the mechanisms of cell death activated by the σ_2 agonists may involve caspase-dependent and -independent apoptosis, generation of reactive oxygen species (ROS), mitochondrial superoxide and autophagy.[102] Meanwhile, recent finding have shown that σ_2 antagonists are involved in the blockage of Aβ neurotoxic effects both in vitro and in vivo, with one compound entering clinical trials for the treatment of AD.[103] However, molecular basis for pharmacological mechanism of action of σ_2 ligands is not understood.

1.3.3. Pharmacological aspect of σ_2R

Highly expressed in liver, kidney, heart, endocrine and immune systems, the σ_2R is also located in the CNS as well as in several cancer cell lines, particularly proliferating versus quiescent tumor cells. Similar localization was found for TMEM97, in fact, several studies showed that TMEM97 is expressed in different normal and cancer human tissues, in which it plays an important role in cell proliferation and, also, in cholesterol metabolism.[95] Since then, the σ_2 receptor/TMEM97 has attracted considerable interest around the diagnosis and treatment of cancer,[104] as well as the treatment of schizophrenia[105] and Alzheimer's disease.[106] TMEM97 has been also attested as a biomarker of proliferative condition, therefore some σ_2 ligands could be used as molecular probes for imaging solid tumors. For example, the radioligand of TMEM97, [^{18}F]ISO-1, has been devised and approved as a PET imaging biomarker of proliferative condition in tumors and as an indicator of the cancer therapy response (Figure 1.10).[107] Nowadays, σ_2 receptor has been also proposed to interfere with the binding of Aβ oligomers and σ_2 antagonists are supposed to prevent and displace the binding of Aβ oligomers to neurons. One of these σ_2 antagonist, named CT1812 (also known as Elayta) underwent a Phase II clinical trial, with promising outcomes coming (Figure 1.10).[108] Hundreds of publications have

addressed the functions of small molecules with affinity for the σ_2R, which has been implicated in cancer and neurodegenerative diseases; but there is still much to discover.

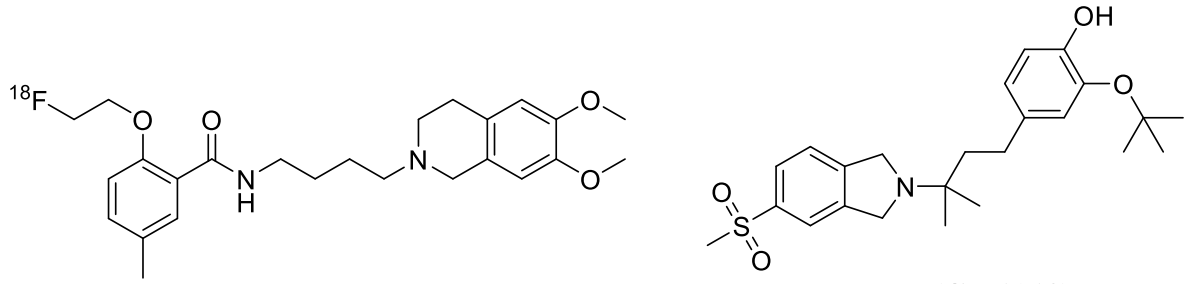

[18F]ISO-1
approved as a PET
imaging biomarker

Elayta (CT-1812)
σ_2 antagonist
phase II - AD

Figure 1.10. Selective σ_2 receptor ligands in human clinical trials.

1.4. Histone deacetylase enzyme (HDAC)

Histone acetylation is an important epigenetic mechanism that modulates expression of certain genes without altering the base sequences of DNA. As is known, genomic DNA in eukaryotic cells is packaged into chromatin, which could exist in a relaxed form, active for transcription (euchromatin), or in a condensed form, inactive for transcription (heterochromatin). Nucleosome, fundamental unit of chromatin, consist of DNA wrapped around an octamer composed of two copies of each histone proteins H2A, H2B, H3 and H4 (Figure 1.11).[109]

Chromatin remodelling is accomplished through three main epigenetic mechanisms, which include DNA methylation, histone modification and miRNA.[110] Histone modifications play a pivotal role in epigenetic regulation of transcription by acetylation and deacetylation, inducing transition between the euchromatin and heterochromatin. Histone acetyltransferase (HAT) is achieved by the action of which adds an acetyl group to a lysine residue. This neutralizes the positive charge of histone tails and reduce their affinity for DNA, resulting in chromatin activation. Conversely, histone deacetylase (HDAC) remove the acetyl groups added by HATs to the histones, by once they enter the nucleus and before their incorporation into chromatin, leading to chromatin inactivation.[111] Lys9, Lys14,

Lys27 on histone H3, and Lys5, Lys8, Lys12 and Lys16 on histone H4 are the main site of acetylation[112] and in addition to these, HDACs are also responsible for the deacetylation of lysine residues in other non-histone proteins, including-tubulin, heat shock protein 90 (Hsp90), as well as a variety of transcription factors and DNA repair proteins.[113]

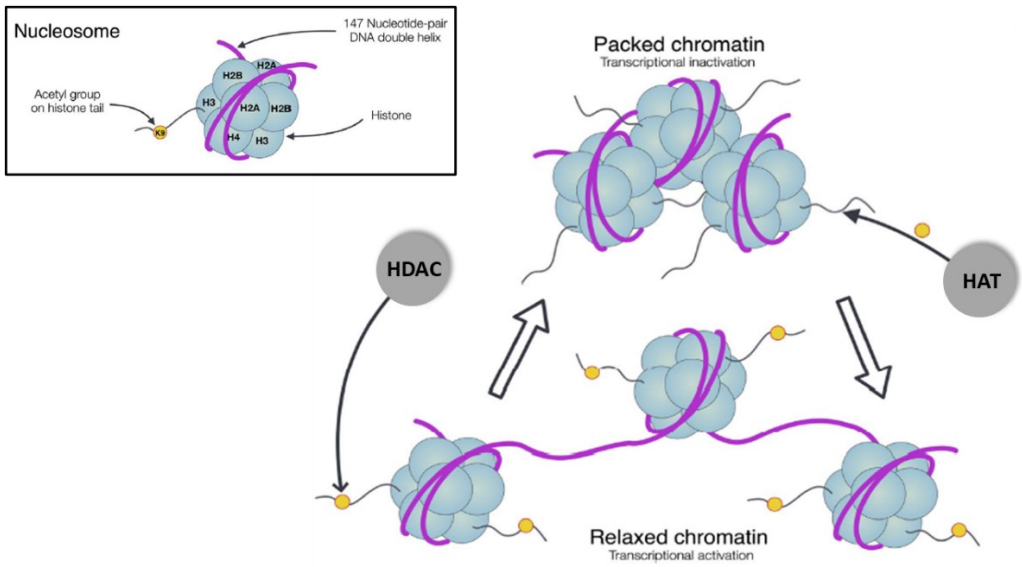

Figure 1.11. Nucleosome structure and schematic diagram illustrating changes in chromatin structure due to histone deacetylase (HDAC)-catalysed deacetylation. Adapted from Huynh *et al.* 2017.[114]

Eighteen members of the human HDACs family have been discovered and divided into two families based on their Zn^{2+} and nicotinamide adenine dinucleotide NAD^{+}-dependency. The Zn^{2+}-dependent subfamily includes the class I HDACs (HDAC 1, 2, 3, and 8) that are widely expressed in many cell types, Class IIa (HDAC 4, 5, 7, 9), class IIb (HDAC 6 and 10) and class IV (HDAC 11) are expressed in a more tissue-specific fashion. Instead, class III sirtuins includes the Sir2 regulator family and requires the cofactor (NAD^{+}) for their active site. The Class I proteins, located in the nucleus and ubiquitously expressed, presents sequence analogy to the yeast transcription regulator reduced potassium dependency 3 (Rdp3). The Class II proteins have cytoplasmic localization and sequence analogy to the yeast Hda1 protein. The Class III proteins have sequence analogy to the yeast Sir2

protein and are differently located in the nucleus, cytoplasm, mitochondria and nucleolus. The Class IV protein shares sequence analogy to both Class I and II proteins.[115]

The first structural and mechanistic information on HDACs was derived from the crystal structure of histone deacetylase-like protein (HDLP), an HDAC1 homologue from *Aquifex aeolicus*, containing an α/β fold with a central 8-stranded parallel β-sheet flanked on each side by four α-helices. From this study, the crystalline structure shows the presence of a Zn^{2+} ion placed on the bottom of the hydrophobic pocket, which emerged as active site, coordinated with Asp168, His170, Asp258 and a water molecule.[115,116] Lately, studies from X-ray crystallography of mammalian HDACs showed the same catalytic domain structure as HDLP conserved across the HDAC family, even though for HDAC8 was suggested a slightly different catalytic mechanism (approximately 30% sequence identity with HDLP). The most significant differences concern the length and structure of loops around the active site and the presence, in addition to the zinc ion, of two potassium ions, one of which interacts with important residues for enzymatic catalysis. In some HDAC isoforms, there is an additional hydrophobic internal cavity lateral to the active site also known as the "foot pocket". This cavity accommodates acyl side chains longer than acetyl in the cases of HDAC8 and HDAC11 and may aid the entry of water and the release of acetate.[115,117]

On the basis of these structural considerations, it is possible to assume a mechanism of enzymatic catalysis. The general mechanism provide for a binding interactions between the acetyl-lysine bearing protein substrate and a tyrosine residue and the zinc cation in the HDAC active site (Figure 1.10A), following by the formation of a tetrahedral oxyanion enzyme intermediate arising from nucleophilic attack by water and the cleavage of the amide bond (Figure 1.12B-C). In particular, the nucleophilic reaction is facilitated by the coordination of the water molecule with the Zn^{2+} ion and the charge transfer system His131-Asp166. Moreover, the Zn^{2+} ion further facilitates deacetylation reaction, reducing the entropy of the reaction itself and coordinating both nucleophile and substrate. The presence of a tyrosine residue further stabilizes the intermediate of reaction and in the last catalytic step the nitrogen atom of lysine receives a proton from the pair Asp173-His132.[118]

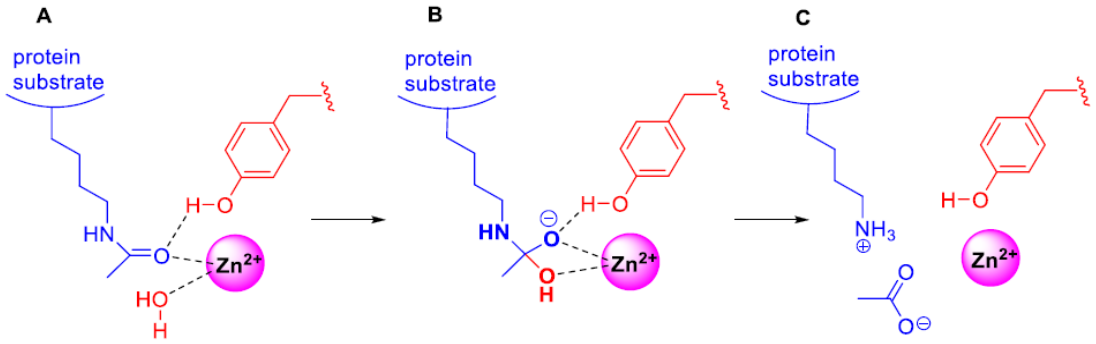

Figure 1.12. Simplified illustration of the catalytic mechanism of deacetylation by HDACs.

1.4.1. HDAC inhibitors

To inhibit HDACs by blocking access to their active site, several natural and synthetic inhibitors have been identified. HDAC inhibitors induce an accumulation of acetylated histones and other non-histone proteins, altering several biological processes including regulation of gene expression, cell proliferation, cell migration, and cell death. The exact mechanisms involved in these processes are not fully understood. HDAC inhibitors (HDACi) are characterized by a common pharmacophore model including: a hydrophobic cap (CAP) able to interact with the rim space at the entrance of N-acetylated lysine binding channel of the enzyme linked to a hydrophobic spacer (HS) through a polar connection unit (CU). At the end of the hydrophobic spacer, a zinc-binding group (ZBG) coordinates the zinc ion in the active site assures the inhibition of enzyme activity (Figure 1.13).

CAP is a variable moiety, ranging from a simple benzene ring to a more complex cyclic tetrapeptide. CU is often a sp2-hybridized group such as ketone, amide or sulphonamide, oxazole or thiazole rings. HS can be represented by linear or cyclic structures, either saturated or unsaturated and to date the most widely used ZBG is the hydroxamate.[119,120]

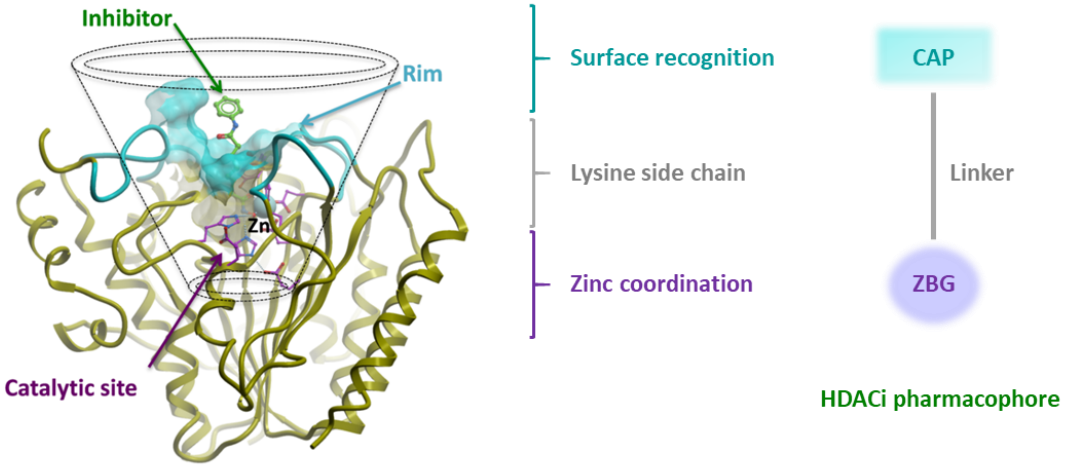

Figure 1.13. Pharmacophore model for HDAC inhibitors.

Despite the shared features of the pharmacophore, HDACi have been discovered with different structural characteristics and classified in four main classes (Figure 1.14) including: A) hydroximates, such as tricostatin A (TSA) and suberoylanilide hydroxamic acid (SAHA, commercially known as Zolinza®); B) short-chain fatty acids, such as valproic acid (VPA) or butyric acid; C) benzamides, such as CI-994 and MS-275 (entiostat); D) cyclic peptides, such as trapoxin B (TPX B) and depsipeptides FK228 (romidepsin).[121]

Among these classes, hydroxamates are the most studied. Indeed, co-crystallization studies of TSA or SAHA with the HDLP have shown that the inhibitors insert their aliphatic chain into the HDLP pocket. The zinc-bound water molecule was replaced by hydroxamate hydroxyl, which coordinates the zinc ion in a bidentate manner through its carbonyl and hydroxyl groups and also establish hydrogen bonds with amino acids located around the zinc, displacing the zinc-bound water molecule with its hydroxy group. The aromatic ring group interacts with amino acids at the edge of the pocket, which allows inhibitors to lock in the pocket.[118] The hydroxamic acid moiety may possess different zinc-binding modalities in the active site of HDAC6 due to its unique three dimensional contour of the catalytic domains. In 2016, a novel hydroxamate-Zn^{2+} coordination mode where the hydroxyl does not replace zinc-bound water was discovered.[122] This unique monodentate binding model, with

free energy of about 0.5 kcal/mol higher than that of the bidentate model, was more suitable for phenylhydroxamate inhibitors, which are unable to bind deeply to the HDAC6 active site owing to the short and bulky linkers.[123]

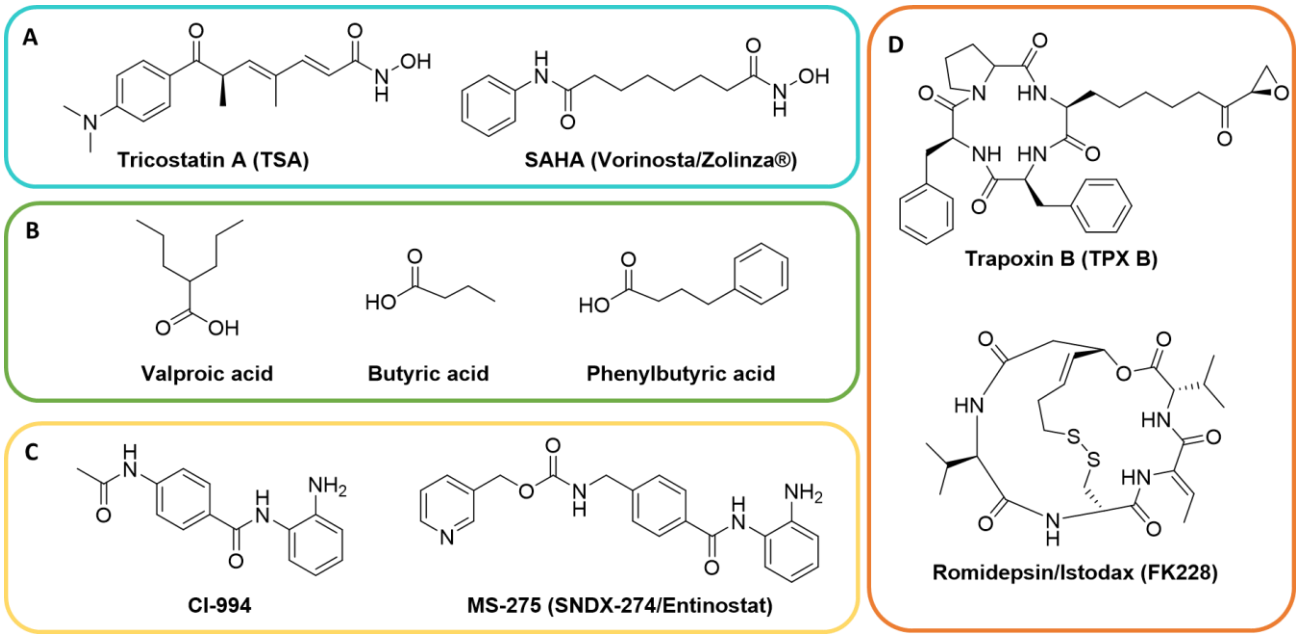

Figure 1.14. The main four classes of HDAC inhibitors. (A) Hydroxamic acids, (B) short-chain fatty acids, (C) benzamides and (D) cyclic peptides.

Certain HDACi may selectively inhibit different HDACs. In effect, MS-275 could be considered a novel isoform-selecive inhibitor, inhibiting preferentially HDAC1 with IC_{50} at 0.3 μM, compared to HDAC3 with an IC_{50} of about 8 μM, while it has little or no inhibitory effect against HDAC6 and HDAC8.[124]

1.4.2. Biological effects of HDAC

Owing to the effect in regulating cellular function, many studies demonstrated that HDAC inhibitors can cure cancer, inflammation, and nerve degradation after brain injury in vivo. The over-expression of HDACs is often related to cancer and HDAC inhibitors represent a class of targeted anti-cancer

agents. They are able, in fact, to induce growth arrest, reduction of angiogenesis and cell migration, differentiation, apoptosis, and autophagocytic cell death of cancer cells (Figure 1.15).[125]

Likewise, HDAC inhibitors seem promising for the treatment of neurodegenerative diseases (like PD, AD, ALS) in which the histone acetylation homeostasis is greatly impaired, shifting towards hypoacetylation. Mainly, HDAC inhibitors beget neuronal differentiation in different neural o ganglion cells, neurons and experimental cell lines such as the PC12 cells.[126]

Hyperacetylation produced by HDAC inhibitors leads to neuroprotective effects such as stimulation of neurogenesis, restoration of memory and learning, enhancement of neuronal differentiation and synaptic plasticity in different disease models.[126] Moreover, HDAC inhibition results in beneficial outcomes in various types of inflammation disorders[127,128] and cardiovascular diseases.[129,130]

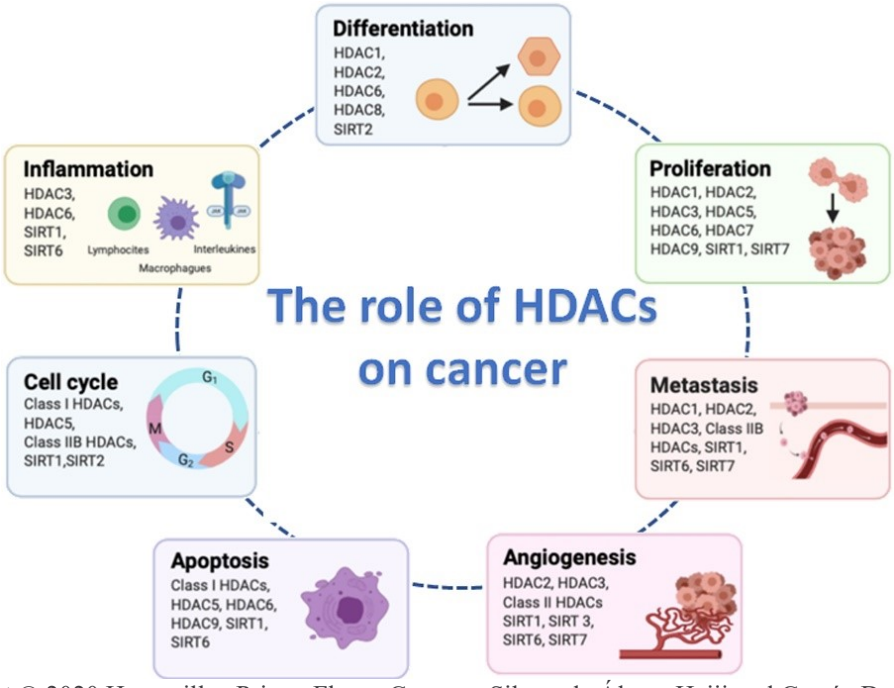

Figure 1.15. Hallmarks of cancer cell biology in which histone deacetylases (HDACs) are involved.

The United States Food and Drug Administration (FDA) has so far approved four HDAC inhibitors for treatment of hematologic cancers with less severe side effects in clinic trial, which also are continuously expanding to address other types of cancer. These include Vorinostat (SAHA)[131],

Romidepsin (FK228),[132,133] and Belinostat (PXD101)[134] for cutaneous and peripheral T-cell lymphomas; while Panobinostat (LBH-589)[135] has been approved for myeloma. In addition, other inhibiting compounds have entered into clinical trials such as TSA, sodium butyrate (NaB), phenylbutyrate, Entinostat (MS-275), depsipeptide, pyroxamide and VPA.

In particular, further work showed that pan-HDAC inhibitors, such as valproic acid, induced an inhibition of growth and survival *in vitro* and *in vivo* uveal melanoma xenograft models, reason why phase II clinical study is ongoing for adjuvant VPA as treatment for high-risk uveal melanoma.[136]

Clinical applications have been limited due to pan-inhibitors which act on many HDAC members leading to a wide range of effects in patients, associated with a lack of HDAC isoform or complex selectivity. An emerging strategy aiming to address these limitations is the development of bifunctional HDAC therapeutics-single molecules comprising a HDAC inhibitor conjugated to another specificity targeting moiety.

2. Aim of the thesis

Uveal melanoma is the most frequently found intra-ocular malignancy in adults and no clinically significant chemotherapeutic treatments are so far available, often due to the occurrence of frequent highly aggressive metastasis and the outcomes that are poor once distant spread appears.

The general attention of the thesis was focused on the development of Sigma/HDACi hybrid molecules that could be considered for the treatment of this rare cancer, testing their effects as possible pharmacological strategy. In the last years, the growing interest as chemotherapeutic agents that have seen both σ receptor ligands and HDACi protagonists suggest the possibility to combine both, obtaining hybrid ligands, capable of carrying out an antiproliferative action through the interaction with two different molecular target. Moreover, the encouraging developments and results achieved with previous works encouraged us to continue on this path. Previous works by our research group identified some dual-target/dual-function ligands (σ and HDACi) which display interesting antiproliferative or antiangiogenic properties such us (±)-MRJF4 and its enantiomers, a novel ester prodrug of haloperidol metabolite II (HP-mII) with the histone deacetylase inhibitor (HDACi) phenylbutyric acid, as well as the σ_1 receptor antagonist (±)-MRJF22, a prodrug of (±)-HP-mII that we achieved by conjugation to VPA.

Meanwhile, both the target object of this thesis are involved for different reasons in uveal melanoma pathways. HDACi reverse the biochemical defect caused by BAP1 loss (i.e., H2A hyperubiquitination), a tumor suppressor gene closely associated with loss of melanocytic differentiation in uveal melanoma and metastasis; while recently some σR ligands seem to induce apoptosis and autophagy in uveal melanoma (although the mechanism is not yet clear).

Thanks to these results, the project has been developed following the scheme summarized in figure 3.1 and, generally, it provides for three groups of compounds, each of which has been then distinguished into several series:

- First of all, the presence of an asymmetry centre (chiral carbon) in the prodrug (±)-MRJF22 suggested the synthesis of the two enantiomers through enantioselective synthetic approach, with the aim to assess whether the possible antiangiogenic effects of the racemic mixture could depend on the prevailing activity of an isomer rather than another one.

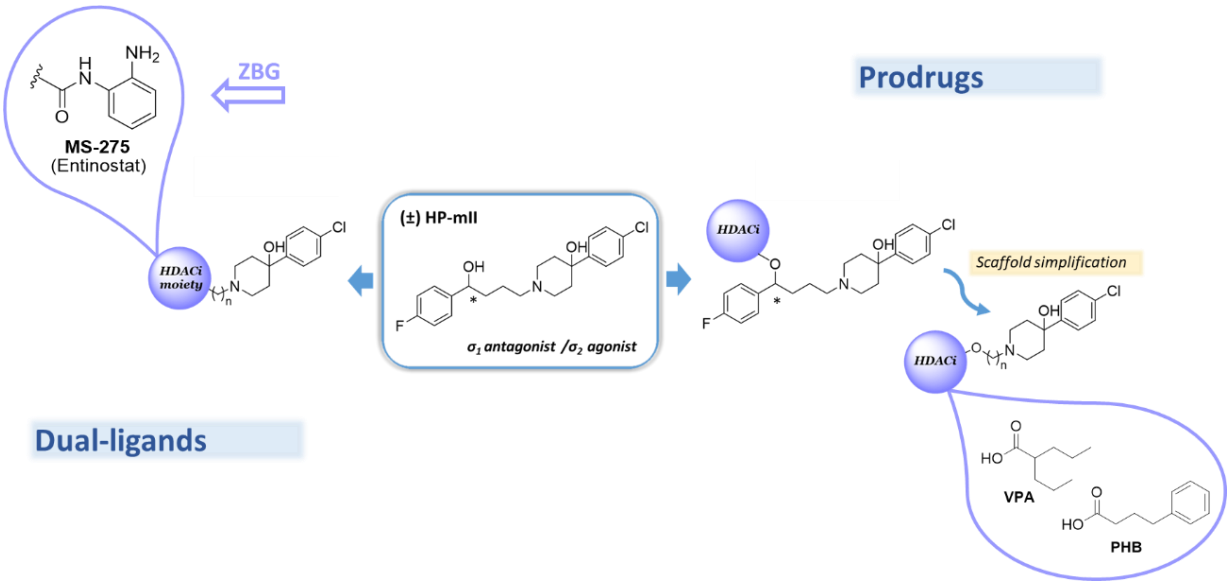

Figure 3.1 General idea for the design of Sigma/HDACi hybrid ligands.

- Afterward, it have been designed different esters of VPA, phenyl butyric and butyric acid, in which the fluorophenyl ring was removed and the length of the methylene chain between nitrogen and the ester carboxyl group was modified. In this way, the excessive steric hindrance on the substituent at the nitrogen of 4-phenylpiperidine of (±)-MRJF22, which could lead to a reduction in affinity for σ receptors, should be reduced.

- Moreover, a multitarget approach has been pursued: the single molecules, called dual-ligands, should be capable of interacting as such on the molecular targets considered in this research project. The rational design for the advancement of these new ligands was based first on the overlap and then the merger of the pharmacophore common to the σ ligands with the

established one for HDACis. In this sense, appropriate functional groups were selected, providing together a single pharmacophore, able to fit into the pharmacophoric model of both molecular targets and ensure optimal binding interaction either with the receptor σ or with the HDAC enzyme.

For all the designed compounds we aim to evaluate the ability to inhibit the proliferation of human uveal melanoma 92-1 cells, and therefore to validate the general idea that the multitarget approach represent a clear advantage, especially in cancer that often is approached through combined therapies. We are hopeful that hybrid ligands could represent a point of departure for a valid strategy in the treatment of a multi-functional pathology and so aggressive disease as uveal melanoma.

3. Results and discussions

Herein are reported proofs of the manuscript or the simple description of the preliminary results obtained with the Sigma/HDACi hybrid ligands previously described.

For all the hybrids compounds synthesis and characterizations have been performed at the Department of Drug and Healthy Science of the University of Catania and at the Department of Organic Chemistry in the Faculty of Science of the University of Zaragoza. Moreover, radioligand binding assay were also carry out at the Department of Drugs and Healthy Science of the University of Catania.

Biological evaluation data on human uveal melanoma 92-1 cell lines have been produced at the laboratory core of Vera Salus s.r.l. (Viagrande, CT).

Additional biological assays and HDAC inhibition assays were made possible thanks to the collaboration and support of the Department of Biomedical and Biotechnological Sciences (School of Medicine) of the University of Catania and the Department of Pharmacy at the University "G. d'Annunzio" of Chieti-Pescara.

Haloperidol metabolite II Valproate ester (±)-MRJF22: asymmetric synthesis and biological evaluation on Human Microvascular Retinal Endothelial and uveal melanoma cells.

Carla Barbaraci[a§], Giovanni Giurdanella[b§], Claudia Leotta[c], Anna Longo[c], Orazio Prezzavento[a], Gabriella Lupo[b], Emanuele Amata[a], Giovanni Mario Pitari[c*], Daniela Anfuso[b*], Agostino Marrazzo[a*]

[a]Department of Health and Drug Sciences, University of Catania, Viale A. Doria 6, 95125 Catania, Italy

[b]Department of Biomedical and Biotechnological Sciences, School of Medicine, University of Catania, Via S. Sofia 97, 95123 Catania, Italy

[c]Vera Salus Ricerca S.r.l, Via Sigmund Freud 62/B, 96100 Siracusa, Italy

ACS Journal of Medicinal Chemistry
(Manuscript almost ready for submission)

ABSTRACT As reported in a previous work, the prodrug **(±)-MRJF22**, consisting of a histone deacetylase inhibitor (valproic acid) and a sigma ligand (haloperidol metabolite II), have shown an antiangiogenic activity comparable to bevacizumab. In continuation of this one, we report the asymmetric synthesis of compounds **(*R*)-(+)-MRJF22** and **(*S*)-(-)-MRJF22** and their biological activity on HREC and human cells of uveal melanoma (92-1), which is the most common primary malignancy of the eye in adults developing for 40-50% metastatic disease usually fatal within a year of onset of symptoms. Good antiangiogenic activity on HREC, associated with the aptitude to reduce cell viability and, most importantly, the highest antimigratory effect on 92-1 cells of **(*S*)-(-)-MRJF22** represent a promising result for the development of a useful therapeutic candidate for the treatment of uveal melanoma.

KEYWORDS: *sigma receptors, HDAC, angiogenesis, VEGF, uveal melanoma*

Author Contributions:
[§]CB and GG contributed equally.

[*]Corresponding Authors
Agostino Marrazzo (marrazzo@unict.it)
Daniela Anfuso (daniela.anfuso@unict.it)
Giovanni Mario Pitari (giovanni.pitari@verasalusricerca.it)

INTRODUCTION

Although uveal melanoma (UM) is the most common primary malignancy of the eye in adults, it is reputed a relatively rare subset of noncutaneous melanoma (less of 5% melanoma cases),[19] which arises from melanocytes as cutaneous melanoma but it is biologically and genetically distinct from it. Approximately 90% of all UMs involve the choroid, while the rest rise in the ciliary body (6%) or iris (4%).[3] Worldwide estimate that there are 7095 new cases of UM annually with a mean age-adjusted incidence of 4.3 per million. The median age at presentation is about 60 and the malignancy affects male and female at the same rate, with an irrelevant predominance among males.[2] Without timely treatment, patients are endangered with visual handicap, pain and facial disfigurement and, despite early diagnosis and proper treatment, about 40-50% of UM patients develop metastatic disease, which is usually fatal within a year of onset of symptoms.[4] Indeed, given the considerable vascularity of the eye and the distinct biology of this tumor, the site of predilection for metastatic diffusion is typically the liver and the presence of a network vascular pattern have also been associated with a worse prognosis.[26] Ocular treatment is aimed at conserving the eye and useful vision, and, if possible, preventing metastatic disease. Adjuvant therapies and screening, in fact, do not seem to provide a significant survival benefit and the apparent benefit may be due to the earlier detection of metastases in an asymptomatic phase (ie, “lead-time bias”). Therapeutic modalities include enucleation and various forms of radio-therapy, tumor resection, and laser therapy. Furthermore, no chemotherapeutic regimen or immunotherapy was demonstrated to be effective and at this stage they are not considered a clinically significant alternative to radiation or surgery.[15,137]

In UM, the signaling pathways regulated by the vascular endothelium growth factor (VEGF) are involved in both neovascularisation and growth of the primary tumor and especially in its metastatization.[7] Certainly, angiogenesis plays a key role in the development and progression of cancer considering that neoplastic cells induce the formation of new blood vessels, which provide nourishment to the growing tumor. Antiangiogenic therapies, in term of neutralisation of angiogenic factors such as VEGF, could be considering for the treatment of cancers in metastatic phases.[25]

As reported in the literature, σ receptors are present at the uveal level (iris and rabbit ciliary body)[138] and, as we reported in recent preliminary studies, both σ receptors are involved in UM, exerting different effects on cell proliferation.[139] First mistaken as a subtype of the opioid receptors, σ receptor are now considered an exceptional class of proteins. Identified as two different σ receptors, Sigma-1 (σ_1) and Sigma-2 (σ_2) receptors, they can be distinguished by molecular weight, tissue distribution, ligand binding profile, pharmacology and activation mechanisms.[140] Widely distributed in the central nervous system, σ receptors are overexpressed in several tumor cell lines and involved in different biological functions including cell proliferation and survival. Interestingly, previous reports showed

that σ_1 receptor is involved in apoptosis due to its location at the mitochondria-associated membranes, and beside σ_1 antagonist and in vivo silencing of the σ receptor may modulate endothelial cell (EC) proliferation and inhibit angiogenesis.[141] Ultimately, treatment with appropriate σ ligands induces apoptosis and autophagy in human uveal melanoma cells, and noteworthy, σ_1 receptor antagonists/σ_2 agonist such as haloperidol metabolite II (HP-mII) reduce the proliferation of human UM cells.[139]
Furthermore, studies suggest that HDACi induced morphologic changes consistent with melanocytic differentiation, and these findings conclude that HDAC inhibitors may play a role in the adjuvant therapy of patients with UM by inducing differentiation and prolonged dormancy of micrometastatic disease.[142] HDACi can induce growth arrest of transformed cells, terminal differentiation, cell death and inhibition of angiogenesis, inducing hyperacetylation of histones and, consequently, affect gene expression.[143] The inhibition of HDACs, in fact, came out as a target for specific epigenetic changes associated with cancer and other diseases.[144] Until now, more than 20 HDAC inhibitors (HDACis) have entered clinical studies, and some of them (e.g., vorinostat, romidepsin) have been approved for the treatment of cutaneous T-cell lymphoma.[145,146] Particularly, studies have shown that the well-known HDACi valproic acid (VPA) inhibits proliferation, inducing G1 cell-cycle arrest in UM cells, and reduces the growth and the final volume of UM in vivo; reason why it underwent phase II clinical trials (NCT02068586).[147-136]
Noting that prodrug approach has been widely employed to improve the delivery of anticancer drugs (camptothecin, paclitaxel, doxorubicin and vinblastine),[148] some dual-target/dual-function ligands (σ_1 and HDAC inhibitors) have been developed, exhibiting both antiangiogenic and antiproliferative properties. On these ground, in our previous work we have shown that **(±)-MRJF4**, a novel ester prodrug of haloperidol metabolite II (HP-mII) with the histone deacetylase inhibitor (HDACi) phenylbutyric acid , and its enatiomers exhibit a good anticancer activity reducing cell viability and increasing cell death by apoptosis.[149,150] Moreover, the σ_1 receptor antagonist **(±)-MRJF22**, a prodrug of (±)-HP-mII that we achieved by conjugation to VPA, showed significant antiangiogenic activity compared to (±)-HP-mII and HP. Indeed, it induced a reduction of the proliferation of the human retinal endothelial cells (HRECs) 20 times higher than (±)-HP-mII and 120 times than VPA and also was able to significantly reduce viable cells count, endothelial cell migration and tube formation in vascular endothelial growth factor A (VEGF-A) stimulated HREC cultures.[151] Based on these results, it could be considered a promising candidate for the development of a therapeutic strategy for the treatment of diseases related to angiogenesis, such as cancer. It should also be remembered that **(±)-MRJF22** can either totally act or be metabolized in the two active molecules (±)-HP-mII and VPA, which has recently undergone phase I/II clinical trials as anticancer drug.[152]

In this study we report the asymmetric synthesis of prodrugs **(*R*)-(+)-MRJF22** and **(*S*)-(−)-MRJF22** (Scheme 1) and the evaluation of them on VEGF-A stimulated human retinal endothelial cells (HRECs), which offers an in vitro model of blood−retinal barrier (BRB) in a proangiogenic tumoral environment. Furthermore, we also investigated their effect on human 92-1 uveal melanoma cells, in order to further validate our previous hypothesis on the possibility of considering σ receptors and, consequently HDAC as a valuable target for uveal melanoma treatment.

RESULTS AND DISCUSSION

Compounds **(*R*)-(+)-2** and **(*S*)-(-)-2** were obtained in two steps through enantioselective reduction, as also reported in literature.[150] In the first step, the 4-cloro-1-(4-fluorophenil)butan-1-one was treated with the reduction agents (+) or (-) diisopinocanphenilcloroborane (DIP-Cl), in THF for 16 h at -25 °C; in the second one, was added dietanolamine (DEA) at room temperature (rt) and let stirred overnight. The intermediate have been used to achieve respectively compounds (*R*)-(+)-HPmII and (*S*)-(-)-HPmII with a nucleophilic substitution with 4-(4-clorophenil)hydroxypiperidine in anhydrous DMF and in presence of $KHCO_3$ at 80 °C for 24h. Subsequently, in order to obtain the final products **(*R*)-(+)-MRJF22** and **(*S*)-(-)-MRJF22,** compounds (*R*)-(+)-HPmII and (*S*)-(-)-HPmII were esterified with 2-propylpentanoil chloride in presence of TEA, in THF at 0 °C and then stirred at rt, according to the procedure already used by us[151] (Scheme 1).

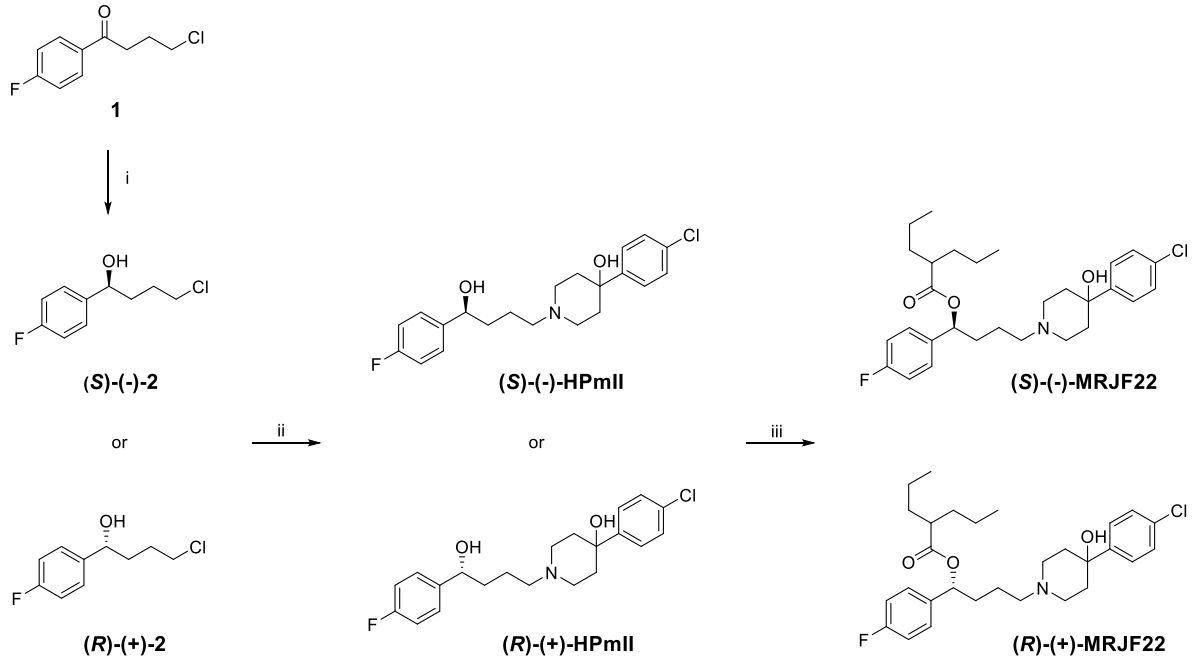

Scheme 1. *Reagents and conditions*: i) 1. (+) o (−) DIP-Cl, THF, -25°C, 16 h; 2. DEA, Et_2O, r.t., overnight; ii) 4-(4-clorophenyl)hydroxipiperidine, $KHCO_3$, DMF dry, 80°C, 24 h; iii) 2-propylpentanoyl chloride, THF, 0°C to r.t, 3h.

All compounds were characterized by their ^{1}H and ^{13}C NMR spectroscopic data that resulted superimposable with the literature ones (see Supporting Information).[150,151]

In table 1 are showed the σ_1 and σ_2 receptor affinities of **(*R*)-(+)-MRJF22**, **(*S*)-(-)-MRJF22**, (*R*)-(+)-HP-mII, and (*S*)-(-)-HP-mII relative to respective racemic mixtures. An high σ_1 binding affinity (K_i = 2.0 ± 0.4 and 3.0 ± 0.8 nM, respectively) was exhibit by the (+)- and (-)-enantiomers of HP-mII; on contrary both the enantiomers display an anomalous lower affinity for σ_2 receptor with respect to racemic mixture (K_i = 2.4 ± 0.5 nM), probably due to a positive allosteric modulation of the two enantiomers as also reported in literature for sigma receptors.[37] In particular, (+)-HP-mII showed lower affinity to σ_2 receptor (K_i = 32.0 ± 2.0 nM) if compared with its opposite isomer (-)-HP-mII and haloperidol (K_i = 9.8 ± 1.3 nM and 18.0 ± 2.2 nM, respectively), these data are in accord to literature ones.[150]

Table 1. σ_1 and σ_2 binding assays, optical activity of (±)-MRJF22, its enantiomers and precursor compounds

	***K*i (nM) ± SD[a]**		***α***
Cmps	**σ_1R**	**σ_2R**	
(±)-MRJF22	13.0±0.4[a]	124±11[a]	-
R-(+)-MRJF22	64.0±0.6	74±1.5	+ 26
S-(-)-MRJF22	16±0.8	56±1.2	- 24
(±)-HPmII	2.9±0.8[a]	2.4±0.5[a]	-
(R)-(+)-HPmII	2.0±0.4[b]	32.0±2.0[b]	+ 66
(S)-(-)-HPmII	3.0±0.8[b]	9.8±1.3[b]	- 65
Haloperidol	2.7±0.5[a]	17.0±0.5[a]	-

Each value is the mean ± SD of at least two experiments performed in duplicate
[a]Ref. 21
[b]Ref. 20

The esterification of the hydroxyl group on the (+)- and (-)-HP-mII enantiomers with VPA decreased, the binding affinity for both σ receptor subtypes, in accordance with previous data on **(±)-MRJF22**. Nevertheless, **(*S*)-(-)-MRJF22** preserve a good affinity for both σ_1 and σ_2 receptor (K_i = 16.0 ± 0.8 nM and 56.0 ± 1.2 nM) compared to **(*R*)-(+)-MRJF22** (K_i = 64.0 ± 0.6 nM and 74.0 ± 1.5 nM), which seem to no discriminate between the two subtype.

In order to characterized the biological properties of racemic mixture **(±)-MRJF22** and the respective enantiomers **(*S*)-(-)-MRJF22** and **(*R*)-(+)-MRJF22**, we first used MTT test to evaluate cell viability in human retinal endothelial cells (HREC) treated with different concentration (1, 2.5, 5, 10 and 20

μM) of compounds for 24, 48 and 72h (Fig. 1). Mainly, all treatments reduced viability in a dose and time dependent manner; the doses of 10 or 20 μM were very toxic as they reduced strongly cell viability up to about 15% in comparison to untreated cells (Fig.1 panel A, B and C).

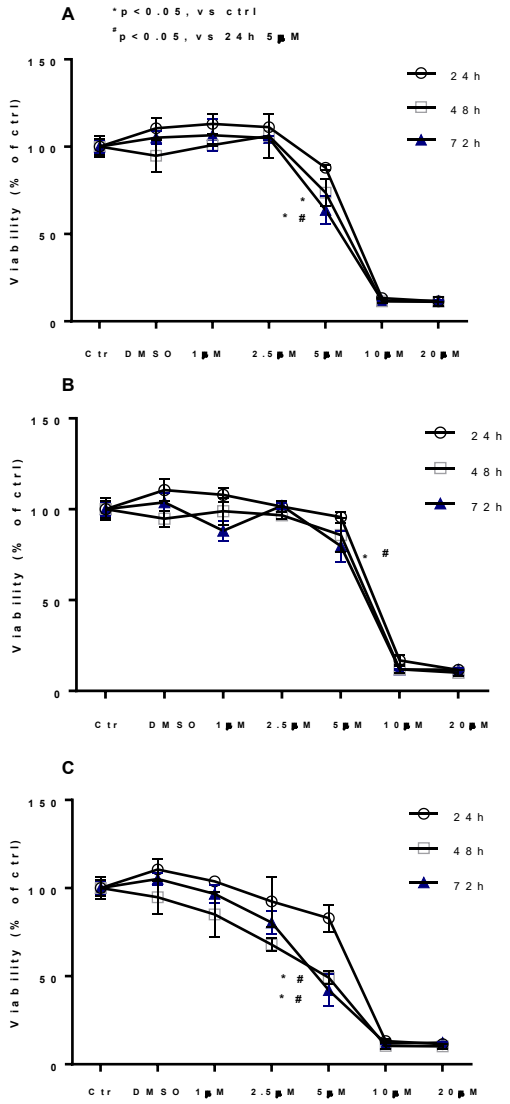

Figure 1. Effects of (±)-MRJF22 , S-(-)-MRJF22, R-(+)-MRJF22 on HREC viability. MTT value obtained in cells treated with increasing concentration (1, 2.5, 5, 10 and 20 μM) of (±)-MRJF22 (A), (*S*)-(-)-MRJF22 (B) and (*R*)-(+)-MRJF22 (C) for 24, 48 and 72h. Ctr, untreated cells; DMSO, vehicle control (DMSO); Data are expressed as a mean ± SEM of three independent experiments, each involving three different wells per condition. Statistical analysis was performed using two-way ANOVA, followed by Tukey's test. *, p<0,05; vs control; # p<0,05 vs 24h 5 μM.

However, compounds impacted on HREC cell viability in different manner at the dose of 5 μM. In fact, 5 μM of **(±)-MRJF22** significantly decreased cell viability up to about 75 and 65% after 48 and

72h of treatment respectively (Fig. 1, panel A). IC_{50} calculated for **(±)-MRJF22** treatment ranged from 5.83 to 5.1 μM at 24, 48 and 72 h respectively. **(*S*)-(-)-MRJF22** reduced significantly of 35% only after 72h of treatment respect to untreated cells ($p<0.05$; Fig. 1, panel B) with IC_{50} of 6.63, 6.23 and 5.44 μM calculated at 24, 48 and 72h of treatment ($p<0.05$). Unlike **(*S*)-** enantiomer, equimolar concentration of **(*R*)-(+)-MRJF22** enantiomer proved to be more toxic, since decreased viability of about 50% just after 48h of treatment and of 60% after 72h (Fig. 1, panel C). IC_{50} calculated for **(*R*)-(+)-MRJF22** treatment ranged from 6.36 to 4.69 μM at 24, 48 and 72 h respectively. In this respect, noteworthy is that 5 μM **(±)-MRJF22**, as reported in the previous work, induced also a significant decrease in cell viability (28% and 32%, respectively) at 24 and 72 h compared to the individual (±)-HP-mII and VPA in equimolar concentrations (5 μM) incubated with HREC.[151]

Low doses of treatments (1 and 2.5μM) with **(±)-MRJF22** and **(*S*)-(-)-MRJF22** do not induced relevant changes in MTT values respect to the controls, despite a not significant trend of reduction was observed in cell treated with **(*R*)-(+)-MRJF22** for 48 and 72h (Fig. 1, panel C). Table S1 (see Supporting information) shows the IC_{50} values of **(±)-MRJF22** compared to **(*S*)-(-)-MRJF22** and **(*R*)-(+)-MRJF22** at 24, 48, and 72h. These data highlighted a greater tolerability of the enantiomer **(*S*)-(-)-MRJF22** in comparison to **(*R*)-(+)-MRJF22** indicating a different involvement of the enantiomers in the viability of HREC. On the other hand, racemic mixture **(±)-MRJF22** seem to be characterized by an intermediate degree of toxicity with respect to the two enantiomers.

Crystal violet assays were carried out to investigate the effects of **(±)-MRJF22**, **(*S*)-(-)-MRJF22**, **(R)-(+)-MRJF22** on the proliferation rate of HREC stimulated with 80 ng/ml of VEGF (Fig 2). As expected, VEGF (at conc. of 80 ng/ml) exerted a pro-angiogenic effect by increasing cell proliferation of about 45 and 35% after 24 and 72h of treatment respectively ($p<0.05$) (Fig 2, panel A and C) in comparison to the controls. We first verified that 5 μM of treatment with **(±)-MRJF22**, **(*S*)-(-)-MRJF22**, **(*R*)-(+)-MRJF22** do not induced any substantial changes in proliferation rate after 24 and 72h of treatment in un-stimulated HREC. The presence of 5 μM of **(±)-MRJF22**, completely prevented the enhancement of cell proliferation induced by 80 ng/ml of VEGF-A at 24h; moreover, equimolar concentration of **(*S*)-(-)-MRJF22** and mainly **(*R*)-(+)-MRJF22** (5 μM) reduced cell proliferation of about 10 and 20% below the control levels in presence of VEGF-A (Fig 2, panel A). These data were further confirmed at 72h; in fact, co-treated HREC with 5 μM of **(±)-MRJF22**, **(*S*)-(-)-MRJF22** and **(*R*)-(+)-MRJF22** and VEGF-A lowered proliferation rate of HREC with the same extent below the control levels ($p<0.05$, Fig 2, paned C).

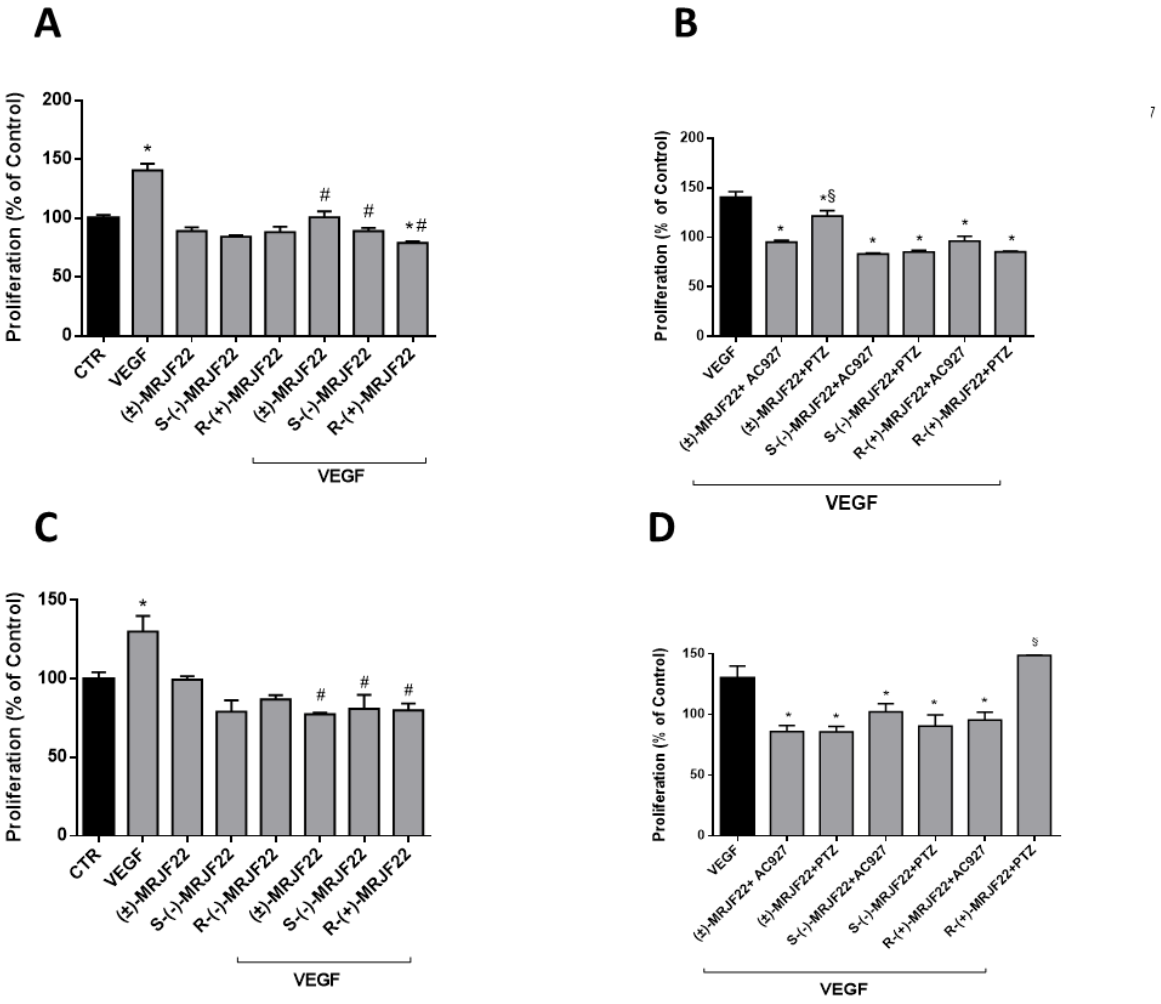

Figure 2. Antiproliferative effects of (±)-MRJF22, (*S*)-(-)-MRJF22 and (*R*)-(+)-MRJF22 in HREC. Cell proliferation of HREC treated with 80 ng/ml of VEGF-A in presence or in absence of 5 μM of (±)-MRJF22, (*S*)-(-)-MRJF22 and (*R*)-(+)-MRJF22 for 24h (A) or 72h (C). Effects of the selective σ_1 agonist PTZ (2 μM) and σ_2 receptors antagonist AC927 (2 μM) tested in HREC co-treated with 5 μM of (±)-MRJF22, (*S*)-(-)-MRJF22 and (*R*)-(+)-MRJF22 and 80 ng/ml of VEGF-A for 24h (B) or 72h (D). CTR, vehicle control (DMSO); PTZ, Pentazocine. Data are expressed as % of proliferation with respect to the vehicle control. *, p<0,05 vs CTR; #, p<0,05 vs VEGF. §, p<0,05 vs the same conditions without agonist or antagonist.

(±)-MRJF22 and its enantiomers have also been used in combination with the σ_1 agonist (+)-pentazocine [(+)-PTZ] (2 μM) and σ_2 receptors antagonist 1-phenethylpiperidine (AC927, 2 μM) to evaluate the role of σ receptors in the anti-proliferative activity of **(±)-MRJF22**, **(*S*)-(-)-MRJF22**, **(*R*)-(+)-MRJF22** in HREC induced by VEGF-A. Treatments with (+)-PTZ partially restored ($p<0.05$ vs the same conditions without agonist or antagonist) the loss of HREC cell proliferation induced by 24h of co-treatment with VEGF-A (80 ng/ml) and 5 μM of **(±)-MRJF22**; however this effect was completely lost at 72h of treatment (Fig 2, panels B and C). AC927 do not changed the effects of the co-treatment with **(±)-MRJF22** and VEGF-A on HREC cell proliferation ($p<0.05$ vs the same

conditions without agonist or antagonist). On the other hand, 24 of incubation with (+)-PTZ and AC927 do not altered the anti-proliferative role of **(*S*)-(-)-MRJF22** at 5 μM. However, we observed a partial restore of VEGF-A proliferative activity of about 40% induced by AC927 in presence of **(*S*)-(-)-MRJF22**. Finally, in presence of (+)-PTZ, **(*R*)-(+)-MRJF22** (5 μM) was completely ineffective in the blockade of cell proliferation induced by VEGF-A at 72h of treatment ($p<0,05$ vs the same conditions without agonist or antagonist) (Fig 2, panel D). These results suggested that VEGF ability to induce cell proliferation is mediated by a synergistic involvement of both σ_1 and σ_2 receptors. Overall, the VEGF-A mediated activation of both these receptors seems to be a necessary condition as indicated by a substantial lack of PTZ and AC927 effect in the blockade of the racemic mixture **(±)-MRJF22** anti-angiogenic activity. The ability of (+)-PTZ to completely block the anti VEGF-A activity of **(*R*)-(+)-MRJF22** enantiomer highlighted its σ_1 receptor antagonist profile. On the other hand, as AC927 partially counteracted the **(*S*)-(-)-MRJF22** effect in VEGF-A stimulated HREC, a σ_2 receptor agonist profile can be attribute to this enantiomer.

In vitro stimulation of endothelial motility by VEGF is suggestive of the enhanced cell migration observed in the pathological process of angiogenesis.[153] Therefore, we evaluated the effects of **(±)-MRJF22**, and relative enantiomers **(*S*)-(-)-MRJF22**, **(*R*)-(+)-MRJF22** on HREC cell motility stimulated by 80 ng/ml of VEGF-A through the wound healing assays. As shown in Fig. 3, wounded HREC monolayers do not complete the closure of the wound even at 48 hours when incubated in a control medium containing 1% FBS (CTR). However, VEGF-A caused an increased migration ($p<0.05$) of HREC compared to unstimulated cells (Fig.3, panel A-B-C), as wound closure was completed already starting from 24h after the scratch of the HREC confluent monolayer.

Treatments with 5 μM of **(±)-MRJF22** do not changed significantly the percentage of wound closure in un-stimulated cells, while completely abrogate VEGF-A-mediated induction of cell migration in HREC. The presence of AC927 or mostly (+)-PTZ reduced **(±)-MRJF22** ability to block VEGF-A-induced wound healing, as indicate d by the percentage of wound closure close to VEGF-A treated HREC levels (Fig.3, panel A).

Interestingly, equimolar concentrations of the enantiomers do not changed cell motility in un-treated HREC significantly (Fig 3 panels B and C); however, they counteracted wound closure in different manner. In particular, HREC stimulated with 80 ng/ml of VEGF-A, and 5 μM of **(*R*)-(+)-MRJF22** showed percentage of wound closure close to controls ($p<0.05$; Fig.3, panel B). The presence of 2 μM (+)-PTZ or AC927 restored the levels of cell motility induced by VEGF-A ($p<0.05$), indicating a putative interaction of **(*R*)-(+)-MRJF22** enantiomer with σ_1 and σ_2 receptors. Moreover, these data are consistent with the idea that the involvement of both σ_1 and σ_2 receptors is necessary for the induction of cellular motility of HREC mediated by VEGF-A. Enantiomer **(*S*)-(-)-MRJF22** (at conc.

of 5 μM) produced a very strong reduction of HREC cell motility, as indicated by the percentages of wound closure much lower than the controls (Fig.3, panel C). Unlike **(*R*)-(+)-MRJF22**, treatment with 2 μM of AC927 restored the loss of cell motility induced by **(*S*)-(-)-MRJF22** in presence of VEGF-A as indicated by the increased wound closure percentage up to control level ($p<0.05$). (+)-PTZ, at 2 μM, did not affect significantly the response of HREC to the treatment with VEGF-A in presence of **(*S*)-(-)-MRJF22** (at 5 μM of conc.).

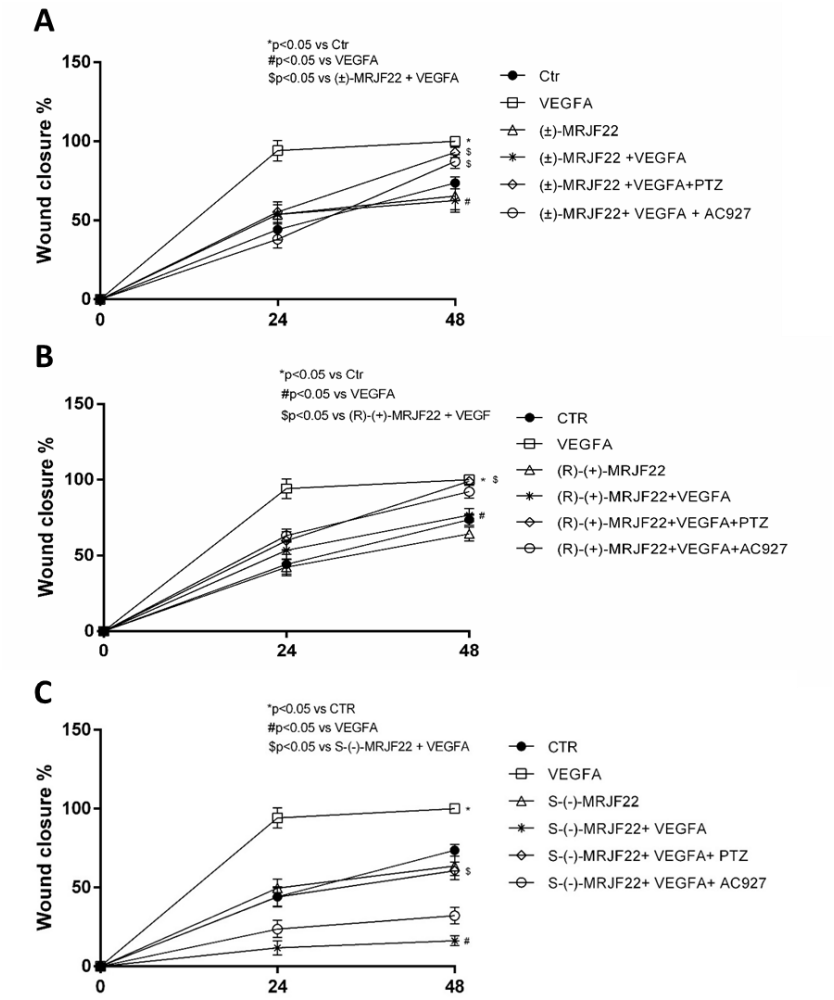

Figure 3. Effects of (±)-MRJF22, (*S*)-(-)-MRJF22 and (*R*)-(+)-MRJF22 on VEGF-A-stimulated HREC migration evaluated by wound healing assay. Evaluation of cell motility in HREC treated with 80 ng/ml of VEGF-A in presence or in absence of 5 μM (±)-MRJF22 (A), (*R*)-(+)-MRJF22 (B) and (*S*)-(-)-MRJF22 (C). Selective σ_1 agonist PTZ (2 μM) or σ_2 receptors antagonist AC927 (2 μM) were added to treatment medium containing 80 ng/ml of VEGF-A and (±)-MRJF22, or (*R*)-(+)-MRJF22 or (*S*)-(-)-MRJF22 were tested. Wound closure percentage was quantified by ImageJ software. CTR, vehicle control (DMSO); PTZ, Pentazocine. Values are expressed as a mean ± SEM of three independent experiments, each involving three different wells per condition. Statistical analysis was performed using one-way ANOVA, followed by Tukey's test. *, $p<0,05$ vs CTR; #, $p<0,05$ vs VEGF. §, $p<0,05$ vs the same conditions without agonist or antagonist.

Representative images of HREC treated with VEGF after the scratch wound are shown in Supporting Information for **(±)-MRJF22** , **(*R*)-(+)-MRJF22** and **(*S*)-(-)-MRJF22** (Figure S1,S2 and S3). These data provide evidence of a highly selective σ_2 agonist profile for the **(S)-(-)-MRJF22** enantiomer, confirming the data reported above. Interestingly, here we show that **(*S*)-(-)-MRJF22** trigger a strong detrimental effect regarding endothelial cell motility in stimulating condition by VEGF-A while do not noticeable alter this property under resting condition.

In Fig. 4 the quantifications of the total tube length from HREC in Matrigel tube formation assays are reported. VEGF conditioning environment results in an upregulation of the total tube length, while treatment with Aflibercept (AFL, 40 μg/ml), also known as VEGF-trap used for the treatment of various ocular abnormalities[154,155] and metastatic colorectal cancer,[156] leads to a reduction of the total tube length.

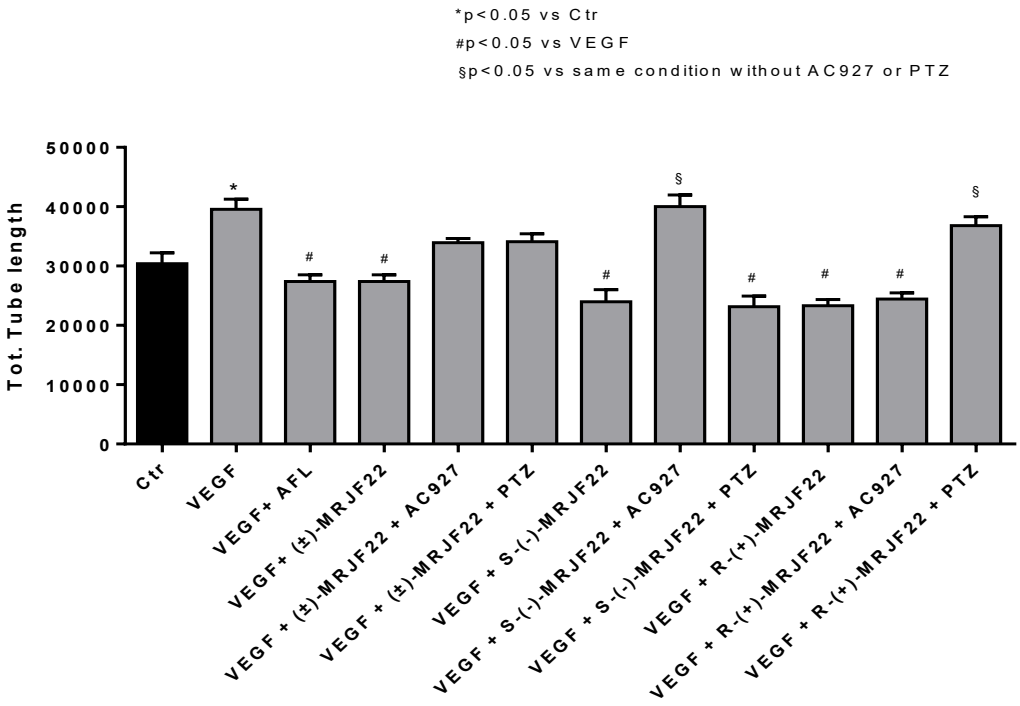

Figure 4. Anti-angiogenic effects of (±)-MRJF22, (*S*)-(-)-MRJF22 and (*R*)-(+)-MRJF22 in VEGF-stimulated HREC. Quantification of tube length was calculated using angiogenesis analyzer tool for Imagej software. CTR, vehicle control (DMSO); PTZ, Pentazocine; AFL, Aflibercept. Values are expressed as a mean ± SEM of three independent experiments, each run in triplicate. Statistical analysis was performed using one-way ANOVA, followed by Tukey's test. *P < 0.05vs. CTRL; #P < 0.05 vs VEGF, § P < 0.05 vs same condition without AC927 or PTZ. One-way ANOVA, followed by Tukey's test. *, p<0,05 vs CTR; #, p<0,05 vs VEGF. §, p<0,05 vs the same conditions without agonist or antagonist.

Moreover, the upregulation of the total tube length induced by VEGF was countered by **(±)-MRJF22**, **(*S*)-(-)-MRJF22**, **(*R*)-(+)-MRJF22**. **(±)-MRJF22** activity was partially blocked by both AC927 and

PTZ with the same extent. The capability of **(*S*)-(-)-MRJF22** was completely blocked by the AC927 but not by PTZ, while the effect of **(*R*)-(+)-MRJF22** was prevented by PTZ and not by AC927. Representative optical phase-contrast micrographs of tube-like structures observed in the Tube Formation assays (Matrigel) are shown in Supporting Information (figure S4).

Immediately afterwards, the effects of **(±)-MRJF22**, **(*R*)-(+)-MRJF22** and **(*S*)-(-)-MRJF22** were explored on human uveal melanoma 92-1 cells in order to assess their inhibitory activity on tumor cells. First of all, gene expression levels of σ_1 and σ_2 receptors were checked, for the first time, by reverse transcription polymerase chain reaction (RT-PCR) and MCF7 human breast cancer cells were used as the positive controls for σ_1/σ_2 gene expression. As shown in Fig. 5A, results indicate 92-1 cells possess the transcripts of both the SIGMAR1 gene (σ_1 receptor) and the TMEM92 gene (σ_2 receptor). Then, actions on cell proliferation were examined as shown in Fig. 5C-D. All precursor compounds, VPA, HP and (±)-HP-mII, significantly inhibited human uveal melanoma 92-1 cell proliferation compared to the vehicle control (Fig. 5B; H_2O_2, positive control). However, all prodrug derivatives exhibited increased antiproliferative effects (Fig.5C) with respect to their chemical precursors (Fig.5B) as indicated by their putative IC_{50} values of about 5.46 μM for **(±)-MRJF22**, 4.95 μM for **(*R*)-(+)-MRJF22** and 4.45 μM for **(*S*)-(-)-MRJF22**. No significant differences in efficacy or potency were observed among the three derivatives (Fig.5C).

Furthermore, application of σ_1 selective agonist (+)-PTZ, σ receptors selective antagonist AC927 or their combination did not perturbed the antiproliferative effects by **(±)-MRJF22** (Fig.5D), indicating that probably σ receptors are not the main antiproliferative targets of **(±)-MRJF22** in human uveal melanoma 92-1 cells.

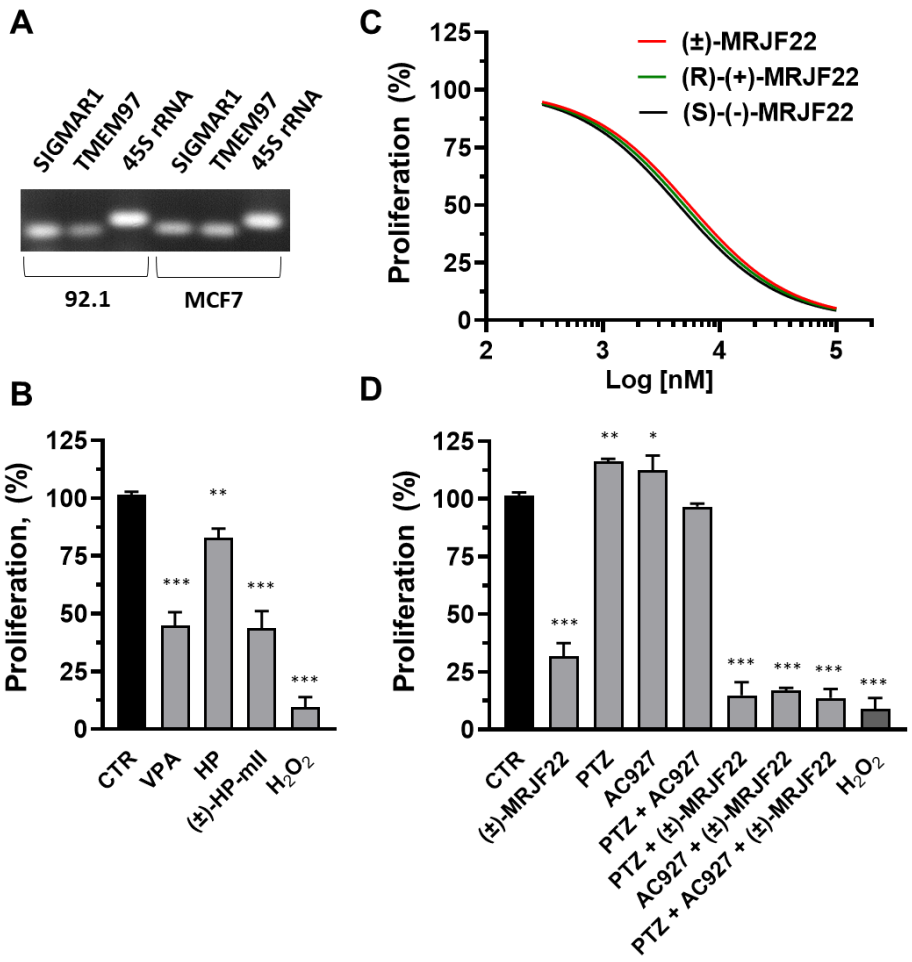

Figure 5.Anticancer effects of (±)-MRJF22, (*R*)-(+)-MRJF22 and (*S*)-(-)-MRJF22 in 92-1 human uveal melanoma cells. A) Reverse transcriptase-polymerase chain reaction (RT-PCR) for σ_1 (SIGMAR1) and σ_2 (TMEM97) receptor expression in 92-1 cells and MCF-7 human breast cancer cells. 45S Ribosomal pre-RNA was used as the positive control. B) Effects of VPA (2 mM), HP (10 µM), (±)-HP-mII (30 µM), H_2O_2 (100 µM) on proliferation. C) Dose-response curves of antiproliferative effects of the indicated compounds. D) Antiproliferative effects of (±)-MRJF22 (5 µM) in combination with the selective σ_1 agonist PTZ (2 µM) and σ receptors antagonist AC927 (2 µM). CTR, vehicle control (DMSO); PTZ, Pentazocine; VPA, Valproic Acid; HP, Haloperidol; (±)-HP-mII, Haloperidol metabolite II. Data in B, C, D represent % of proliferation with respect to the vehicle control. *, p<0,05; **, p<0,01; ***, p<0,001 vs vehicle control.

Finally, tumor cell migration was explored by the wound healing assay (Fig. 6). **(±)-MRJF22**, **(*R*)-(+)-MRJF22** and **(*S*)-(-)-MRJF22** inhibited 92-1 cell migration over 48 h time courses (Fig. 6A). Unexpectedly, sigmoid dose-response curves calculated at the 48 h time point demonstrated significant different antimigratory potencies by the three derivatives (Fig. 6B), displaying IC_{50} values of about 4.22 µM for **(±)-MRJF22**, 1.15 µM for **(*R*)-(+)-MRJF22** and 0.09 µM for **(*S*)-(-)-MRJF22)**. In particular, the derivative **(*S*)-(-)-MRJF22** exerted the highest antimigratory effect (Fig. 6B) compared to **(*R*)-** enantiomer and the racemic mixture **(±)-MRJF22**.

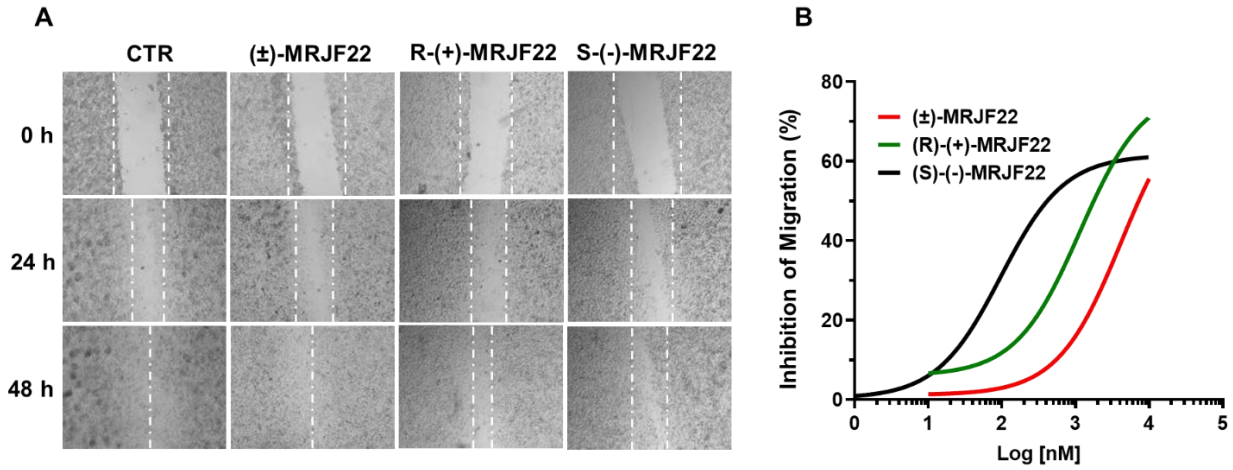

Figure 6. Effect of (±)-MRJF22, (*R*)-(+)-MRJF22 and (*S*)-(-)-MRJF22 on 92-1 human uveal melanoma cell migration. (A) Representative images of wound healing assay. Magnification, 4x. All compounds were used at 3 µM. CTR, vehicle control (DMSO). Panel B shows dose-response curves of inhibition of cell migration by the indicated compounds at the 48-h time point. Data are shown as % inhibition of cell migration with respect to the vehicle control.

CONCLUSION

We describe the synthesis and the pharmacological characterization of the two enantiomers of (±)-HP-mII valproate ester, **(±)-MRJF22**. Results indicate that the racemic mixture and its enantiomers exhibit a good antiangiogenic activity, comparable to aflibercept for **(±)-MRJF22** and moderately improved for the two enantiomers, **(*R*)-(+)-MRJF22** and **(*S*)-(-)-MRJF22**. Moreover, we have shown that all compounds lead to significantly reduce the viable cell count, endothelial cell migration, and tube formation in VEGF stimulated HREC cultures. Notably, **(*S*)-(-)-MRJF22** have shown an improved tolerability in HREC viability, a lowered proliferation rate of HREC stimulated with 80 ng/ml of VEGF and a very strong antimigratory effect at 5 µM on VEGF-stimulated HREC. Co-treatment with σ_1 agonist (+)-PTZ and σ_2 receptors antagonist AC927 provide evidence of a σ_1 receptor antagonist profile for **(*R*)-(+)-MRJF22** and a highly selective σ_2 receptor agonist profile for **(*S*)-(-)-MRJF22**, underling a synergistic involvement of both σ receptors in VEGF ability to induce cell proliferation and cellular motility of HREC.

Furthermore, RT-PCR demonstrated the presence of both σ_1 and σ_2 receptors in human uveal melanoma 92-1 cells, on which it has also been assessed the cytotoxic effects of **(±)-MRJF22** and both enantiomers. All compounds significantly inhibited 92-1 cell proliferation compared to HP, (±)-HP-mII and VPA, without any significant difference in efficacy or potency among the three derivatives but with a really slight better extent for **(*S*)-** enantiomer (IC_{50}= 4.45 µM). On the other hand, **(*S*)-(-)-MRJF22** displayed an excellent antimigratory activity, with an IC_{50} value of 0.09 µM

assessed by the wound healing assay, compared to **(±)-MRJF22** and **(*R*)-(+)-MRJF22**. Unlike what happens in HREC, employment of (+)-PTZ and AC927 or their combination seem to indicate that σ receptors are not the main antiproliferative targets of **(±)-MRJF22** in 92-1 uveal melanoma cells. However, in which way the receptors are involved in the mechanism, even with respect to the HDAC inhibition, is unclear and will be objects of further studies.

Based on our findings, **(*S*)-(-)-MRJF22** shows a considerable antiangiogenic and antimigratory activity compared to the racemic mixture and the **(*R*)-** enantiomer, which also seems to be more toxic in HREC. For this reason, **(*S*)-(-)-MRJF22** might represent a promising candidate for the development of a therapeutic strategy for the treatment of uveal melanoma, a disease closely related to angiogenesis and early-stage development of metastases.

EXPERIMENTAL SECTION

Chemistry. Reagent grade chemicals were purchased from Sigma-Aldrich (St. Louis, MO, USA) or TCI (Tokio, Japan) and were used without further purification. All reactions involving air-sensitive reagents were performed under N_2 in oven-dried glassware using the syringe-septum cap technique. All reactions were monitored by thin-layer chromatography (TLC) which was performed on silica gel Merck 60 F254 plates; the spots were visualized by UV light (λ = 254 and 366 nm) and iodine chamber. Melting points were determined on a Büchi B-450 apparatus in glass capillary tubes and are uncorrected. Optical rotations were taken at 20 °C with a PerkineElmer 241 polarimeter. Flash chromatography purification was performed on a Merck silica gel 60, 0.040−0.063 mm (230−400 mesh), stationary phase using glass columns with a diameter between 1 and 4 cm. Nuclear magnetic resonance spectra (^{1}H NMR and ^{13}C NMR recorded at 500 MHz) were obtained on Varian INOVA spectrometers using $CDCl_3$, D_2O e DMSO-d_6 with a 0.03% of TMS as internal standard. Coupling constants (*J*) are reported in hertz. Signal multiplicities are characterized as s (singlet), d (doublet), t (triplet), q (quartet), m (multiplet), br (broad). Purities of all compounds was determined by microanalysis (C, H, N) that was performed on a Carlo Erba instrument model E1110; all the results agreed within ±0.4% of the theoretical values. Compound nomenclatures were generated with ChemBioDraw Ultra version 16.0.0.82.

General procedure for the synthesis (*S*)-(-)- and (*R*)-(+)-4-cloro-1-(4-fluorophenyl)butan-1-ol, (*R*)-(+)-2 and **(*S*)-(-)-2**

Both compounds were synthesized as already reported in literature,[150] and all analytical and spectral data are consistent with the reported ones. Here we report only the data inherent to purity, obtained after flash chromatography Cy/EtOAc 80-20%.

(*R*)-(+)-2, white solid; 95% of yeld, $[a]_D$= +37.0 (c1 in $CHCl_3$); Anal. Calcd for $C_{10}H_{12}ClFO$: C, 59.27; H, 5.97; N, 17.49. Found: C, 59.50; H, 6.07; N, 17.58.

(*S*)-(-)-2, white solid; 84% of yeld, $[a]_D$= - 41.0 (c1.2 in $CHCl_3$); Anal. Calcd for $C_{10}H_{12}ClFO$: C, 59.27; H, 5.97; N, 17.49. Found: C, 59.45; H, 6.07; N, 17.79.

General procedure for the synthesis (*S*)-(-)- and (*R*)-(+)-4-(4-clorophenyl)-1-[4(4-fluorophenyl)-4-hidroxybutyl]piperidin-4-ol, (*R*)-(+)-HPmII and **(*S*)-(-)-HPmII.**

Both compounds were synthesized as already reported in literature,[150] and all analytical and spectral data are consistent with the reported ones. Here we report only the data inherent to purity, obtained after flash chromatography a gradient CH_2Cl_2/CH_3OH.

(*R*)-(+)-HPmII, white solid, mp: 145-146.5 °C; 80% of yeld, $[a]_D$= +66,5 (c1 $CHCl_3$); Anal. Calcd for $C_{21}H_{25}ClFNO_2$: C, 65.19; H, 6.77; N, 3.62. Found: C, 65.37; H, 7.02; N, 3.20.

(*S*)-(-)-HPmII, white solid, mp: 145-146 °C; 77% of yeld, $[a]_D$= -65 (c1 $CHCl_3$); Anal. Calcd for $C_{21}H_{25}ClFNO_2$: C, 65.19; H, 6.77; N, 3.62. Found: C, 64.97; H, 6.47; N, 3.99.

General procedure for the synthesis (*S*)-(-) and (*R*)-(+)-4-[(4-clorophenyl)-4-hidrosxypiperidin-1-il]-1-(4-fluorophenyl)butil-2-propylpentanoate, (*R*)-(+)-MRJF22 and **(*S*)-(-)-MRJF22.**

To a solution of ***R*-(+)-3** or ***S*-(-)-3** (0.5 mmol) and TEA (1 mmol) in anhydrous THF (6 ml) was added 4-phenylbutanoyl chloride (2 mmol) at 0 °C and under stirring. The reaction was left for 24 h at r.t. under a nitrogen atmosphere. Subsequently, 15 ml of water was added and the mixture let stirred for 30 minutes. To the reaction mixture was added CH_2Cl_2 and the organic phase separated and washed with a solution of $NaHCO_3$ 4%. The organic phase was anhydrified with Na_2SO_4 and evaporated. The crude was purified by flash chromatography to obtain the final compound **(*R*)-(+)-MRJF22** or **(*S*)-(-)-MRJF22** as a colourless oil. Both enantiomers were transformed into oxalate salts to best preserve them for biological tests.

(*R*)-(+)-MRJF22 oxalate, white solid, mp: 159-164 °C, 63% of yeld, $[a]_D$= +26 (c1 $CHCl_3$);. ^{1}H NMR (500 MHz, DMSO-d_6): δ 7.48 (d, J = 8.31 Hz, 2H), 7.41−7.38 (m, 4H), 7.18 (t, J = 8.80 Hz, 2H), 5.71 (t, J=7.09 Hz, 1H), 2.49 (br d, J = 10.76 Hz, 2H), 2.38−2.33 (m, 4H), 2.22−2.07 (m, 2H), 1.91−1.85 (m, 1H), 1.81−1.78 (m, 2H), 1.75 (br d, J = 12.72 Hz, 2H), 1.52−1.32 (m, 10H), 0.82 (t, J = 7.34 Hz, 3H), 0.77 (t, J = 7.34 Hz, 3H). ^{13}C NMR (125 MHz, DMSO-d_6): δ (ppm) 174.6, 164.5 (d, J_{CF} = 245.00 Hz), 146.9, 136.5 (d, J_{CF} = 3.30 Hz), 131.4, 128.5, 128.4 (d, J_{CF} = 8.05 Hz), 126.6, 115.2

(d, J_{CF} = 21.25 Hz), 73.8, 67.9, 47.9, 48.99, 44.4, 37.9, 35.0, 34.03, 33.98, 20.0, 19.9, 19.8, 13.7. Anal. Calcd for $C_{31}H_{41}ClFNO_7$: C, 74.17; H, 8.58; N, 2.98. Found: C, 74.22; H, 8.61; N, 2.98.

(*S*)-(-)-MRJF22 oxalate, white solid, mp: 158-160 °C, 99.7% of yeld, $[a]_D$= -24 (c1 $CHCl_3$). ^{1}H NMR (500 MHz, DMSO-d_6): δ 7.48 (d, *J* = 8.31 Hz, 2H), 7.41−7.38 (m, 4H), 7.18 (t, *J* = 8.80 Hz, 2H), 5.71 (t, *J*=7.09 Hz, 1H), 2.49 (br d, *J* = 10.76 Hz, 2H), 2.38−2.33 (m, 4H),2.22−2.07 (m, 2H), 1.91−1.85 (m, 1H), 1.81−1.78 (m, 2H), 1.75 (br d, *J* = 12.72 Hz, 2H), 1.52−1.32 (m, 10H), 0.82 (t, *J* = 7.34 Hz, 3H), 0.77 (t, *J* = 7.34 Hz, 3H). ^{13}C NMR (125 MHz, DMSO-d_6): δ (ppm) 164.7 (d, J_{CF}=325.5 Hz), 145.7, 138.3, 130.4, 130.4 (d, J_{CF}=8.5 Hz), 120.9, 115.8 (d, J_{CF}=35.5 Hz), 73.0, 71.1, 55.7, 48.1, 39.6, 39.4, 24.8. Anal. Calcd for $C_{31}H_{41}ClFNO_7$: C, 74.17; H, 8.58; N, 2.98. Found: C, 74.22; H, 8.61; N, 2.98.

Receptor Binding studies. The σ_1 and σ_2 receptor binding studies were performed according to literature.[157,158] Briefly, for the σ_1 binding assay guinea pig brain membranes (400ml, 500 µg protein) were incubated 150 min at 37 °C with 3 nM [3H]-(+)-pentazocine (45 Ci/mmol) and increasing concentrations of tested compounds or displacing ligands in 50 mM Tris-HCl (pH 7.4) to a total volume of 1 ml. Nonspecific binding was assessed in the presence of 10 µM of unlabelled haloperidol. σ_2 binding assays were made according to the following protocol: the membranes (300 ml, 360 µg protein) were incubated 120 min at room temperature with 3 nM [3H]-DTG (31 Ci/mmol) in the presence of 0.4 mM (+)-SKF10,047 to block the σ_1 sites. The incubation was performed in 50 mM Tris-HCl (pH 8.0) to a total volume of 0.5 ml with increasing concentration of each test compound. Nonspecific binding was evaluated in the presence of 5 µM DTG.

Each sample was filtered through Whatman GF/B glass fibres filters, which were presoaked for 1 h in a 0.5% poly(ethylenimine) solution, using a Millipore filter apparatus. Filters were washed twice with 4 ml of ice-cold buffer. Radioactivity was counted in 4 ml of 'Ultima Gold MV' in a 1414 Winspectral PerkinElmer Wallac or Beckman LS6500 scintillation counter. Inhibition constants (Ki values) were calculated using the EBDA/LIGAND program purchased from Elsevier/Biosoft.

Cell cultures. Primary human retinal endothelial cells (HREC) were purchased from Innoprot (Elexalde Derio, Spain) and were fed with culture EC medium, supplemented with 5% FBS, 1% ECGS (Endothelial cell Growth supplement), 100 U/ml penicillin and 100 µg/ml streptomycin, provided by Innoprot. Cells were plated in T25 culture flasks (Costar; Corning, New York, NY, USA), precoated with fibronectin (Innoprot) for 1 h at 37 °C. Human uveal melanoma cell line 92-1 (passages 2-15), a gift from Professor Gabriella Lupo,[159] were maintained at 37°C (5% CO_2) in RPMI-1640 medium, containing 10% fetal bovine serum (FBS), 2 mM L-glutamine, 100 units/ml penicillin and 100 µg/mL streptomycin. Breast cancer cell line MCF-7, obtained from the American Type

Culture Collection (ATCC; Manassas, VA, USA), were maintained at 37 °C (5% CO_2) in Eagle's Minimum Essential Medium, containing 10% FBS, 2 mM L-glutamine, 100 units/ml penicillin, 100 μg/mL streptomycin and 0.01 mg/ml human recombinant insulin. All cell media and reagents were from Euroclone S.p.A. (Pero, Milan, Italy). PTZ and AC927 were synthesized in the laboratory of Prof. Agostino Marrazzo (University of Catania, Italy), as reported in literature.[160,161]

MTT assay. For cell viability assays, the 3-[4,5–dimethylthiazol-2-yl]-2,5-diphenyl tetrasodium bromide (MTT assay, Chemicon, Temecula, CA) was used. Cells were seeded in 96-well plates at a density of $1{,}5\times10^4$ cells/well and were incubated overnight at 37 °C before experiment. Afterwards, cells were treated for 24h, 48h and 72h in presence of different concentration (1, 2.5, 5,10, 20 μM) of **(±)-MRJF22**, **(*R*)-(+)-MRJF22** or **(*S*)-(-)-MRJF22**. After the treatments, the cells were incubated with MTT (5 mg/mL) for 3 hours and then 100 μL dimethyl sulfoxide was added and the absorbance was read in a plate reader (Synergy 2-BioTek) with a wavelength of 570 nm.

Cell proliferation. HREC proliferation was measured using crystal violet staining after treatment in 96-well plates with **(±)-MRJF22**, **(*R*)-(+)-MRJF22** or **(*S*)-(-)-MRJF22** with or without VEGF (80 ng/ml), AC927 and PTZ. At the end of the treatment, each well was washed with phosphate-buffered saline (PBS). Following this, cells were fixed and stained with 0.5% crystal violet solution in 20% methanol for 10 min. Subsequently, the plate was washed with water and left to dry. Each assay was carried out in triplicate. Crystal violet staining was evaluated by measuring the absorbance at 570 nm with the microplate reader (Synergy 2-BioTek).
92-1 cell line were seeded ($4x10^3$) in 96-well plates and grown for 72 h at optimum culture conditions. Then, cells were treated with the indicated concentrations of chemicals for additional 48 h. Control cells received an equal volume of vehicle (DMSO). At the end of incubations, cells were fixed (in 4% paraformaldehyde) and stained with crystal violet (1%, aqueous solution). For quantification, after crystal violet extraction with 10% acetic acid (at room temperature for 10 min) the absorbance (at 590 nm) was measured with a spectrophotometer (Synergy HT, BioTek).

Wound healing assay. HREC were seeded in 24 well tissue culture plates until complete confluence. Monolayers of confluent cells were scratched with a p200 pipet tip. Cells were treated for 72hours in the presence of **(±)-MRJF22**, **(*R*)-(+)-MRJF22** or **(*S*)-(-)-MRJF22** with or without VEGF (80 ng/ml), AC927 and PTZ. Wound closure was monitored by photographs at 40× using a phase-contrast microscope in each culture condition and at each time point (0, 24, and 48 h). The numbers of cells toward the wounds were counted using ImageJ software (ImageJ 1.50e, National Institutes of Health, NIH, Bethesda, MD) and were quantified by measuring the distance travelled over time by both cell fronts into the wound area.

92-1 cells were seeded (2.5×10^5 cells/well) into 24 well plates and grown to confluency. Confluent cell monolayers were scratched with a sterile 200 µl pipette tip to create 1 mm wide wounds. After washing (3 times) with PBS to remove cell debris, wounded monolayers were incubated for 48 h (37 °C) in complete medium in the presence of the indicated treatments. Wound closures were photographed at 0, 6, 24, 30 and 48 h and quantified by measuring the remaining cell unmigrated area using the NIH-ImageJ program.

Tubule formation assay. Tube formation assay was analyzed in vitro in BD Matrigel, following manufacturer's instructions (BD, Bedford). In brief, 96-well plates were coated with 50 µl of Matrigel for well and allowed to solidify at 37 °C for 2 h. HREC were seeded at 1.5×10^4 cells/well in 100 µl medium with **(±)-MRJF22**, **(*R*)-(+)-MRJF22** or **(*S*)-(-)-MRJF22** in presence of absence VEGF (80 ng/ml), AC927 and PTZ. After 8h of incubation, tube-like structures were photographed at 10X magnification by using an inverted microscope (Leica DM IRB) equipped with a CCDcamera. Tube formations were quantified with the Image J software (NIH, Bethesda, MD).

Total RNA and RT-PCR. Total RNAs were extracted from cell cultures employing Direct-zol RNA Miniprep (Zymo Research, California, USA) as to manufacturer's instructions, and redissolved in 30 µL RNase-free water. RNA concentrations and purity were estimated by optical density at 260 and 280 nm. The first-strand cDNA was reversely transcribed using High-Capacity cDNA Reverse Transcription Kit (Applied Biosystems™, California, USA) in a 20 µL reaction volume.

Aliquots of cDNA were amplified using specific primers for the σ_1 receptor (SIGMAR1, F: 5′-GTGAGGTCTTCTACCCAG-3' and R: 5′-GAAGAGGGTGAGGAAGTC-3′), σ_2 receptor (TMEM97, F:5'-CCTGGTTTAAGTCCTTTCTG-3'; R:CTCAAACAGAAATGTGGAGAG-3') and the positive control 45S Ribosomal pre-RNA (F: CGCGCTCTACCTTACCTACCT and R:CGTCGGCATGTATTAGCTCT), producing three specific amplification products of 173 bp, 173 bp and 199 bp, respectively. PCR reactions were carried out employing Wonder Taq kit (Euroclone). PCR parameters were: initial denaturing, 95 °C for 3 min; 35 cycles of denaturing at 95 °C for 15 s, annealing at 54 °C (SIGMAR1), 56°C (TMEM97) or 59°C (45S Ribosomal pre-RNA) for 15 s and extension at 72 °C for 30 s; final extension step, 72 °C for 7 min. Primers for RT-PCR were purchased from SIGMA ALDRICH (St. Louis, Missouri, USA).

Statistical Analysis. All results are reported as mean ± SEM from at least 3 independent experiments (n=3) performed at least in duplicate. The results were analysed using one-way ANOVA followed by Tukey–Kramer multiple comparisons test; differences between groups were considered significant for p-value < 0.05.

Abbreviations used

UM, uveal melanoma; VEGF, vascular endothelial growth factor; EC, endothelial cell; HDACi, histone deacetylase inhibitor; HP, haloperidol; HREC, human retinal endothelial cell; VPA, valproic acid; DIP-Cl, diisopinocanphenilcloroborane;(+)-PTZ, (+)-pentazocine; AFL, aflibercept; FBS, fetal bovine serum; RT-PCR, reverse transcription polymerase chain reaction; TLC, thin-layer chromatography.

Supporting Information. Table S1, Figure S1-S4 and NMR spectra of all compounds were reported in the Experimental section of Supporting Information.

References

1. Kaliki, S.; Shields, C. L., Uveal melanoma: relatively rare but deadly cancer. *Eye (Lond)* **2017,** *31* (2), 241-257.
2. Andreoli, M. T.; Mieler, W. F.; Leiderman, Y. I., Epidemiological trends in uveal melanoma. *Br J Ophthalmol* **2015,** *99* (11), 1550-3.
3. Maheshwari, A.; Finger, P. T., Cancers of the eye. *Cancer Metastasis Rev* **2018,** *37* (4), 677-690.
4. Virgili, G.; Gatta, G.; Ciccolallo, L.; Capocaccia, R.; Biggeri, A.; Crocetti, E.; Lutz, J. M.; Paci, E.; Group, E. W., Survival in patients with uveal melanoma in Europe. *Arch Ophthalmol* **2008,** *126* (10), 1413-8.
5. Buder, K.; Gesierich, A.; Gelbrich, G.; Goebeler, M., Systemic treatment of metastatic uveal melanoma: review of literature and future perspectives. *Cancer Med* **2013,** *2* (5), 674-86.
6. Dogrusoz, M.; Jager, M. J.; Damato, B., Uveal Melanoma Treatment and Prognostication. *Asia Pac J Ophthalmol (Phila)* **2017,** *6* (2), 186-196.
7. Chattopadhyay, C.; Kim, D. W.; Gombos, D. S.; Oba, J.; Qin, Y.; Williams, M. D.; Esmaeli, B.; Grimm, E. A.; Wargo, J. A.; Woodman, S. E.; Patel, S. P., Uveal melanoma: From diagnosis to treatment and the science in between. *Cancer* **2016,** *122* (15), 2299-312.
8. Boyd, S. R.; Tan, D. S.; de Souza, L.; Neale, M. H.; Myatt, N. E.; Alexander, R. A.; Robb, M.; Hungerford, J. L.; Cree, I. A., Uveal melanomas express vascular endothelial growth factor and basic fibroblast growth factor and support endothelial cell growth. *Br J Ophthalmol* **2002,** *86* (4), 440-7.
9. Maj, E.; Papiernik, D.; Wietrzyk, J., Antiangiogenic cancer treatment: The great discovery and greater complexity (Review). *Int J Oncol* **2016,** *49* (5), 1773-1784.
10. Jiang, G.; Mysona, B.; Dun, Y.; Gnana-Prakasam, J. P.; Pabla, N.; Li, W.; Dong, Z.; Ganapathy, V.; Smith, S. B., Expression, subcellular localization, and regulation of sigma receptor in retinal muller cells. *Invest Ophthalmol Vis Sci* **2006,** *47* (12), 5576-82.
11. Longhitano, L.; Castracani, C. C.; Tibullo, D.; Avola, R.; Viola, M.; Russo, G.; Prezzavento, O.; Marrazzo, A.; Amata, E.; Reibaldi, M.; Longo, A.; Russo, A.; Parrinello, N. L.; Volti, G. L., Sigma-1 and Sigma-2 receptor ligands induce apoptosis and autophagy but have opposite effect on cell proliferation in uveal melanoma. *Oncotarget* **2017,** *8* (53), 91099-91111.

12. Bowen, W. D., Sigma receptors: recent advances and new clinical potentials. *Pharm Acta Helv* **2000,** *74* (2-3), 211-8.
13. Smith, S. B., Introduction to Sigma Receptors: Their Role in Disease and as Therapeutic Targets. *Adv Exp Med Biol* **2017,** *964*, 1-4.
14. Landreville, S.; Agapova, O. A.; Matatall, K. A.; Kneass, Z. T.; Onken, M. D.; Lee, R. S.; Bowcock, A. M.; Harbour, J. W., Histone deacetylase inhibitors induce growth arrest and differentiation in uveal melanoma. *Clin Cancer Res* **2012,** *18* (2), 408-16.
15. Damaskos, C.; Karatzas, T.; Nikolidakis, L.; Kostakis, I. D.; Karamaroudis, S.; Boutsikos, G.; Damaskou, Z.; Kostakis, A.; Kouraklis, G., Histone Deacetylase (HDAC) Inhibitors: Current Evidence for Therapeutic Activities in Pancreatic Cancer. *Anticancer Research* **2015,** *35* (6), 3129-3135.
16. Li, Z.; Zhu, W.-G., Targeting Histone Deacetylases for Cancer Therapy: From Molecular Mechanisms to Clinical Implications. *International Journal of Biological Sciences* **2014,** *10* (7), 757-770.
17. Mann, B. S.; Johnson, J. R.; He, K.; Sridhara, R.; Abraham, S.; Booth, B. P.; Verbois, L.; Morse, D. E.; Jee, J. M.; Pope, S.; Harapanhalli, R. S.; Dagher, R.; Farrell, A.; Justice, R.; Pazdur, R., Vorinostat for treatment of cutaneous manifestations of advanced primary cutaneous T-cell lymphoma. *Clin Cancer Res* **2007,** *13* (8), 2318-22.
18. Prince, H. M.; Dickinson, M., Romidepsin for cutaneous T-cell lymphoma. *Clin Cancer Res* **2012,** *18* (13), 3509-15.
19. Landreville, S.; Agapova, O. A.; Matatall, K. A.; Kneass, Z. T.; Onken, M. D.; Lee, R. S.; Bowcock, A. M.; Harbour, J. W., Histone Deacetylase Inhibitors Induce Growth Arrest and Differentiation in Uveal Melanoma. *Clinical Cancer Research* **2012,** *18* (2), 408-416.
20. Sato, T.; Orloff, M. M.; Valsecchi, M. E.; Shimada, A.; Chervoneva, I.; Sharpe-Mills, E.; Klose, H.; Norcini, J.; Belinsky, J.; Sato, S.; Hulse, L.; Shields, C. L.; Shields, J. A.; Mastrangelo, M. J., A randomized phase II study of adjuvant sunitinib or valproic acid in high-risk patients with uveal melanoma. *Journal of Clinical Oncology* **2020,** *38* (15_suppl), e22059-e22059.
21. Kratz, F.; Muller, I. A.; Ryppa, C.; Warnecke, A., Prodrug strategies in anticancer chemotherapy. *ChemMedChem* **2008,** *3* (1), 20-53.
22. Marrazzo, A.; Fiorito, J.; Zappala, L.; Prezzavento, O.; Ronsisvalle, S.; Pasquinucci, L.; Scoto, G. M.; Bernardini, R.; Ronsisvalle, G., Antiproliferative activity of phenylbutyrate ester of haloperidol metabolite II [(+/-)-MRJF4] in prostate cancer cells. *Eur J Med Chem* **2011,** *46* (1), 433-8.
23. Sozio, P.; Fiorito, J.; Di Giacomo, V.; Di Stefano, A.; Marinelli, L.; Cacciatore, I.; Cataldi, A.; Pacella, S.; Turkez, H.; Parenti, C.; Rescifina, A.; Marrazzo, A., Haloperidol metabolite II prodrug: asymmetric synthesis and biological evaluation on rat C6 glioma cells. *Eur J Med Chem* **2015,** *90*, 1-9.
24. Olivieri, M.; Amata, E.; Vinciguerra, S.; Fiorito, J.; Giurdanella, G.; Drago, F.; Caporarello, N.; Prezzavento, O.; Arena, E.; Salerno, L.; Rescifina, A.; Lupo, G.; Anfuso, C. D.; Marrazzo, A., Antiangiogenic Effect of (+/-)-Haloperidol Metabolite II Valproate Ester [(+/-)-MRJF22] in Human Microvascular Retinal Endothelial Cells. *J Med Chem* **2016,** *59* (21), 9960-9966.
25. Tan, J.; Cang, S.; Ma, Y.; Petrillo, R. L.; Liu, D., Novel histone deacetylase inhibitors in clinical trials as anti-cancer agents. *Journal of Hematology & Oncology* **2010,** *3* (1), 5.

26. Walker, J. M.; Bowen, W. D.; Walker, F. O.; Matsumoto, R. R.; De Costa, B.; Rice, K. C., Sigma receptors: biology and function. *Pharmacol Rev* **1990,** *42* (4), 355-402.
27. Bao, P.; Kodra, A.; Tomic-Canic, M.; Golinko, M. S.; Ehrlich, H. P.; Brem, H., The role of vascular endothelial growth factor in wound healing. *The Journal of surgical research* **2009,** *153* (2), 347-58.
28. Brown, D. M.; Heier, J. S.; Clark, W. L.; Boyer, D. S.; Vitti, R.; Berliner, A. J.; Zeitz, O.; Sandbrink, R.; Zhu, X.; Haller, J. A., Intravitreal aflibercept injection for macular edema secondary to central retinal vein occlusion: 1-year results from the phase 3 COPERNICUS study. *Am J Ophthalmol* **2013,** *155* (3), 429-437 e7.
29. Campochiaro, P. A.; Clark, W. L.; Boyer, D. S.; Heier, J. S.; Brown, D. M.; Vitti, R.; Kazmi, H.; Berliner, A. J.; Erickson, K.; Chu, K. W.; Soo, Y.; Cheng, Y.; Haller, J. A., Intravitreal aflibercept for macular edema following branch retinal vein occlusion: the 24-week results of the VIBRANT study. *Ophthalmology* **2015,** *122* (3), 538-44.
30. Tabernero, J.; Van Cutsem, E.; Lakomy, R.; Prausova, J.; Ruff, P.; van Hazel, G. A.; Moiseyenko, V. M.; Ferry, D. R.; McKendrick, J. J.; Soussan-Lazard, K.; Chevalier, S.; Allegra, C. J., Aflibercept versus placebo in combination with fluorouracil, leucovorin and irinotecan in the treatment of previously treated metastatic colorectal cancer: prespecified subgroup analyses from the VELOUR trial. *Eur J Cancer* **2014,** *50* (2), 320-31.
31. Mach, R. H.; Smith, C. R.; Childers, S. R., Ibogaine possesses a selective affinity for sigma 2 receptors. *Life Sci* **1995,** *57* (4), PL57-62.
32. Matsumoto, R. R.; Bowen, W. D.; Tom, M. A.; Vo, V. N.; Truong, D. D.; De Costa, B. R., Characterization of two novel sigma receptor ligands: antidystonic effects in rats suggest sigma receptor antagonism. *Eur J Pharmacol* **1995,** *280* (3), 301-10.
33. Anfuso, C. D.; Longo, A.; Distefano, A.; Amorini, A. M.; Salmeri, M.; Zanghi, G.; Giallongo, C.; Giurdanella, G.; Lupo, G., Uveal Melanoma Cells Elicit Retinal Pericyte Phenotypical and Biochemical Changes in an in Vitro Model of Coculture. *Int J Mol Sci* **2020,** *21* (15).
34. Albertson, N. F.; Wetterau, W. F., The synthesis of pentazocine. *J Med Chem* **1970,** *13* (2), 302-3.
35. Maeda, D. Y.; Williams, W.; Kim, W. E.; Thatcher, L. N.; Bowen, W. D.; Coop, A., N-Arylalkylpiperidines as High-Affinity Sigma-1 and Sigma-2 Receptor Ligands: Phenylpropylamines as Potential Leads for Selective Sigma-2 Agents. *Bioorganic & Medicinal Chemistry Letters* **2002,** *12* (3), 497-500.

Development of new Sigma/HDACi prodrugs

Based on the structure of the compound **(±)-MRJF22** and its enantiomers reported in the previous work, several esters of VPA, 4-phenyl butyric acid and butyric acid have been designed, in which the fluorophenyl ring was removed and the length of the methylene chain between nitrogen and the ester carboxyl group was modified (Figure 1).

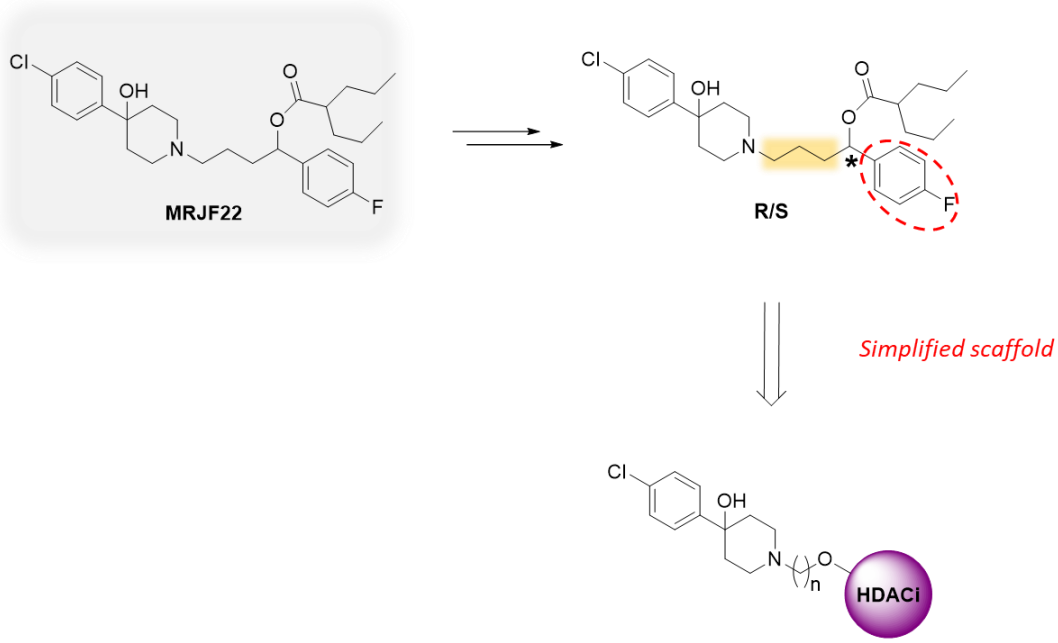

Figure 1. Rational design and general structure of Sigma/HDACi prodrugs.

After having established that conjugate ester of HDACi and HP-mII (σ_2 agonist/σ_1 antagonist ligand) in comparison with the single compounds or the equimolar mixture of both of them acquired an enhanced potency to produce anticancer effects, the focusing of the investigation was on prodrugs with a simplified structure in order to reduce the excessive steric hindrance on the substituent at the nitrogen of 4-phenylpiperidine moiety which could lead to a reduction in affinity for σ receptors. But it means that we should always obtain a synergy of action designing esters which, after a hydrolysis reaction, provide two different active compounds on two distinct molecular targets. All of these is aimed to explore the potential effects of the combination in the same molecule of HDAC inhibition

activity and σ_1 antagonist/σ_2 agonist properties as a useful strategy to develop novel anticancer agents. Further studies are in progress in our laboratories and will be reported in the future.

Synthesis

The synthesis of the prodrug derivatives, including the modified functions before described, are shown in the synthetic scheme 1. Starting from the commercially available 4-(4-chlorophenyl)-hydroxypiperidine the intermediate **1a-c** have been synthesized by nucleophilic substitution with the respective bromo-alcohol. Only thereafter the esterification of the primary alcoholic function of intermediate compounds with the chloride of butyric acid, 4-phenyl butyric acid or VPA respectively, the corresponding final compounds have been obtained. The purity of compounds has been evaluated by ^{1}H and ^{13}C NMR spectroscopy.

.

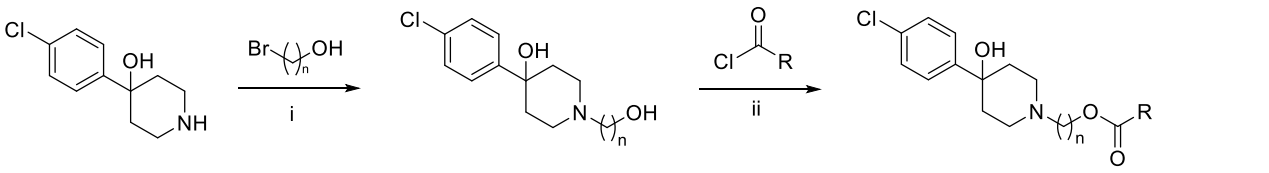

1a-c, n= 2,3,4

2a-c, n= 2,3,4; R= -$(CH_2)_3$
3a-c, n= 2,3,4; R= -$(CH_2)_3$Ph
4a-c, n= 2,3,4; R= -$CH(CH_2CH_2CH_3)_2$

Scheme 1. *Reagents e conditions*: (i) CH_3CN, K_2CO_3, reflux; (ii) THF, DMAP, r.t.

Radioligand binding and HDAC inhibition assays for the compounds described are being processed, while biological evaluation will be carried out soon.

Dual-ligands Sigma/HDACi: a multitarget approach as potential strategy for uveal melanoma with shiftable application in neurodegenerative diseases.

(Manuscript in preparation)

The new single molecules, synthesized and named by us "dual-ligands", should be able to interact as such on the molecular targets considered, antagonizing the σ_1 receptor and inhibiting HDAC enzyme. The rational design for the synthesis of these new ligands was based on overlapping of the pharmacophore common to the σ ligands with that developed for HDACis. In this way, appropriate functional groups were selected, providing together a single pharmacophore, allowed to fit into the pharmacophoric model of both molecular targets and ensure optimal binding interaction either with the σ receptor or with the HDAC enzyme (Figure 1). The σ receptor pharmacophore provide for the presence of certain essential functional groups: one nitrogen atom and two hydrophobic regions, placed at an appropriate distance from the nitrogen atom. However, the pharmacophore common to HDACis consists of a hydrophobic region that blocks the access to the enzyme active site (CAP), a linker made up of a saturated or unsaturated carbon chain with a length between 4 and 6 units, including also aromatic or aliphatic rings, and a functional group chelating the Zn^{2+} cation at the bottom of the catalytic pocket (ZBG).

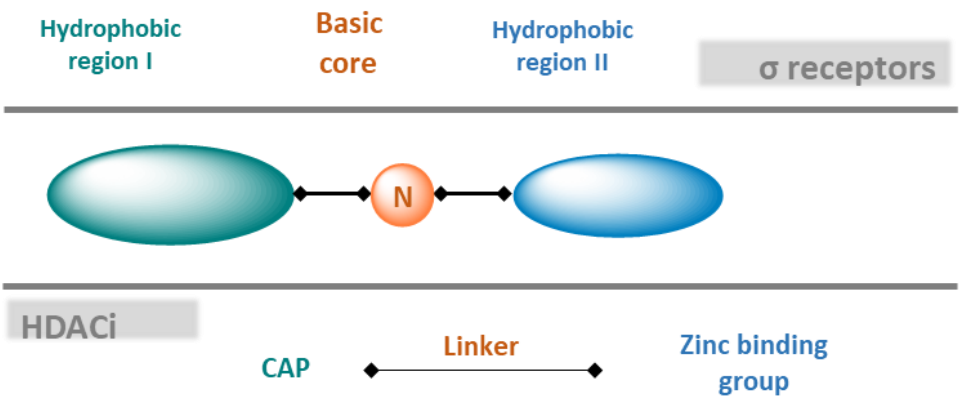

Figure 1. Overlapping of the pharmacophoric models of both σR and HDACi into a single one.

In light of the foregoing, three series of compounds with dual activity have been designed (**Figure 2**). The new ligands include amino moiety of well-knowed σ ligands linked with the hydroxyamino-cinnamic group of LBH-589, developed by Novartis Pharmaceutical under the name of Panobinostat, or with the benzamide-benzylic group of Entinostat (MS-275), both recognized as ZBG functional group. Moreover, both the ZBG have been switched each other so as to achieve benzamide-cinnamic group and N-hydroxybenzamide. In order to simplify the structure of the previous series of compounds, we have also designed dual-ligand compounds in which the amino moiety was replaced by the 4-(4-chlorophenyl)-4-hydroxypiperidine nucleus of HP, well-knowed as σ_1R antagonist, linked with the benzamide group of Entinostat but separated each other just by a saturated hydrocarbon chain. The idea was to consider whether the benzamide group could act simultaneously as ZBG about HDAC inhibition and the II hydrophobic region for the σR affinity.

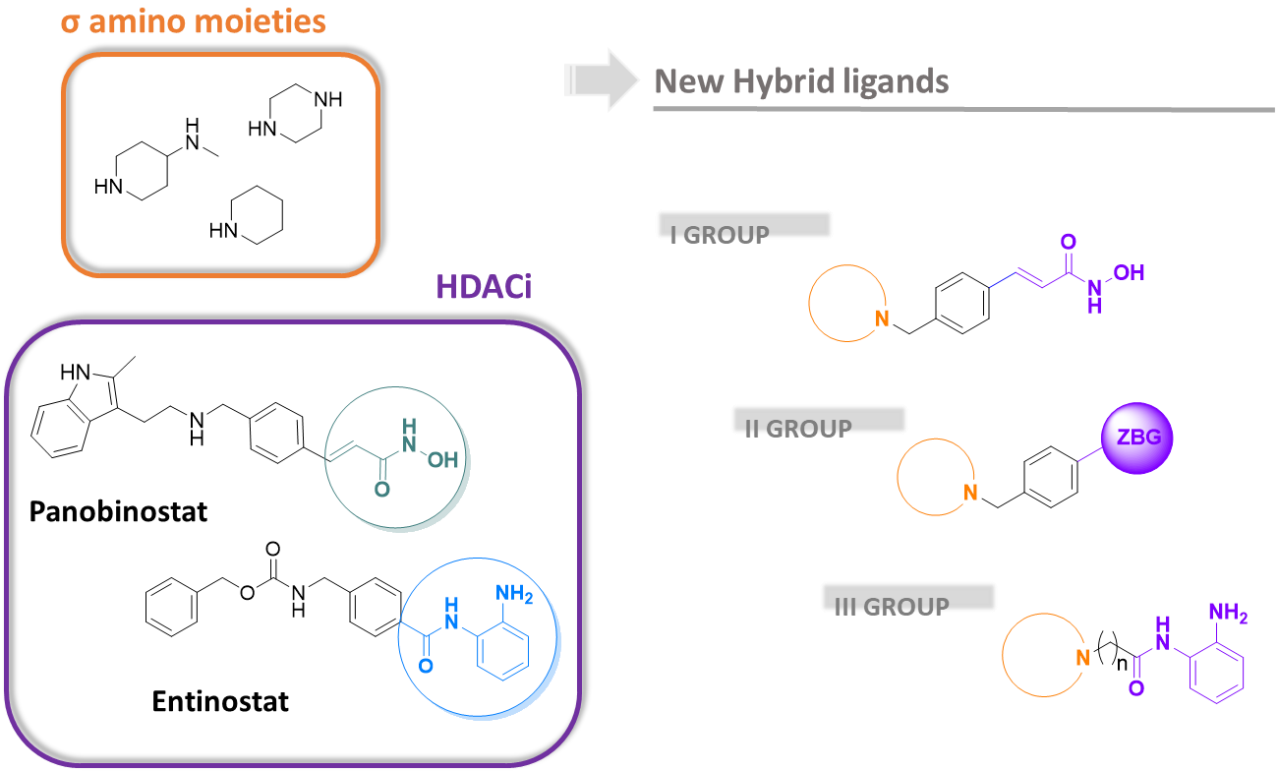

Figure 2. Graphic representation of the design of dual-ligands σ/HDAC series.

Synthesis

Compounds including the hydroxyamino-cinnamic group of LBH-589 or the modified benzamide-cinnamic group of MS-275 were synthesized, providing for an esterification of trans-4-formilcinnamic acid with methyl iodide in N,N-dimethylformamide (DMF) to obtain the compound (*E*)-3-(4-formilphenyl)methyl acrylate. It was subjected to reductive amination reaction with 4-benzylpiperazine in THF and in the presence of $NaBH(OAc)_3$ and acetic acid to give the intermediate **2**. The hydrolysis of compound **2** and the subsequent reaction with o-phenylenediamine, in presence of HOBt (*N*-hydroxybenzotriazole) and EDC (1-ethyl-3-(3-)-dimethylaminopropyl) carbodiimide) supplied the final compound **3**.

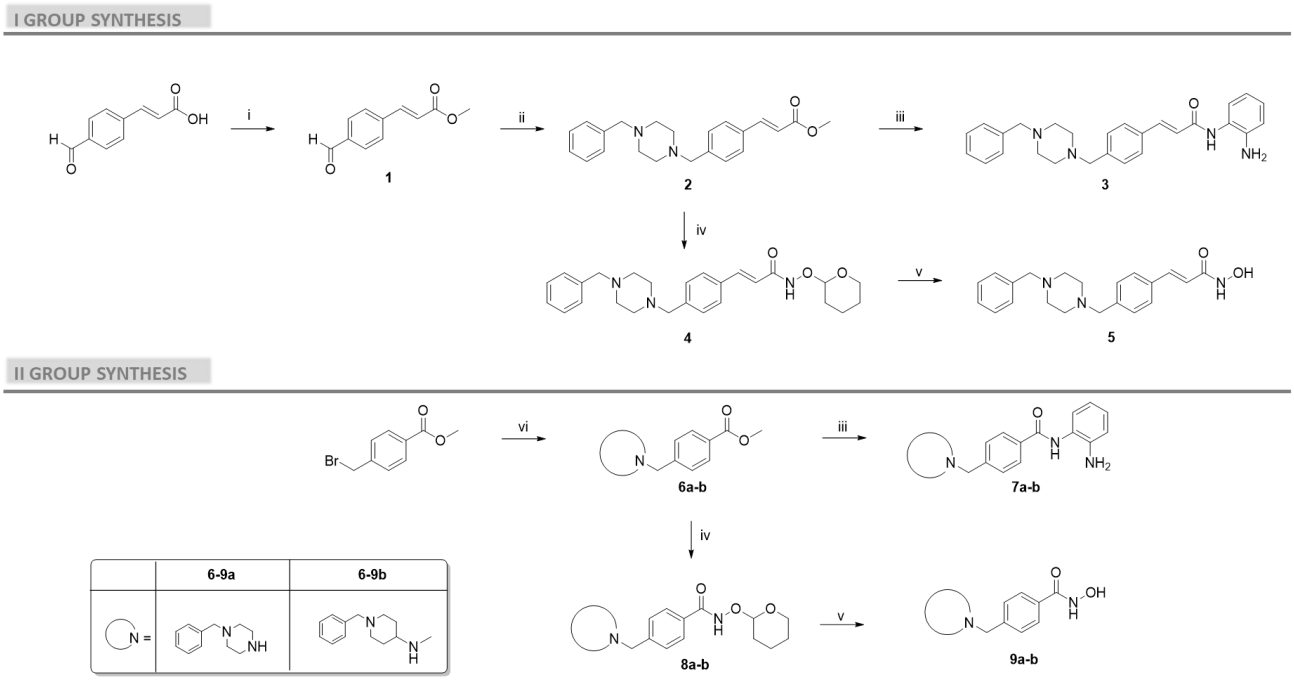

Scheme 1. *Reagent and conditions:* (i) MeI, DMF, rt; (ii) 4-benzylpiperazine, AcOH, $NaBH(OAc)_3$, THF, rt; (iii) 1. LiOH 1M, MeOH, rt; 2. *o*-phenylendiamine, HOBt, EDC, DMF; (iv) 1. LiOH 1M, MeOH, rt; 2. $ClCO_2Et$, TEA, THF, rt; 3. NH_2OTHP, THF, rt; (v) HCl 1.25M; (vi) 4-benzylpiperazine or 1-benzyl-4-(methylamino)piperidine, EtOH, $NaHCO_3$, 70°C.

Instead, the hydrolysis of the ester group of **2** in methanol and LiOH 1M, followed by activation of the carboxylic acid with ethyl chloroformate and triethylamine (TEA), nucleophilic reaction with *O*-(tetrahydro-2H-piran-2-yl)-hydroxylamine (NH_2OTHP) and, finally, the deprotection of the hydroxyl

aminic group, performed by hydrolysis with a solution of HCl 1.25 M in EtOH, provide the final product **5**. The second group of compounds was synthesized providing for a nucleophilic substitution of methyl-4-(bromidemethyl)-benzoate with 4-benzylpiperazine or 1-benzyl-4-(methylamino) piperidine in EtOH to give the intermediates **6a-b**. The synthetic route to obtain the final products **7a-b** and **9a-b** proceed as previously reported (Scheme 1).

The general synthetic scheme of benzamide derivatives, including HP and MS-275 cores previous described, involves the reaction between *o*-phenylendiamine and its appropriate acylic chloride in methylene chloride and in the presence of TEA. Intermediate products are subjected to a nucleophilic substitution reaction with 4-(4-chlorophenyl)-4-hydroxypiperidine in DMF and K_2CO_3, in order to obtain the final compounds **11a-c** (Scheme 2).

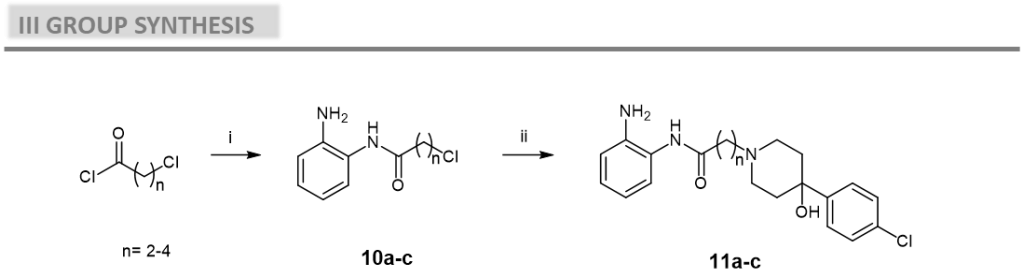

Scheme 2. (i) o-phenylendiamine, TEA, CH_2Cl_2, rt; (ii) 4-(4-chlorophenyl)-4-hydroxypiperidine, K_2CO_3, DMF, 80 °C.

Radioligand Binding assays

All the synthesized compounds were evaluated for affinity at both σ_1R and σ_2R through radioligand binding assay (**Table 1**). The lack of the double bond of the benzamide-cinnamic group or hydroxyamino-cinnamic group in **7a** and **9a** leads to a loss of affinity for the σ_1R, together with an improved selectivity over σ_2R. Moreover, a worsening of the affinity for σ_1R is observed for compounds including o-phenylenediamine **3** and **7a** (respectively $K_i\sigma_1$R= 1330±239 and 3758±929 nM) with respect to the corresponding compound with hydroxamic acid as ZBG **5** and **9a** (respectively $K_i\sigma_1$R= 38±3.7 and 93±10.9 nM); except for compounds **7b** ($K_i\sigma_1$R=52±3.9 nM**)** that

show just a decrease compared to **9b** ($K_i\sigma_1R$=41±6.5 nM**)**. All the compounds of these series show a poor affinity for σ_2R; while **7a** and **9a**, including 4-benzylpiperazine moiety and without the double bound as mentioned above, completely lost the capacity to bind σ_2R ($K_i\sigma_2R$ >10000 nM).

Despite a lower affinity over both σ receptor for all compounds including *o*-phenylenediamine in the previous groups, the third series of dual-ligands restored the affinity towards σ_1R, in particular the affinity decrease and the selectivity toward σ_2R improves increasing the chain lenght. Indeed, compound **11a** had a K_i for σ_1R of about 47 vs K_i for σ_2R of 738 nM, compound **11b** arrange a K_i of 55 nM for σ_1R *vs* 2799 nM for $K_i\sigma_2R$, while compound **11c** holds $K_i\sigma_1R$ = 107 nM and completely lost affinity for σ_2R with $K_i\sigma_2R$ >10000.

Table 1. σ_1R and σ_2R binding assays for dual-ligands

	K_i (nM) ± SD[a]	
Compounds	**σ_1R**	**σ_2R**
3	1330±239	2691±1254
5	38±3.7	2917±769
7a	3758±929	>10000
7b	52±3.9	1588±233
9a	93±10.9	>10000
9b	41±6.5	1656±14.8
11a	47±4.6	738±117
11b	55±3.2	2799±609
11c	107±17	>10000
Haloperidol	2.6 ± 0.4	77 ± 18
(+)-Pentazocine	4.3 ± 0.5	1465 ± 224
DTG	124 ± 19	18 ± 1
BD-1063	14 ± 2.7	-

[a]Each value is the mean ± SD of at least two experiments performed in duplicate.

Included in the tested compounds, it has been evaluated also compound named **X**, for which it was decided to hidden the structure, due to its extraordinary antiproliferative activity as explained in the following section and for this reason we are also considering the possibility of a future patent. Regarding its σ receptor affinity, compound **X** exhibit a marked affinity for σ_1R with a K_i value of about 18.97 nM associated to an high selectivity toward σ_2R (K_i=2051±737 nM).

Biological evaluation

Biological screening has been realized through MTT assays, performed with the employ of several tumor cell lines to determine the anticancer activity of these new Sigma/HDACi dual-ligands, which were further selected for their preferential cytotoxicity towards these ones. First of all, all the compounds were tested on human gastric adenocarcinoma cells (AGS), treated with 1, 5 and 10 µM of all the synthetized compounds for 24, 48 and 72 hours respectively (Figure 1 and 2).

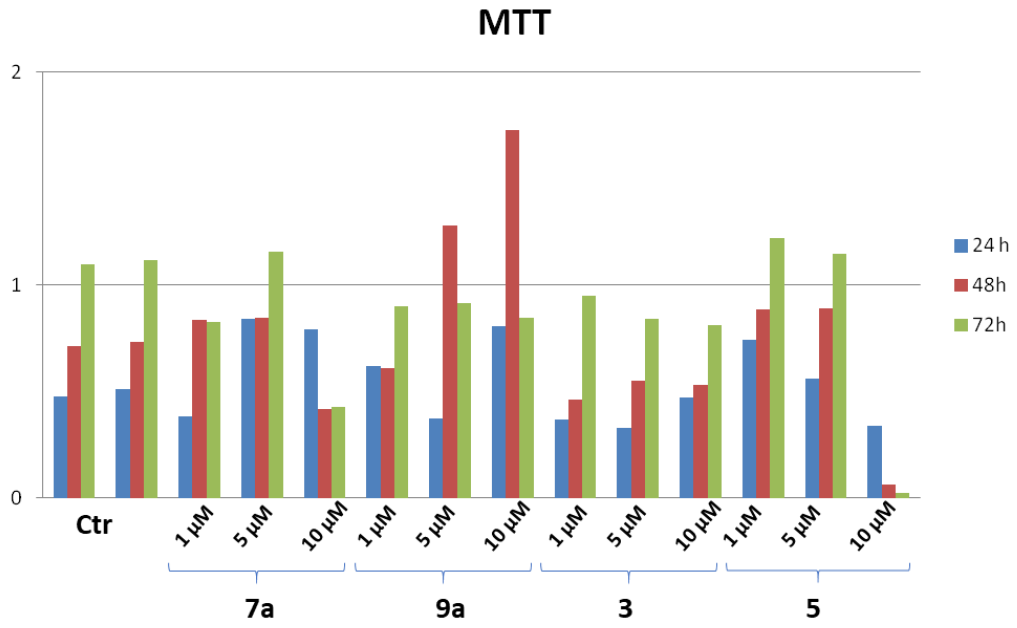

Figure 1. MTT assay of AGS cell lines treated with 1, 5 and 10 µM of compounds **7a**, **9a**, **3** and **5**. Graph represents OD values in control and treated samples. Ctr: untreated cells.

A visible antitumoral activity was displayed by compounds **7b** and **5**, in particular at the higher dose in a time-dependent manner, while compound **7a** exhibited a slight cytotoxicity in a dose but not a time-dependent manner. Likewise, compound **3** seemed to display a good cytotoxicity, but neither dose nor time-dependent manner.

Notably, the highest and interesting antitumoral activity has been showed by compound **X**, reason why right now we reserve the possibility to show the structure.

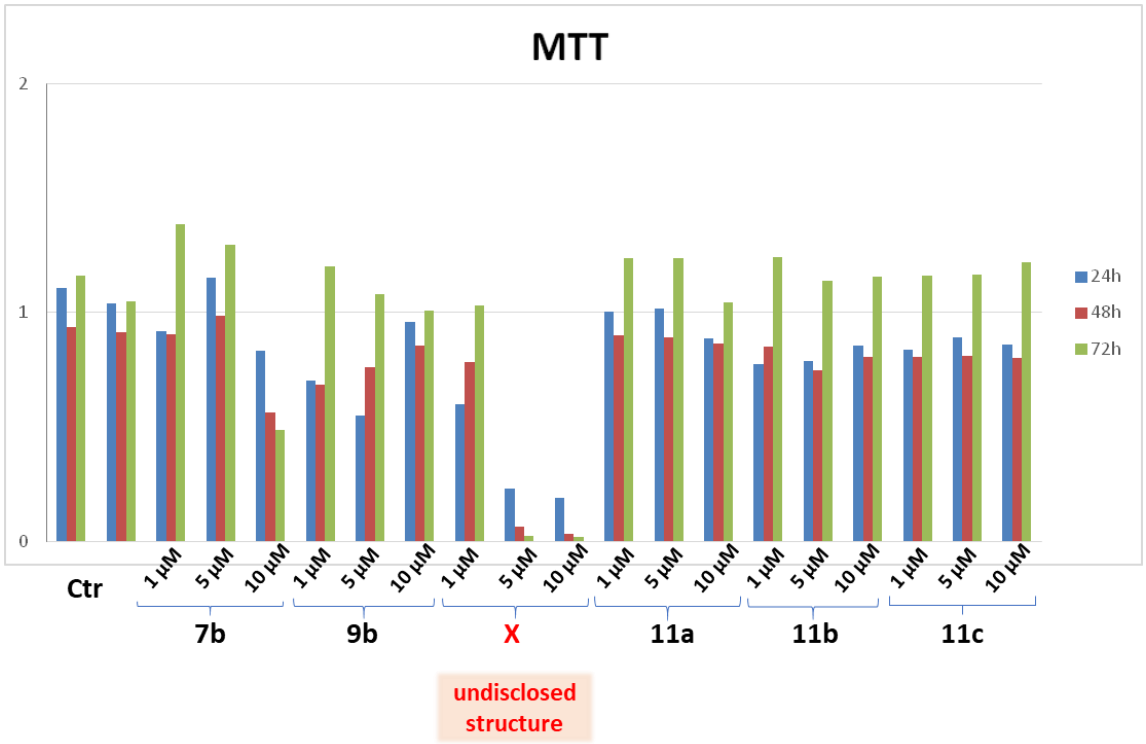

Figure 2. MTT assay of AGS cell lines treated with 1, 5 and 10 µM of compounds **7b**, **9b**, **11a**, **11b**, **11c** and the unrevealed compound **X**. Graph represents OD values in control and treated samples. Ctr: untreated cells.

Based on these preliminary results, we focused our attention on the more interesting compounds. Compounds **5**, **7a** and **7b** were investigated on three more tumor cell lines, such us human breast cancer (MCF-7), human prostate adenocarcinoma (PC3) and human colorectal carcinoma (HTC 116), considering also the expression of σ_2R, σ_1R and HDAC enzyme respectively.

All tested compounds were utilized at increasing concentration from 1 to 80 µM for 48 hours. The viability of all the cell lines appears strongly reduced by the exposure to the compound **5** (Figure 3), which seems effective also at very low concentrations, especially against AGS and HCT 116 cell lines with respect to MCF-7 and PC3.

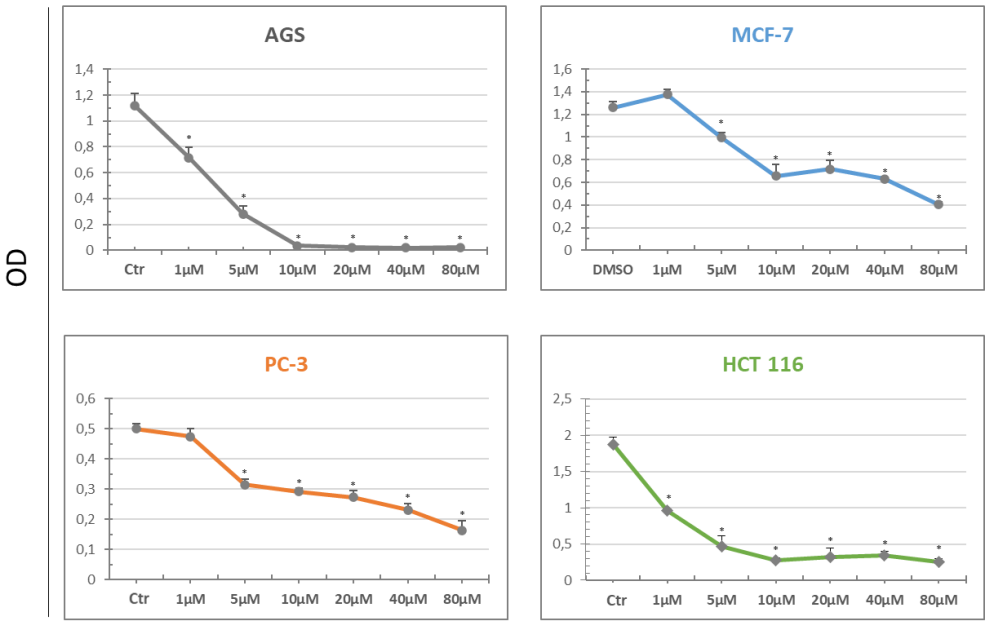

Figure 3. MTT assay of AGS; MCF-7, PC-3, HCT 116 cell lines treated with 0, 1, 5, 10, 20, 40, 80 µM of compound **5**. Graph represents OD values in control and treated samples. Data shown are the mean (±SD) of three separate experiments. Ctr: untreated cells. *$p < 0.05$ vs Ctr.

Instead, compound **7a** (Figure 4) shows a good anti-proliferative activity against three, namely AGS, MCF-7, HCT 116, of the four cell lines tested. As for the prostate cancer PC3 cells, they seemed poorly affected by the **7a**, even at the highest concentration.

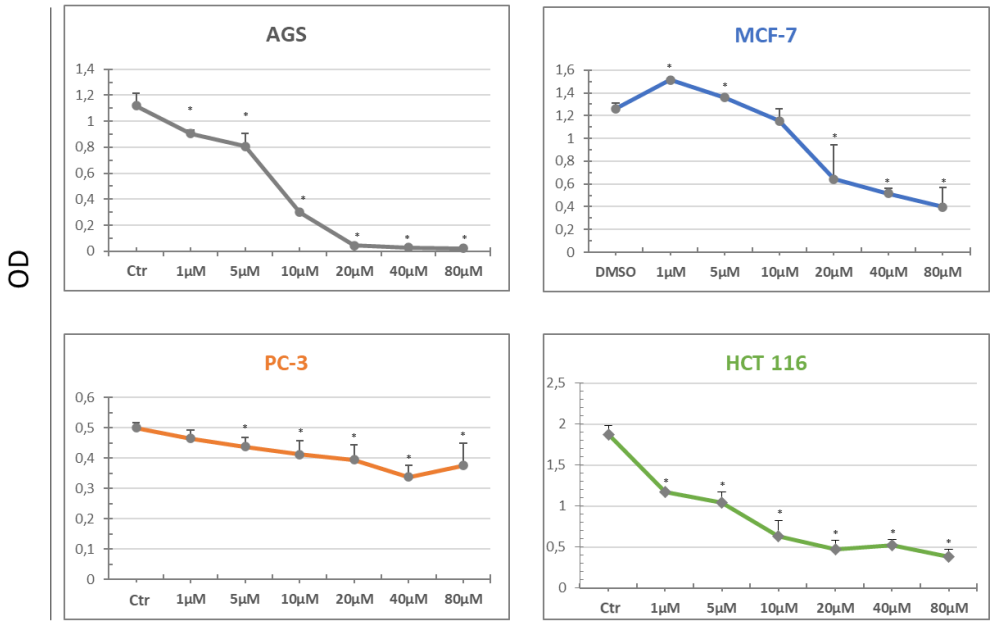

Figure 4. MTT assay of AGS; MCF-7, PC-3, HCT 116 cell lines treated with 0, 1, 5, 10, 20, 40, 80 μM of compound **7a**. Graph represents OD values in control and treated samples. Data shown are the mean (±SD) of three separate experiments. Ctr: untreated cells. *p < 0.05 vs Ctr.

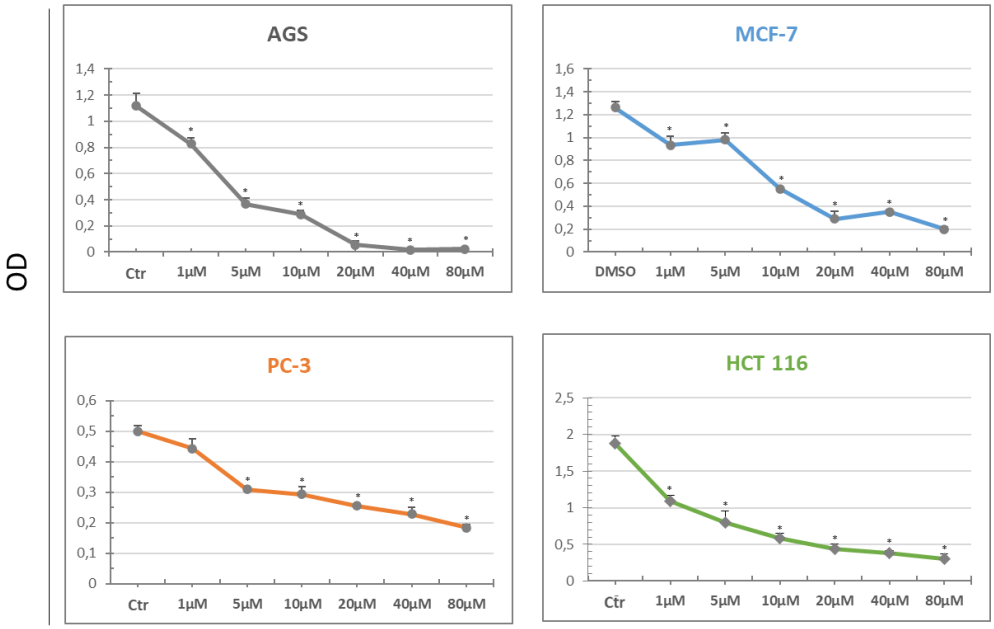

Figure 5. MTT assay of AGS; MCF-7, PC-3, HCT 116 cell lines treated with 0, 1, 5, 10, 20, 40, 80 μM of compound **7b**. Graph represents OD values in control and treated samples. Data shown are the mean (±SD) of three separate experiments. Ctr: untreated cells. *p < 0.05 vs Ctr.

The results shown for the compound **7b** (Figure 5) resembles what was found for compound **5**, being the highest anti proliferative activity exerted against the two cell lines from different region of the digestive tract, AGS and HCT 116.

Consequently, the concentration causing the 50% inhibition of cell growth (IC_{50}) was calculated for each compound at 48 hours and the values are shown in table 2. Compound **5** appears to be the most active compound, being its IC_{50} values always below 10 μM, with the IC_{50} for HCT 116 in a sub-micromolar range (0.87 μM).

In the same way, compound **X** has been evaluated on MCF-7, PC3 and HCT 116 at the same conditions of time and concentration, displaying for all the tumor cells used an IC_{50} value that is around the 0.1 and 0.01 μM as listed in table 2.

Table 2. Dual-ligands IC_{50} values on different cancer cells.

Cmpds	7a (μM)	5 (μM)	7b (μM)	X (μM)
AGS	8.2	3.5	2.93	0.16
MCF-7	15.01	8.4	8.82	0.03
PC-3	26.80	7.5	5.80	0.05
HCT 116	2.9	0.87	3.4	0.009

[a]Each value is the mean ± SD of at least three experiments performed in duplicate.

In light of these preparatory studies on varied tumors cell lines and considering in addition the binding affinity data for σ receptors, the effects of some of the hybrid ligands **3**, **7a**, **7b**, **9a**, **11a**, **11b**, **11c** and compound **X** were explored on human uveal melanoma 92-1 cells with the intention of assessing their inhibitory activity on these specific cell line, in keeping with the aim of the thesis.

As shown in Figures 5 and 6, their effect on 92-1 cell proliferation were examined with 300 nM, 1, 3 and 10 μM of the hybrid ligands for 48 hours. Once again, compound **X** exibits a surprising antiproliferative activity, already clearly observable in the nM range. Among the chosen ligands seem

to reveal a good and a slight antiproliferative activity respectively compounds **7b** and **11c** at concentration of 3 and 10 μM, otherwise all the remaining dual-ligands do not seem to have any cytotoxic activity on human melanoma 92-1 cells.

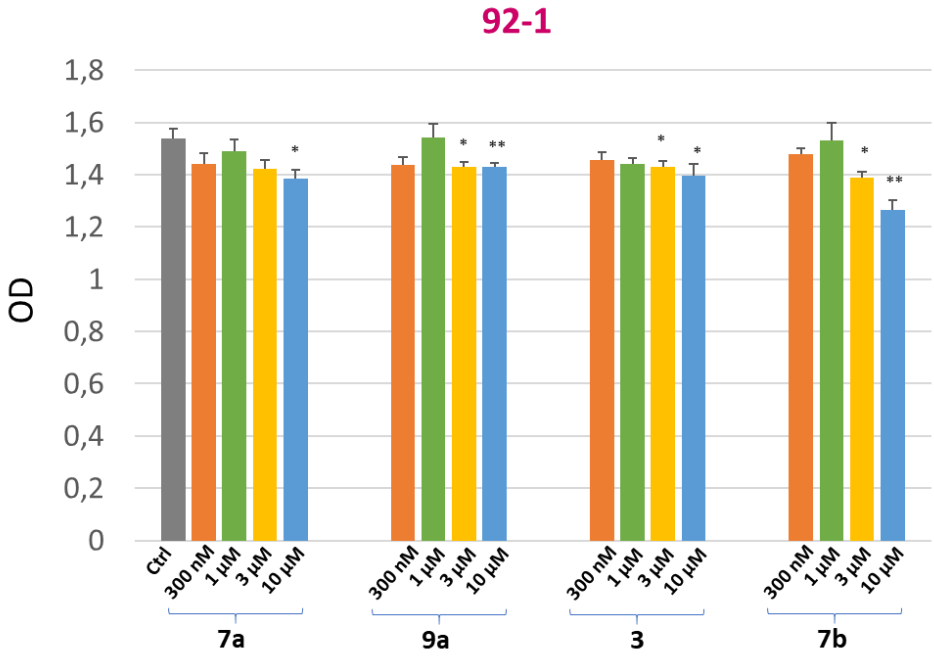

Figure 5 Effects of compounds **3**, **7a**, **7b** and **9a** on 92-1 cells proliferation. Graph represents OD values in control and treated samples. Data shown are the mean (±SD) of two separate experiments. Ctr: untreated cells. *$p < 0.05$, **$p < 0.01$ and ***$p < 0.0001$ vs Ctr.

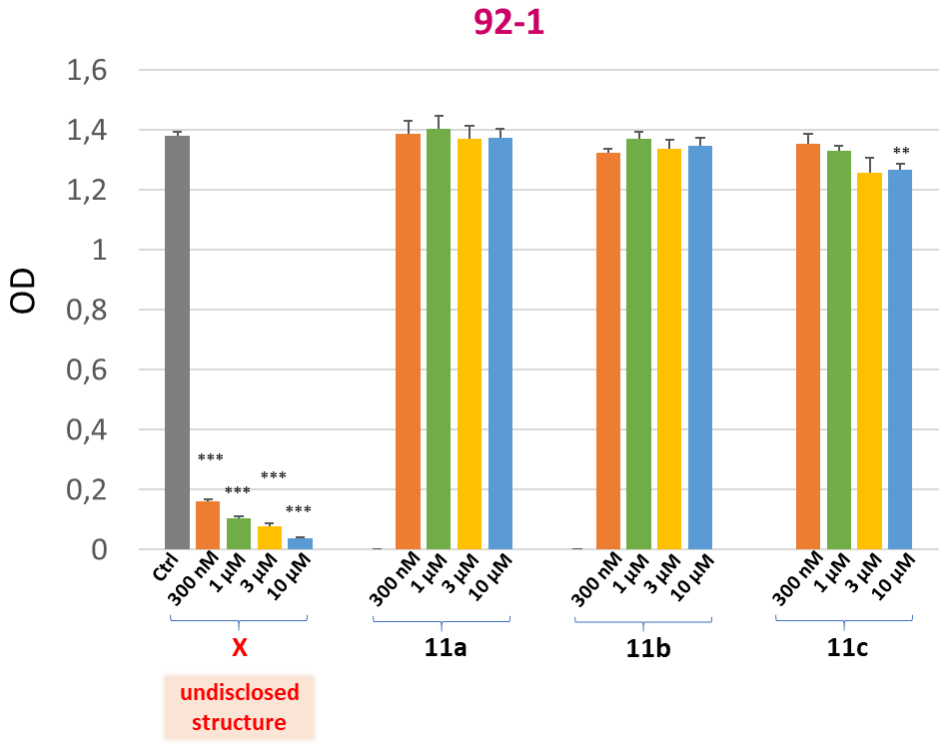

Figure 6 Effects of compounds **11a**, **11b**, **11c** and compound **X** on 92-1 cells proliferation. Graph represents OD values in control and treated samples. Data shown are the mean (±SD) of two separate experiments. Ctr: untreated cells. *$p < 0.05$, **$p < 0.01$ and ***$p < 0.0001$ vs Ctr.

On these grounds, the antiproliferative effect of compounds **7b**, **11c** and **X** has been evaluated at lowest concentration than the ones used in the previous experiment, mainly in the µM for compounds **7b** and **11c** but in the nM range for the unrevealed compound **X**, with the purpose to attest their antiproliferative activity as shown in Figure 7. In fact, compounds confirmed their attitude to inhibit the proliferation of 92-1 and in particular compound **11c** exibits an higher antiproliferative activity compared to compound **7b** for which however the effect became significant at 10 µM ($p < 0.0001$ vs Ctr) with respect to 10 µM of **11c** ($p < 0.05$ vs Ctr). Chart show that at the same concentrations of both compounds, generally **11c** retains a better cytotoxic activity, even if with a considerable effect at 30 µM, in comparison with **7b** which therefore manifest a good activity. A separate consideration should be done for **X**, which demonstrated a behavior clearly superior, considering that were used nM concentration, respect to compounds **7b** and **11c**, and that the antiproliferative effect is yet

meaningful at 10 nM ($p < 0.01$ vs Ctr). Calculation of IC_{50} on 92-1 cells for the these compounds is ongoing.

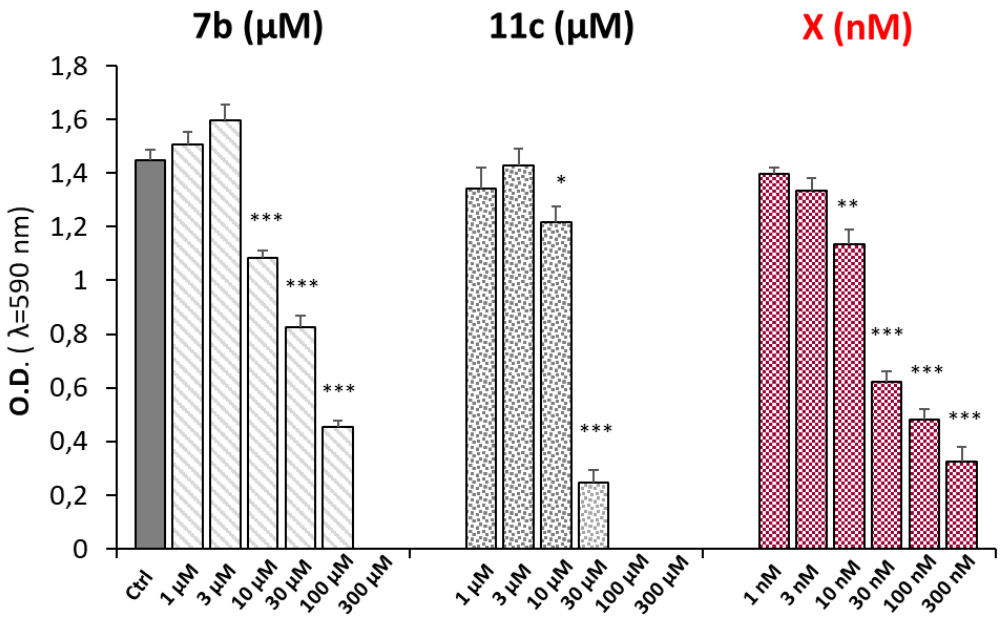

Figure 7 Effects of compounds **7b**, **11c** and compound **X** on 92-1 cells proliferation at lower concentration. Graph represents OD values in control and treated samples. Ctr: untreated cells. *$p < 0.05$, **$p < 0.01$ and ***$p < 0.0001$ vs Ctr.

In addition, all the most relevant compounds have been tested on human primary gingival fibroblasts (HGFs), in order to considering its toxicity rate (data not shown), displaying a good tolerability in normal cells. Furthermore, HDAC inhibition assays for the compounds described are currently ongoing and other biological evaluations will be carried out.

CONCLUSIONS

Screening on cancer cell lines identifies multiple opportunities for the probable different employment of the designed Sigma/HDACi ligands as a possible way for the treatment not only of uveal melanoma but even of different cancer types. Particularly, it has been shown that compound **5** strongly reduces the viability of the cells from different region of the digestive tract, AGS and HCT 116 and equally

compound **7b**, although to a lesser extent, while compound **7a** exhibit a good anti-proliferative activity especially against HCT 116. Furthermore, an appreciable cytotoxic activity against human melanoma 92-1 cells has been demonstrate for compound **7b**. Remarkably, compound **11c** have displayed a good anti proliferative effects after treatment with lower concentrations on 92-1cells. On these grounds, both **7b** and **11c** will be subject of further studies on 92-1.

Really noteworthy is the attitude of compound **X** to inhibit tumor proliferation in the range of nM on all the tumor cell lines considered in these investigations, in particular on 92-1cells; as well its tolerability towards fibroblasts for which **X** is not toxic. Assuming these excellent results the structure has been momently disclosed and further research will be carried out about its peculiar activity.

Finally, data provided by the screening on cancer cell lines have suggested an alternative switchable employment of the designed Sigma/HDACi ligands with a poor antiproliferative effects or no cytotoxic activity as possible treatment of other multifactorial disease such as neurodegenerative diseases. Certainly, it is renowned that both σ receptor ligands and HDACi are involved in treatment of different neurodegenerative diseases and, in this respect, an evaluation should not also be excluded in the field of neuroprotection.

MATERIALS AND METHODS

Chemistry. Reagent grade chemicals were purchased from Sigma-Aldrich (St. Louis, MO, USA) or TCI (Tokio, Japan) and were used without further purification. All reactions involving air-sensitive reagents were performed under N_2 in oven-dried glassware using the syringe-septum cap technique. All reactions were monitored by thin-layer chromatography (TLC) which was performed on silica gel Merck 60 F254 plates; the spots were visualized by UV light (λ = 254 and 366 nm) and iodine chamber. Melting points were determined on a Büchi B-450 apparatus in glass capillary tubes and are uncorrected. Flash chromatography purification was performed on a Merck silica gel 60, 0.040−0.063 mm (230−400 mesh), stationary phase using glass columns with a diameter between 1 and 4 cm. Nuclear magnetic resonance spectra (^{1}H NMR and ^{13}C NMR recorded at 500 MHz) were

obtained on Varian INOVA spectrometers using $CDCl_3$, D_2O e DMSO-d_6 with a 0.03% of TMS as internal standard. Coupling constants (*J*) are reported in hertz. Signal multiplicities are characterized as s (singlet), d (doublet), t (triplet), q (quartet), m (multiplet), br (broad), app (apparent). Purities of all compounds was determined by microanalysis (C, H, N) that was performed on a Carlo Erba instrument model E1110; all the results agreed within ±0.4% of the theoretical values. Compound nomenclatures were generated with ChemBioDraw Ultra version 16.0.0.82.

General procedure for methyl (*E*)-3-[4-(4-benzylpiperazin-1-yl)phenyl]acrylate (2).

To a solution of 4-formil-cinnamic acid (5 g; 28.4 mmol) in N,N-dimethylformamide anhydrous (DMF) was added K_2CO_3 (5.10 g; 37mmol) and dropwise methyl iodide (5.68 g; 40 mmol) at room temperature and in nitrogen atmosphere. The reaction mixture was stirred for 24 hours at room temperature. Then the solvent was evaporated under vacuum, the resulting residue treated with EtOAc and washed saturated solution of $NaHCO_3$. The organic and the aqueous phase were repeatedly separated, and the aqueous phase extracted with EtOAc. The combined organics phases have been dried with anhydrous Na_2SO_4, filtered and evaporated under vacuum to obtain 4.61 g of pure **1** (yield 85.4%). The obtained solid was did not require any further purification. Characterization and NMR data for compound **1** is reported in Supporting information. To a solution of 4-benzylpiperazine (1.26 ml; 7.3mmol) in 10 ml of anhydrous tetrahydrofuran (THF) was added dropwise at room temperature and in nitrogen atmosphere compound **1** (1,4 g; 7.3 mmol) in 6 ml anhydrous THF. AcOH was added to the solution (0.420 ml, 7.3 mmol) and reaction mixture was stirred for about 30 minutes and added dropwise a $NaBH(OAc)_3$ solution (2,31 g; 10,9 mmol) in 1,85 ml of anhydrous THF at room temperature and in nitrogen atmosphere. The reaction mixture was stirred overnight at room temperature. Subsequently, a saturated solution of $NaHCO_3$ has been added and the aqueous phase has been repeatedly extracted with $CHCl_3$. The combined organic phases were dried with Na_2SO_4 anhydrous, filtered and evaporated under vacuum. The crude was purified by MPLC using EtOAc as eluent to get 1.76 g of intermediate **2** (69% yield) as a white solid. mp 107-109 °C; ^{1}H NMR (500 MHz, D_2O): δ 3.46 (s, 8H); 3.65 (s, 3H); 4.31 (s, 4H); 6.43 (d, *J*=5.0 Hz, 1H); 7.34-7.56 (m, 10H);

^{13}C NMR (125 MHz, D_2O): 50.48, 50.53, 54.66, 62.30, 62.82, 121.24, 129.83, 131.34, 131.79, 132.09, 132.96, 133.53, 134.09, 138.37, 146.77, 171.86. Anal. Calcd. for $C_{22}H_{26}N_2O_2$: C, 75.36; H, 7.60; N, 7.99. Found: C, 75.40; H, 7.48; N, 8.04.

General procedure for the synthesis of methyl esters (6a-b)

To a solution of the specific ammine (1 mmol) and $NaHCO_3$ in absolute EtOH was added (1 mmol) dropwise methyl (*E*)-3-(4-(bromomethyl)phenyl)acrylate (1 mmol) at 50 °C and in nitrogen atmosphere. The reaction mixture was stirred for 7 hours at 50 °C and then stirred at room temperature overnight. Then the solvent was evaporated under vacuum, the resulting residue treated with EtOAc and washed with a saturated solution of $NaHCO_3$. The organic and the aqueous phase were repeatedly separated, the aqueous phase extracted with EtOAc and subsequently adjusted at pH 9 with Na_2CO_3. The aqueous phase was extracted with EtOAc and the combined organics phases have been dried with anhydrous Na_2SO_4, filtered and evaporated under vacuum. The crude was purified by MPLC using EtOAc as eluent. According to this procedure, the following products have been obtained.

*Methyl 4-[(4-benzylpiperazin-1-yl)methyl]benzoate (**6a**).* White solid (86 %): mp 82-83 °C; ^{1}H NMR (500 MHz, $CDCl_3$): δ 2.47 (s, 8H), 3.51 (s, 2H), 3.54 (s, 2H), 3.89 (s, 3H), 7.21-7.31 (m, 5H), 7.38 (d, *J*=25.0 Hz, 2H), 7.96 (d, *J*=25.0 Hz, 2H); ^{13}C NMR (125 MHz, $CDCl_3$): 51.98, 53.02, 53.13, 62.62, 63.01, 127.00, 128.16, 128.92, 129.18, 129.51, 129.83, 133.47, 138.04, 140.34, 143.81, 167.03. Anal. Calcd. for $C_{20}H_{24}N_2O_2$: C, 75.05, H, 7.46, N, 8.63. Found: C, 74.79, H, 7.79, N, 8.45.

*Methyl 4-{[(1-benzylpiperidin-4-yl)(methyl)amino]methyl}benzoate (**6b**).* White solid (49 %): mp 240-242 °C; ^{1}H NMR (500 MHz, $CDCl_3$): δ 1.60-1.70 (m, 2H), 1.73-1.79 (m, 2H), 1.91-2.07 (m, 2H), 2.18 (s, 3H), 2.37-2.46 (m, 1H), 2.90-2.98 (m, 2H), 3.48 (s, 4H), 3.61 (s, 2H), 3.89 (s, 3H), 7.20-7.32 (m, 4H), 7.38 (d, *J*=8.0 Hz, 2H), 7.96 (d, *J*=8.0 Hz, 2H,); ^{13}C NMR (125 MHz, $CDCl_3$): 27.87, 37.85, 51.91, 53.23, 57.69, 61.04, 63.05, 126.89, 128.11, 128.45, 128.64, 129.08, 129.50, 138.43, 145.86, 167.07. Anal. Calcd. for $C_{22}H_{28}N_2O_2$: C, 62.25, H, 7.32, N, 6.50. Found: C, 62.12, H, 7.11, N, 6.59.

General procedure for *N*-(2-aminophenyl)amide (3, 7a-b)

To a solution of esters **2**, **6a** or **6b** (1 mmol) in MeOH was added dropwise an aqueous solution of LiOH 1M (2 mmol) at 50 °C. The reaction mixture was stirred at a temperature of 50º C overnight. The solvent was evaporated under vacuum, the resulting residue dissolved in anhydrous DMF and o-phenylenediamine (4 mmol) was added in DMF, followed by the addition of HOBt (3 mmol) and EDC (3 mmol). The reaction was stirred at room temperature for 24 hours. Subsequently EtOAc was added and the organic phase was repeatedly washed with a saturated solution of $NaHCO_3$ and with a solution of NaCl. The combined organic phases were dried with anhydrous Na_2SO_4, filtered and evaporated under vacuum. The crude was purified by MPLC using EtOAc as eluent. According to this procedure, the following products have been obtained.

*(E)-N-(2-aminophenyl)-3-{4-[(4-benzylpiperazin-1-yl)methyl]phenyl}acrylamide (**3**).* Beige solid (70%): mp 164-166 °C; ^{1}H NMR (500 MHz, $CDCl_3$): δ 2.49 (s, 8H); 3.52 (s, 4H); 3.88 (br s, 2H); 6.57 (d, *J*=25.0 Hz, 1H); 6.77-6.84 (m, 2H); 7.00-7.38 (m, 9H); 7.4-7.5 (m, 2H); 7.55 (br s, 1H); 7.71 (d, *J*=25.0 Hz,1H); ^{13}C NMR (125 MHz, $CDCl_3$): 52.94, 52.99, 62.58, 62.95, 116.71, 118.20, 119.17, 119.54, 124.49, 125.09, 127.06, 127.86, 128.18, 129.23, 129.57, 133.47, 137.83, 140.34, 140.71, 142.06, 164.37. Anal. Calcd. for $C_{27}H_{30}N_4O$: C, 76.03; H, 7.09; N, 13.13. Found: C, 75.99; H, 7.23; N, 13.18.

*N-(2-aminophenyl)-4-[(4-benzylpiperazin-1-yl)methyl]benzamide (**7a**).* Beige solid (75%): mp 148-150 °C; ^{1}H NMR (500 MHz, $CDCl_3$): δ 2.49 (s, 8H), 3.52 (d, 2H), 3.56 (s, 2H), 4.75 (br s, 2H), 6.82-7.32 (m, 9H), 7.42 (d, *J*= 15.0 Hz, 2H), 7.38 (d, *J*= 15.0 Hz, 2H), 7.92 (br s, 1H); ^{13}C NMR (125 MHz, $CDCl_3$): 52.96, 53.03, 62.47, 62.95, 118.36, 119.75, 124.62, 125.16, 127.08, 127.16, 127.25, 128.20, 129.23, 129.34, 132.93, 137.83, 140.67, 142.67, 165.66. Anal. Calcd. for $C_{25}H_{28}N_4O$: C, 74.97; H, 7.05; N, 13.99. Found: C, 74.77; H, 6.90; N, 14.10.

*N-(2-aminophenyl)-4-{[(1-benzylpiperidin-4-yl)(methyl)amino]methyl}benzamide (**7b**).* Yellow solid (62%): mp 141-143 °C; ^{1}H NMR (500 MHz, $CDCl_3$): δ 1.60-1.71 (m, 2H), 1.73-1.80 (m, 2H), 1.92-

2.00 (m, 2H), 2.38-2.48 (m, 1H), 2.92-3.00 (m, 2H), 3.49 (s, 2H), 3.63 (s, 2H), 3.88 (br s, 1H), 6.80-7.35 (m, 9H), 7.42 (d, *J*= 7.5 Hz, 1H), 7.83 (d, *J*= 7.5 Hz, 1H), 7.88 (br s, 1H); ^{13}C NMR (125 MHz, $CDCl_3$): 27.85, 37.84, 53.22, 57.62, 60.95, 63.04, 118.30, 119.68, 124.60, 125.21, 126.94, 127.12, 127.25, 128.14, 128.86, 129.13, 132.64, 138.35, 140.72, 144.79, 165.77. Anal. Calcd. for $C_{27}H_{32}N_4O$: C, 75.67; H, 7.53; N, 13.07. Found: C, 75.54; H, 7.47; N, 13.19.

General procedure for the synthesis of methyl esters (5, 9a-b)

To a solution of esters **2**, **6a** or **6b** (1 mmol) in MeOH was added dropwise an aqueous solution of LiOH 1M (2 mmol) at 50 °C and the reaction mixture was stirred overnight. The solvent was evaporated under vacuum, the resulting residue dissolved in 15 ml of an anhydrous solution of THF/DMF (1:1) and was added TEA (2 mmol), followed by the addition of a ethyl chloroformate solution (4 mmol) in 12 ml of THF dropwise at 0 °C and in inert atmosphere. The reaction was stirred at room temperature for 3 hours. Subsequently, has been added at room temperature and under nitrogen atmosphere O-(tetrahydro-2H-pyran-2-yl)-hydroxylamine (5 mmol) and the reaction stirred at room temperature overnight. The resulting residue was washed with a saturated solution of $NaHCO_3$ and the aqueous phase extracted with $CHCl_3$, the combined organic phases were dried with anhydrous Na_2SO_4, filtered and evaporated under vacuum. The crude was purified by MPLC in order to obtain the intermediates **4** and **8a-b**. Characterization and NMR data for compounds **4** and **8a-b** are reported in Supporting information. To a solution of the intermediates in EtOH was added dropwise a solution of HCl 1,25 M in EtOH at 0 °C. The reaction was stirred at room temperature for 24 hours. Subsequently, the solvent was evaporated under vacuum, the resulting residue dissolved in EtOH and precipitated with Et_2O. According to this procedure, the following products have been obtained.

*4.1.4.1. (E)-3-{4-[(4-benzylpiperazin-1-yl)methyl]phenyl}-N-hydroxyacrylamide (**5**).* White solid (63%): mp 230-231 °C; ^{1}H NMR (500 MHz, DMSO-d_6): δ 3.21-3.70 (m, 8H), 4.34 (s, 4H), 6.55 (d, *J*= 5.0 Hz, 1H), 7.44-7.65 (m, 10H), 10.89 (br s, 1H), 12.12(br s, 1H); ^{13}C NMR (125 MHz, DMSO-d_6): δ 47.51, 58.30, 58.72, 79.30, 120.44, 128.12, 129.17, 129.32, 130.00, 130.65, 131.58, 132.12,

136.23, 137.89, 162.84. Anal. Calcd. for $C_{21}H_{25}N_3O_2 \cdot 2HCl$: C, 59.44; H, 6.41; N, 9.90. Found: C, 59.28; H, 6.50; N, 9.77.

*4-[(4-benzylpiperazin-1-yl)methyl]-N-hydroxybenzamide (**9a**).* White solid (88%): mp 230-232 °C; ^{1}H NMR (500 MHz, DMSO-d_6): δ 3.44 (s, 8H), 4.34 (s, 2H), 4.39 (s, 2H), 7.40-7.54 (m, 5H), 7.61 (d, *J*=25.0 Hz, 2H,), 7.77 (d, *J*=25.0 Hz, 2H), 11.34 (br s, 1H) 11.34 (br s, 1H); ^{13}C NMR (125 MHz, $CDCl_3$): δ 47.76, 58.48, 58.97, 79.02, 127.8, 129.1, 129.4, 130.3, 131.82, 131.86, 132.73, 133.93, 164.2. Anal. Calcd. for $C_{19}H_{23}N_3O_2 \cdot 2HCl$: C, 57.29; H, 6.33; N, 10.55. Found: C, 57.04; H, 6.21; N, 10.68.

*4-{[(1-benzylpiperidin-4-yl)(methyl)amino]methyl}-N-hydroxybenzamide (**9b**).* Pink solid (93%): mp 229-231 °C; ^{1}H NMR (500 MHz, D_2O): δ 2.15-2.25 (m, 2H), 2.48-2.55 (m, 2H), 2.83 (s, 3H), 3.20-3.30 (m, 2H), 3.75-3.80 (m, 2H), 4.42 (s, 2H); 4.49 (br. s, 1H), 4.55 (s, 2H), 7.55-8.15 (m, 9H); ^{13}C NMR (125 MHz, D_2O): δ 35.76, 50.24, 56.81, 59.36, 60.52, 62.53, 65.96, 127.98, 128.17, 129.32, 130.37, 131.16, 131.40, 132.66, 133.82, 167.48. Anal. Calcd. for $C_{21}H_{25}N_3O_2 \cdot 2HCl$: C, 59.15; H, 6.86; N, 9.86. Found: C, 59.26; H, 6.83; N, 10.05.

General procedure for the synthesis of (11a-c)

To a solution of o-phenylenediamine (3 mmol) in anhydrous CH_2Cl_2 was added dropwise a solution of the different acyl chloride (1 mmol) in 6 ml of CH_2Cl_2 at 0 °C and inert atmosphere, then the reaction mixture was stirred 24 hours at room temperature. Subsequently, a saturated solution of $NaHCO_3$ was added and the aqueous phase extracted with CH_2Cl_2. The combined organic phases were dried with anhydrous Na_2SO_4, filtered and evaporated under vacuum. The crude was purified by flash chromatography with CH_2Cl_2/EtOAc 50-50% in order to obtain the intermediates **10a-c**. Characterization and NMR data for compounds **10a-c** are reported in Supporting information. The intermediate were added dropwise and under nitrogen atmosphere to a solution of 4-(4-chlorophenyl)-4-hydroxypiperidine and K_2CO_3 in anhydrous DMF, and the reaction mixture was stirred 21 hours at 80 °C. The solvent was evaporated under vacuum, the resulting residue treated with EtOAc and washed with a saturated solution of $NaHCO_3$. The organic and the aqueous phase were repeatedly

separated, the aqueous phase extracted with EtOAc. The crude was purified by flash chromatography with EtOAc/MeOH 70-30% as eluent. According to this procedure, the following products have been obtained.

N-(2-aminophenyl)-3-[4-(4-chlorophenyl)-4-hydroxypiperidin-1-yl]propanamide ***(11a)*** White solid (85%): mp 171-174 °C; ^{1}H NMR (500 MHz, DMSO-d_6): δ 9.37 (s, 1H), 7.51-7.35 (m, 4H), 7.12-6.51 (m, 4H), 4.99-4.91 (br s, 2H), 3.33 (m, 2H), 2.80-2.78 (m. 2H), 2.49-2.41 (m, 4H), 1.96-1.90 (m, 2H), 1.60-1.57 (m, 2H); ^{13}C NMR (125 MHz, DMSO-d_6): δ 170.28, 149.04, 142.70, 130.76, 127.69, 126.85, 126.01, 125.74, 123.35, 115.94, 115.44, 69.42, 48.79, 37.74, 33.64. Anal. Calcd. for $C_{20}H_{24}ClN_3O_2$: C, 64.25; H, 6.47; N, 11.24. Found: C, 63.92; H, 6.32; N, 11.42.

N-(2-aminophenyl)-3-[4-(4-chlorophenyl)-4-hydroxypiperidin-1-yl]butanamide ***(11b)*** White solid (70%): mp 157-160 °C; ^{1}H NMR (500 MHz, DMSO-d_6): δ 9.21 (s, 1H), 7.45-7.32 (m, 4H), 7.20-6.51 (m, 4H), 4.85 (br s, 2H), 3.51 (br s, 1H), 2.67-2.65 (m, 2H), 2.37-2.33 (m, 6H), 1.91-1.85 (m, 2H), 1.77 (m, 2H), 1.55-1.53 (m, 2H).; ^{13}C NMR (125 MHz, DMSO-d_6): δ 171.15, 149.21, 141.76, 130.64, 127.62, 126.78, 125.48, 125.08, 123.68, 116.06, 115.77, 69.56, 57.59, 48.99, 37.92, 34.07, 22.67. Anal. Calcd. for $C_{21}H_{26}N_3O_2$: C, 65.02; H, 6.76; N, 10.83. Found: C, 64.79; H, 7.01; N, 11.15.

N-(2-aminophenyl)-3-[4-(4-chlorophenyl)-4-hydroxypiperidin-1-yl]pentanamide ***(11c)*** White solid (60%): mp 163-166 °C; ^{1}H NMR (500 MHz, DMSO-d_6): δ 9.15 (s, 1H), 7.49-7.33 (m, 4H), 7.16-6.51 (m, 4H), 4.82 (br s, 2H), 3.43 (br s, 1H), 2.65-2.63 (m, 2H), 2.36-2.32 (m, 6H), 1.91-1.85 (m, 2H), 1.64-1.46 (m, 6H); ^{13}C NMR (125 MHz, DMSO-d_6): δ 171.12, 149.21, 141.84, 130.67, 127.65, 126.82, 125.60, 125.19, 123.58, 116.11, 115.84, 69.55, 57.83, 49.04, 37.92, 35.63, 26.13, 23.40. Anal. Calcd. for $C_{22}H_{28}N_3O_2$: C, 64.25; H, 6.47; N, 11.24. Found: C, 63.92; H, 6.32; N, 11.42.

Radioligand Binding assay. Brain and liver homogenates for σ_1R and σ_2R receptor binding assays were prepared from male Dunkin-Hartley guinea pigs and Sprague Dawley rats, respectively (ENVIGO RMS S.R.L., Udine, Italy). Animals (200-250 g) were euthanized with CO_2 in an euthanasia chamber and sacrificed by decapitation. Guinea pig brains without cerebellum (~2.5 g each) and rat livers (~7 g each) were kept on dry ice and stored at -80 °C. [^{3}H](+)-Pentazocine (26.9

Ci/mmol) and [^{3}H]1,3-di-o-tolylguanidine ([^{3}H]DTG, 35.5 Ci/mmol) were purchased from PerkinElmer (Zaventem, Belgium). Ultima Gold MV Scintillation cocktail was from PerkinElmer (Milan, Italy). All the other materials were obtained from Merck Life Science S.r.l. (Milan, Italy). The test compound solutions were prepared by dissolving approximately 10 μmol of test compound in DMSO so that a 10 mM stock solution was obtained. The required test concentrations for the assay (from 10−5 to 10−11 M) have been prepared by diluting the DMSO stock solution with the respective assay buffer. All experiments were performed using ultrapure water obtained with a Millipore Milli-Q Reference Ultrapure Water Purification System. All the laboratory glassware was first washed with 6 M HCl water solution and then rinsed with ultrapure water. For membrane homogenates preparation and protein determination see Experimental section of Supporting information.

σ_1R Ligand Binding Assays. In vitro σ_1R ligand binding assays were carried out in Tris buffer (50 mM, pH 7.4) for 150 min at 37 °C. The thawed membrane preparation of guinea pig brain cortex (250 μg/sample) was incubated with increasing concentrations of test compounds and [^{3}H](+)-pentazocine (2 nM) in a final volume of 0.5 mL. The K_d value of [^{3}H](+)-pentazocine was 2.9 nM. Unlabeled (+)-pentazocine (10 μM) was used to measure non-specific binding. Bound and free radioligand were separated by fast filtration under reduced pressure using a Millipore filter apparatus through Whatman GF/6 glass fiber filters, which were presoaked in a 0.5% poly(ethyleneimine) water solution for 120 min. Each filter paper was rinsed three times with 3 mL ice-cold Tris buffer (50 mM, pH 7.4), dried at rt, and incubated overnight with 3 mL scintillation cocktail into pony vials. The bound radioactivity has been determined using a liquid scintillation counter (Beckman LS 6500).

σ_2R Ligand Binding Assays. In vitro σ_2R ligand binding assays were carried out in Tris buffer (50 mM, pH 8.0) for 120 min at rt. The thawed membrane preparation of rat liver (250 μg/sample) was incubated with increasing concentrations of test compounds and [^{3}H]DTG (2 nM) in the presence of (+)-pentazocine (5 μM) as σ_1R masking agent in a final volume of 0.5 mL. The K_d value of [^{3}H]DTG was 17.9 nM. Non-specific binding was evaluated with unlabeled DTG (10 μM). Bound and free radioligand were separated by fast filtration under reduced pressure using a Millipore filter apparatus

through Whatman GF/6 glass fiber filters, which were presoaked in a 0.5% poly(ethyleneimine) water solution for 120 min. Each filter paper was rinsed three times with 3 mL ice-cold Tris buffer (10 mM, pH 8), dried at rt, and incubated overnight with 3 mL scintillation cocktail into pony vials. The bound radioactivity has been determined using a liquid scintillation counter (Beckman LS 6500).

Data analysis. The K_i-values were calculated with the program GraphPad Prism® 7.0 (GraphPad Software, San Diego, CA, USA). The K_i-values are given as mean value ± SD from at least two independent experiments performed in duplicate.

Cell culture. Human breast cancer MCF-7 cells were purchased from American Type Culture Collection (ATCC) and the human colorectal carcinoma cell line HCT116 was purchased from ECACC. Both cell lines were maintained in Dulbecco's modified Eagle's medium (DMEM) high glucose (EuroClone, Milan, Italy). The human gastric adenocarcinoma cell line AGS and the human prostate adenocarcinoma PC-3 cells were both purchased by ECACC and maintained in Ham's F-12 medium (EuroClone). Human uveal melanoma cell line 92-1 (passages 2-15), a gift from Professor Gabriella Lupo,[159] were maintained at 37°C (5% CO_2) in RPMI-1640 medium, containing 10% fetal bovine serum (FBS), 2 mM L-glutamine, 100 units/ml penicillin and 100 µg/mL streptomycin. Breast cancer cell line MCF-7, obtained from the ATCC (Manassas, VA, USA), were maintained at 37°C (5% CO_2) in Eagle's Minimum Essential Medium, containing 10% FBS, 2 mM L-glutamine, 100 units/ml penicillin, 100 µg/mL streptomycin and 0.01 mg/ml human recombinant insulin. All cell media and reagents were from Euroclone S.p.A. (Pero, Milan, Italy). HGFs were cultured in DMEM high glucose. All culture media were supplemented with 10% of fetal bovine serum (FBS) and 1% of penicillin/streptomycin (Gibco - Thermofisher Scientific, MD, USA) and all the cells were kept at 37°C in a humidified atmosphere of 5% (v/v) CO_2.

Cell viability assay (MTT). Cell viability was assessed by MTT (3-(4,5-Dimethylthiazol-2-yl)-2,5-DiphenyltetrazoliumBromide) test (Sigma Aldrich, Milan, Italy). Since the compounds were dissolved in DMSO, cell susceptibility to the latter was previously investigated (data not shown). The MCF-7 cells only showed a significant decrease in viability when exposed to DMSO, therefore in the

MTT assay DMSO was added to the control sample of MCF-7 cells at the concentration of 80 μM, i. e. the highest concentration tested. Cells were seeded (8 x 10^4/well) in a 96-well tissue culture-treated plate (Falcon®, Corning Incorporated, NY, USA) and let them adhere for 24 h. Next, medium was removed and the cell monolayers were exposed to different concentrations (0-80 μM) of the compounds **7a**, **5** and **7b**. After 48 h, cells were incubated with 100 μl/well of MTT (1 mg/ml) 1:10 with fresh growth medium for 4 h at 37°C and 5% CO_2. Finally, the MTT solution was replaced with 100 μl/well of DMSO (Sigma Aldrich). Cells were incubated for additional 20 min at 37°C and 5% CO_2. The optical density was measured at 540 nm by means of a spectrophotometer (Multiskan GO, Thermo Scientific, Monza, Italy). The IC_{50} value for each molecule was calculated as the compound concentration able to inhibit the growth of the 50% of the cells using Graph Pad Prism (GraphPad Software, San Diego, Ca, USA). Each experiment was performed three times in triplicate.

Cell proliferation. 92-1 cell line were seeded (3x10^3/well) in 96-well plates and grown for 72 h at optimum culture conditions. Then, cells were treated with the indicated concentrations of chemicals for additional 48 h. Control cells received an equal volume of vehicle (DMSO). At the end of incubations, cells were fixed (in 4% paraformaldehyde) and stained with crystal violet (1%, aqueous solution). For quantification, after crystal violet extraction with 10% acetic acid (at room temperature for 10 min) the absorbance (at 590 nm) was measured with a spectrophotometer (Synergy HT, BioTek).

Developments of new Sigma/HDACi dual-ligands

Supported by the previous results about Sigma/HDACi dual-ligands on uveal melanoma and different tumor cell lines, we decide to continue with these series of hybrid dual-ligands with some modification. The sigma ammino moieties of the III group, described in the previous paragraph, was replaced with piperazine variously substituted, keeping up the ZBG *o*-phenylenediamine unchanged and limiting to a minimum of two and three methylenes the chain length (Figure 1). Indeed, compounds including 4 methylene lengths in the III group holds σ_1R affinity but in a rate of K_i=107 nM and completely lost affinity for σ_2R with K_i= >10000.

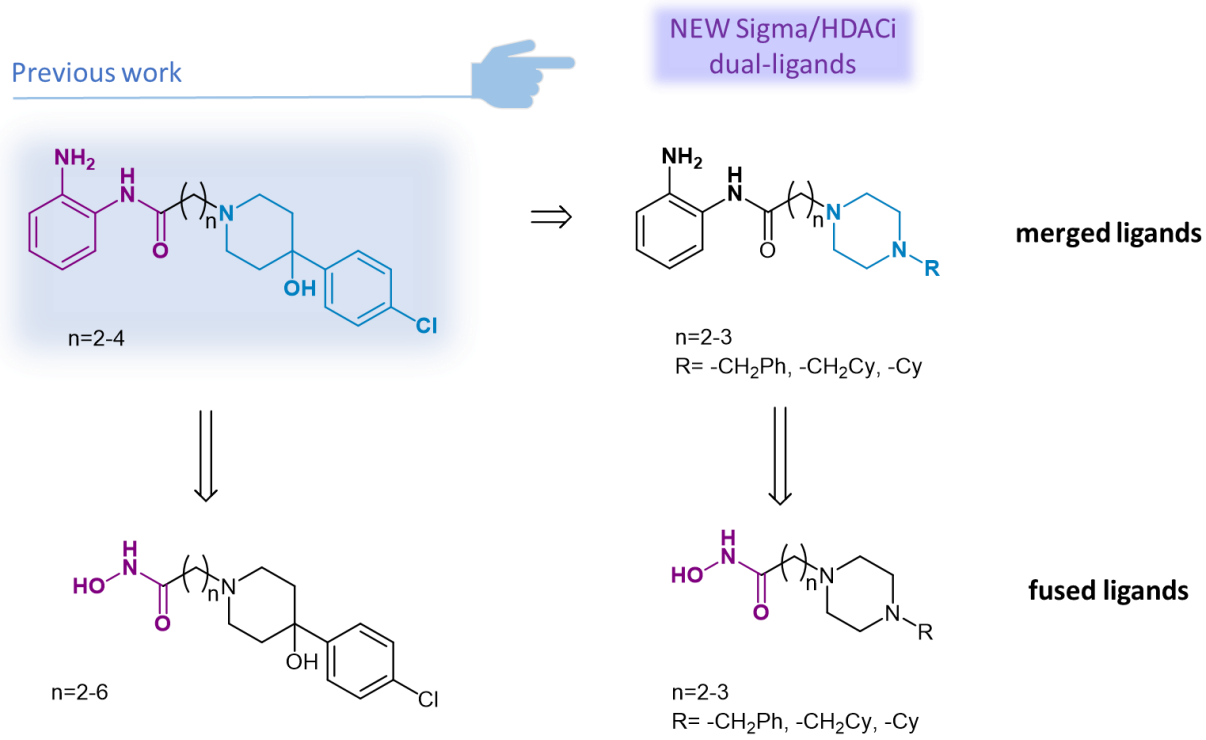

Figure 1. Design of new Sigma/HDACi hybrids as merged or fused ligands.

On the other hands, considering both σ receptor and HDAC enzyme pharmacophore models, new multiple ligands were designed as fused ligands, in which some pharmacophore elements of both targets are strictly connected and not overlapped like the precedent one (Figure 2). In this direction, appropriate functional groups have been chosen which, taken as a whole, could provide a single

pharmacophore model, capable of being part of the pharmacophoric model of both molecular targets and guaranteeing in the same way an excellent binding interaction with both the σ receptor and the enzyme HDAC. In particular, the new fused ligands preserve the structural features of the previous one above described, changing the ZBG *o*-phenylenediamine for the ZBG hydroxamic acid (see figure 1).

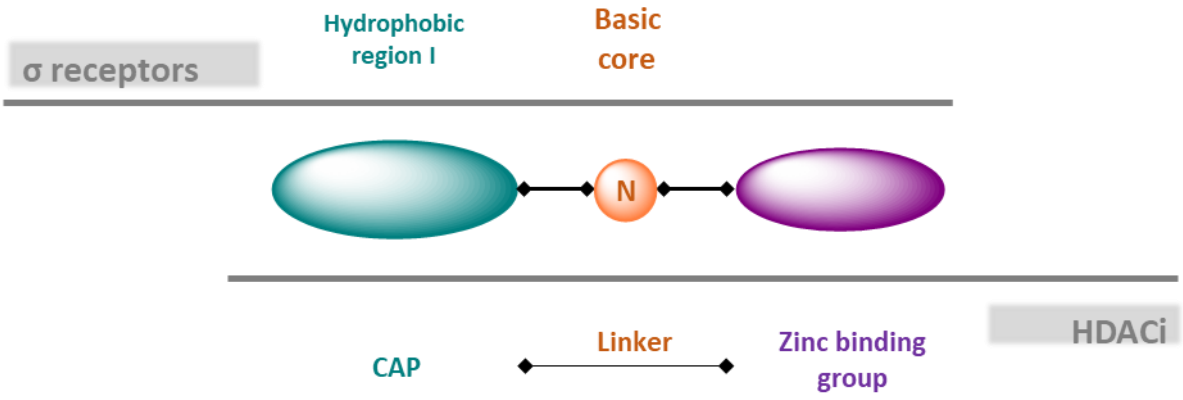

Figure 2. Design of new Sigma/HDACi hybrids as merged or fused ligands.

Synthesis

The synthesis of the *N*-(2-aminophenyl)amide derivatives is shown in the synthetic scheme 1. Starting from the commercially available 3-chloropropionyl and 4-chlorobutyryl chloride, the intermediates **1a-b** have been synthesized respectively by amidation with *o*-phenylenediamine.

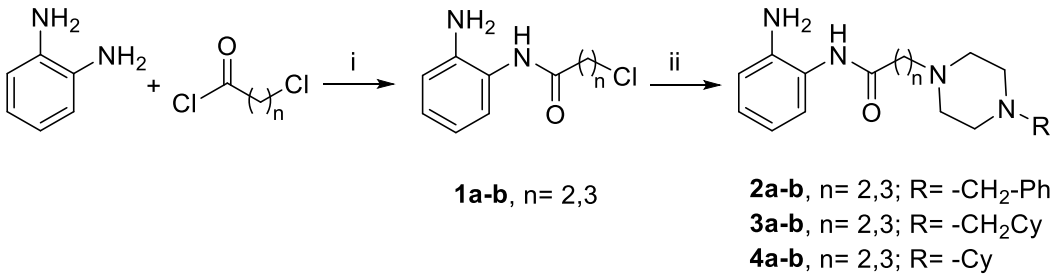

1a-b, n= 2,3

2a-b, n= 2,3; R= -CH_2-Ph
3a-b, n= 2,3; R= -CH_2Cy
4a-b, n= 2,3; R= -Cy

Scheme 1. *Reagent and conditions:* i) DCM anh., 0 °C to r.t; ii) piperazine variously substitued, $KHCO_3$, KI, ACN, 50 °C, 48h.

Intermediate products are objected to a nucleophilic substitution reaction with 1-benzylpiperazine, 1-(cyclohexylmethyl)piperazine or 1-cyclohexylpiperazine respectively in order to obtain the final compounds **2a-b, 3a-b** and **4a-b**. The purity of compounds has been evaluated by ^{1}H and ^{13}C NMR spectroscopy.

However, the synthetic route for the preparation of the hydroxamic acid derivatives is shown in scheme 2. Starting from the commercially available 1-benzylpiperazine, 1-(cyclohexylmethyl)piperazine, 1-cyclohexylpiperazine and 4-(4-chlorophenyl)piperidin-4-ol, the intermediate **5a-b**, **6a-b**, **7a-b** and **8a-e** have been synthesized by nucleophilic substitution with respectively methyl 3-bromopropanoate and 4-chlorobutanoate. The corresponding final compounds **9a-b**, **10a-b**, **11a-b** and **12a-e** were provided by direct reaction of the esters **5a-b**, **6a-b**, **7a-b** and **8a-e** with hydroxylamine hydrochloride in the presence of a base, used to generate free hydroxylamine in situ from hydroxylamine hydrochloride. Free hydroxylamine in a solution is slightly volatile, so a large excess of the reagent is required (~5-10 equivalent) to complete the reaction. The purity of compounds has been evaluated by 1H and 13C NMR spectroscopy.

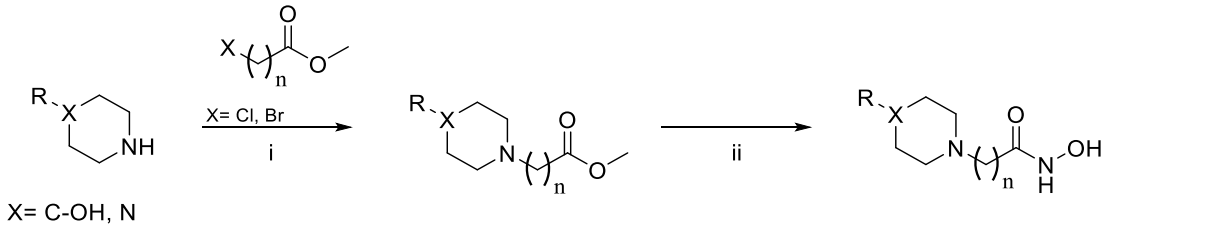

Scheme 2. *Reagents e conditions*: (i) ACN, K_2CO_3, 50 °C, overnight; (ii) MeOH, $NH_2OH{\cdot}HCl$, NaOH, r.t, overnight.

Radioligand binding and HDAC inhibition assays for the compounds described are currently in development, while biological evaluation will be carried out after the binding affinity results.

4. Concluding remarks

This research aimed to achieve new synthetic compounds for treatment of a rare and aggressive malignancy as uveal melanoma. With this purpose, the PhD project was developed in the hope of being able to identify new σR/HDACi hybrid ligands, which act on two molecular targets and will perform a double enhanced function, antiangiogenic and antiproliferative.

The design and the development of these hybrid compounds allowed to deepen the multitarget approach, sweeping from the prodrug to the overlapped and merged ligands, and to improve several competences among other compounds preparation and purification but in particular preclinical evaluation.

By analyzing results obtained up to now, the new hybrid compounds seem to represent promising candidate for the treatment of uveal melanoma and not beyond. Some of them exhibit interesting antiproliferative activity on human uveal melanoma 92-1 cells and also particular behaviors, supporting the initial idea of this work. In addition, these results give cause for hope about the cytotoxic activity of the prodrugs with simplified structure and the new "merged" dual-ligands, which are under preclinical evaluation.

While the consciousness of a no-specific mechanism limits the generalizability of the results, this approach provides anyway new purpose for further studies on possible mechanisms involving both targets in a unique cytotoxic activity. For these reasons, the more promising compounds will be object of additional biological evaluation, in order to understand the involved pathways and mechanisms, and pharmacological characterization in zebrafish xenograft model for uveal.

.

References

(1) Jager, M. J.; Shields, C. L.; Cebulla, C. M.; Abdel-Rahman, M. H.; Grossniklaus, H. E.; Stern, M. H.; Carvajal, R. D.; Belfort, R. N.; Jia, R.; Shields, J. A.et al. Uveal melanoma. *Nature reviews. Disease primers* **2020,** *6* (1), 24.

(2) Maheshwari, A.; Finger, P. T. Cancers of the eye. *Cancer Metastasis Rev* **2018,** *37* (4), 677.

(3) Andreoli, M. T.; Mieler, W. F.; Leiderman, Y. I. Epidemiological trends in uveal melanoma. *Br J Ophthalmol* **2015,** *99* (11), 1550.

(4) Virgili, G.; Gatta, G.; Ciccolallo, L.; Capocaccia, R.; Biggeri, A.; Crocetti, E.; Lutz, J. M.; Paci, E.; Group, E. W. Survival in patients with uveal melanoma in Europe. *Arch Ophthalmol* **2008,** *126* (10), 1413.

(5) Spagnolo, F.; Caltabiano, G.; Queirolo, P. Uveal melanoma. *Cancer Treat Rev* **2012,** *38* (5), 549.

(6) Mäkitie, T.; Summanen, P.; Tarkkanen, A.; Kivelä, T. Microvascular density in predicting survival of patients with choroidal and ciliary body melanoma. *Invest Ophthalmol Vis Sci* **1999,** *40* (11), 2471.

(7) Boyd, S. R.; Tan, D. S.; de Souza, L.; Neale, M. H.; Myatt, N. E.; Alexander, R. A.; Robb, M.; Hungerford, J. L.; Cree, I. A. Uveal melanomas express vascular endothelial growth factor and basic fibroblast growth factor and support endothelial cell growth. *Br J Ophthalmol* **2002,** *86* (4), 440.

(8) Logan, P.; Burnier, J.; Burnier, M. N., Jr. Vascular endothelial growth factor expression and inhibition in uveal melanoma cell lines. *Ecancermedicalscience* **2013,** *7*, 336.

(9) Mäkitie, T.; Summanen, P.; Tarkkanen, A.; Kivelä, T. Microvascular Loops and Networks as Prognostic Indicators in Choroidal and Ciliary Body Melanomas. *JNCI: Journal of the National Cancer Institute* **1999,** *91* (4), 359.

(10) Singh, A. D.; Turell, M. E.; Topham, A. K. Uveal melanoma: trends in incidence, treatment, and survival. *Ophthalmology* **2011,** *118* (9), 1881.

(11) Nayman, T.; Bostan, C.; Logan, P.; Burnier, M. N. Uveal Melanoma Risk Factors: A Systematic Review of Meta-Analyses. *Current Eye Research* **2017,** *42* (8), 1085.

(12) Ortega, M. A.; Fraile-Martinez, O.; Garcia-Honduvilla, N.; Coca, S.; Alvarez-Mon, M.; Bujan, J.; Teus, M. A. Update on uveal melanoma: Translational research from biology to clinical practice (Review). *Int J Oncol* **2020,** *57* (6), 1262.

(13) Wang, J. Z.; Lin, V.; Toumi, E.; Wang, K.; Zhu, H.; Conway, R. M.; Madigan, M. C.; Murray, M.; Cherepanoff, S.; Zhou, F.et al. Development of new therapeutic options for the treatment of uveal melanoma. *The FEBS Journal n/a* (n/a).

(14) Bakhoum, M. F.; Esmaeli, B. Molecular Characteristics of Uveal Melanoma: Insights from the Cancer Genome Atlas (TCGA) Project. *Cancers* **2019,** *11* (8), 1061.

(15) Chattopadhyay, C.; Kim, D. W.; Gombos, D. S.; Oba, J.; Qin, Y.; Williams, M. D.; Esmaeli, B.; Grimm, E. A.; Wargo, J. A.; Woodman, S. E.et al. Uveal melanoma: From diagnosis to treatment and the science in between. *Cancer* **2016,** *122* (15), 2299.

(16) Jager, M. J.; Brouwer, N. J.; Esmaeli, B. The Cancer Genome Atlas Project: An Integrated Molecular View of Uveal Melanoma. *Ophthalmology* **2018,** *125* (8), 1139.

(17) Onken, M. D.; Worley, L. A.; Ehlers, J. P.; Harbour, J. W. Gene expression profiling in uveal melanoma reveals two molecular classes and predicts metastatic death. *Cancer Res* **2004,** *64* (20), 7205.

(18) Fallico, M.; Raciti, G.; Longo, A.; Reibaldi, M.; Bonfiglio, V.; Russo, A.; Caltabiano, R.; Gattuso, G.; Falzone, L.; Avitabile, T. Current molecular and clinical insights into uveal melanoma (Review). *Int J Oncol* **2021,** *58* (4), 10.

(19) Kaliki, S.; Shields, C. L. Uveal melanoma: relatively rare but deadly cancer. *Eye (Lond)* **2017,** *31* (2), 241.

(20) Kujala, E.; Mäkitie, T.; Kivelä, T. Very long-term prognosis of patients with malignant uveal melanoma. *Invest Ophthalmol Vis Sci* **2003,** *44* (11), 4651.
(21) Onken, M. D.; Worley, L. A.; Char, D. H.; Augsburger, J. J.; Correa, Z. M.; Nudleman, E.; Aaberg, T. M., Jr.; Altaweel, M. M.; Bardenstein, D. S.; Finger, P. T.et al. Collaborative Ocular Oncology Group report number 1: prospective validation of a multi-gene prognostic assay in uveal melanoma. *Ophthalmology* **2012,** *119* (8), 1596.
(22) Brouwer, N. J.; Gezgin, G.; Wierenga, A. P. A.; Bronkhorst, I. H. G.; Marinkovic, M.; Luyten, G. P. M.; Versluis, M.; Kroes, W. G. M.; van der Velden, P. A.; Verdijk, R. M.et al. Tumour Angiogenesis in Uveal Melanoma Is Related to Genetic Evolution. *Cancers (Basel)* **2019,** *11* (7).
(23) Piperno-Neumann, S.; Diallo, A.; Etienne-Grimaldi, M. C.; Bidard, F. C.; Rodrigues, M.; Plancher, C.; Mariani, P.; Cassoux, N.; Decaudin, D.; Asselain, B.et al. Phase II Trial of Bevacizumab in Combination With Temozolomide as First-Line Treatment in Patients With Metastatic Uveal Melanoma. *Oncologist* **2016,** *21* (3), 281.
(24) https://ClinicalTrials.gov/show/NCT00596362.
(25) Maj, E.; Papiernik, D.; Wietrzyk, J. Antiangiogenic cancer treatment: The great discovery and greater complexity (Review). *Int J Oncol* **2016,** *49* (5), 1773.
(26) Buder, K.; Gesierich, A.; Gelbrich, G.; Goebeler, M. Systemic treatment of metastatic uveal melanoma: review of literature and future perspectives. *Cancer Med* **2013,** *2* (5), 674.
(27) Nathan, P.; Cohen, V.; Coupland, S.; Curtis, K.; Damato, B.; Evans, J.; Fenwick, S.; Kirkpatrick, L.; Li, O.; Marshall, E.et al. Uveal Melanoma UK National Guidelines. *Eur J Cancer* **2015,** *51* (16), 2404.
(28) Chua, V.; Mattei, J.; Han, A.; Johnston, L.; LiPira, K.; Selig, S. M.; Carvajal, R. D.; Aplin, A. E.; Patel, S. P. The Latest on Uveal Melanoma Research and Clinical Trials: Updates from the Cure Ocular Melanoma (CURE OM) Science Meeting (2019). *Clin Cancer Res* **2021,** *27* (1), 28.
(29) Medina-Franco, J. L.; Giulianotti, M. A.; Welmaker, G. S.; Houghten, R. A. Shifting from the single to the multitarget paradigm in drug discovery. *Drug Discov Today* **2013,** *18* (9-10), 495.
(30) Zhang, W.; Pei, J.; Lai, L. Computational Multitarget Drug Design. *J Chem Inf Model* **2017,** *57* (3), 403.
(31) Peters, J. U. Polypharmacology - foe or friend? *J Med Chem* **2013,** *56* (22), 8955.
(32) Cavalli, A.; Bolognesi, M. L.; Minarini, A.; Rosini, M.; Tumiatti, V.; Recanatini, M.; Melchiorre, C. Multi-target-directed ligands to combat neurodegenerative diseases. *J Med Chem* **2008,** *51* (3), 347.
(33) Olsen, J.; Overvad, K. The concept of multifactorial etiology of cancer. *Pharmacol Toxicol* **1993,** *72 Suppl 1*, 33.
(34) Morphy, R.; Rankovic, Z. Designed multiple ligands. An emerging drug discovery paradigm. *J Med Chem* **2005,** *48* (21), 6523.
(35) Kondej, M.; Stepnicki, P.; Kaczor, A. A. Multi-Target Approach for Drug Discovery against Schizophrenia. *International journal of molecular sciences* **2018,** *19* (10).
(36) Schmidt, H. R.; Kruse, A. C. The Molecular Function of sigma Receptors: Past, Present, and Future. *Trends in pharmacological sciences* **2019,** *40* (9), 636.
(37) Walker, J. M.; Bowen, W. D.; Walker, F. O.; Matsumoto, R. R.; De Costa, B.; Rice, K. C. Sigma receptors: biology and function. *Pharmacol Rev* **1990,** *42* (4), 355.
(38) Hellewell, S. B.; Bowen, W. D. A sigma-like binding site in rat pheochromocytoma (PC12) cells: decreased affinity for (+)-benzomorphans and lower molecular weight suggest a different sigma receptor form from that of guinea pig brain. *Brain Res* **1990,** *527* (2), 244.
(39) Glennon, R. A. Pharmacophore identification for sigma-1 (sigma1) receptor binding: application of the "deconstruction-reconstruction-elaboration" approach. *Mini Rev Med Chem* **2005,** *5* (10), 927.

(40) Wunsch, B. Pharmacophore models and development of spirocyclic ligands for sigma1 receptors. *Current pharmaceutical design* **2012,** *18* (7), 930.
(41) Schmidt, H. R.; Betz, R. M.; Dror, R. O.; Kruse, A. C. Structural basis for sigma1 receptor ligand recognition. *Nat Struct Mol Biol* **2018,** *25* (10), 981.
(42) Su, T. P.; London, E. D.; Jaffe, J. H. Steroid Binding at Sigma-Receptors Suggests a Link between Endocrine, Nervous, and Immune-Systems. *Science* **1988,** *240* (4849), 219.
(43) Fontanilla, D.; Johannessen, M.; Hajipour, A. R.; Cozzi, N. V.; Jackson, M. B.; Ruoho, A. E. The hallucinogen N,N-dimethyltryptamine (DMT) is an endogenous sigma-1 receptor regulator. *Science (New York, N.Y.)* **2009,** *323* (5916), 934.
(44) Ramachandran, S.; Chu, U. B.; Mavlyutov, T. A.; Pal, A.; Pyne, S.; Ruoho, A. E. The sigma1 receptor interacts with N-alkyl amines and endogenous sphingolipids. *European journal of pharmacology* **2009,** *609* (1-3), 19.
(45) Cobos, E. J.; Entrena, J. M.; Nieto, F. R.; Cendan, C. M.; Del Pozo, E. Pharmacology and therapeutic potential of sigma(1) receptor ligands. *Current neuropharmacology* **2008,** *6* (4), 344.
(46) Brailoiu, E.; Chakraborty, S.; Brailoiu, G. C.; Zhao, P.; Barr, J. L.; Ilies, M. A.; Unterwald, E. M.; Abood, M. E.; Taylor, C. W. Choline Is an Intracellular Messenger Linking Extracellular Stimuli to IP(3)-Evoked Ca(2+) Signals through Sigma-1 Receptors. *Cell reports* **2019,** *26* (2), 330.
(47) Schmidt, H. R.; Zheng, S.; Gurpinar, E.; Koehl, A.; Manglik, A.; Kruse, A. C. Crystal structure of the human sigma1 receptor. *Nature* **2016,** *532* (7600), 527.
(48) Hayashi, T.; Su, T. P. Sigma-1 receptor chaperones at the ER-mitochondrion interface regulate Ca(2+) signaling and cell survival. *Cell* **2007,** *131* (3), 596.
(49) Chu, U. B.; Ruoho, A. E. Biochemical Pharmacology of the Sigma-1 Receptor. *Molecular pharmacology* **2016,** *89* (1), 142.
(50) Weng, T. Y.; Tsai, S. A.; Su, T. P. Roles of sigma-1 receptors on mitochondrial functions relevant to neurodegenerative diseases. *Journal of biomedical science* **2017,** *24* (1), 74.
(51) Johannessen, M.; Ramachandran, S.; Riemer, L.; Ramos-Serrano, A.; Ruoho, A. E.; Jackson, M. B. Voltage-gated sodium channel modulation by sigma-receptors in cardiac myocytes and heterologous systems. *Am J Physiol Cell Physiol* **2009,** *296* (5), C1049.
(52) Kourrich, S.; Su, T. P.; Fujimoto, M.; Bonci, A. The sigma-1 receptor: roles in neuronal plasticity and disease. *Trends Neurosci* **2012,** *35* (12), 762.
(53) Pabba, M.; Sibille, E. Sigma-1 and N-Methyl-d-Aspartate Receptors: A Partnership with Beneficial Outcomes. *Mol Neuropsychiatry* **2015,** *1* (1), 47.
(54) Ye, N.; Qin, W.; Tian, S.; Xu, Q.; Wold, E. A.; Zhou, J.; Zhen, X.-C. Small Molecules Selectively Targeting Sigma-1 Receptor for the Treatment of Neurological Diseases. *Journal of Medicinal Chemistry* **2020,** *63* (24), 15187.
(55) Hanner, M.; Moebius, F. F.; Flandorfer, A.; Knaus, H. G.; Striessnig, J.; Kempner, E.; Glossmann, H. Purification, molecular cloning, and expression of the mammalian sigma1-binding site. *Proc Natl Acad Sci U S A* **1996,** *93* (15), 8072.
(56) Kekuda, R.; Prasad, P. D.; Fei, Y. J.; Leibach, F. H.; Ganapathy, V. Cloning and functional expression of the human type 1 sigma receptor (hSigmaR1). *Biochem Biophys Res Commun* **1996,** *229* (2), 553.
(57) Seth, P.; Fei, Y. J.; Li, H. W.; Huang, W.; Leibach, F. H.; Ganapathy, V. Cloning and functional characterization of a sigma receptor from rat brain. *J Neurochem* **1998,** *70* (3), 922.
(58) Gromek, K. A.; Suchy, F. P.; Meddaugh, H. R.; Wrobel, R. L.; LaPointe, L. M.; Chu, U. B.; Primm, J. G.; Ruoho, A. E.; Senes, A.; Fox, B. G. The Oligomeric States of the Purified Sigma-1 Receptor Are Stabilized by Ligands. *J Biol Chem* **2014,** *289* (29), 20333.
(59) Kurcinski, M.; Jaronczyk, M.; Lipinski, P. F. J.; Dobrowolski, J. C.; Sadlej, J. Structural Insights into sigma(1) Receptor Interactions with Opioid Ligands by Molecular Dynamics Simulations. *Molecules* **2018,** *23* (2).

(60) Yano, H.; Bonifazi, A.; Xu, M.; Guthrie, D. A.; Schneck, S. N.; Abramyan, A. M.; Fant, A. D.; Hong, W. C.; Newman, A. H.; Shi, L. Pharmacological profiling of sigma 1 receptor ligands by novel receptor homomer assays. *Neuropharmacology* **2018,** *133*, 264.
(61) Mishra, A. K.; Mavlyutov, T.; Singh, D. R.; Biener, G.; Yang, J.; Oliver, J. A.; Ruoho, A.; Raicu, V. The sigma-1 receptors are present in monomeric and oligomeric forms in living cells in the presence and absence of ligands. *Biochem J* **2015,** *466* (2), 263.
(62) Schmidt, H. R.; Betz, R. M.; Dror, R. O.; Kruse, A. C. Structural basis for σ(1) receptor ligand recognition. *Nature structural & molecular biology* **2018,** *25* (10), 981.
(63) Nguyen, L.; Lucke-Wold, B. P.; Mookerjee, S. A.; Cavendish, J. Z.; Robson, M. J.; Scandinaro, A. L.; Matsumoto, R. R. Role of sigma-1 receptors in neurodegenerative diseases. *Journal of pharmacological sciences* **2015,** *127* (1), 17.
(64) Castany, S.; Gris, G.; Vela, J. M.; Verdú, E.; Boadas-Vaello, P. Critical role of sigma-1 receptors in central neuropathic pain-related behaviours after mild spinal cord injury in mice. *Scientific reports* **2018,** *8* (1), 3873.
(65) Bruna, J.; Videla, S.; Argyriou, A. A.; Velasco, R.; Villoria, J.; Santos, C.; Nadal, C.; Cavaletti, G.; Alberti, P.; Briani, C.et al. Efficacy of a Novel Sigma-1 Receptor Antagonist for Oxaliplatin-Induced Neuropathy: A Randomized, Double-Blind, Placebo-Controlled Phase IIa Clinical Trial. *Neurotherapeutics : the journal of the American Society for Experimental NeuroTherapeutics* **2018,** *15* (1), 178.
(66) Mancuso, R.; Oliván, S.; Rando, A.; Casas, C.; Osta, R.; Navarro, X. Sigma-1R agonist improves motor function and motoneuron survival in ALS mice. *Neurotherapeutics : the journal of the American Society for Experimental NeuroTherapeutics* **2012,** *9* (4), 814.
(67) Li, D.; Zhang, S. Z.; Yao, Y. H.; Xiang, Y.; Ma, X. Y.; Wei, X. L.; Yan, H. T.; Liu, X. Y. Sigma-1 receptor agonist increases axon outgrowth of hippocampal neurons via voltage-gated calcium ions channels. *CNS neuroscience & therapeutics* **2017,** *23* (12), 930.
(68) Das, D.; Persaud, L.; Dejoie, J.; Happy, M.; Brannigan, O.; De Jesus, D.; Sauane, M. Tumor necrosis factor-related apoptosis-inducing ligand (TRAIL) activates caspases in human prostate cancer cells through sigma 1 receptor. *Biochem Biophys Res Commun* **2016,** *470* (2), 319.
(69) Maurice, T.; Su, T. P. The pharmacology of sigma-1 receptors. *Pharmacol Ther* **2009,** *124* (2), 195.
(70) Georgiadis, M. O.; Karoutzou, O.; Foscolos, A. S.; Papanastasiou, I. Sigma Receptor (sigmaR) Ligands with Antiproliferative and Anticancer Activity. *Molecules* **2017,** *22* (9).
(71) Alonso, G.; Phan, V.; Guillemain, I.; Saunier, M.; Legrand, A.; Anoal, M.; Maurice, T. Immunocytochemical localization of the sigma(1) receptor in the adult rat central nervous system. *Neuroscience* **2000,** *97* (1), 155.
(72) Bangaru, M. L.; Weihrauch, D.; Tang, Q. B.; Zoga, V.; Hogan, Q.; Wu, H. E. Sigma-1 receptor expression in sensory neurons and the effect of painful peripheral nerve injury. *Molecular pain* **2013,** *9*, 47.
(73) Palacios, G.; Muro, A.; Verdú, E.; Pumarola, M.; Vela, J. M. Immunohistochemical localization of the sigma1 receptor in Schwann cells of rat sciatic nerve. *Brain research* **2004,** *1007* (1-2), 65.
(74) Ryskamp, D. A.; Korban, S.; Zhemkov, V.; Kraskovskaya, N.; Bezprozvanny, I. Neuronal Sigma-1 Receptors: Signaling Functions and Protective Roles in Neurodegenerative Diseases. *Frontiers in Neuroscience* **2019,** *13* (862).
(75) van Waarde, A.; Ramakrishnan, N. K.; Rybczynska, A. A.; Elsinga, P. H.; Ishiwata, K.; Nijholt, I. M.; Luiten, P. G. M.; Dierckx, R. A. The cholinergic system, sigma-1 receptors and cognition. *Behavioural Brain Research* **2011,** *221* (2), 543.
(76) Hong, J.; Wang, L.; Zhang, T.; Zhang, B.; Chen, L. Sigma-1 receptor knockout increases α-synuclein aggregation and phosphorylation with loss of dopaminergic neurons in substantia nigra. *Neurobiology of Aging* **2017,** *59*, 171.

(77) Mishina, M.; Ishiwata, K.; Ishii, K.; Kitamura, S.; Kimura, Y.; Kawamura, K.; Oda, K.; Sasaki, T.; Sakayori, O.; Hamamoto, M.et al. Function of sigma1 receptors in Parkinson's disease. *Acta Neurologica Scandinavica* **2005,** *112* (2), 103.
(78) Herrando-Grabulosa, M.; Gaja-Capdevila, N.; Vela, J. M.; Navarro, X. Sigma 1 receptor as a therapeutic target for amyotrophic lateral sclerosis. *British Journal of Pharmacology n/a* (n/a).
(79) Hampel, H.; Williams, C.; Etcheto, A.; Goodsaid, F.; Parmentier, F.; Sallantin, J.; Kaufmann, W. E.; Missling, C. U.; Afshar, M. A precision medicine framework using artificial intelligence for the identification and confirmation of genomic biomarkers of response to an Alzheimer's disease therapy: Analysis of the blarcamesine (ANAVEX2-73) Phase 2a clinical study. *Alzheimer's & Dementia: Translational Research & Clinical Interventions* **2020,** *6* (1), e12013.
(80) Fox, S. H.; Lang, A. E.; Brotchie, J. M. Translation of nondopaminergic treatments for levodopa-induced dyskinesia from MPTP-lesioned nonhuman primates to phase IIa clinical studies: Keys to success and roads to failure. *Movement Disorders* **2006,** *21* (10), 1578.
(81) Abadias, M.; Escriche, M.; Vaqué, A.; Sust, M.; Encina, G. Safety, tolerability and pharmacokinetics of single and multiple doses of a novel sigma-1 receptor antagonist in three randomized phase I studies. *British journal of clinical pharmacology* **2013,** *75* (1), 103.
(82) de la Puente, B.; Nadal, X.; Portillo-Salido, E.; Sánchez-Arroyos, R.; Ovalle, S.; Palacios, G.; Muro, A.; Romero, L.; Entrena, J. M.; Baeyens, J. M.et al. Sigma-1 receptors regulate activity-induced spinal sensitization and neuropathic pain after peripheral nerve injury. *Pain* **2009,** *145* (3), 294.
(83) Entrena, J. M.; Cobos, E. J.; Nieto, F. R.; Cendán, C. M.; Gris, G.; Del Pozo, E.; Zamanillo, D.; Baeyens, J. M. Sigma-1 receptors are essential for capsaicin-induced mechanical hypersensitivity: studies with selective sigma-1 ligands and sigma-1 knockout mice. *Pain* **2009,** *143* (3), 252.
(84) Vilner, B. J.; John, C. S.; Bowen, W. D. Sigma-1 and Sigma-2 Receptors Are Expressed in a Wide Variety of Human and Rodent Tumor-Cell Lines. *Cancer Res* **1995,** *55* (2), 408.
(85) Crottès, D.; Guizouarn, H.; Martin, P.; Borgese, F.; Soriani, O. The sigma-1 receptor: a regulator of cancer cell electrical plasticity? *Frontiers in physiology* **2013,** *4*, 175.
(86) Maher, C. M.; Thomas, J. D.; Haas, D. A.; Longen, C. G.; Oyer, H. M.; Tong, J. Y.; Kim, F. J. Small-Molecule Sigma1 Modulator Induces Autophagic Degradation of PD-L1. *Molecular cancer research : MCR* **2018,** *16* (2), 243.
(87) Spruce, B. A.; Campbell, L. A.; McTavish, N.; Cooper, M. A.; Appleyard, M. V. L.; O'Neill, M.; Howie, J.; Samson, J.; Watt, S.; Murray, K.et al. Small Molecule Antagonists of the σ-1 Receptor Cause Selective Release of the Death Program in Tumor and Self-Reliant Cells and Inhibit Tumor Growth in Vitro and in Vivo. *Cancer Res* **2004,** *64* (14), 4875.
(88) Happy, M.; Dejoie, J.; Zajac, C. K.; Cortez, B.; Chakraborty, K.; Aderemi, J.; Sauane, M. Sigma 1 Receptor antagonist potentiates the anti-cancer effect of p53 by regulating ER stress, ROS production, Bax levels, and caspase-3 activation. *Biochemical and biophysical research communications* **2015,** *456* (2), 683.
(89) Spruce, B. A.; Campbell, L. A.; McTavish, N.; Cooper, M. A.; Appleyard, M. V.; O'Neill, M.; Howie, J.; Samson, J.; Watt, S.; Murray, K.et al. Small molecule antagonists of the sigma-1 receptor cause selective release of the death program in tumor and self-reliant cells and inhibit tumor growth in vitro and in vivo. *Cancer research* **2004,** *64* (14), 4875.
(90) Xu, J.; Zeng, C.; Chu, W.; Pan, F.; Rothfuss, J. M.; Zhang, F.; Tu, Z.; Zhou, D.; Zeng, D.; Vangveravong, S.et al. Identification of the PGRMC1 protein complex as the putative sigma-2 receptor binding site. *Nature Communications* **2011,** *2* (1), 380.
(91) Abate, C.; Niso, M.; Infantino, V.; Menga, A.; Berardi, F. Elements in support of the 'non-identity' of the PGRMC1 protein with the σ2 receptor. *Eur J Pharmacol* **2015,** *758*, 16.

(92) Chu, U. B.; Mavlyutov, T. A.; Chu, M.-L.; Yang, H.; Schulman, A.; Mesangeau, C.; McCurdy, C. R.; Guo, L.-W.; Ruoho, A. E. The Sigma-2 Receptor and Progesterone Receptor Membrane Component 1 are Different Binding Sites Derived From Independent Genes. *EBioMedicine* **2015,** *2* (11), 1806.
(93) Pati, M. L.; Groza, D.; Riganti, C.; Kopecka, J.; Niso, M.; Berardi, F.; Hager, S.; Heffeter, P.; Hirai, M.; Tsugawa, H.et al. Sigma-2 receptor and progesterone receptor membrane component 1 (PGRMC1) are two different proteins: Proofs by fluorescent labeling and binding of sigma-2 receptor ligands to PGRMC1. *Pharmacological Research* **2017,** *117*, 67.
(94) Alon, A.; Schmidt, H. R.; Wood, M. D.; Sahn, J. J.; Martin, S. F.; Kruse, A. C. Identification of the gene that codes for the sigma2 receptor. *Proc Natl Acad Sci U S A* **2017,** *114* (27), 7160.
(95) Zeng, C.; Riad, A.; Mach, R. H. The Biological Function of Sigma-2 Receptor/TMEM97 and Its Utility in PET Imaging Studies in Cancer. *Cancers* **2020,** *12* (7).
(96) Ye, R.; Holland, W. L.; Gordillo, R.; Wang, M.; Wang, Q. A.; Shao, M.; Morley, T. S.; Gupta, R. K.; Stahl, A.; Scherer, P. E. Adiponectin is essential for lipid homeostasis and survival under insulin deficiency and promotes β-cell regeneration. *eLife* **2014,** *3*.
(97) Ebrahimi-Fakhari, D.; Wahlster, L.; Bartz, F.; Werenbeck-Ueding, J.; Praggastis, M.; Zhang, J.; Joggerst-Thomalla, B.; Theiss, S.; Grimm, D.; Ory, D. S.et al. Reduction of TMEM97 increases NPC1 protein levels and restores cholesterol trafficking in Niemann-pick type C1 disease cells. *Human molecular genetics* **2016,** *25* (16), 3588.
(98) Ramalho-Carvalho, J.; Goncalves, C. S.; Graca, I.; Bidarra, D.; Pereira-Silva, E.; Salta, S.; Godinho, M. I.; Gomez, A.; Esteller, M.; Costa, B. M.et al. A multiplatform approach identifies miR-152-3p as a common epigenetically regulated onco-suppressor in prostate cancer targeting TMEM97. *Clinical epigenetics* **2018,** *10*, 40.
(99) Qiu, G.; Sun, W.; Zou, Y.; Cai, Z.; Wang, P.; Lin, X.; Huang, J.; Jiang, L.; Ding, X.; Hu, G. RNA interference against TMEM97 inhibits cell proliferation, migration, and invasion in glioma cells. *Tumour biology : the journal of the International Society for Oncodevelopmental Biology and Medicine* **2015,** *36* (10), 8231.
(100) Zeng, C.; Weng, C. C.; Schneider, M. E., Jr.; Puentes, L.; Riad, A.; Xu, K.; Makvandi, M.; Jin, L.; Hawkins, W. G.; Mach, R. H. TMEM97 and PGRMC1 do not mediate sigma-2 ligand-induced cell death. *Cell death discovery* **2019,** *5*, 58.
(101) Zeng, C.; Rothfuss, J. M.; Zhang, J.; Vangveravong, S.; Chu, W.; Li, S.; Tu, Z.; Xu, J.; Mach, R. H. Functional assays to define agonists and antagonists of the sigma-2 receptor. *Analytical Biochemistry* **2014,** *448*, 68.
(102) Niso, M.; Abate, C.; Contino, M.; Ferorelli, S.; Azzariti, A.; Perrone, R.; Colabufo, N. A.; Berardi, F. Sigma-2 receptor agonists as possible antitumor agents in resistant tumors: hints for collateral sensitivity. *ChemMedChem* **2013,** *8* (12), 2026.
(103) Izzo, N. J.; Staniszewski, A.; To, L.; Fa, M.; Teich, A. F.; Saeed, F.; Wostein, H.; Walko, T., 3rd; Vaswani, A.; Wardius, M.et al. Alzheimer's therapeutics targeting amyloid beta 1-42 oligomers I: Abeta 42 oligomer binding to specific neuronal receptors is displaced by drug candidates that improve cognitive deficits. *PLoS One* **2014,** *9* (11), e111898.
(104) Georgiadis, M.-O.; Karoutzou, O.; Foscolos, A.-S.; Papanastasiou, I. Sigma Receptor (σR) Ligands with Antiproliferative and Anticancer Activity. *Molecules* **2017,** *22* (9), 1408.
(105) Davidson, M.; Saoud, J.; Staner, C.; Noel, N.; Luthringer, E.; Werner, S.; Reilly, J.; Schaffhauser, J. Y.; Rabinowitz, J.; Weiser, M.et al. Efficacy and Safety of MIN-101: A 12-Week Randomized, Double-Blind, Placebo-Controlled Trial of a New Drug in Development for the Treatment of Negative Symptoms in Schizophrenia. *Am J Psychiatry* **2017,** *174* (12), 1195.
(106) Grundman, M.; Morgan, R.; Lickliter, J. D.; Schneider, L. S.; DeKosky, S.; Izzo, N. J.; Guttendorf, R.; Higgin, M.; Pribyl, J.; Mozzoni, K.et al. A phase 1 clinical trial of the sigma-2 receptor complex allosteric antagonist CT1812, a novel therapeutic candidate for

Alzheimer's disease. *Alzheimer's & Dementia: Translational Research & Clinical Interventions* **2019,** *5*, 20.
(107) Zeng, C.; Riad, A.; Mach, R. H. The Biological Function of Sigma-2 Receptor/TMEM97 and Its Utility in PET Imaging Studies in Cancer. *Cancers* **2020,** *12* (7), 1877.
(108) Abate, C.; Niso, M.; Berardi, F. Sigma-2 receptor: past, present and perspectives on multiple therapeutic exploitations. *Future Med Chem* **2018,** *10* (16), 1997.
(109) Fyodorov, D. V.; Zhou, B. R.; Skoultchi, A. I.; Bai, Y. Emerging roles of linker histones in regulating chromatin structure and function. *Nature reviews. Molecular cell biology* **2018,** *19* (3), 192.
(110) Vrtačnik, P.; Marc, J.; Ostanek, B. Epigenetic mechanisms in bone. *Clinical chemistry and laboratory medicine* **2014,** *52* (5), 589.
(111) Gregory, P. D.; Wagner, K.; Hörz, W. Histone Acetylation and Chromatin Remodeling. *Experimental Cell Research* **2001,** *265* (2), 195.
(112) Yan, C.; Boyd, D. D. Histone H3 acetylation and H3 K4 methylation define distinct chromatin regions permissive for transgene expression. *Molecular and cellular biology* **2006,** *26* (17), 6357.
(113) Xu, W. S.; Parmigiani, R. B.; Marks, P. A. Histone deacetylase inhibitors: molecular mechanisms of action. *Oncogene* **2007,** *26* (37), 5541.
(114) Huynh, N. C.-N.; Everts, V.; Ampornaramveth, R. S. Histone deacetylases and their roles in mineralized tissue regeneration. *Bone Reports* **2017,** *7*, 33.
(115) Seto, E.; Yoshida, M. Erasers of histone acetylation: the histone deacetylase enzymes. *Cold Spring Harb Perspect Biol* **2014,** *6* (4), a018713.
(116) Finnin, M. S.; Donigian, J. R.; Cohen, A.; Richon, V. M.; Rifkind, R. A.; Marks, P. A.; Breslow, R.; Pavletich, N. P. Structures of a histone deacetylase homologue bound to the TSA and SAHA inhibitors. *Nature* **1999,** *401* (6749), 188.
(117) Wu, R.; Lu, Z.; Cao, Z.; Zhang, Y. Zinc chelation with hydroxamate in histone deacetylases modulated by water access to the linker binding channel. *Journal of the American Chemical Society* **2011,** *133* (16), 6110.
(118) Finnin, M. S.; Donigian, J. R.; Cohen, A.; Richon, V. M.; Rifkind, R. A.; Marks, P. A.; Breslow, R.; Pavletich, N. P. Structures of a histone deacetylase homologue bound to the TSA and SAHA inhibitors. *Nature* **1999,** *401* (6749), 188.
(119) Miller, T. A.; Witter, D. J.; Belvedere, S. Histone deacetylase inhibitors. *Journal of medicinal chemistry* **2003,** *46* (24), 5097.
(120) Mai, A.; Massa, S.; Rotili, D.; Pezzi, R.; Bottoni, P.; Scatena, R.; Meraner, J.; Brosch, G. Exploring the connection unit in the HDAC inhibitor pharmacophore model: novel uracil-based hydroxamates. *Bioorganic & medicinal chemistry letters* **2005,** *15* (21), 4656.
(121) Li, W.; Sun, Z. Mechanism of Action for HDAC Inhibitors-Insights from Omics Approaches. *International journal of molecular sciences* **2019,** *20* (7).
(122) Hai, Y.; Christianson, D. W. Histone deacetylase 6 structure and molecular basis of catalysis and inhibition. *Nature Chemical Biology* **2016,** *12* (9), 741.
(123) Porter, N. J.; Mahendran, A.; Breslow, R.; Christianson, D. W. Unusual zinc-binding mode of HDAC6-selective hydroxamate inhibitors. *Proceedings of the National Academy of Sciences* **2017,** *114* (51), 13459.
(124) Hu, E.; Dul, E.; Sung, C. M.; Chen, Z.; Kirkpatrick, R.; Zhang, G. F.; Johanson, K.; Liu, R.; Lago, A.; Hofmann, G.et al. Identification of novel isoform-selective inhibitors within class I histone deacetylases. *J Pharmacol Exp Ther* **2003,** *307* (2), 720.
(125) Dokmanovic, M.; Marks, P. A. Prospects: histone deacetylase inhibitors. *Journal of cellular biochemistry* **2005,** *96* (2), 293.
(126) Shukla, S.; Tekwani, B. L. Histone Deacetylases Inhibitors in Neurodegenerative Diseases, Neuroprotection and Neuronal Differentiation. *Front Pharmacol* **2020,** *11*, 537.

(127) Lohman, R.-J.; Iyer, A.; Fairlie, T. J.; Cotterell, A.; Gupta, P.; Reid, R. C.; Vesey, D. A.; Sweet, M. J.; Fairlie, D. P. Differential Anti-inflammatory Activity of HDAC Inhibitors in Human Macrophages and Rat Arthritis. *Journal of Pharmacology and Experimental Therapeutics* **2016,** *356* (2), 387.
(128) Zhang, H.; Li, X.; Zhang, Q.; Yang, F.; Chu, X.; Zhang, D.; Wang, L.; Gong, Z. Role of histone deacetylase expression levels and activity in the inflammatory responses of patients with chronic hepatitis B. *Mol Med Rep* **2017,** *15* (5), 2744.
(129) Pons, D.; de Vries, F. R.; van den Elsen, P. J.; Heijmans, B. T.; Quax, P. H. A.; Jukema, J. W. Epigenetic histone acetylation modifiers in vascular remodelling: new targets for therapy in cardiovascular disease. *European Heart Journal* **2009,** *30* (3), 266.
(130) Cardinale, J. P.; Sriramula, S.; Pariaut, R.; Guggilam, A.; Mariappan, N.; Elks, C. M.; Francis, J. HDAC inhibition attenuates inflammatory, hypertrophic, and hypertensive responses in spontaneously hypertensive rats. *Hypertension* **2010,** *56* (3), 437.
(131) Mann, B. S.; Johnson, J. R.; Cohen, M. H.; Justice, R.; Pazdur, R. FDA approval summary: vorinostat for treatment of advanced primary cutaneous T-cell lymphoma. *Oncologist* **2007,** *12* (10), 1247.
(132) Whittaker, S. J.; Demierre, M. F.; Kim, E. J.; Rook, A. H.; Lerner, A.; Duvic, M.; Scarisbrick, J.; Reddy, S.; Robak, T.; Becker, J. C.et al. Final results from a multicenter, international, pivotal study of romidepsin in refractory cutaneous T-cell lymphoma. *Journal of clinical oncology : official journal of the American Society of Clinical Oncology* **2010,** *28* (29), 4485.
(133) Coiffier, B.; Pro, B.; Prince, H. M.; Foss, F.; Sokol, L.; Greenwood, M.; Caballero, D.; Borchmann, P.; Morschhauser, F.; Wilhelm, M.et al. Results from a pivotal, open-label, phase II study of romidepsin in relapsed or refractory peripheral T-cell lymphoma after prior systemic therapy. *Journal of clinical oncology : official journal of the American Society of Clinical Oncology* **2012,** *30* (6), 631.
(134) Poole, R. M. Belinostat: first global approval. *Drugs* **2014,** *74* (13), 1543.
(135) Oki, Y.; Buglio, D.; Fanale, M.; Fayad, L.; Copeland, A.; Romaguera, J.; Kwak, L. W.; Pro, B.; de Castro Faria, S.; Neelapu, S.et al. Phase I study of panobinostat plus everolimus in patients with relapsed or refractory lymphoma. *Clin Cancer Res* **2013,** *19* (24), 6882.
(136) Sato, T.; Orloff, M. M.; Valsecchi, M. E.; Shimada, A.; Chervoneva, I.; Sharpe-Mills, E.; Klose, H.; Norcini, J.; Belinsky, J.; Sato, S.et al. A randomized phase II study of adjuvant sunitinib or valproic acid in high-risk patients with uveal melanoma. *Journal of Clinical Oncology* **2020,** *38* (15_suppl), e22059.
(137) Dogrusoz, M.; Jager, M. J.; Damato, B. Uveal Melanoma Treatment and Prognostication. *Asia Pac J Ophthalmol (Phila)* **2017,** *6* (2), 186.
(138) Jiang, G.; Mysona, B.; Dun, Y.; Gnana-Prakasam, J. P.; Pabla, N.; Li, W.; Dong, Z.; Ganapathy, V.; Smith, S. B. Expression, subcellular localization, and regulation of sigma receptor in retinal muller cells. *Invest Ophthalmol Vis Sci* **2006,** *47* (12), 5576.
(139) Longhitano, L.; Castracani, C. C.; Tibullo, D.; Avola, R.; Viola, M.; Russo, G.; Prezzavento, O.; Marrazzo, A.; Amata, E.; Reibaldi, M.et al. Sigma-1 and Sigma-2 receptor ligands induce apoptosis and autophagy but have opposite effect on cell proliferation in uveal melanoma. *Oncotarget* **2017,** *8* (53), 91099.
(140) Bowen, W. D. Sigma receptors: recent advances and new clinical potentials. *Pharm Acta Helv* **2000,** *74* (2-3), 211.
(141) Smith, S. B. Introduction to Sigma Receptors: Their Role in Disease and as Therapeutic Targets. *Adv Exp Med Biol* **2017,** *964*, 1.
(142) Landreville, S.; Agapova, O. A.; Matatall, K. A.; Kneass, Z. T.; Onken, M. D.; Lee, R. S.; Bowcock, A. M.; Harbour, J. W. Histone deacetylase inhibitors induce growth arrest and differentiation in uveal melanoma. *Clin Cancer Res* **2012,** *18* (2), 408.
(143) DAMASKOS, C.; KARATZAS, T.; NIKOLIDAKIS, L.; KOSTAKIS, I. D.; KARAMAROUDIS, S.; BOUTSIKOS, G.; DAMASKOU, Z.; KOSTAKIS, A.;

KOURAKLIS, G. Histone Deacetylase (HDAC) Inhibitors: Current Evidence for Therapeutic Activities in Pancreatic Cancer. *Anticancer Research* **2015,** *35* (6), 3129.
(144) Li, Z.; Zhu, W.-G. Targeting Histone Deacetylases for Cancer Therapy: From Molecular Mechanisms to Clinical Implications. *International Journal of Biological Sciences* **2014,** *10* (7), 757.
(145) Mann, B. S.; Johnson, J. R.; He, K.; Sridhara, R.; Abraham, S.; Booth, B. P.; Verbois, L.; Morse, D. E.; Jee, J. M.; Pope, S.et al. Vorinostat for treatment of cutaneous manifestations of advanced primary cutaneous T-cell lymphoma. *Clin Cancer Res* **2007,** *13* (8), 2318.
(146) Prince, H. M.; Dickinson, M. Romidepsin for cutaneous T-cell lymphoma. *Clin Cancer Res* **2012,** *18* (13), 3509.
(147) Landreville, S.; Agapova, O. A.; Matatall, K. A.; Kneass, Z. T.; Onken, M. D.; Lee, R. S.; Bowcock, A. M.; Harbour, J. W. Histone Deacetylase Inhibitors Induce Growth Arrest and Differentiation in Uveal Melanoma. *Clinical Cancer Research* **2012,** *18* (2), 408.
(148) Kratz, F.; Muller, I. A.; Ryppa, C.; Warnecke, A. Prodrug strategies in anticancer chemotherapy. *ChemMedChem* **2008,** *3* (1), 20.
(149) Marrazzo, A.; Fiorito, J.; Zappala, L.; Prezzavento, O.; Ronsisvalle, S.; Pasquinucci, L.; Scoto, G. M.; Bernardini, R.; Ronsisvalle, G. Antiproliferative activity of phenylbutyrate ester of haloperidol metabolite II [(+/-)-MRJF4] in prostate cancer cells. *Eur J Med Chem* **2011,** *46* (1), 433.
(150) Sozio, P.; Fiorito, J.; Di Giacomo, V.; Di Stefano, A.; Marinelli, L.; Cacciatore, I.; Cataldi, A.; Pacella, S.; Turkez, H.; Parenti, C.et al. Haloperidol metabolite II prodrug: asymmetric synthesis and biological evaluation on rat C6 glioma cells. *Eur J Med Chem* **2015,** *90*, 1.
(151) Olivieri, M.; Amata, E.; Vinciguerra, S.; Fiorito, J.; Giurdanella, G.; Drago, F.; Caporarello, N.; Prezzavento, O.; Arena, E.; Salerno, L.et al. Antiangiogenic Effect of (+/-)-Haloperidol Metabolite II Valproate Ester [(+/-)-MRJF22] in Human Microvascular Retinal Endothelial Cells. *J Med Chem* **2016,** *59* (21), 9960.
(152) Tan, J.; Cang, S.; Ma, Y.; Petrillo, R. L.; Liu, D. Novel histone deacetylase inhibitors in clinical trials as anti-cancer agents. *Journal of Hematology & Oncology* **2010,** *3* (1), 5.
(153) Bao, P.; Kodra, A.; Tomic-Canic, M.; Golinko, M. S.; Ehrlich, H. P.; Brem, H. The role of vascular endothelial growth factor in wound healing. *The Journal of surgical research* **2009,** *153* (2), 347.
(154) Brown, D. M.; Heier, J. S.; Clark, W. L.; Boyer, D. S.; Vitti, R.; Berliner, A. J.; Zeitz, O.; Sandbrink, R.; Zhu, X.; Haller, J. A. Intravitreal aflibercept injection for macular edema secondary to central retinal vein occlusion: 1-year results from the phase 3 COPERNICUS study. *Am J Ophthalmol* **2013,** *155* (3), 429.
(155) Campochiaro, P. A.; Clark, W. L.; Boyer, D. S.; Heier, J. S.; Brown, D. M.; Vitti, R.; Kazmi, H.; Berliner, A. J.; Erickson, K.; Chu, K. W.et al. Intravitreal aflibercept for macular edema following branch retinal vein occlusion: the 24-week results of the VIBRANT study. *Ophthalmology* **2015,** *122* (3), 538.
(156) Tabernero, J.; Van Cutsem, E.; Lakomy, R.; Prausova, J.; Ruff, P.; van Hazel, G. A.; Moiseyenko, V. M.; Ferry, D. R.; McKendrick, J. J.; Soussan-Lazard, K.et al. Aflibercept versus placebo in combination with fluorouracil, leucovorin and irinotecan in the treatment of previously treated metastatic colorectal cancer: prespecified subgroup analyses from the VELOUR trial. *Eur J Cancer* **2014,** *50* (2), 320.
(157) Mach, R. H.; Smith, C. R.; Childers, S. R. Ibogaine possesses a selective affinity for sigma 2 receptors. *Life Sci* **1995,** *57* (4), PL57.
(158) Matsumoto, R. R.; Bowen, W. D.; Tom, M. A.; Vo, V. N.; Truong, D. D.; De Costa, B. R. Characterization of two novel sigma receptor ligands: antidystonic effects in rats suggest sigma receptor antagonism. *Eur J Pharmacol* **1995,** *280* (3), 301.

(159) Anfuso, C. D.; Longo, A.; Distefano, A.; Amorini, A. M.; Salmeri, M.; Zanghi, G.; Giallongo, C.; Giurdanella, G.; Lupo, G. Uveal Melanoma Cells Elicit Retinal Pericyte Phenotypical and Biochemical Changes in an in Vitro Model of Coculture. *Int J Mol Sci* **2020,** *21* (15).
(160) Albertson, N. F.; Wetterau, W. F. The synthesis of pentazocine. *J Med Chem* **1970,** *13* (2), 302.
(161) Maeda, D. Y.; Williams, W.; Kim, W. E.; Thatcher, L. N.; Bowen, W. D.; Coop, A. N-Arylalkylpiperidines as High-Affinity Sigma-1 and Sigma-2 Receptor Ligands: Phenylpropylamines as Potential Leads for Selective Sigma-2 Agents. *Bioorganic & Medicinal Chemistry Letters* **2002,** *12* (3), 497.

Supplementary Information

Haloperidol metabolite II Valproate ester (±)-MRJF22: asymmetric synthesis and biological evaluation on Human Microvascular Retinal Endothelial and uveal melanoma cells.

Carla Barbaraci[a§], Giovanni Giurdanella[b§], Claudia Leotta[c], Anna Longo[c], Orazio Prezzavento[a], Gabriella Lupo[b], Emanuele Amata[a], Giovanni Mario Pitari[c*], Daniela Anfuso[b*], Agostino Marrazzo[a*]

[a] Department of Health and Drug Sciences, University of Catania, Viale A. Doria 6, 95125 Catania, Italy.

[b] Department of Biomedical and Biotechnological Sciences, School of Medicine, University of Catania, Via S. Sofia 97, 95123 Catania, Italy.

[c] Vera Salus Ricerca S.r.l, Via Sigmund Freud 62/B, 96100 Siracusa, Italy.

Corresponding Authors:
*A.M.: phone, (+39 0957384250; email: marrazzo@unict.it)
*Daniela Anfuso (+39 0954781170; email: daniela.anfuso@unict.it)
*Giovanni Mario Pitari (+39 09311987360; email: giovanni.pitari@verasalusricerca.it)

Author Contributions:
§CB and GG contributed equally.

Table of contents

Table S1. MTT Viability Test on HREC: IC_{50} at three Different Time Periods of (±)MRJF22, (*S*)-(-)-MRJF22, (*R*)-(+)-MRJF22

Cmps	Period (h)	IC_{50} (µM)	(pIC_{50} ± SE)
	24	5.83 mM	5.222 (± 0.041)
(±)-MRJF22	48	5.45 mM	5.284 (± 0.068)
	72	5.1 mM	5.373 (± 1.065)
	24	6.63 mM	5,179 (± 0.025)
S-(-)-MRJF22	48	6.23 mM	5,205 (± 0.083)
	72	5.44 mM	5,265 (± 0.142)
	24	6.36 mM	5,196 (± 0.030)
R-(+)-MRJF22	48	4.832 mM	5,316 (± 0.186)
	72	4.69 mM	5,326 (± 0.186)

IC_{50} values have been calculated with GraphPad Prism 5 for Windows using a nonlinear fit transform sigmoidal dose-response (variable slope). pIC_{50} is defined as the $-\log(IC_{50})$. IC_{50} values are averaged from multiple determinations (n = 6). IC_{50} values are averaged from multiple determinations (n = 3).

Figure S1. Wound healing assay: effects of (±)-MRJF22 on VEGF-stimulated HREC.

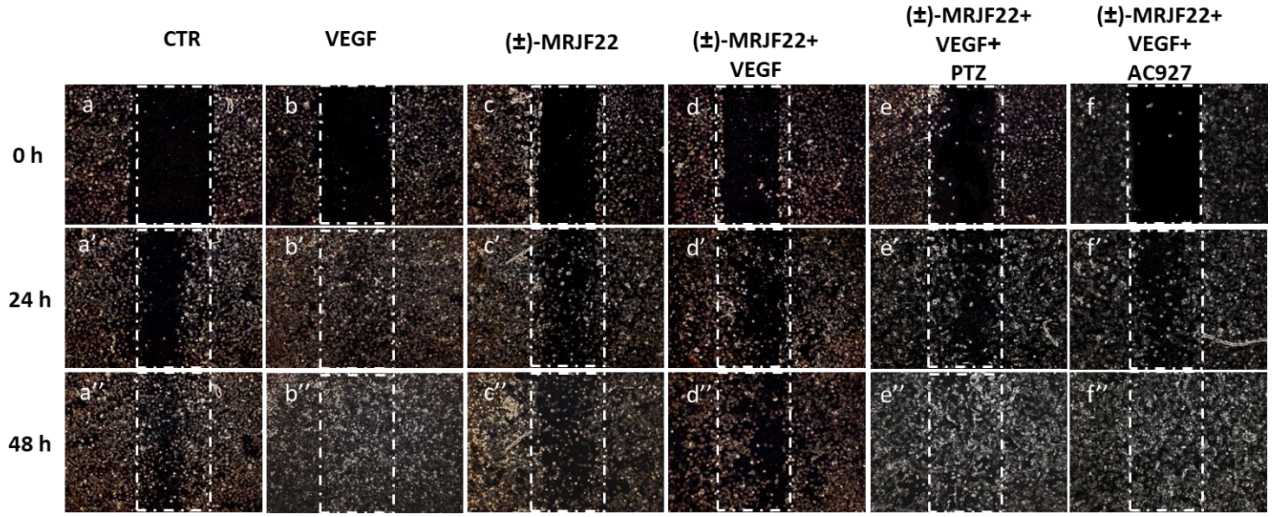

Representative images of scratched cells treated with VEGF (80 ng/ml; b, b' and b''), 5 μM of (±)-MRJF22 (c, c' and c''), VEGF plus 5 μM of (±)-MRJF22 (d, d' and d''), VEGF plus 5 μM (±)-MRJF22 plus 2 μM of PTZ (e, e' and e''), VEGF plus 5 μM of (±)-MRJF22 plus 2 μM of AC927 (f, f' and f''). Untreated cells were considered as control samples (CTR; a, a' and a''). Images show cells at the starting points (0 h after scratch: a, b, c, d, e and f), after 24 h (a', b', c', d', e' and f') and 48 h (a'', b'', c'', d'', e'' and f'') from the starting of the assays.

Figure S2. Wound healing assay: effects of (*R*)-(+)-MRJF22 on VEGF-stimulated HREC.

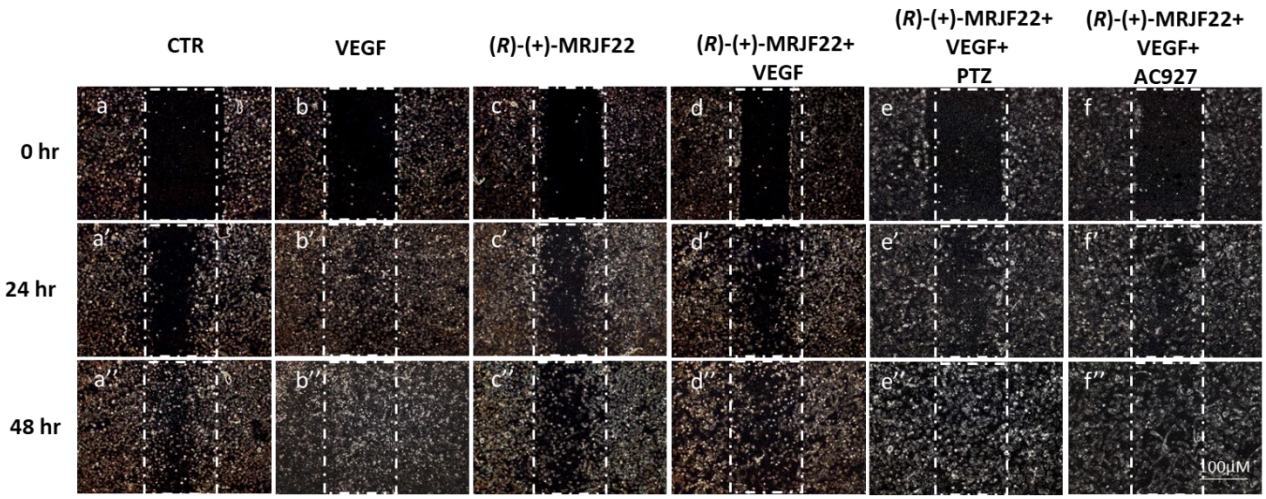

Representative images of scratched cells treated with VEGF (80 ng/ml; b, b' and b''), 5 μM of (*R*)-(+)-MRJF22 (c, c' and c''), VEGF plus 5 μM of (*R*)-(+)-MRJF22 (d, d' and d''), VEGF plus 5 μM (*R*)-(+)-MRJF22 plus 2 μM of PTZ (e, e' and e''), VEGF plus 5 μM of (*R*)-(+)-MRJF22 plus 2 μM of AC927 (f, f' and f''). Untreated cells were considered as control samples (CTRL; a, a' and a''). Images show cells at the starting points (0 h after scratch: a, b, c, d, e and f), after 24 h (a', b', c', d', e' and f') and 48 h (a'', b'', c'', d'', e'' and f'') from the starting of the assays.

Figure S3. Wound healing assay: effects of (*S*)-(-)-MRJF22 on VEGF-stimulated HREC.

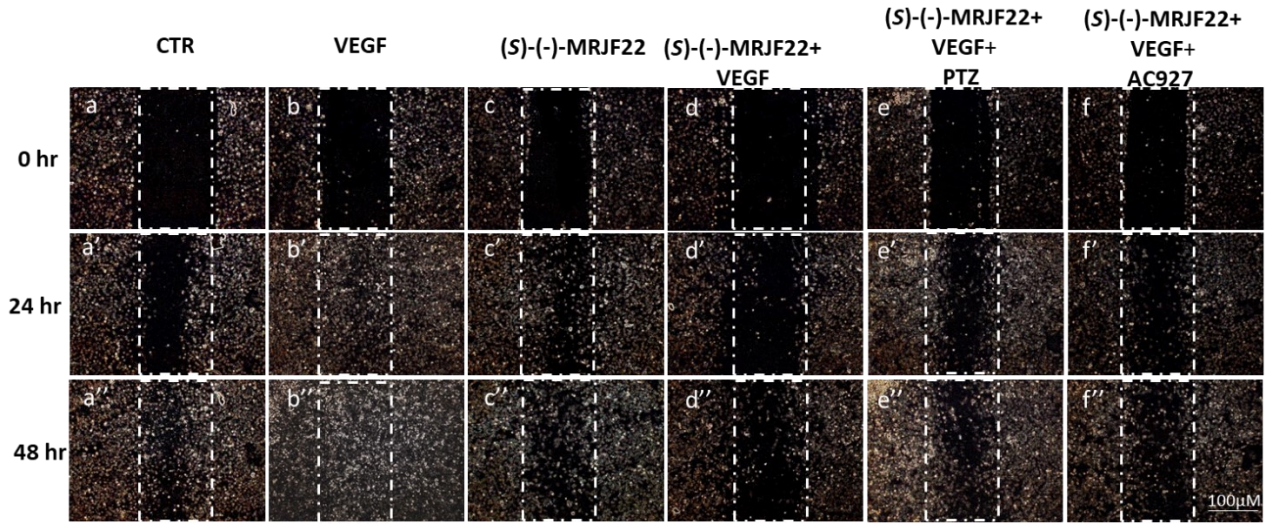

Representative images of scratched cells treated with VEGF (80 ng/ml; b, b' and b''), 5 µM of (*S*)-(-)-MRJF22 (c, c' and c''), VEGF plus 5 µM of (*S*)-(-)-MRJF22 (d, d' and d''), VEGF plus 5 µM (*S*)-(-)-MRJF22 plus 2 µM of PTZ (e, e' and e''), VEGF plus 5 µM of (*S*)-(-)-MRJF22 plus 2 µM of AC927 (f, f' and f''). Untreated cells were considered as control samples (CTRL; a, a' and a''). Images show cells at the starting points (0 h after scratch: a, b, c, d, e and f), after 24 h (a', b', c', d', e' and f') and 48 h (a'', b'', c'', d'', e'' and f'') from the starting of the assays.

Figure S4 Tube formation on Matrigel: effects of (±)-MRJF22, (*S*)-(-)-MRJF22 and (*R*)-(+)-MRJF22 in VEGF-stimulated HREC

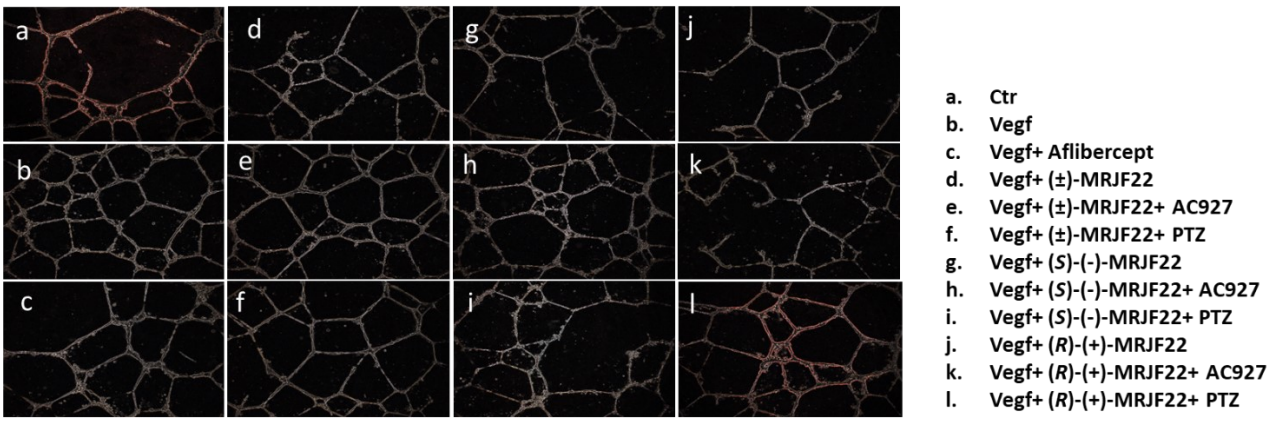

Representative optical phase-contrast micrographs of tube-like structures observed in the Tube Formation assays (Matrigel) at 24h from the starting of the assays (40X of magnification). We tested HREC treated with 80 ng/ml of VEGF in presence or in absence of 5 µM of (±)-MRJF22, (*S*)-(-)-MRJF22 and (*R*)-(+)-MRJF22 or further supplemented with selective σ1 agonist PTZ (2 µM) and σ receptors antagonist AC927 (2 µM). We included HREC treated with 40 µg/ml of Aflibercept (AFL).

EXPERIMENTAL SECTION

NMR spectra

^{1}H NMR (500 MHz,$CDCl_3$) for (*R*)-(+)-4-cloro-1-(4-fluorophenyl)butan-1-ol, (*R*)-(+)-2

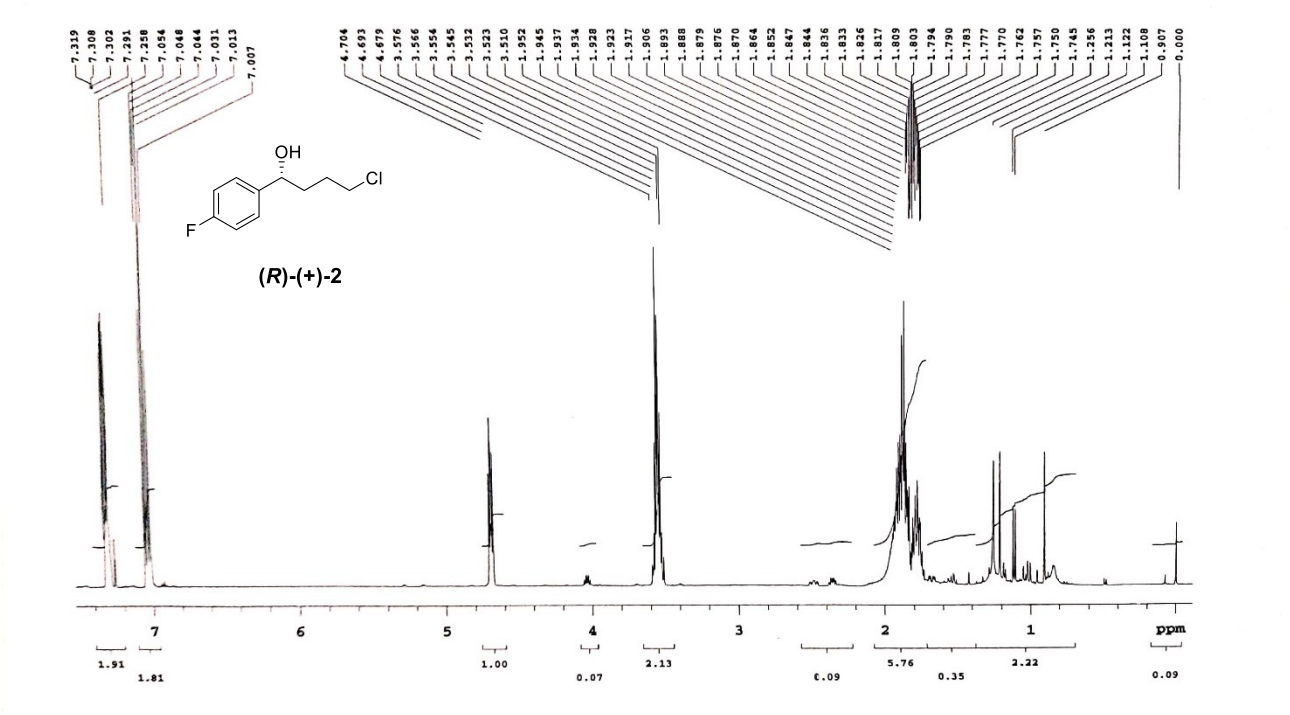

^{1}H NMR (500 MHz,$CDCl_3$) for (*S*)-(-)-4-cloro-1-(4-fluorophenyl)butan-1-ol, (*S*)-(-)-2

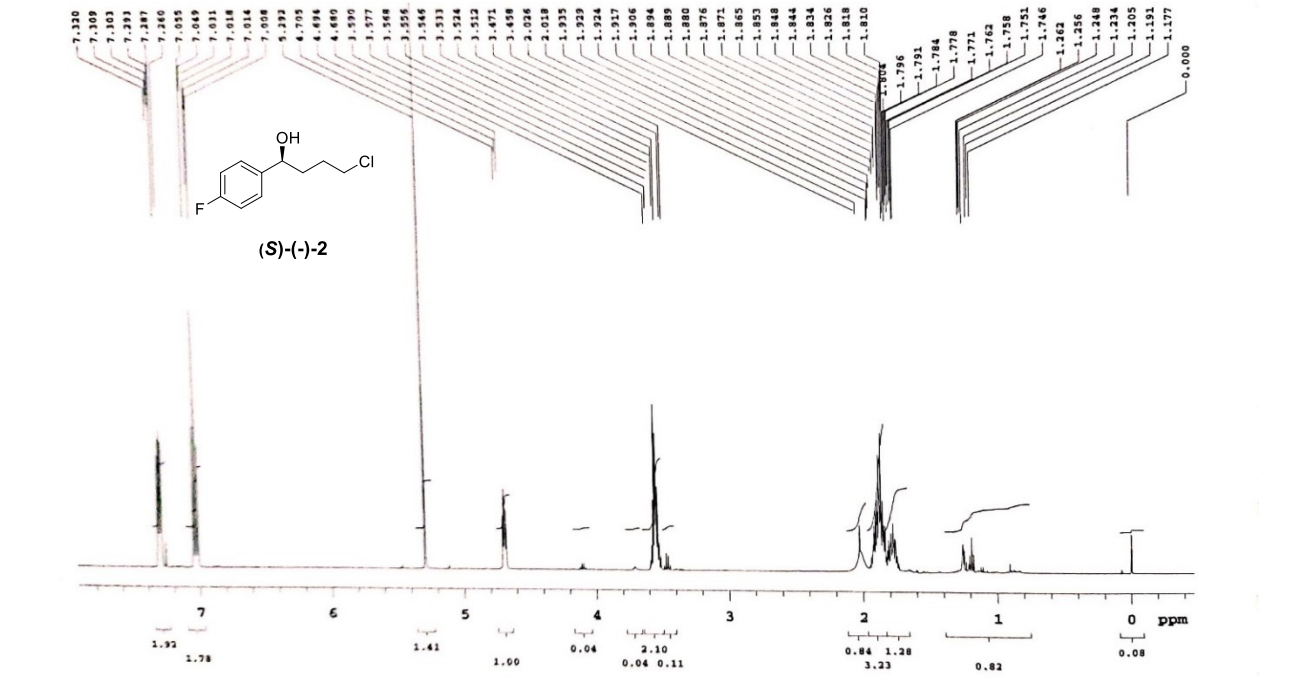

^{1}H NMR (500 MHz,$CDCl_3$) for (*R*)-(+)-4-(4-clorophenyl)-1-[4(4-fluorophenyl)-4-hidroxybutyl] piperidin-4-ol, (*R*)-(+)-HPmII

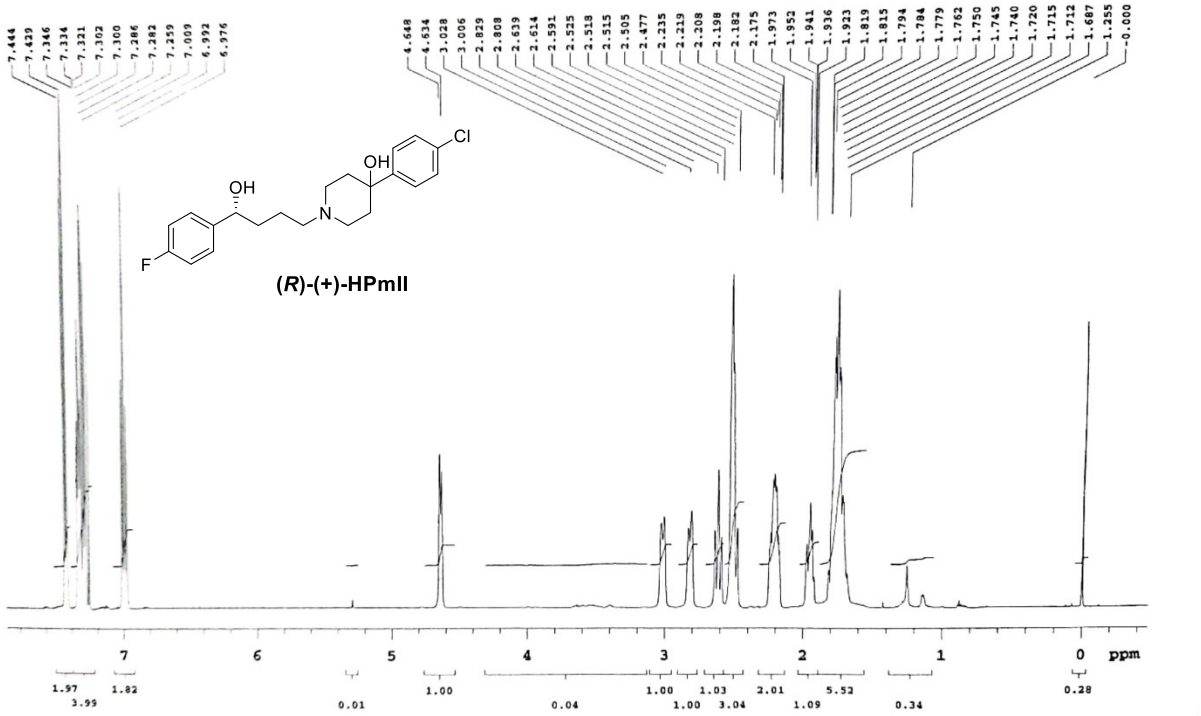

^{1}H NMR (500 MHz,$CDCl_3$) for (*S*)-(-)- 4-(4-clorophenyl)-1-[4(4-fluorophenyl)-4-hidroxybutyl] piperidin-4-ol, (*S*)-(-)-HPmII

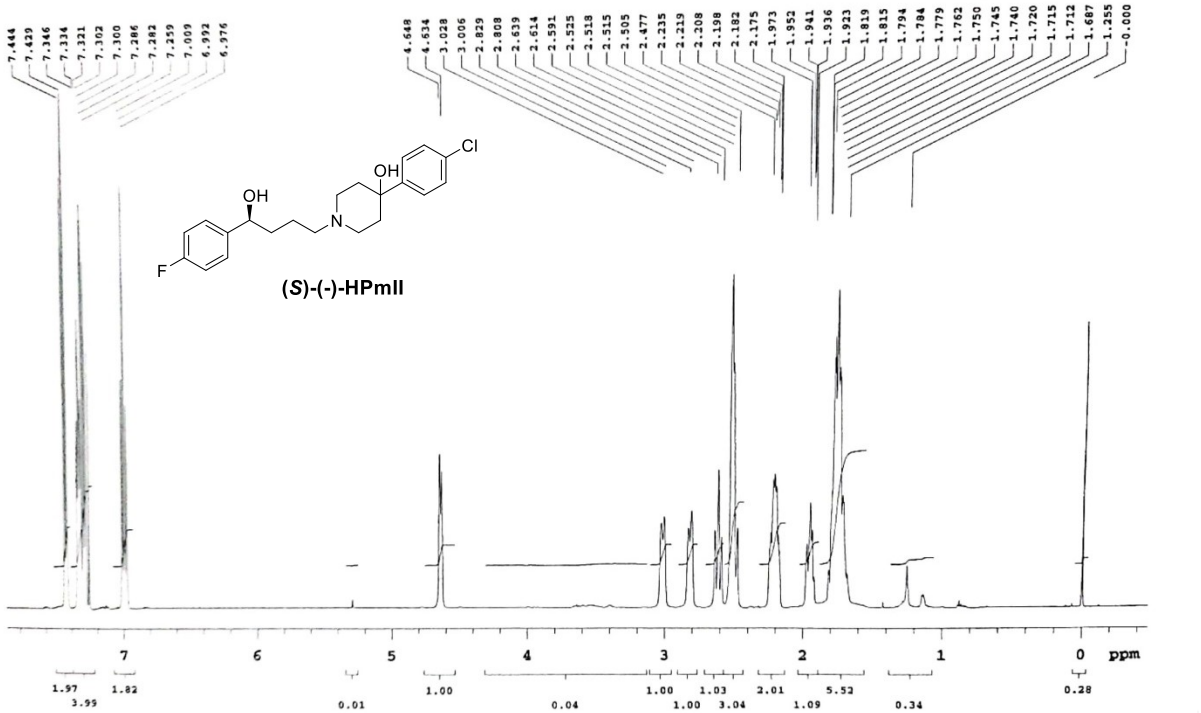

^{1}H NMR (500 MHz, DMSO-d_6) for (*R*)-(+)-4-[(4-clorophenyl)-4-hidrosxypiperidin-1-il]-1-(4-fluorophenyl) butil-2-propylpentanoate, (*R*)-(+)-MRJF22(oxalate)

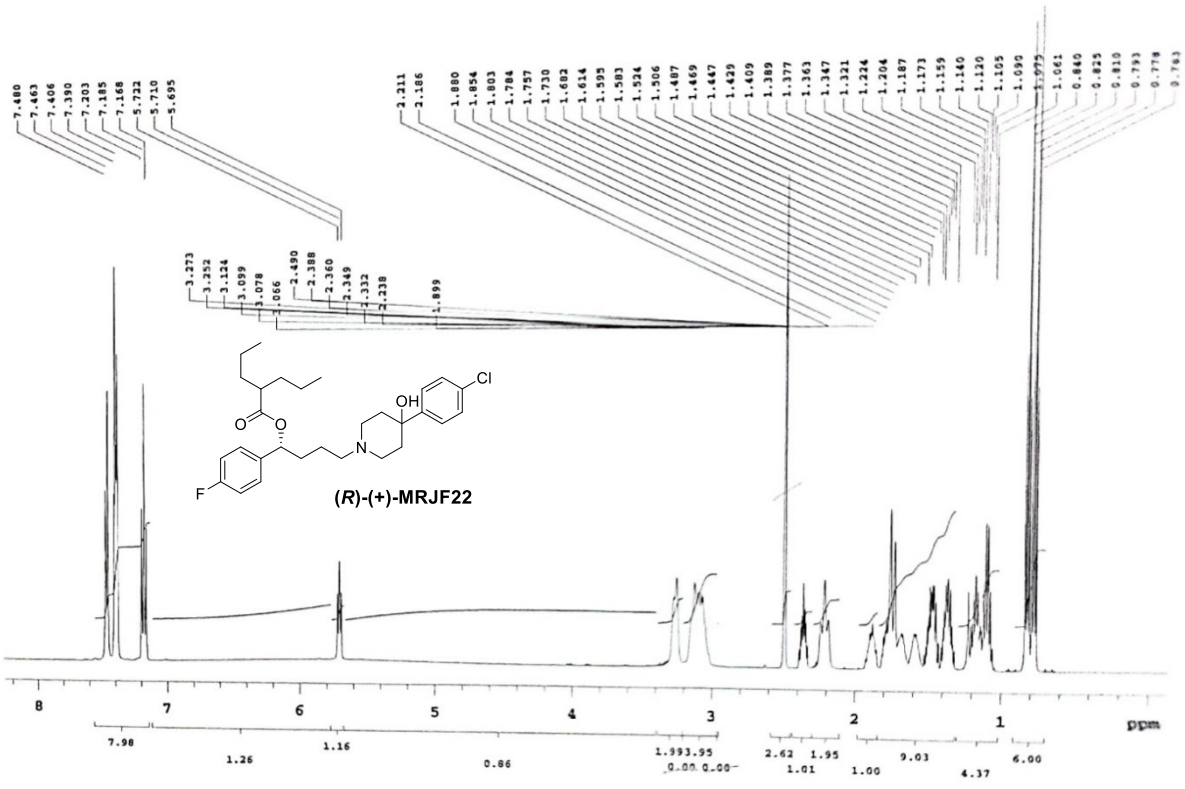

^{13}C NMR-APT (500 MHz, DMSO-d_6) for (*R*)-(+)-4-[(4-clorophenyl)-4-hidrosxypiperidin-1-il]-1-(4-fluorophenyl) butil-2-propylpentanoate, (*R*)-(+)-MRJF22(oxalate)

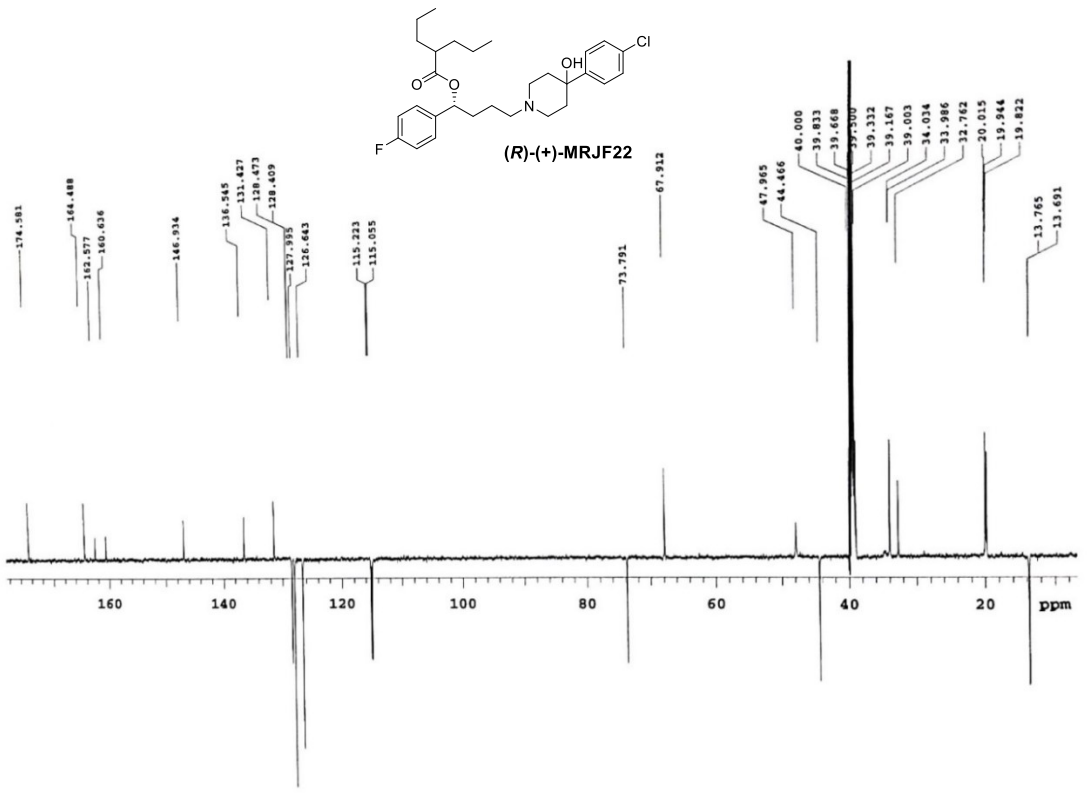

^{1}H NMR (500 MHz, DMSO-d_6) for (*S*)-(-)-4-[(4-clorophenyl)-4-hidrosxypiperidin-1-il]-1-(4-fluorophenyl) butil-2-propylpentanoate, (*S*)-(-)-MRJF22

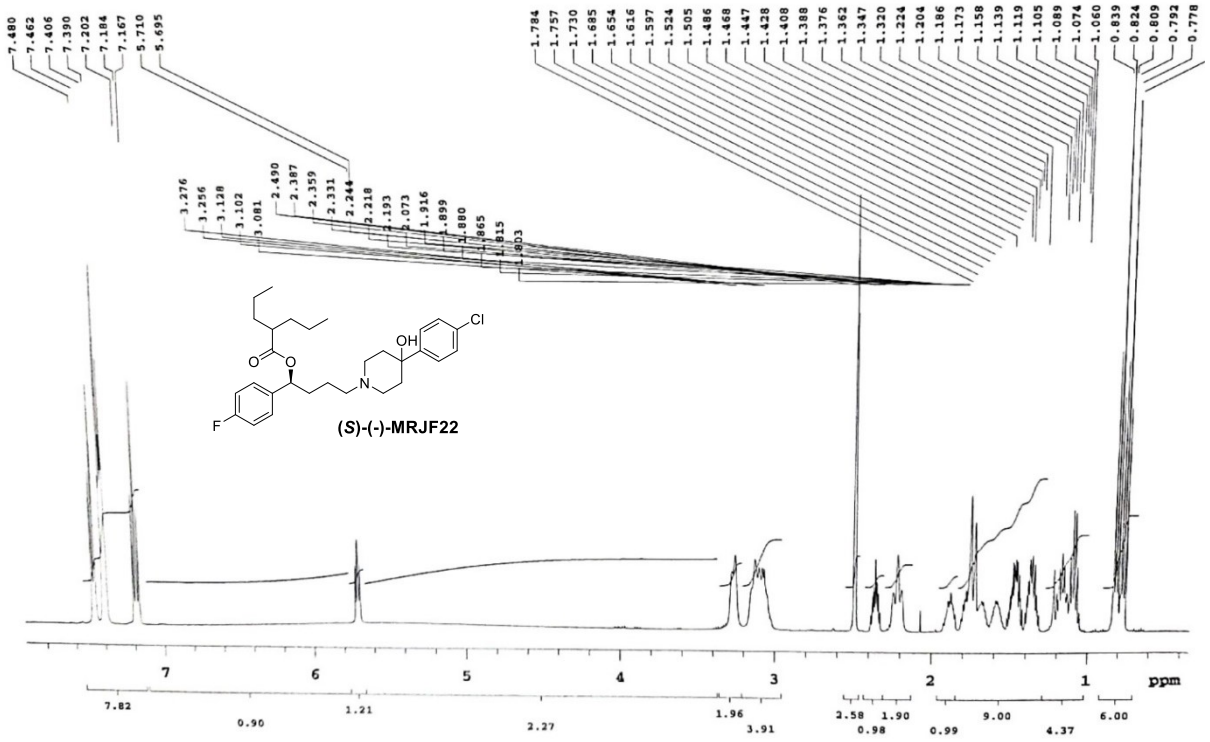

^{13}C NMR-APT (500 MHz, DMSO-d_6) for (*S*)-(-)-4-[(4-clorophenyl)-4-hidrosxypiperidin-1-il]-1-(4-fluorophenyl) butil-2-propylpentanoate, (*S*)-(-)-MRJF22

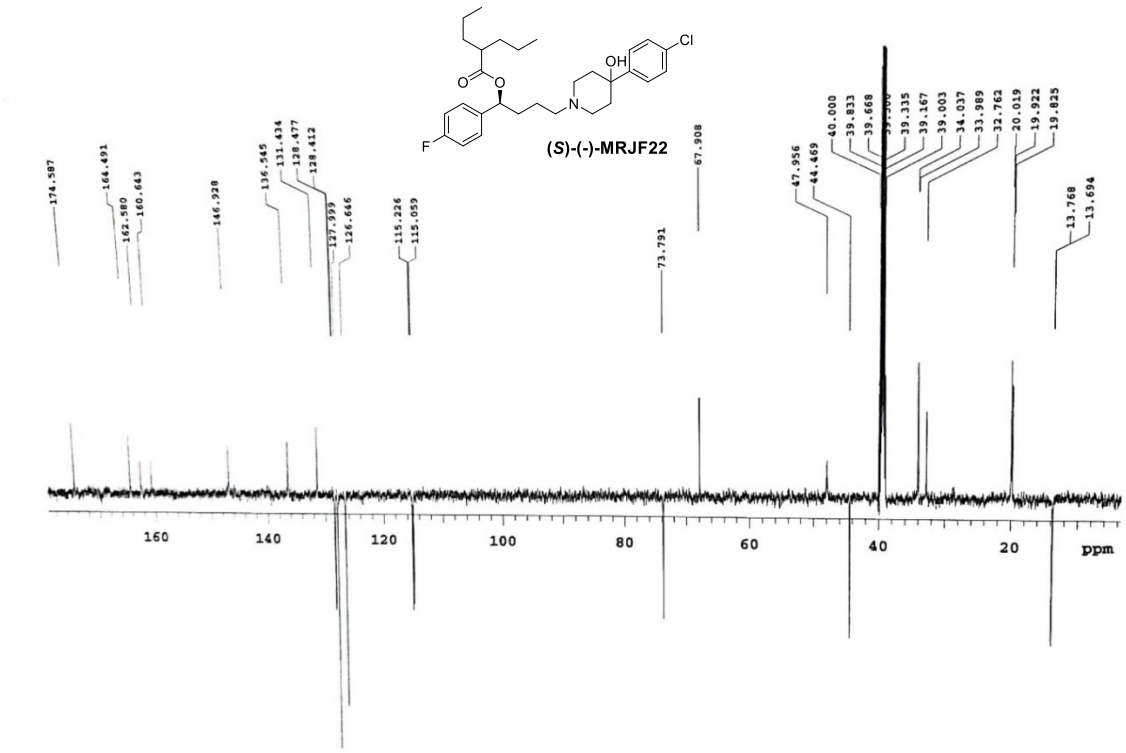

Development of Sigma/HDAC prodrugs

Supplemental materials - Experimental section

General details. Reagent grade chemicals were purchased from Sigma-Aldrich (St. Louis, MO, USA) or TCI (Tokio, Japan) and were used without further purification. All reactions involving air-sensitive reagents were performed under N2 in oven-dried glassware using the syringe-septum cap technique. All reactions were monitored by thin-layer chromatography (TLC) which was performed on silica gel Merck 60 F254 plates; the spots were visualized by UV light (λ = 254 and 366 nm) and iodine chamber. Melting points were determined on a Büchi B-450 apparatus in glass capillary tubes and are uncorrected. Flash chromatography purification was performed on a Merck silica gel 60, 0.040−0.063 mm (230−400 mesh), stationary phase using glass columns with a diameter between 1 and 4 cm. Nuclear magnetic resonance spectra (^{1}H NMR and ^{13}C NMR recorded at 500 MHz) were obtained on Varian INOVA spectrometers using $CDCl_3$ e DMSO-d_6 with a 0.03% of TMS as internal standard. Coupling constants (J) are reported in hertz. Signal multiplicities are characterized as s (singlet), d (doublet), t (triplet), q (quartet), m (multiplet), br (broad), app (apparent). Purities of all compounds was determined by microanalysis (C, H, N) that was performed on a Carlo Erba instrument model E1110; all the results agreed within ±0.4% of the theoretical values. Compound nomenclatures were generated with ChemBioDraw Ultra version 16.0.0.82.

General procedure for nucleophilic substitution

To a solution of 4-(4-chlorophenyl)-4-hydroxypiridine (1g, 4.7 mmol) in ACN was added K_2CO_3 (0.974 g, 7.05 mmol) and 2-bromoethanol,3-bromopropanolo or 4-bromobutanolo (4.7 mmol) dropwise. The reaction mixture was stirred under reflux for 4 hours. Then, the solvent was evaporated and saturated solution $NaHCO_3$ was added. The aqueous phase was extracted with CH_2Cl_2 (3x50 ml), the collected organic phases dried over anhydrous Na_2SO_4, filterd and evaporated to dryness. The residue obtained was purified by flash chromatography on silica gel to afford the desired product.

4-(4-chlorophenyl)-1-(2-hydroxyethyl)piperidin-4-ol (1a)

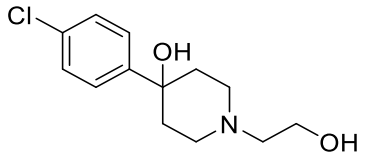

The compound has been prepared using 4-(4-chlorophenyl)-4-hydroxypiridine (1 g, 4.7 mmol) and 2-bromoethanol (335 µl, 4,7 mmol) following the general procedure. The residue has been purified by flash chromatography on silica gel eluting with an eluent mixture CH_2Cl_2/MeOH/NH_4OH (90-10-2%). Compound **1a** was obtained as yellow oil (0.868 g, 72% yield).

Chemical Formula: $C_{13}H_{18}ClNO_2$ (255.74 g/mol)

^{1}H NMR (300 MHz, $CDCl_3$) δ 7.50 – 7.21 (m, 4H), 3.61 (br s, 2H), 3.35 (s, 2H), 2.77 (d, J = 10.5 Hz, 2H), 2.56 (dd, J = 12.6, 9.3 Hz, 4H), 2.04 (t, J = 11.6 Hz, 2H), 1.70 (d, J = 13.6 Hz, 2H).

^{13}C NMR (50 MHz, $CDCl_3$) δ 146.92, 133.08, 128.64, 126.30, 71.00, 59.66, 58.04, 49.43, 38.52.

4-(4-chlorophenyl)-1-(3-hydroxypropyl)piperidin-4-ol (1b)

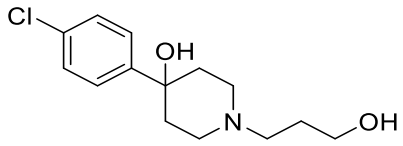

The compound has been prepared using 4-(4-chlorophenyl)-4-hydroxypiridine (1 g, 4.7 mmol) and 3-bromopropanol (408 µl, 4,7 mmol) following the general procedure. The residue obtained has been purified by flash chromatography on silica gel eluting with an eluent mixture CH_2Cl_2/MeOH/NH_4OH (90-10-2%). Compound **1b** was obtained as yellow oil (1 g, 79% yield).

Chemical Formula: $C_{14}H_{20}ClNO_2$ (269.77 g/mol)

^{1}H NMR (400 MHz, $CDCl_3$) δ 7.38 - 7.30 (m, 2H), 7.25 - 7.18 (m, 2H), 3.71 (t, *J*= 8.0 Hz, 2H), 2.89 (d, *J*= 8.0 Hz, 2H), 2.63 (t, *J*= 8.0 Hz, 2H), 2.44 (td, 2H), 1.99 (td, *J*= 4.0, 12.0 Hz, 2H), 1.72 - 1.63 (m, 4H).

^{13}C NMR (100 MHz, $CDCl_3$) δ 146.62, 133.04, 128.55, 126.29, 70.77, 64.46, 58.89, 49.65, 38.34, 27.34.

4-(4-chlorophenyl)-1-(4-hydroxybutyl)piperidin-4-ol (1c)

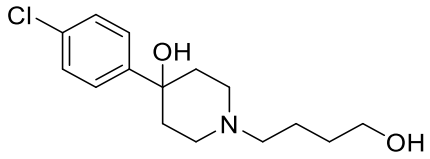

The compound has been prepared using 4-(4-chlorophenyl)-4-hydroxypiridine (1 g, 4.7 mmol) and 4-bromobutanol (0.719 g, 4.7 mmol) following the general procedure. The residue obtained has been purified by flash chromatography on silica gel eluting with an eluent mixture CH_2Cl_2/MeOH/NH_4OH (90-10-2%). Compound **1c** was obtained as white solid (0.746 g, 56% yield).

Chemical Formula: $C_{15}H_{22}ClNO_2$ (283.80 g/mol)

^{1}H NMR (200 MHz, $CDCl_3$) δ 7.54 - 7.43 (m, 2H), 7.35 - 7.25 (m, 2H), 3.62 - 3.54 (m, 2H), 2.89 (d, *J*= 12.0 Hz, 2H), 2.65 - 2.40 (m, 4H), 2.16 (td, *J* = 6.0, 12.0 Hz, 2H), 1.85 - 1.65 (m, 6H)

^{13}C NMR (50 MHz, $CDCl_3$) δ 146.64, 132.75, 128.33, 126.16, 70.70, 62.63, 58.50, 49.15, 37.90, 32.74, 25.83.

General procedure for esterification

To a solution of **1a-c** (1.564 mmol) in THF was added DMAP (1.564 mmol) and butanoyl chloride, 4-phenylbutanoyl or 2-propylvaleryl (3.128 mmol) dropwise. The reaction mixture was left to stir under N_2 at room temperature for 24 hours. Then, the reaction mixture was quenched with a saturated solution $NaHCO_3$ and extracted with EtOAc (3 x 50 ml). The organic layer was dried over Na_2SO_4, filtered and concentrated in vacuo. The crude product was purified by column chromatography on silica gel to afford the desired product. After purification, all the pure final product were dissolved in EtOAc/Et_2O and added to a solution of anhydrous oxalic acid in EtOAc/Et_2O dropwise to obtain the desired product as hydrochloride salt (white solid)

2-(4-(4-chlorophenyl)-4-hydroxypiperidin-1-yl)ethyl butyrate (2a)

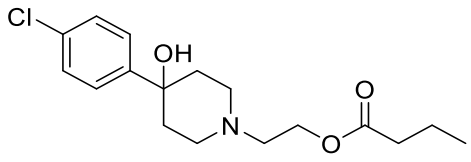

The compound has been prepared using intermediate **1a** (0.400 g, 1.564 mmol) and butanoyl chloride (327 µl, 3.128 mmol) following procedure B. The residue obtained has been purified by column chromatography on

silica gel using a gradient elution with EtOAc/EtOH. Compound **2a** was obtained as colorless oil (0.302 g, 59% yield) and converted as oxalic acid salt (white solid).

Chemical Formula: $C_{17}H_{24}ClNO_3 \cdot (COOH)_2$ (415.87 g/mol)

m.p: 155.0-156.0 °C

^{1}H NMR (free base): (500 MHz, $CDCl_3$) δ 7.46-7.40 (m, 2H), 7.35-7.25 (m, 2H), 4.24 (t, *J*=6.0 Hz, 2H), 2.85-2.80 (m, 2H), 2.70 (t, *J*=6.0 Hz, 2H), 2.61-2.48 (td, *J*=4.0, 12 Hz, 2H), 2.31 (t, *J*=8.0 Hz, 2H) , 2.19-2.04 (td, *J*=4.0, 12 Hz, 2H), 1.85 (br s, OH), 1.74-1.56 (m, 4H), 0.95 (t, *J*=8.0 Hz, 3H).

^{13}C NMR (free base): (125 MHz, $CDCl_3$) δ 173.67, 146.81, 132. 76, 128.76, 126.07, 70.81, 61.73, 56.77, 49.58, 38.34, 36.18, 18.42, 13.56.

Exact mass: Anal. calcd: C, 55.24; H, 6.32; N, 3.52.
Found: C, 54.88; H, 6.30; N, 3.37.

3-(4-(4-chlorophenyl)-4-hydroxypiperidin-1-yl)propyl butyrate (2b)

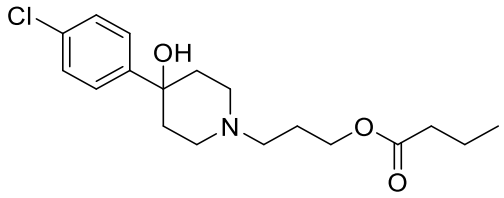

The compound has been prepared using intermediate **1b** (0,400 g, 1,48 mmol) and butanoyl chloride (316 µl, 2.96 mmol) following procedure B. The residue obtained has been purified by column chromatography on silica gel using a gradient elution with EtOAc/EtOH. Compound **2b** was obtained as colorless oil (0.411 g, 81% yield) and converted as oxalic acid salt (white solid).

Chemical Formula: $C_{18}H_{26}ClNO_3 \cdot (COOH)_2$ (429.89 g/mol)

m.p: 191.5-191.5 °C

^{1}H NMR (oxalate): (500 MHz, DMSO-d_6) δ 7.51-7.36 (m, 4H), 5.30 (br s, 3H), 4.07 (t, *J*=6.0 Hz, 2H), 3.13-3.07 (m, 2H), 2.93-2.81 (m,4H), 2.28 (t, *J*=6.0 Hz, 2H), 2.17-2.05 (m, 2H), 1.94 (m, 2H), 1.99-1.88 (m, 2H), 1.72-1.49 (m, *J*=6.0 Hz, 4H), 0.88 (t, *J*=6.0 Hz, 2H).

^{13}C NMR (oxalate): (125 MHz, DMSO-d_6) δ 172.78, 164.01, 147.81, 131.19, 127.92, 126.75, 66.532, 61.574, 53.39, 48.45, 24.25, 17.90, 13.44.

Exact mass: Anal. calcd: C, 55.99; H, 6.32; N, 3.22.
Found: C, 55.88; H, 6.78; N, 3.26.

4-(4-(4-chlorophenyl)-4-hydroxypiperidin-1-yl)butyl butyrate (2c)

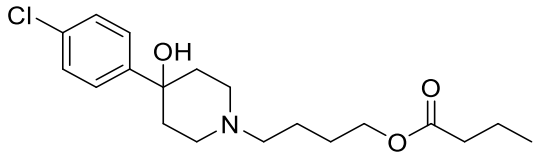

The compound has been obtained using **1c** (0.300 g, 1.06 mmol) and butanoyl chloride (225 µl, 2.11 mmol) following procedure B. The residue obtained has been purified by column chromatography on silica gel using a gradient elution with EtOAc/EtOH. Compound **2c** was obtained as colorless oil (0.218 g, 58% yield) and converted as oxalic acid salt (white solid).

Chemical Formula: $C_{19}H_{28}ClNO_3 \cdot (COOH)_2$ (443.17 g/mol)
m.p: 98.5-100.5 °C

^{1}H NMR (oxalate)	(200 MHz, DMSO-d_6) δ 7.52-7-39 (m, 4H), 5.76 (br s, 3H), 4.04 (t, *J*=6.0 Hz, 2H), 3.37-3.32 (m, 2H), 3.22-3.04 (m, 4H), 2.32-2.20 (m, 4H), 1.79-1.45 (m, 8H), 0.88 (t, *J*= 8.0 Hz, 3H).
^{13}C NMR (oxalate)	(50 MHz, DMSO-d_6) δ 172.83, 164.89, 147.03, 131.46, 128.05, 126.71, 68.0, 63.02, 55.08, 47.99, 35.32, 34.77, 25.48, 20.36, 17.94, 13.46.
Exact mass	Anal. calcd: C, 56.51; H, 6.68; N, 3.22. Found: C, 56.82; H, 6.81; N, 3.16.

2-(4-(4-chlorophenyl)-4-hydroxypiperidin-1-yl)ethyl 4-phenylbutanoate (3a)

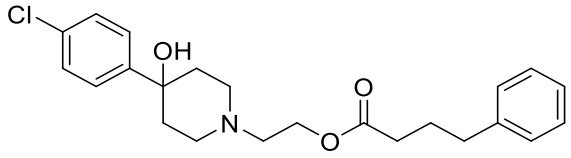

The product has been obtained using the intermediate **1a** (0.452 g, 1.77 mmol) and 4-phenylbutanoyl chloride (591 µl, 3.54 mmol) following procedure B. The crude product has been purified by column chromatography on silica gel using a gradient elution with EtOAc/EtOH. Compound **3a** was obtained as colorless oil (0.436 g, 61% yield) and converted as oxalic acid salt (white solid).

Chemical Formula: $C_{23}H_{28}ClNO_3 \cdot (COOH)_2$ (491.97 g/mol)
m.p: 148.0-150.0 °C

^{1}H NMR (free base)	(200 MHz, $CDCl_3$) δ 7.43- 7.16 (m, 9H), 4.23 (t, *J*=6.0 Hz, 2H), 2.85-2.79 (m, 2H), 2.72-2.62 (m, 4H), 2.59-2.46 (td, *J*=2.0, 12.0 Hz, 2H), 2.35 (t, *J*=8.0 Hz, 2H), 2.17-2.02 (td, *J*=4.0, 12.0 Hz, 2H), 1.96 (t, *J*=8.0 Hz, 2H), 1.73-1.66 (dd, *J*=2.0, 12.0 Hz, 2H).
^{13}C NMR (free base)	(50 MHz, $CDCl_3$) δ 173.46, 146.79, 141.35, 132.76, 128.47, 128.37, 126.05, 125.97, 70.84, 61.73, 56.78, 49.58, 38.36, 35.04, 33.60, 26.51.
Exact mass	Anal. calcd: C, 61.51; H, 6.28; N, 2.42. Found: C, 61.04; H, 6.15; N, 2.85.

3-(4-(4-chlorophenyl)-4-hydroxypiperidin-1-yl)propyl 4-phenylbutanoate (3b)

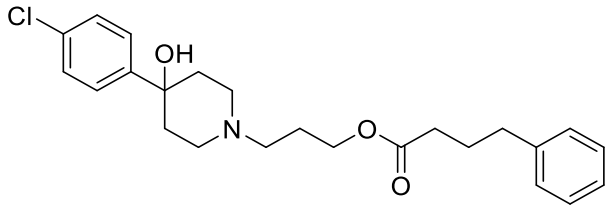

The product has been obtained using the intermediate **1b** (0.300 g, 1.11 mmol) in THF and 4-phenylbutanoyl chloride (371 µl, 2.22 mmol) following procedure B. The crude product was purified by column chromatography on silica gel using a gradient elution with EtOAc/EtOH. Compound **3b** was obtained as colorless oil (0.328 g, 70% yield) and converted as oxalic acid salt (white solid).

Chemical Formula: $C_{24}H_{30}ClNO_3 \cdot (COOH)_2$ (505.99 g/mol)
m.p: 131.5-132.5 °C

^{1}H NMR (free base)	(200 MHz, $CDCl_3$) δ 7.46-7.16 (m, 9H), 4.13 (t, *J*=6.0 Hz, 2H), 2.82-2.77 (m, 2H), 2.65 (t, *J*=8.0 Hz, 2H), 2.51-2.44 (m, 3H), 2.33 (t, *J*=6.0 Hz, 2H), 2.18-1.68 (m, 10H).
^{13}C NMR (free base)	(50 MHz, $CDCl_3$) δ 173.74, 147.01, 141.53, 132.94, 128.64, 128.57, 126.26, 126.15, 71.23, 63.01, 55.31, 49.47, 38.61, 35.29, 33.79, 29.68, 26.49.
Exact mass	Anal. calcd: C, 61.84; H, 6.28; N, 3.38. Found: C, 61.72; H, 6.37; N, 2.77.

4-(4-(4-chlorophenyl)-4-hydroxypiperidin-1-yl)butyl 4-phenylbutanoate (3c)

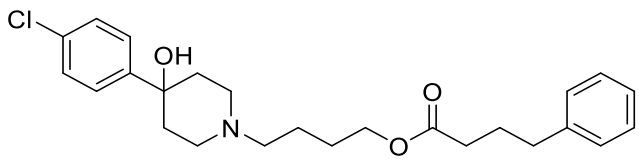

The product has been obtained using the intermediate **1c** (0.152 g, 0.53 mmol) and 4-phenylbutanoyl chloride (179 µl, 1.07 mmol) following procedure B. The crude product was purified by column chromatography on silica gel using a gradient elution with EtOAc/EtOH. Compound **3c** was obtained as colorless oil (0.177 g, 76% yield) and converted as oxalic acid salt (white solid).

Chemical Formula: $C_{25}H_{32}ClNO_3 \cdot (COOH)_2$ (520.02 g/mol)
m.p: 106.0-108.0 °C

^{1}H NMR (free base)	(200 MHz, $CDCl_3$) δ 7.46-7.16 (m, 9H), 4.09 (t, *J*=6.0 Hz, 2H), 2.84-2.79 (m, 2H), 2.65 (t, *J*=8.0 Hz, 2H), 2.47-2.42 (m, 2H), 2.32 (t, *J*=6.0 Hz, 2H), 2.24 (br s, OH), 2.19-2.03 (m, 2H), 1.98-1,87 (m, 4H), 1.74-1.56 (m, 6H).
^{13}C NMR (free base)	(50 MHz, $CDCl_3$) δ 173.57, 146.81, 141.36, 132.75, 128.45, 128.38, 126.07, 125.96, 71.03, 64.19, 58.16, 49.33, 35.13, 33.64, 26.72, 26.52, 23.41.
Exact mass	Anal. calcd: C, 62.59; H, 6.68; N, 2.88. Found: C, 62.36; H, 6.59; N, 2.69.

2-(4-(4-chlorophenyl)-4-hydroxypiperidin-1-yl)ethyl 2-propylpentanoate (4a)

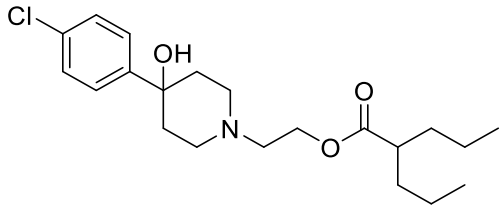

The product has been obtained using the intermediate **1a** (0.580 g, 2.27 mmol) and 2-propylvaleryl chloride (780 µl, 4.55 mmol) following procedure B. The crude product was purified by column chromatography on silica gel using a gradient elution with EtOAc/EtOH. Compound **4a** was obtained as colorless oil (0.458 g, 53% yield) and converted as oxalic acid salt (white solid).

Chemical Formula: $C_{21}H_{32}ClNO_3 \cdot (COOH)_2$ (471.98 g/mol)
m.p: 84.0-85.0 °C

^{1}H NMR (free base)	(200 MHz, $CDCl_3$) δ 7.49 - 7.38 (m, 2H), 7.36 - 7.23 (m, 2H), 4.25 (t, *J*= 6.0 Hz, 2H), 2.84 (d, *J*= 12.0 Hz, 2H), 2.70 (t, *J*= 6.0 Hz, 2H), 2.54 (m, 2H), 2.45 – 2.31 (m, 1H), 2.10 (td, *J*= 4.0, 12.0 Hz, 2H), 1.87 (s, 1H), 1.75 (m, 1H), 1.69 (m, 1H), 1.64 – 1.21 (m, 8H), 0.90 (t, *J*= 6.0 Hz, 6H).
^{13}C NMR (free base)	(50 MHz, $CDCl_3$) δ 176.63; 147.34; 133.01; 128.71; 126.27; 71.21; 61.49; 57.16; 49.73; 45.29; 38.32; 34.97; 20.84; 14.06.

Exact mass Anal. calcd: C, 58.65; H, 7.30; N, 2.52.
Found: C,58.53; H, 7.26; N, 2.97.

3-(4-(4-chlorophenyl)-4-hydroxypiperidin-1-yl)propyl 2-propylpentanoate (4b)

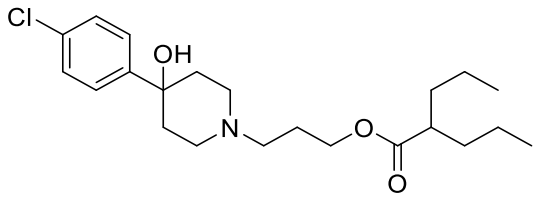

The product has been obtained using the intermediate **1b** (0.300 g, 1.11 mmol) and 2-propylvaleryl chloride (380 µl, 2.22 mmol) following procedure B. The crude product has been purified by column chromatography on silica gel using a gradient elution with EtOAc/EtOH. Compound **4b** was obtained as colorless oil (0.340 g, 87% yield) and converted as oxalic acid salt (white solid).

Chemical Formula: $C_{22}H_{34}ClNO_3 \cdot (COOH)_2$ (486.0 g/mol)
m.p: 127.0-133.0 °C
^{1}H NMR (oxalate) (500 MHz, DMSO-d_6) δ 7.50 - 7.48 (m, 2H), 7.42 - 7.40 (m, 2H), 4.09 (t, *J*=5.0 Hz, 2H), 3.32 (d, *J*=11.5 Hz, 2H), 3.16 (t, *J*=11.5 Hz, 2H), 3.08 (t, *J*=8.0 Hz, 2H), 2.38 - 2.32 (m, 1H), 2.26 - 2.19 (td, *J*=5.0, 15.0 Hz, 2H), 2.01 (m, 2H), 1.77 (d, *J*=10.0 Hz, 2H), 1.54 - 1.47 (m, 2H), 1.43 – 1.36 (m, 2H), 1.28 – 1.20 (m, 4H), 0.86 (t, *J*=5.0 Hz, 6H).
^{13}C NMR (oxalate) (125 MHz, DMSO-d_6) δ 175.33, 164.63, 146.98, 131.43, 127.99, 126.66, 67.93, 61.11, 48.14, 44.30, 34.85, 33.97, 23.35, 20.01, 13.81.
Exact mass Anal. calcd: C, 58.59; H, 7.70; N, 2.91.
Found: C,59.31; H, 7.47; N, 2.88.

4-(4-(4-chlorophenyl)-4-hydroxypiperidin-1-yl)butyl 2-propylpentanoate (4c)

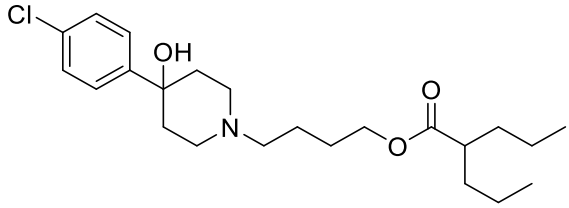

The product has been obtained using **1c** (0.706 g, 2.49 mmol) and 2-propylvaleryl chloride (850 µl, 4.97 mmol) following procedure B. The crude product was purified by column chromatography on silica gel using a

gradient elution with EtOAc/EtOH. Compound **4c** was obtained as colorless oil (0.458 g, 45% yield) and converted as oxalic acid salt (white solid).

Chemical Formula: $C_{23}H_{36}ClNO_3 \cdot (COOH)_2$ (500.03 g/mol)

m.p: 112.0-113.0 °C

^{1}H NMR (free base)	(200 MHz, $CDCl_3$) δ 11.12 (s, 1H), 7.41 - 7.28 (m, 2H), 7.26 - 7.14 (m, 2H), 4.04 - 3.95 (m,2H), 3.54 – 2.91 (m, 6H), 2.44 - 2.22 (m, 3H), 1.98 - 1.78 (m, 2H), 1.75 - 1.34 (m, 8H), 1.30 - 1.12 (m, 4H), 0.87 (t, *J*=4.0 Hz, 6H).
^{13}C NMR (free base)	(50 MHz, $CDCl_3$) δ 176.83; 163.55; 144.87; 133.48; 128.74; 126.23; 68.92; 62.87; 57.02; 49.11; 45.30; 35.34; 34.68; 26.10; 20.77; 20.70; 14.13.
Exact mass	Anal. calcd: C, 60.15; H, 7.30; N, 2.92. Found: C,60.05; H, 7.66; N, 2.80.

^{1}H and ^{13}C NMR spectra

^{1}H (300 MHz, $CDCl_3$) and ^{13}C (50 MHz, $CDCl_3$) for 4-(4-chlorophenyl)-1-(2-hydroxyethyl)piperidin-4-ol (1a)

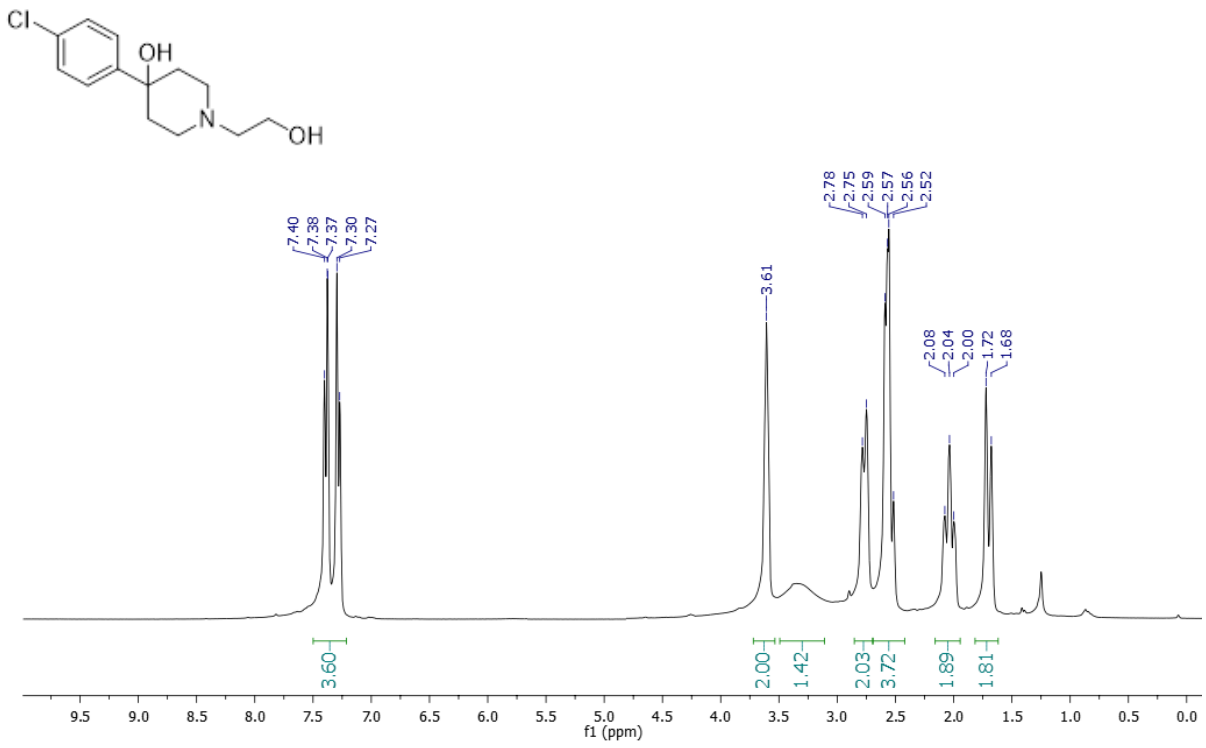

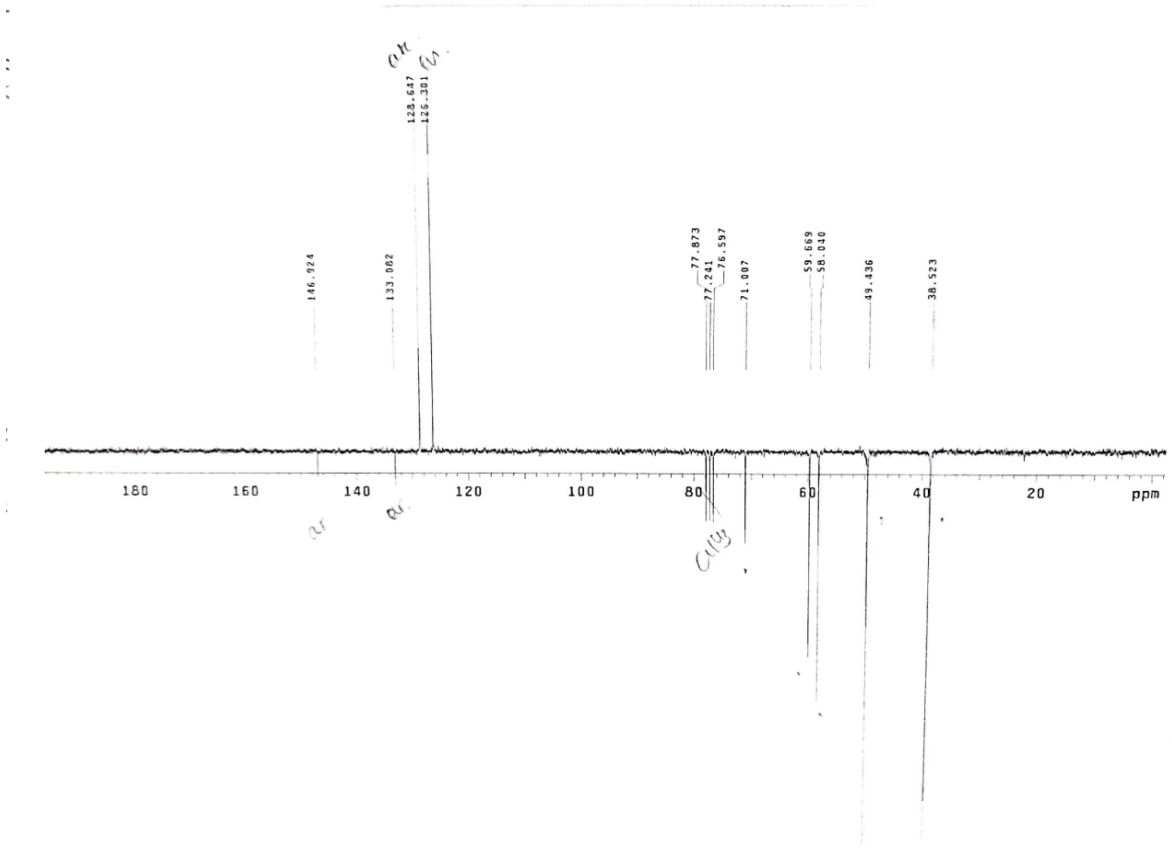

^{1}H (400 MHz, $CDCl_3$) and ^{13}C (100 MHz, $CDCl_3$) for 4-(4-chlorophenyl)-1-(3-hydroxypropyl)piperidin-4-ol (1b)

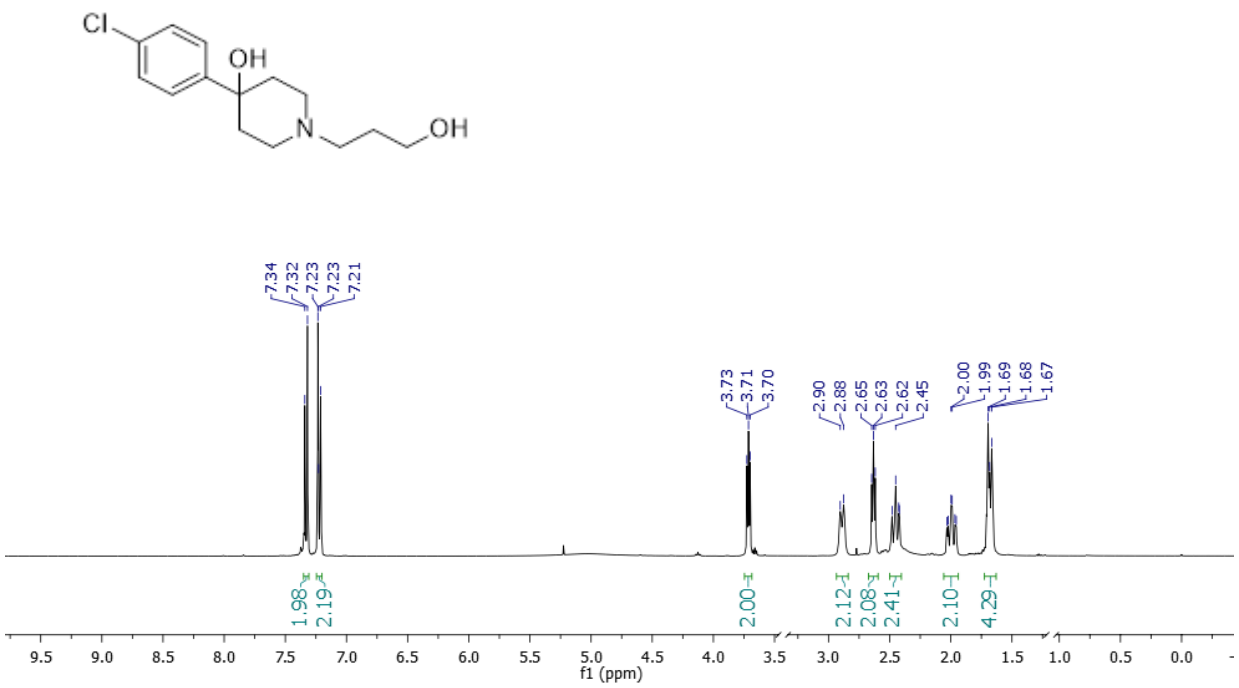

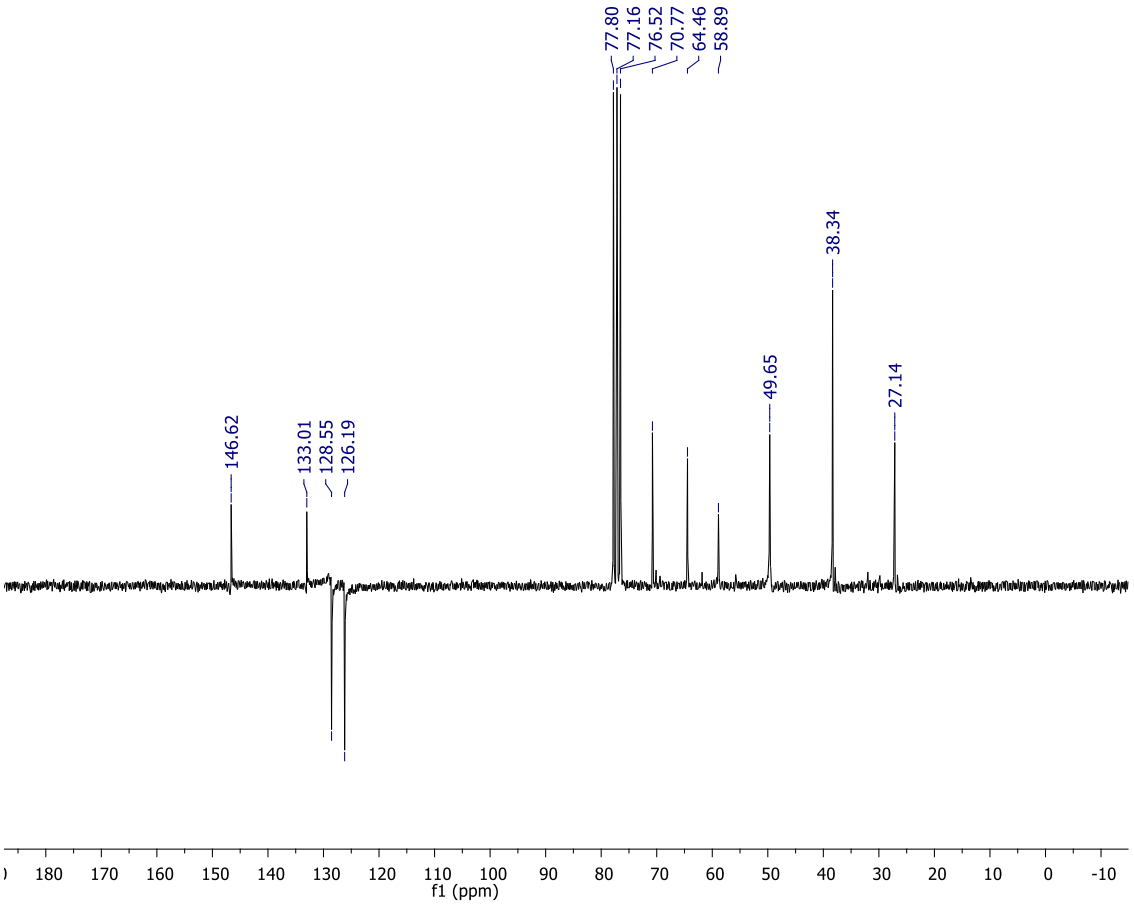

^{1}H (200 MHz, $CDCl_3$) and ^{13}C (50 MHz, $CDCl_3$) for 4-(4-chlorophenyl)-1-(4-hydroxybutyl)piperidin-4-ol (1c)

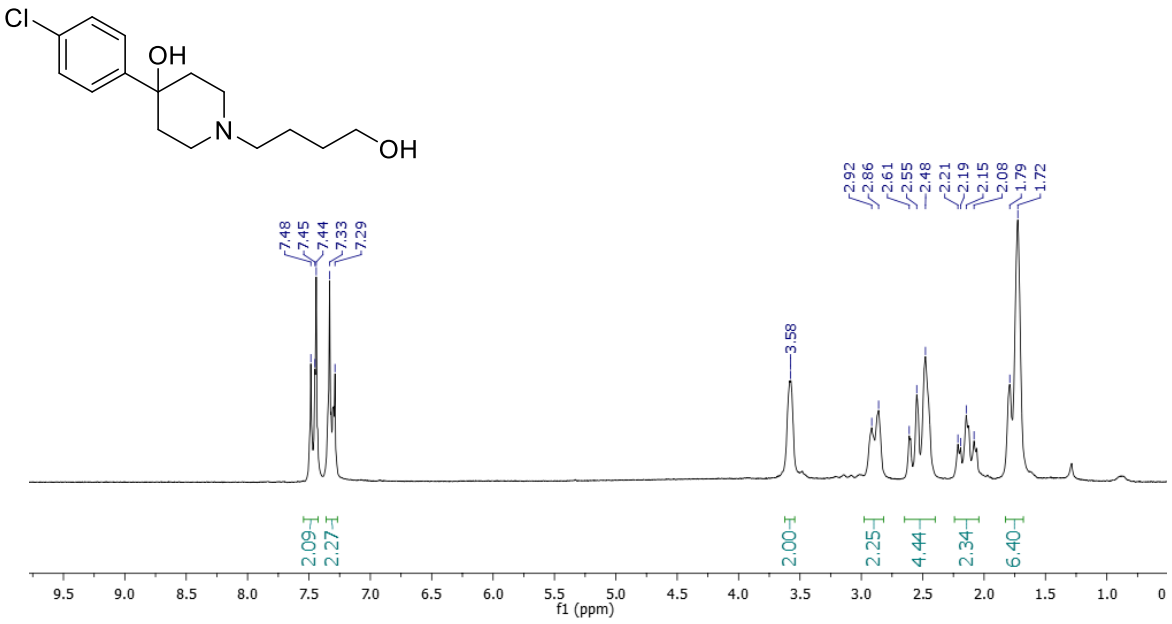

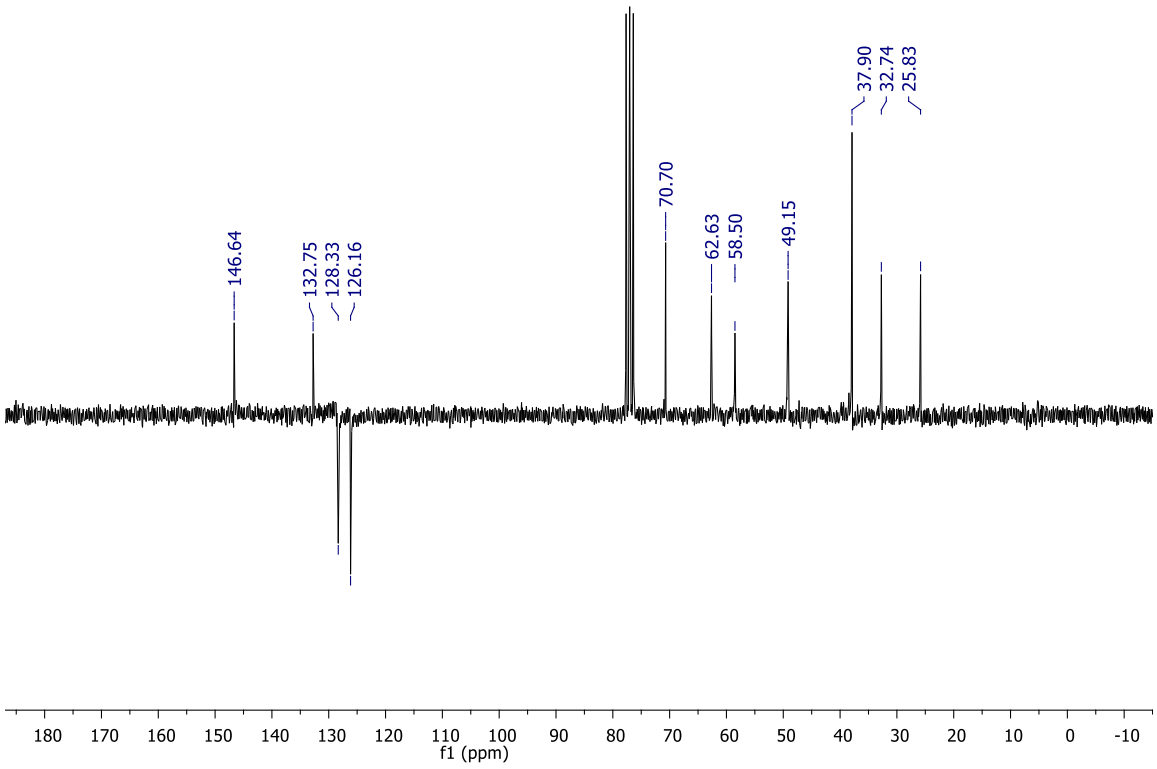

^{1}H (500 MHz, $CDCl_3$) and ^{13}C (125 MHz, $CDCl_3$) for 2-(4-(4-chlorophenyl)-4-hydroxypiperidin-1-yl)ethyl butyrate (2a)

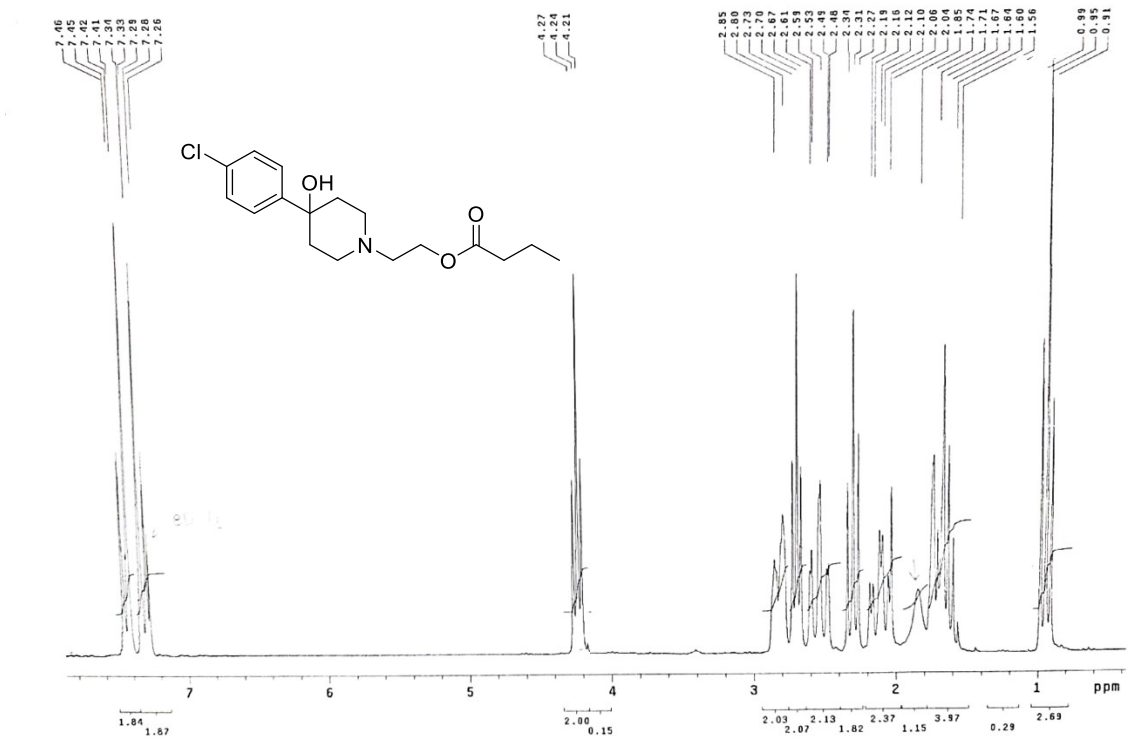

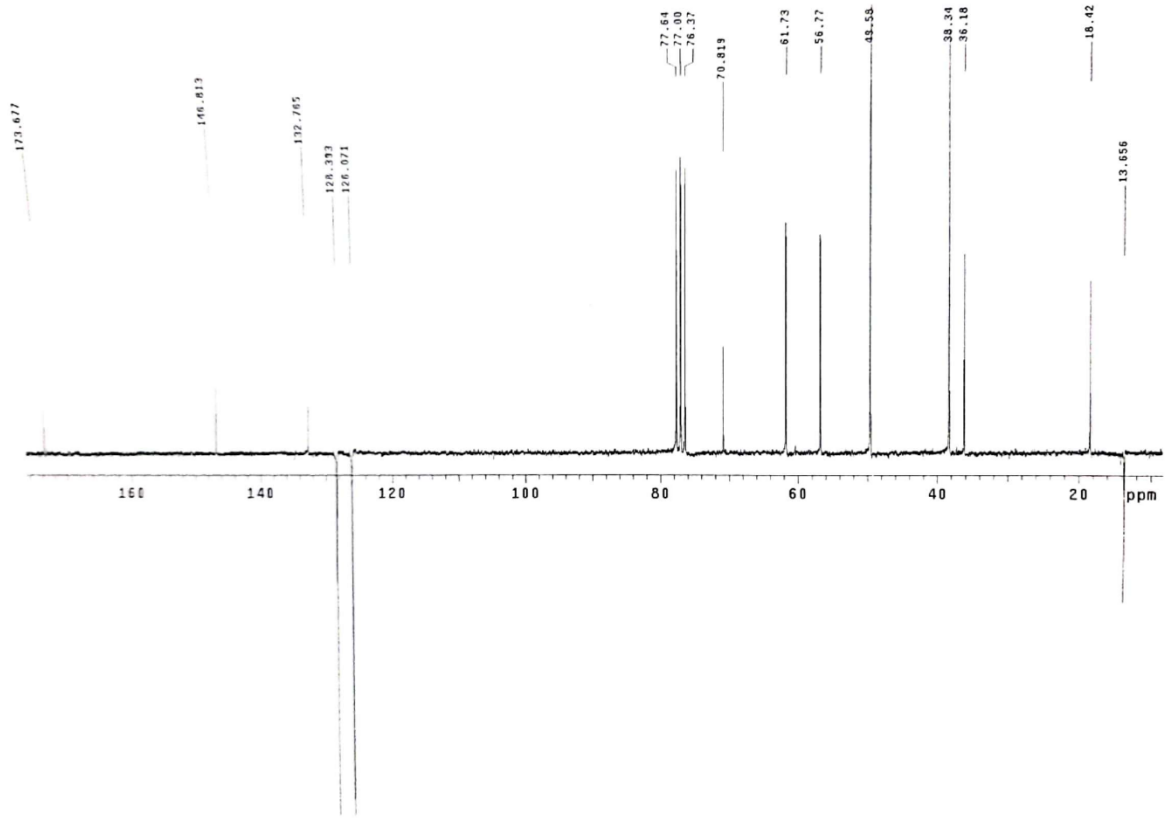

^{1}H (500 MHz, DMSO-d_6) and ^{13}C (125 MHz, DMSO-d_6) for 3-(4-(4-chlorophenyl)-4-hydroxypiperidin-1-yl)propyl butyrate-oxalate (2b)

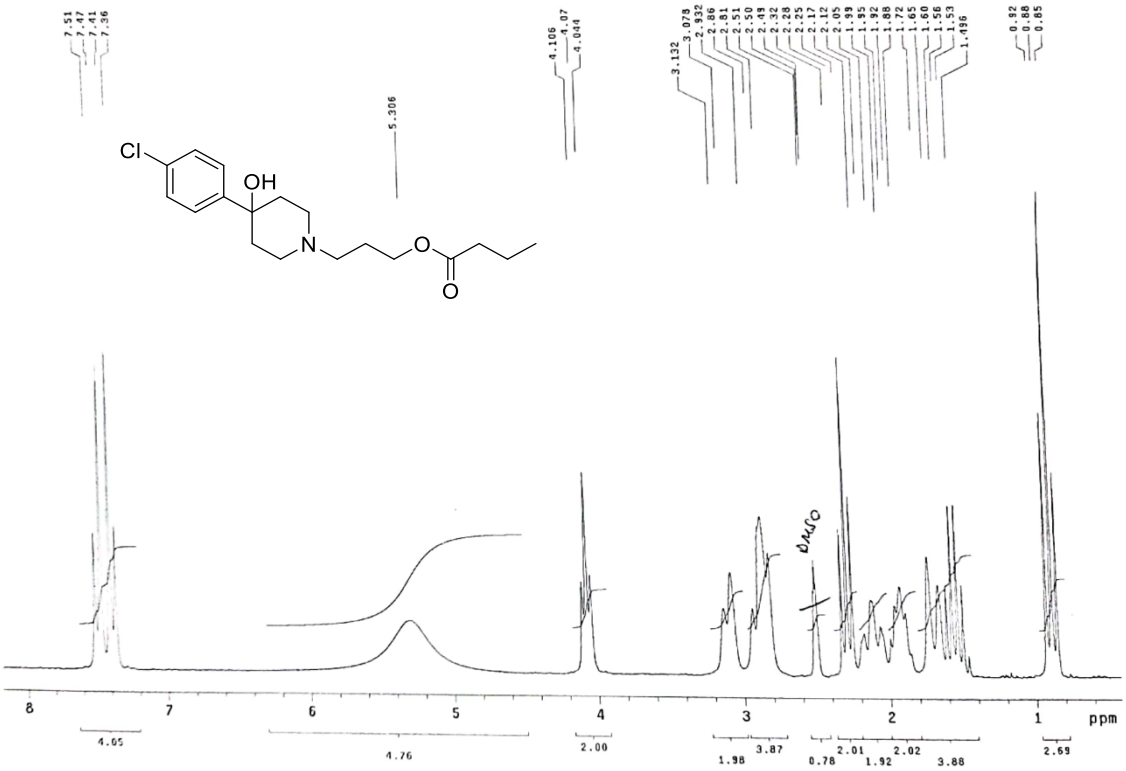

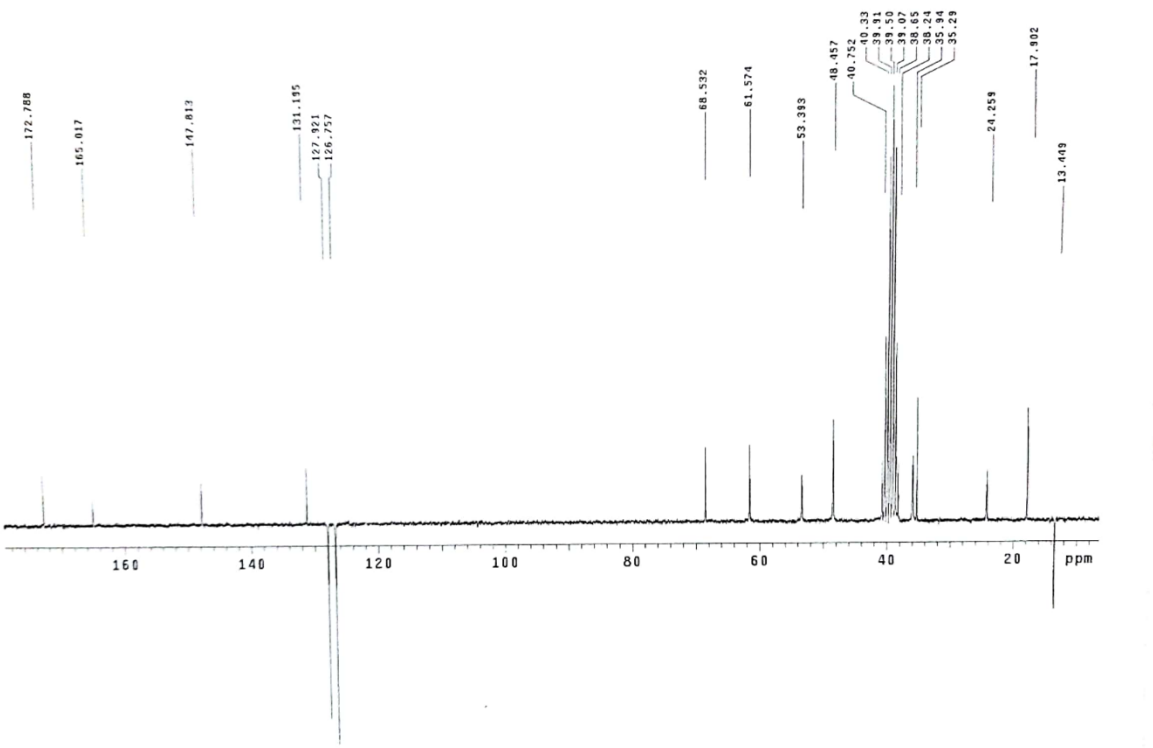

^{1}H (500 MHz, DMSO-d_6) and ^{13}C (125 MHz, DMSO-d_6) for 4-(4-(4-chlorophenyl)-4-hydroxypiperidin-1-yl)butyl butyrate-oxalate (2c)

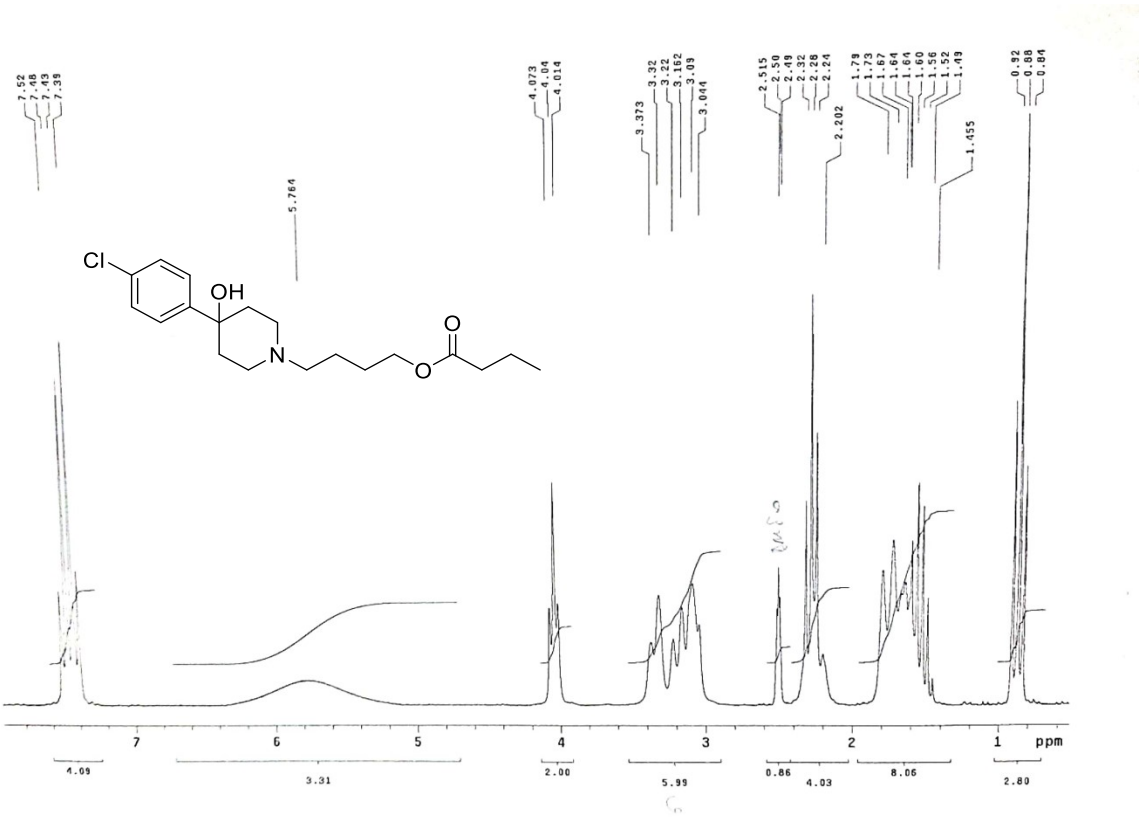

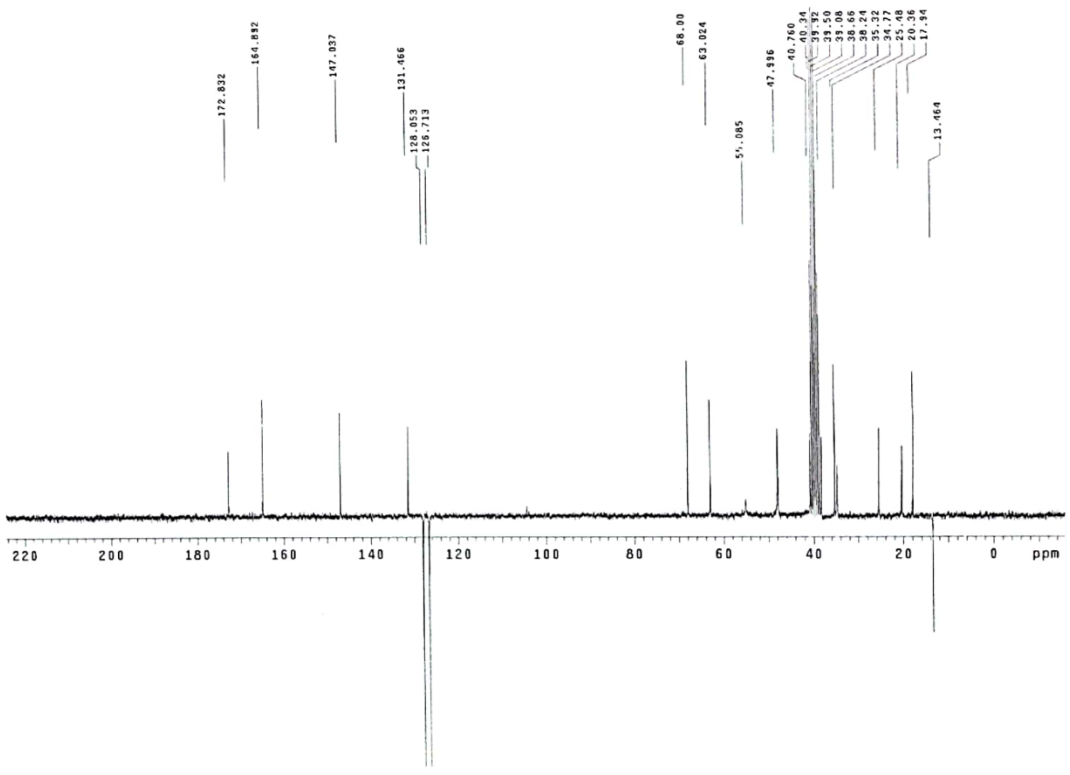

^{1}H (500 MHz, $CDCl_3$) and ^{13}C (125 MHz, $CDCl_3$) for 2-(4-(4-chlorophenyl)-4-hydroxypiperidin-1-yl)ethyl 4-phenylbutanoate (3a)

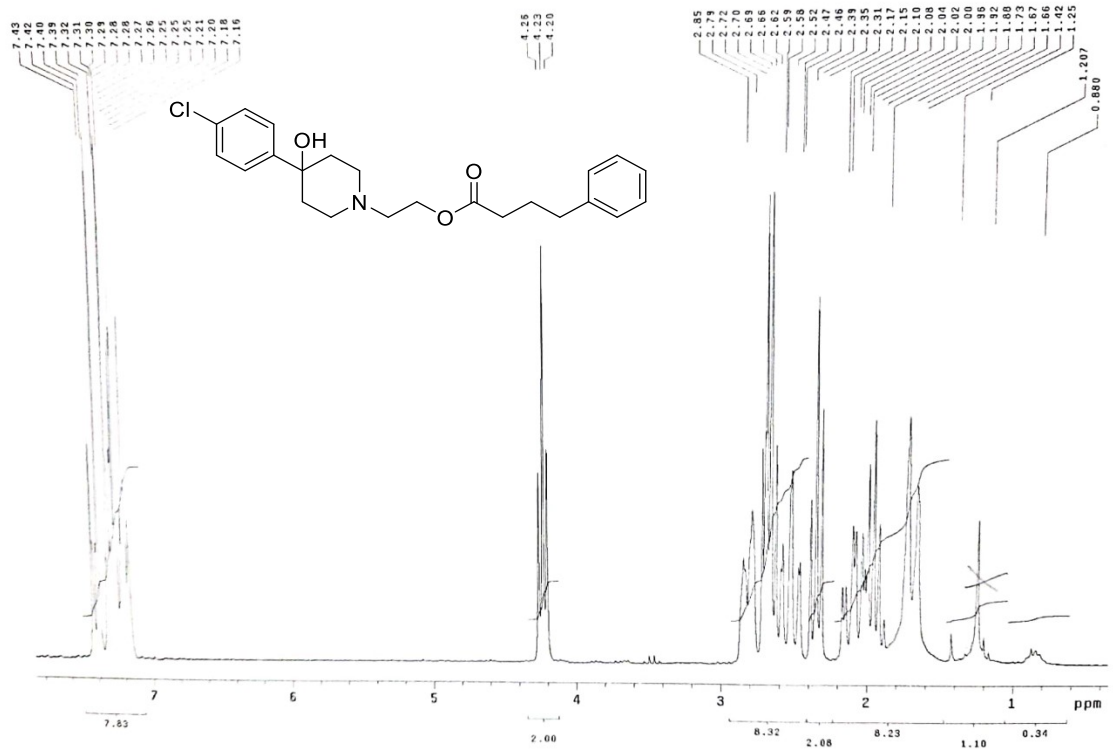

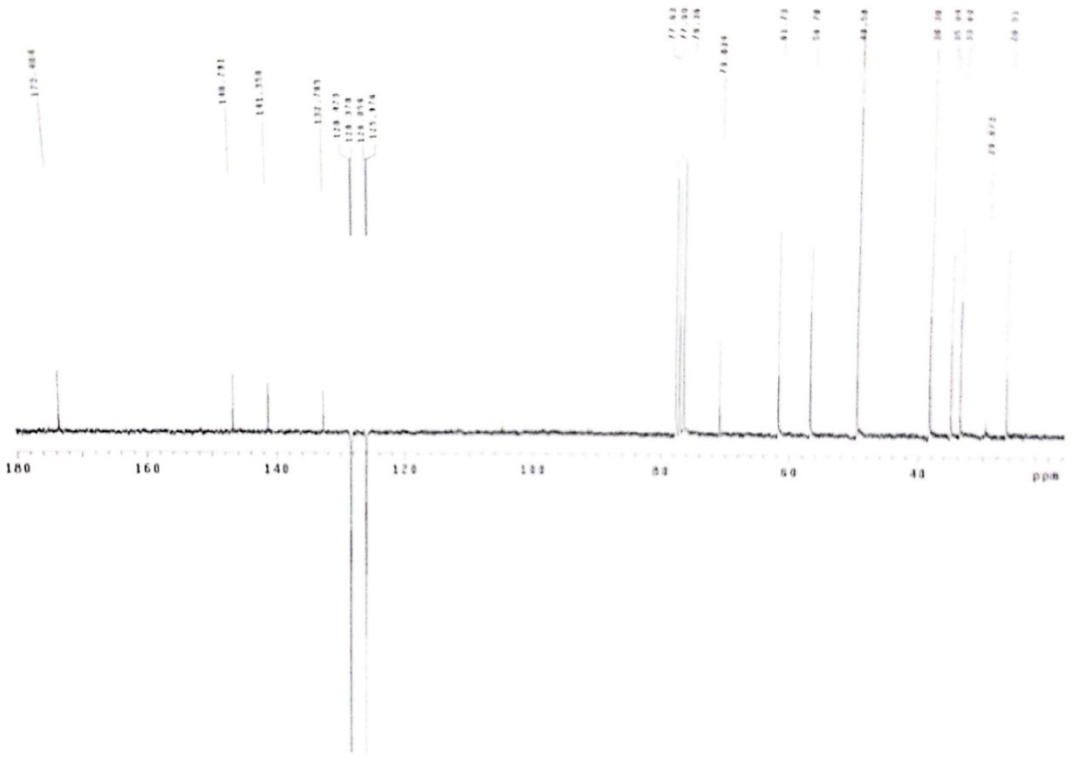

^{1}H (500 MHz, $CDCl_3$) and ^{13}C (125 MHz, $CDCl_3$) for 3-(4-(4-chlorophenyl)-4-hydroxypiperidin-1-yl)propyl 4-phenylbutanoate (3b)

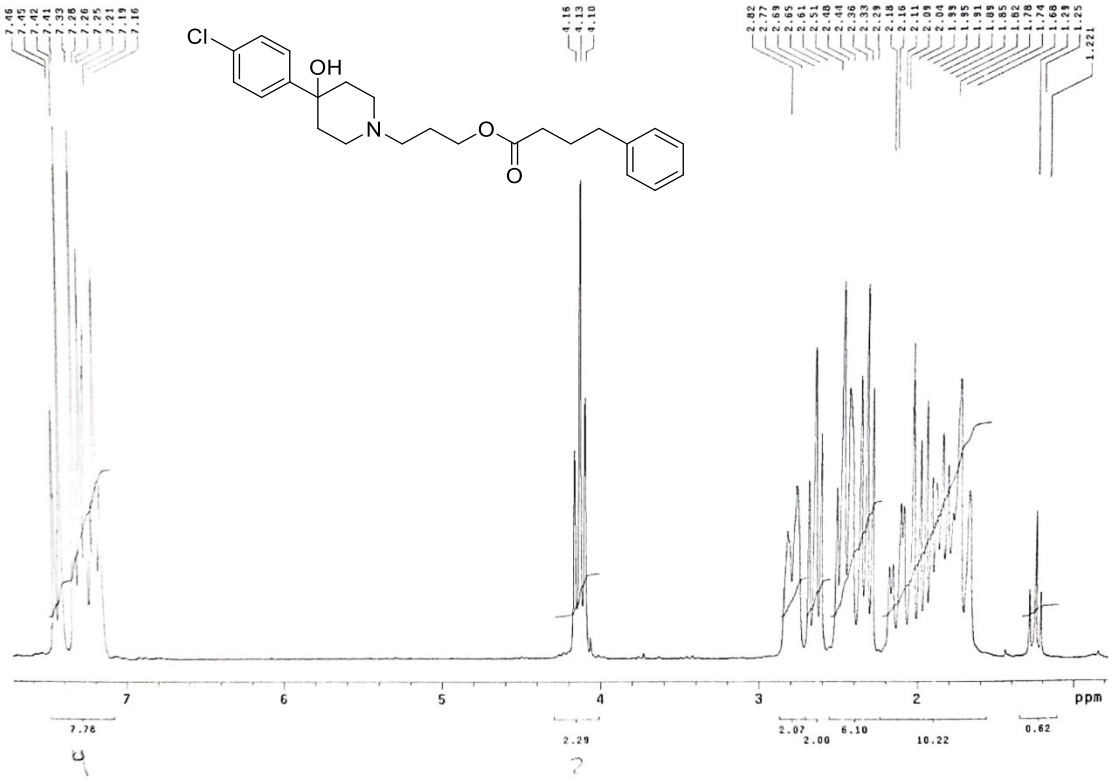

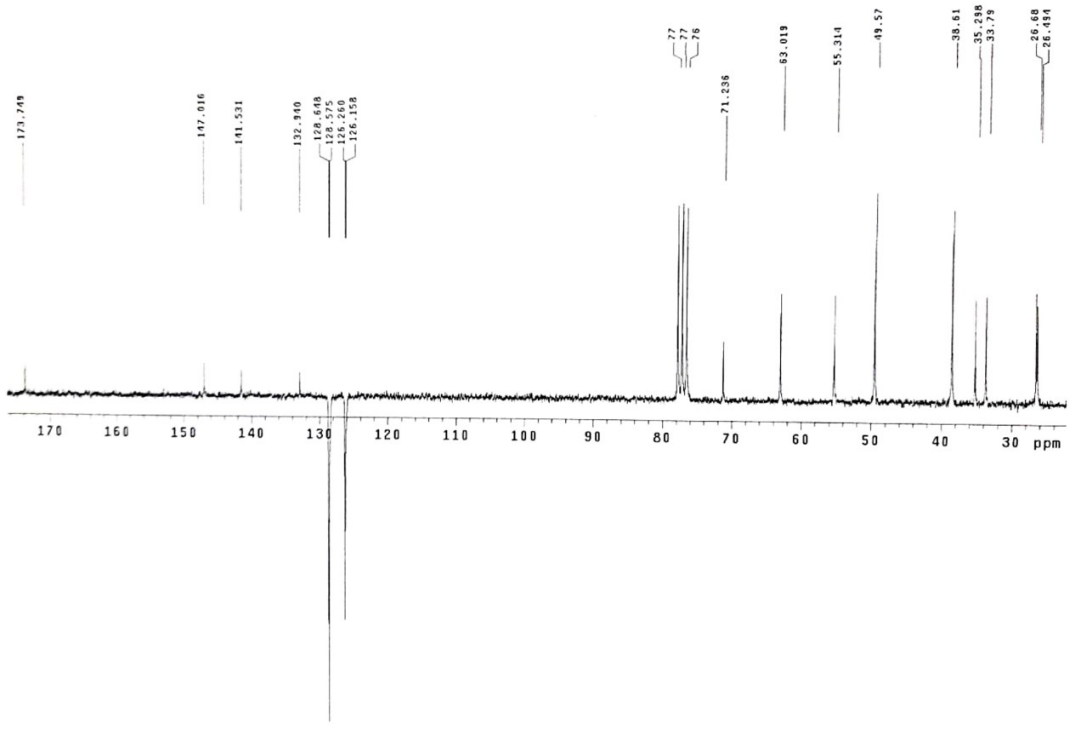

^{1}H (500 MHz, $CDCl_3$) and ^{13}C (125 MHz, $CDCl_3$) for 4-(4-(4-chlorophenyl)-4-hydroxypiperidin-1-yl)butyl 4-phenylbutanoate (3c)

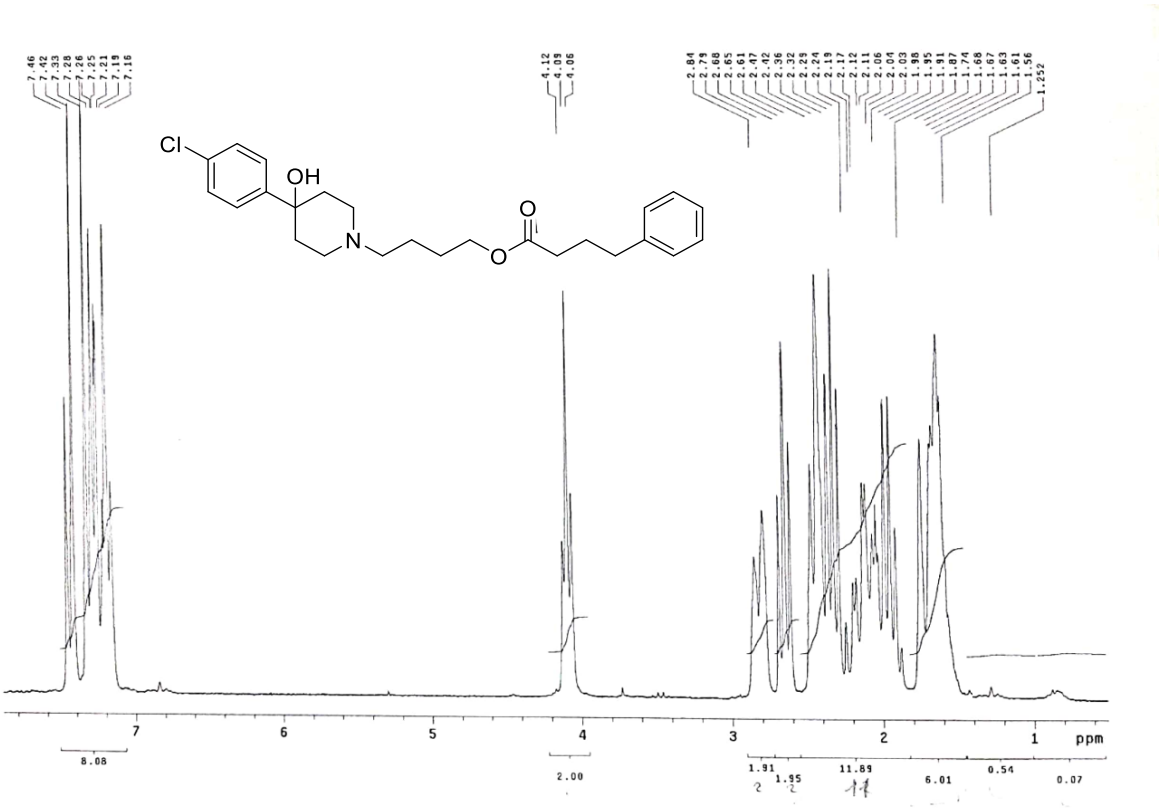

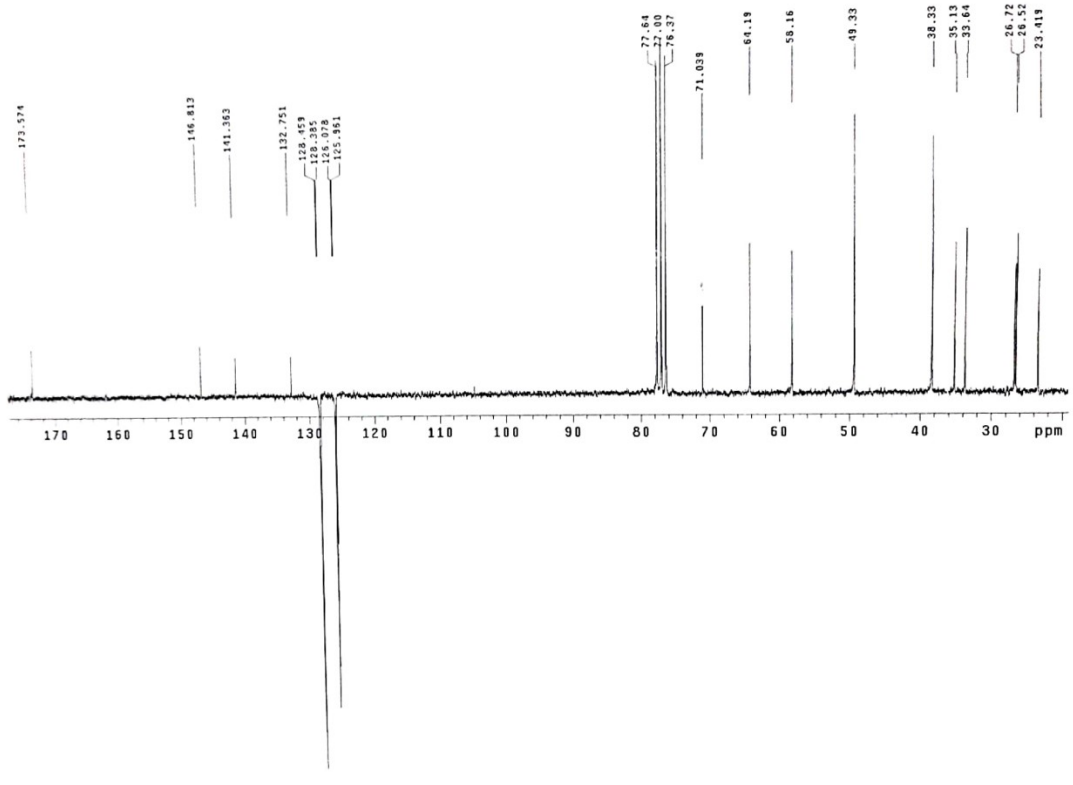

^{1}H (500 MHz, $CDCl_3$) and ^{13}C (125 MHz, $CDCl_3$) for 2-(4-(4-chlorophenyl)-4-hydroxypiperidin-1-yl)ethyl 2-propylpentanoate (4a)

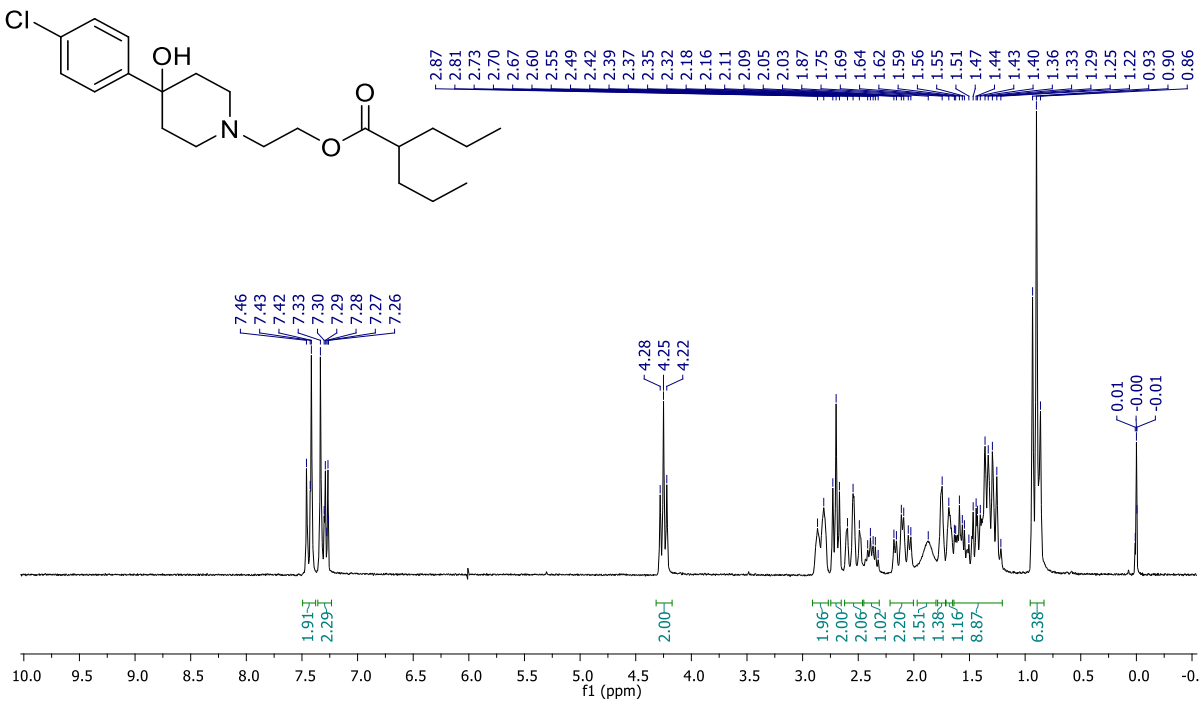

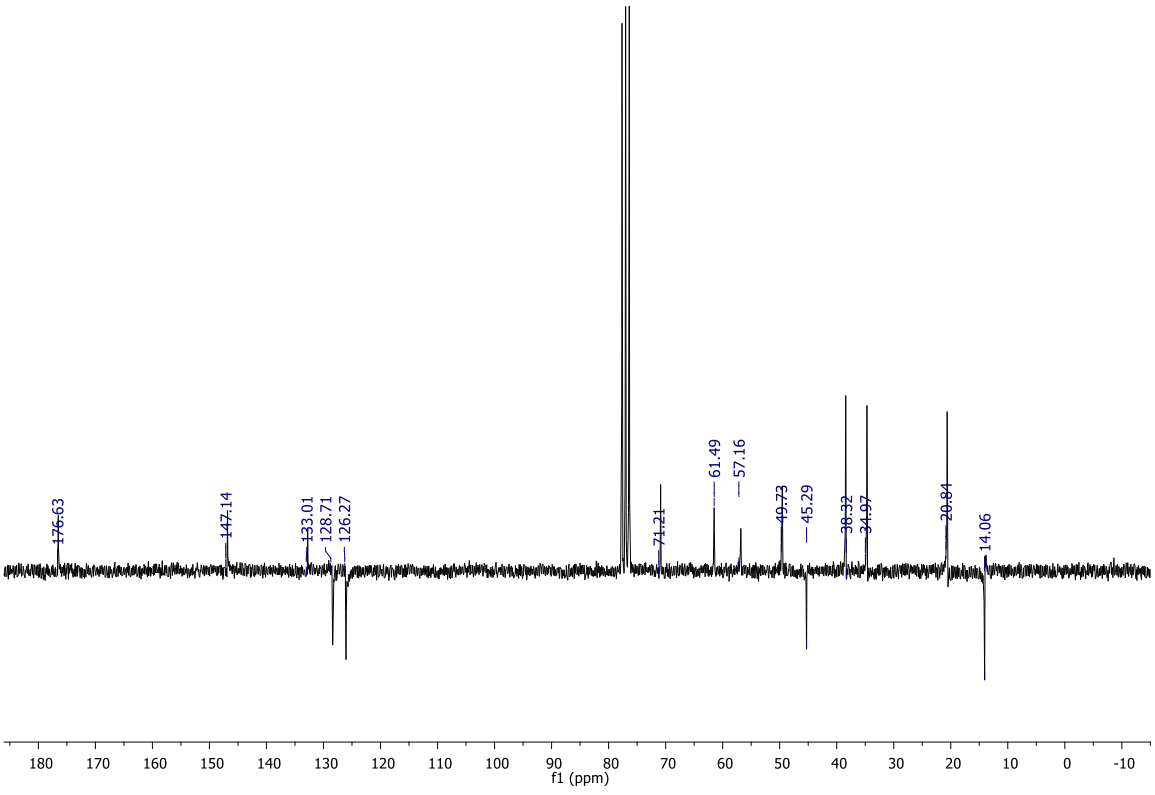

^{1}H (500 MHz, $CDCl_3$) and ^{13}C (125 MHz, $CDCl_3$) for 3-(4-(4-chlorophenyl)-4-hydroxypiperidin-1-yl)propyl 2-propylpentanoate (4b)

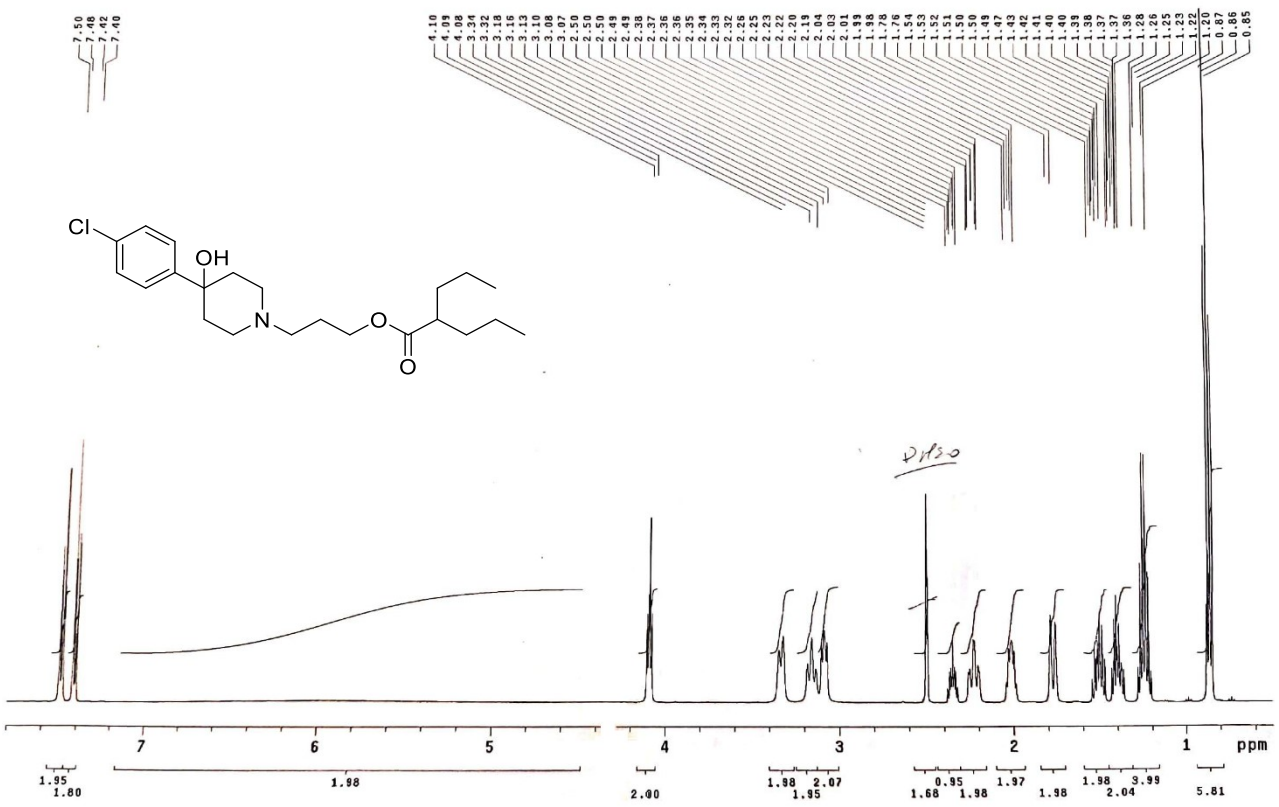

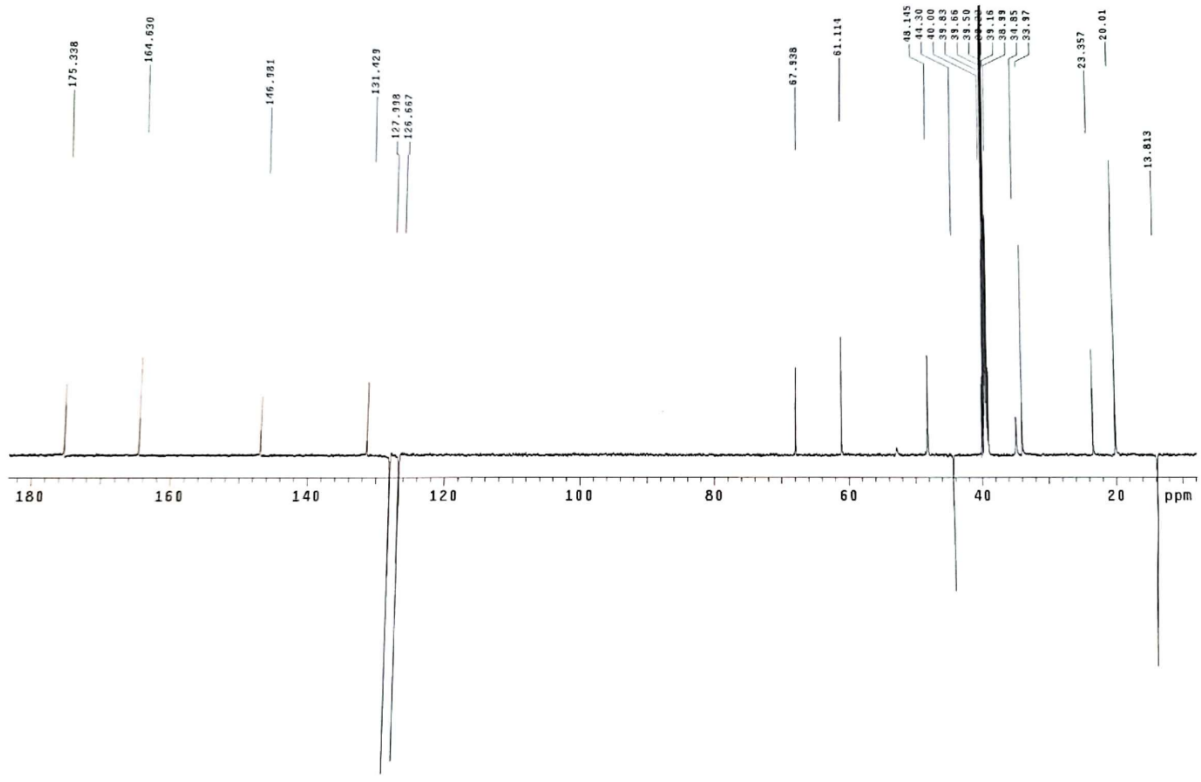

^{1}H (500 MHz, $CDCl_3$) and ^{13}C (125 MHz, $CDCl_3$) for 4-(4-(4-chlorophenyl)-4-hydroxypiperidin-1-yl)butyl 2-propylpentanoate (4c)

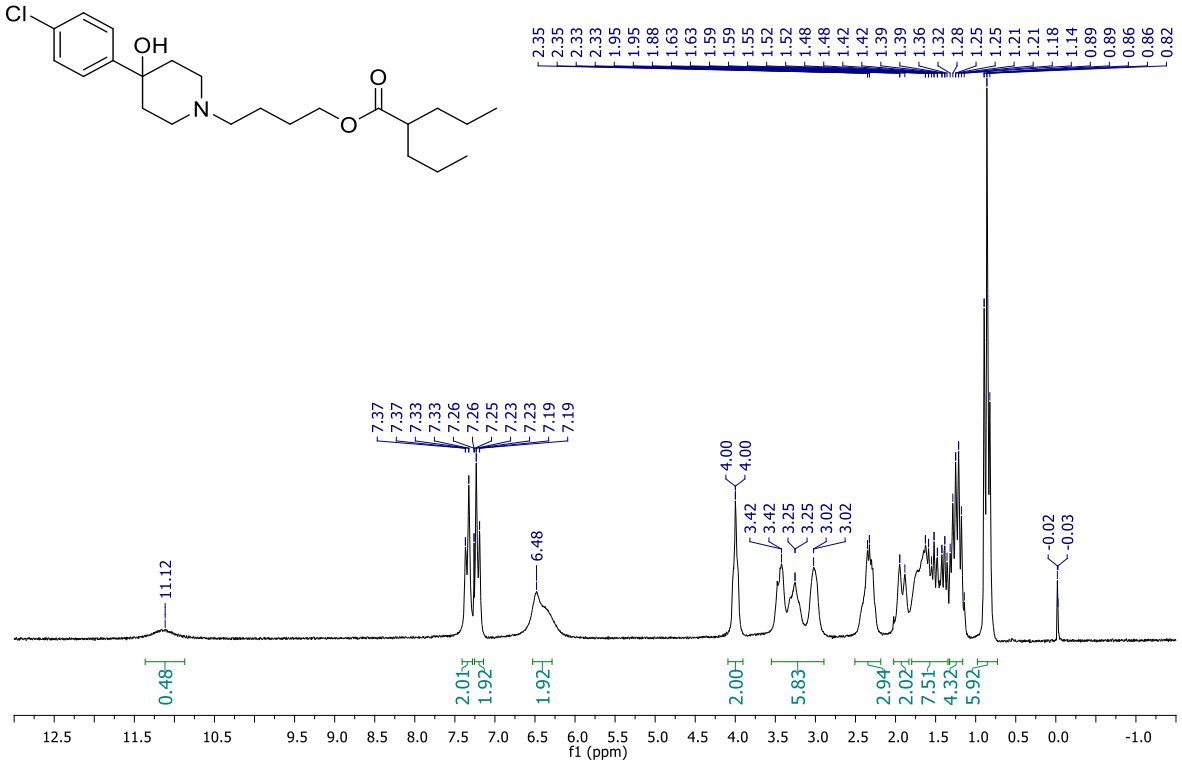

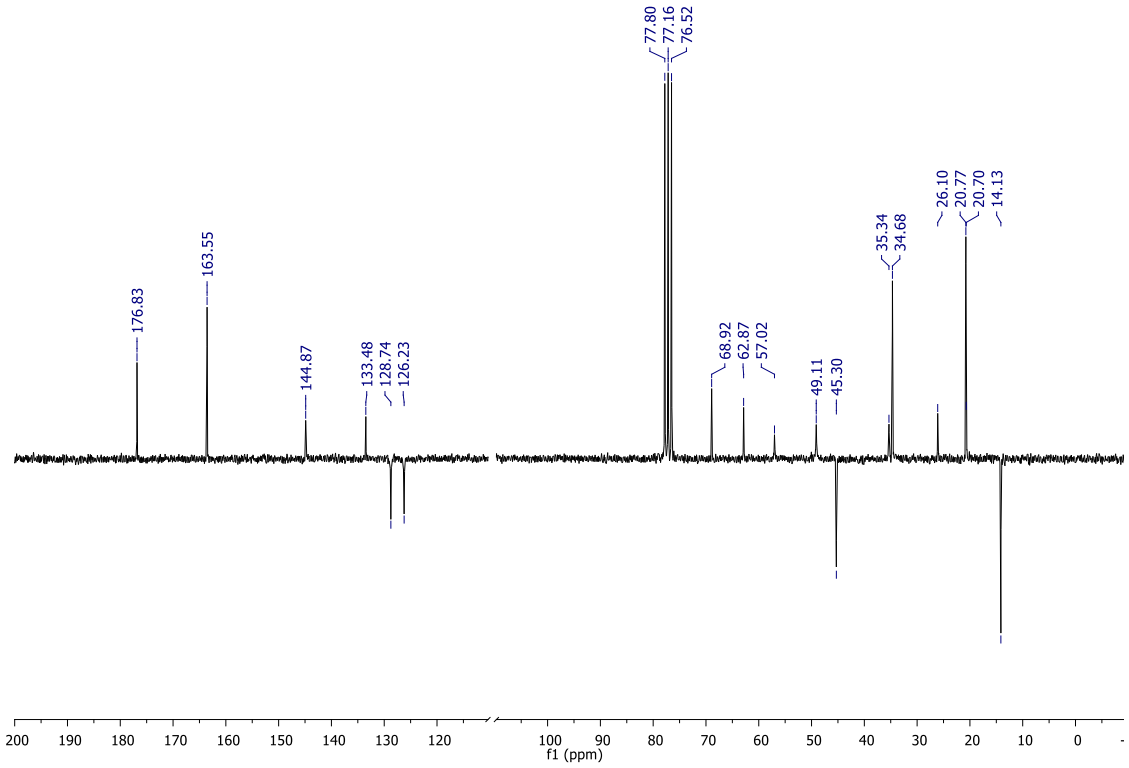

Dual-ligands Sigma/HDACi: a multitarget approach as potential strategy for uveal melanoma with shiftable application in neurodegenerative diseases.

EXPERIMENTAL SECTION

Table of contents

EXPERIMENTAL SECTION

Chemistry

Methyl (E)-3-(4-formylphenyl)acrylate (1). ^{1}H NMR (500 MHz, $CDCl_3$): δ 3.80 (s, 3H), 6.53 (d, *J*=16.0 Hz, 1H), 7.63-7.90 (m, 5H), 10.01(s, 1H); ^{13}C NMR (125 MHz, $CDCl_3$): 53.41, 116.80, 128.52, 129.53, 134.90, 138.15, 142.28, 163.69, 191.22.

(E)-3-{4-[(4-benzylpiperazin-1-yl)methyl]phenyl}-N-[(tetrahydro-2H-pyran-2-yl)oxy]acrylamide (4). The crude was purified by MPLC using EtOAc as eluent to obtain a white solid (76%). ^{1}H NMR (500 MHz, $CDCl_3$): δ 1.58-1.78 (m, 3H), 1.79-1.98 (m, 3H), 2.48 (s, 8H), 3.50 (s, 2H), 3.51 (s, 2H), 3.62-3.68 (m, 1H), 3.93-4.09 (m, 1H), 4.88-5.06 (m, 1H), 6.37 (d, 1H, J=5), 7.18-7.48 (m, 9H), 7.75 (d, *J*=5.0 Hz, 1H), 8.76 (br s, 1H); ^{13}C NMR (125 MHz, $CDCl_3$): 18.74, 24.96, 28.10, 52.97, 53.03, 62.61, 62.73, 62.98, 106.3, 118.8, 127.03, 127.82, 128.17, 129.22, 129.57, 133.48, 137.91, 140.35, 140.49, 166.5.

4-[(4-benzylpiperazin-1-yl)methyl]-N-(tetrahydro-2H-pyran-2-yloxy)benzamide (8a). The crude was purified by MPLC using EtOAc/$CHCl_3$ (7:3) as eluents to obtain a white solid (73%). ^{1}H NMR (500 MHz, $CDCl_3$): δ 1.45-1.72 (m, 3H), 1.81-1.92 (m, 3H), 2.74 (s, 8H), 3.52 (s, 2H), 3.53 (s, 2H), 3.64-3.68 (m, 1H), 3.97-4.04 (m, 1H), 5.00-5.20 (m, 1H), 7.22-7.32 (m, 5H), 7.37 (d, *J*=20.0 Hz, 2H), 7.69 d, *J*=20.0 Hz, 2H), 8.95 (br s, 1H); ^{13}C NMR (125 MHz, $CDCl_3$): 18.69, 25.00, 27.80, 28.08, 52.93, 52.98, 62.47, 62.70, 62.93, 102.69, 127.07, 127.10, 128.18, 129.22, 129.50, 130.70, 137.80, 142.71, 166.50.

4-{[(1-benzylpiperidin-4-yl)(methyl)amino]methyl}-N-(tetrahydro-2H-pyran-2-yloxy)benzamide (8b). The crude was purified by MPLC using EtOAc/$CHCl_3$ (7:3) as eluents to obtain a white solid (42%). ^{1}H NMR (500 MHz, $CDCl_3$): δ 1.55-1.71 (m, 5H), 1.73-1.78 (m, 2H), 1.80-2.00 (m, 5H), 2.18 (s, 3H), 2.37-2.44 (m, 1H), 2.92-2.97 (m, 2H), 3.49 (s, 2H), 3.60 (s, 2H), 3.64-3.70 (m, 1H), 3.95-4.00 (m, 1H), 5.01 (br., s, 1H), 7.20-7.32 (m, 5H), 7.37 (d, *J*=8.0 Hz, 2H), 7.68 d, *J*=8.0 Hz, 2H), 8.93 (br s, 1H); ^{13}C NMR (125 MHz, $CDCl_3$): 18.69, 25.01, 27.80, 28.08, 37.79, 53.20, 57.62, 60.88, 62.71, 63.02, 102.68, 126.94, 127.09, 128.13, 128.78, 129.14, 130.40, 138.32, 144.86, 166.12.

N-(2-aminophenyl)-3-chloropropanamide (10a). ^{1}HNMR (500 MHz, $CDCl_3$): δ 7.50 (s, 1H), 7.20-6.76 (m, 4H), 3.87 (t, *J*= 5.0 Hz, 2H), 3.52 (br s, 2H), 2.82 (t, *J*= 5.0 Hz, 2H); ^{13}CNMR (500 MHz, $CDCl_3$): δ 168.39, 140.72, 127.58, 125.78, 123.67, 119.54, 117.95, 40.30, 39.79.

N-(2-aminophenyl)-4-chlorobutanamide (10b). ^{1}HNMR (500 MHz, $CDCl_3$): δ 7.40 (br s, 1H), 7.21-7.04 (m, 2H), 6.83-6,75 (m, 2H), 3.66 (t, *J*=16.0 Hz, 2H), 3.48 (br s, 2H), 2.57 (t, *J*=17.0 Hz, 2H), 2.34-2.03 (m, 2H); ^{13}CNMR (500 MHz, $CDCl_3$): δ 170.55, 140.53, 127.29, 125.28, 124.14, 119.65, 118.22, 44.45, 33.39, 27.98.

N-(2-aminophenyl)-5-chloropentanamide (10c). ^{1}HNMR (500 MHz, DMSO-d6): δ 9.09 (s, 1H), 7.15-6,51 (m, 4H), 4.80 (br s, 2H), 3.67 (t, *J*=10.0 Hz, 2H), 2.35 (t, *J*=10.0 Hz, 2H), 1.80-1.69 (m, 4H); ^{13}CNMR (500 MHz, DMSO-d6): δ 170.71, 141.85, 125.68, 125.24, 123.43, 116.12, 115.83, 45.07, 34.77, 31.56, 22.60.

Binding affinity assay

Preparation of membrane homogenates from pig brain. Fresh guinea pig brain cortices (~25 g) were homogenized in two portions with 10 volumes of ice-cold Tris (50 mM, pH 7.4) containing 0.32 M sucrose with a Potter-Elvehjem glass homogenizer. The suspension was centrifuged at 1,030 × g for 10 min at 4 °C. The supernatant was separated and centrifuged at 41,200 × g for 20 min at 4 °C. The obtained pellet was suspended with 3 volumes of ice-cold Tris (50 mM, pH 7.4), incubated at rt for 15 min and centrifuged at 41,200 × g for 15 min at 4 °C. The final pellet was resuspended with ~2 volumes of ice-cold Tris buffer, and frozen at -80 °C in ~1 mL portions containing about 5 mg protein/ml.

Preparation of membrane homogenates from rat liver. Rat livers (~21 g) were cut into small pieces with a scalpel and homogenized in two portions with 6 volumes of cold 0.32 M sucrose with a Potter-Elvehjem glass homogenizer. The suspension was centrifuged at 1,030 × g for 10 min at 4 °C. The supernatant was separated and centrifuged at 31,100 × g for 20 min at 4 °C. The pellet was resuspended with 6 volumes of ice-cold Tris buffer (50 mM, pH 8) and incubated at rt for 30 min. Then, the suspension was centrifuged at 31,100 × g for 20 min at 4 °C. The final pellet was

resuspended with 6 volumes of ice-cold Tris buffer and stored at -80 °C in ~1 mL portions containing about 6 mg protein/ml.

Protein determination. The protein concentration was determined by the method of Bradford. The Bradford solution was prepared by dissolving 10 mg of Coomassie Brilliant Blue G 250 in 5 mL of 95% ethanol. To this solution, 10 mL of 85% phosphoric acid were added and the mixture was stirred and filled to a total volume of 100 mL with ultrapure water. The calibration was carried out with bovine serum albumin as a standard at different concentrations. In a 96-well plate, 30 µL of the calibration solution or 30 µL of the membrane receptor preparation were mixed with 240 µL of the Bradford solution, respectively. After 5 min of incubation at rt, the UV absorbance was measured at λ=595 nm using a microplate spectrophotometer reader (Synergy HT, BioTek).

^{1}H and ^{13}C NMR SPECTRA

^{1}H (500 MHz, $CDCl_3$) and ^{13}C (125 MHz, $CDCl_3$) for (*E*)-*N*-(2-aminophenyl)-3-{4-[(4-benzylpiperazin-1-yl)methyl]phenyl}acrylamide (3)

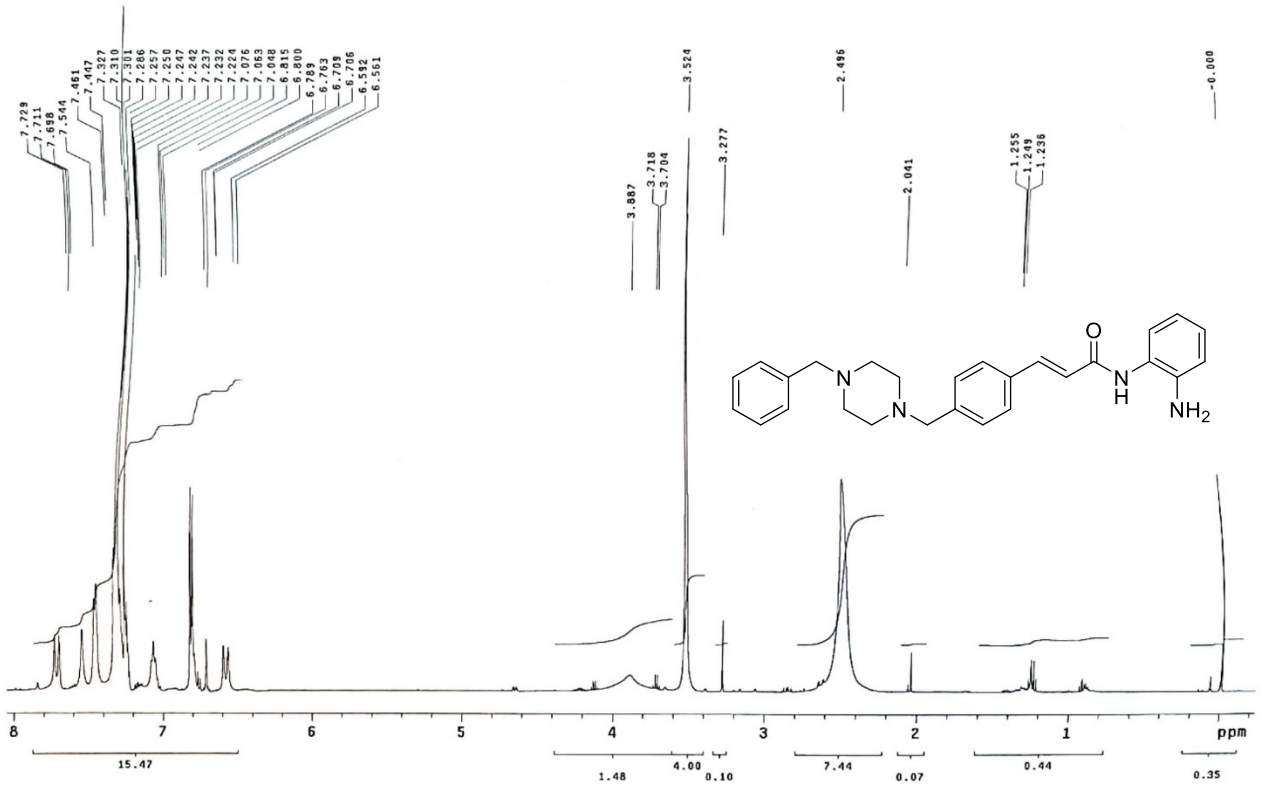

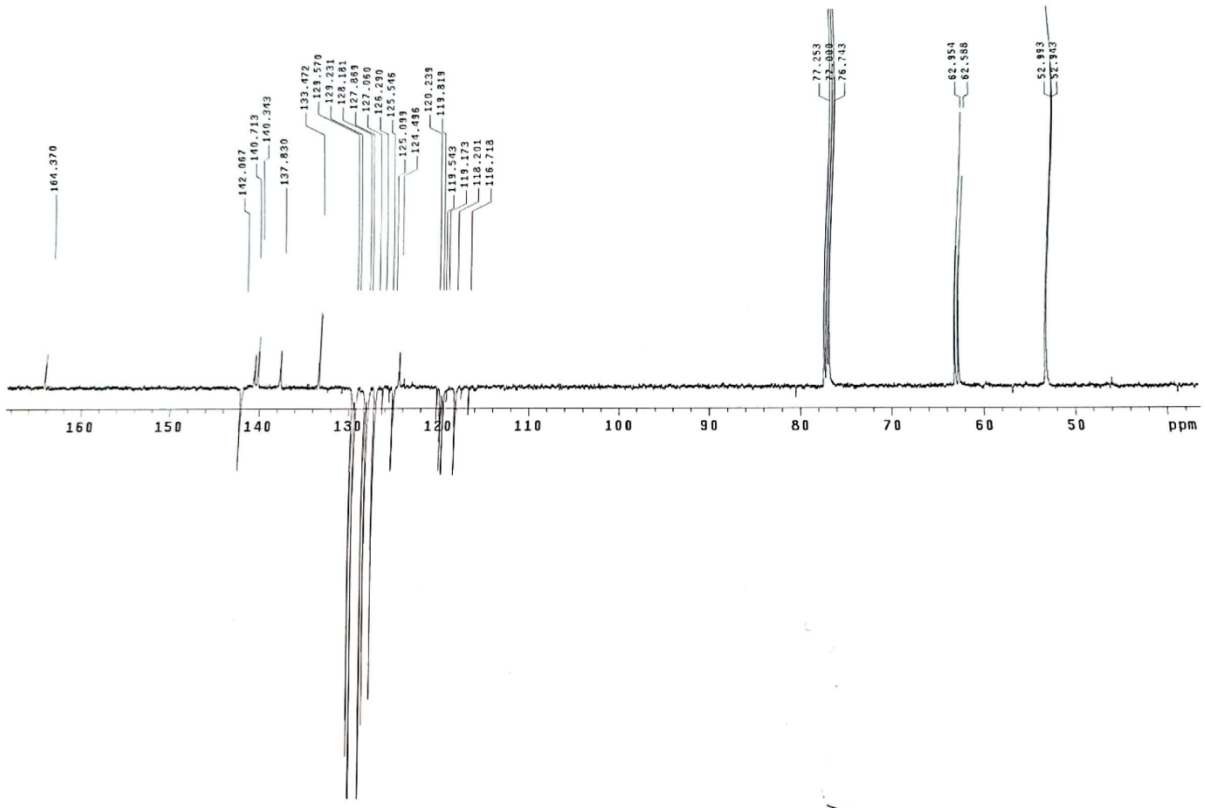

^{1}H (500 MHz, $CDCl_3$) and ^{13}C (125 MHz, $CDCl_3$) for *N*-(2-aminophenyl)-4-[(4-benzylpiperazin-1-yl)methyl]benzamide (7a)

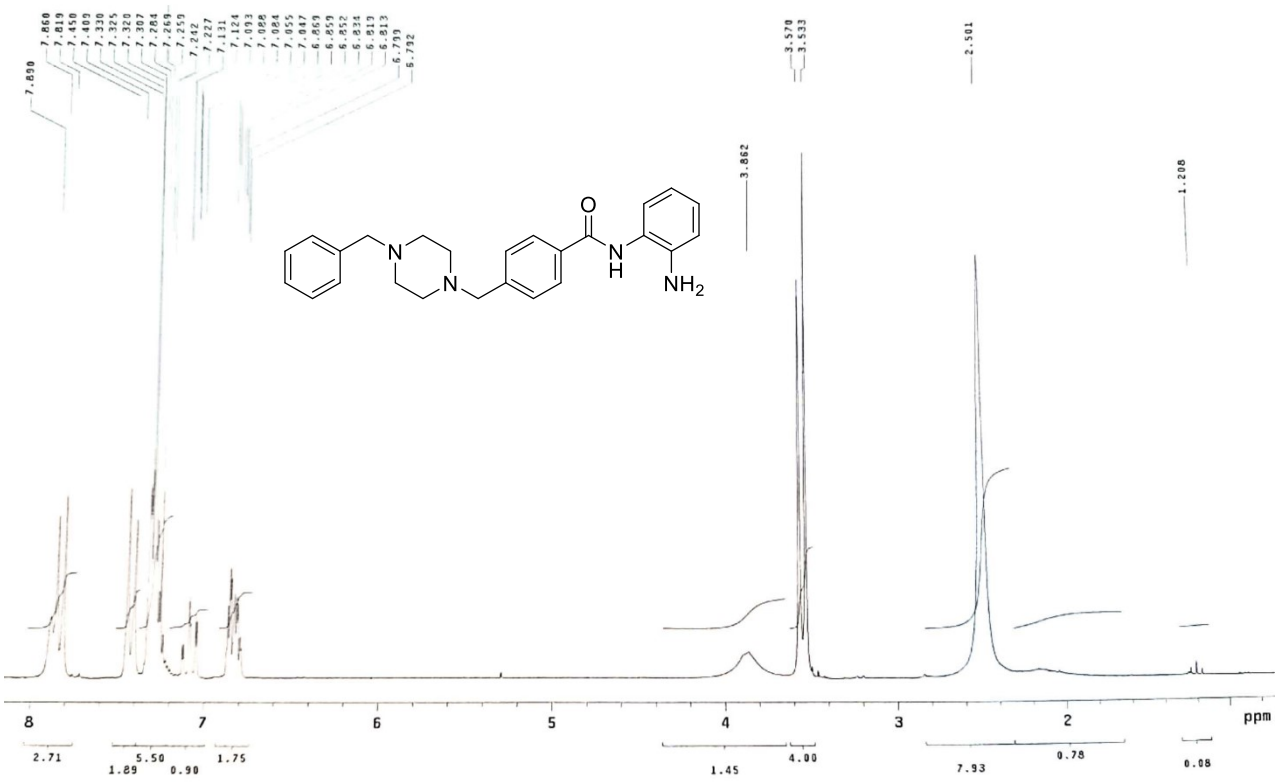

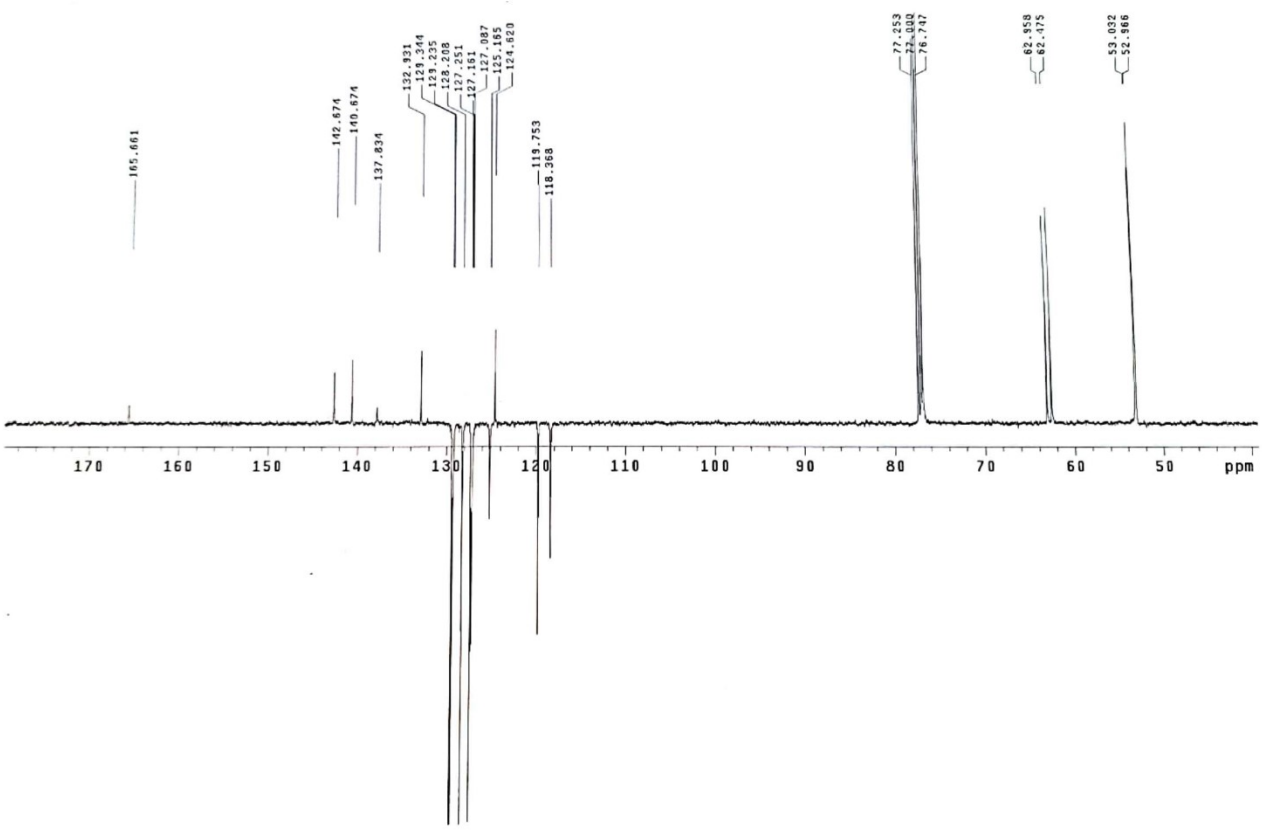

^{1}H (500 MHz, $CDCl_3$) and ^{13}C (125 MHz, $CDCl_3$) for *N*-(2-aminophenyl)-4-{[(1-benzylpiperidin-4-yl)(methyl)amino]methyl}benzamide (7b).

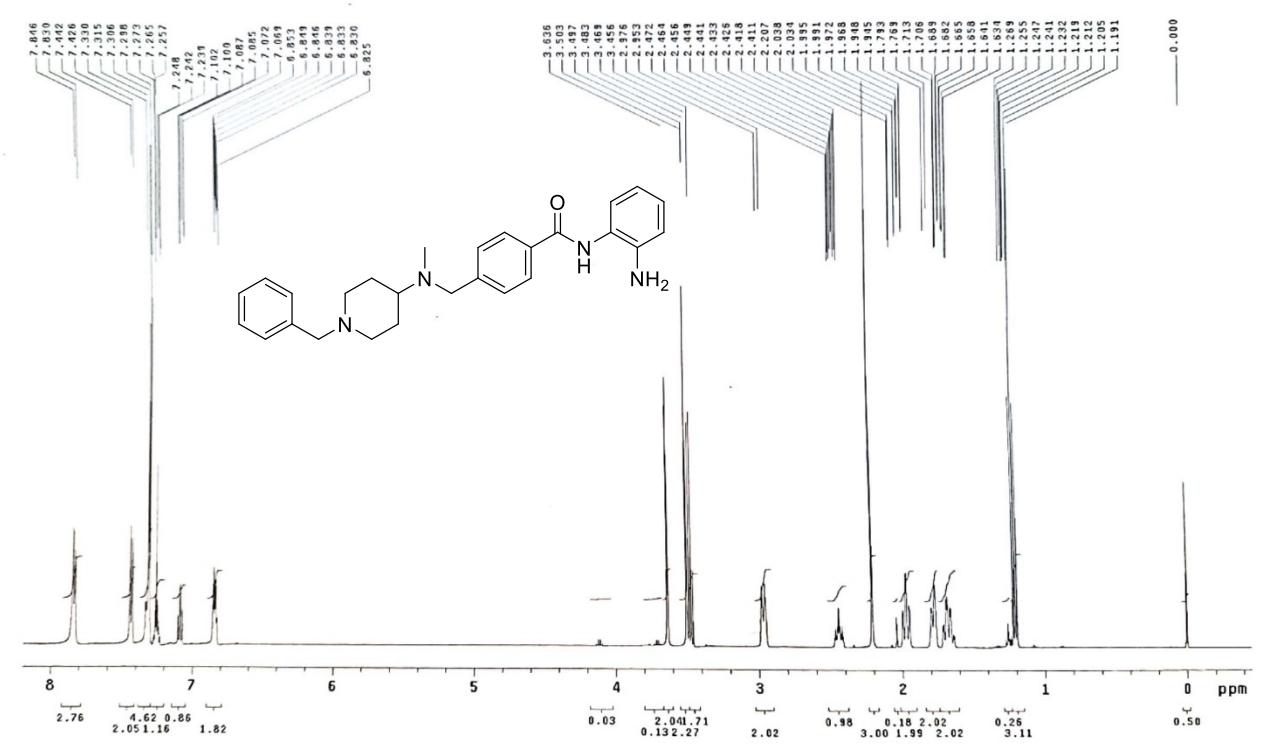

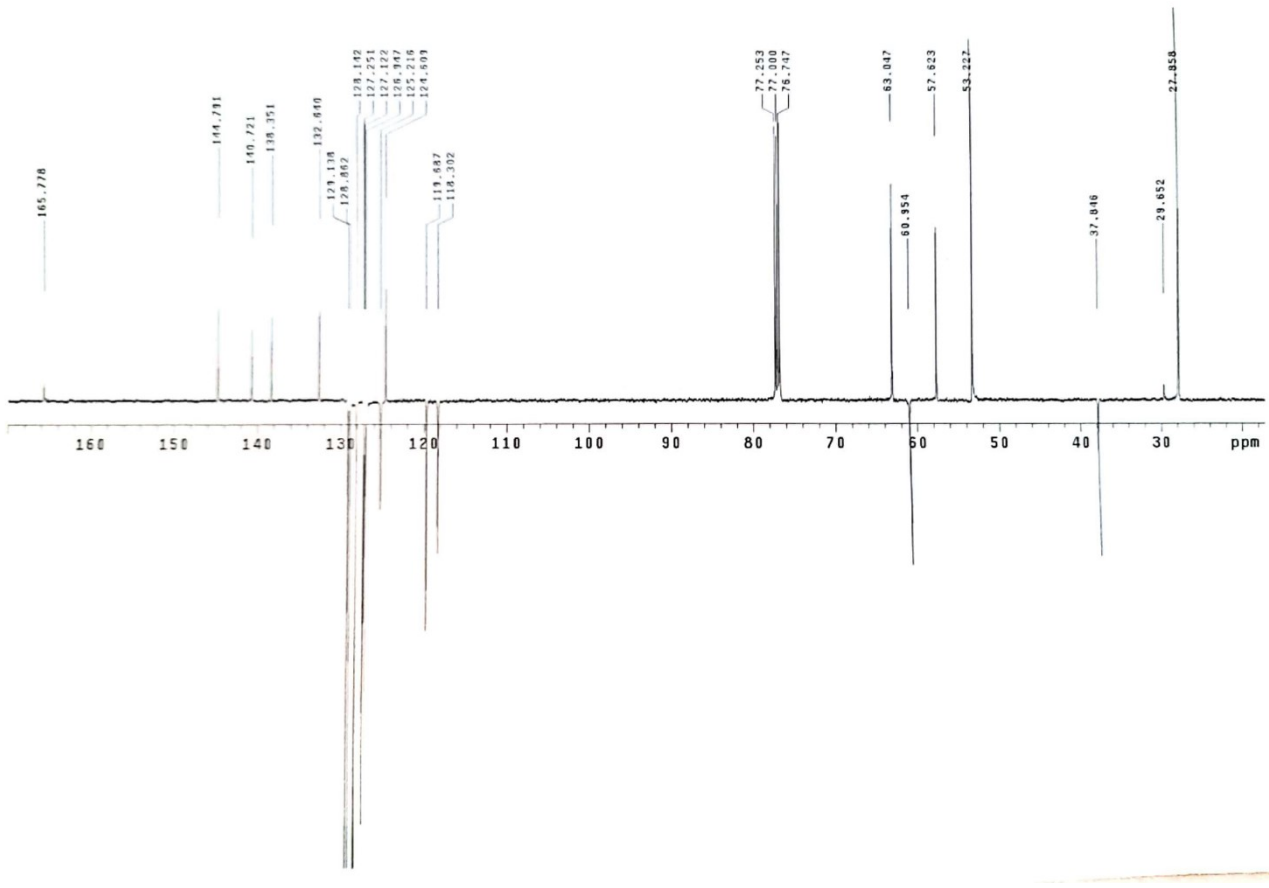

^{1}H (500 MHz, DMSO-d_6) and ^{13}C (125 MHz, DMSO-d_6) for (*E*)-3-{4-[(4-benzylpiperazin-1-yl)methyl]phenyl}-N-hydroxyacrylamide (5)

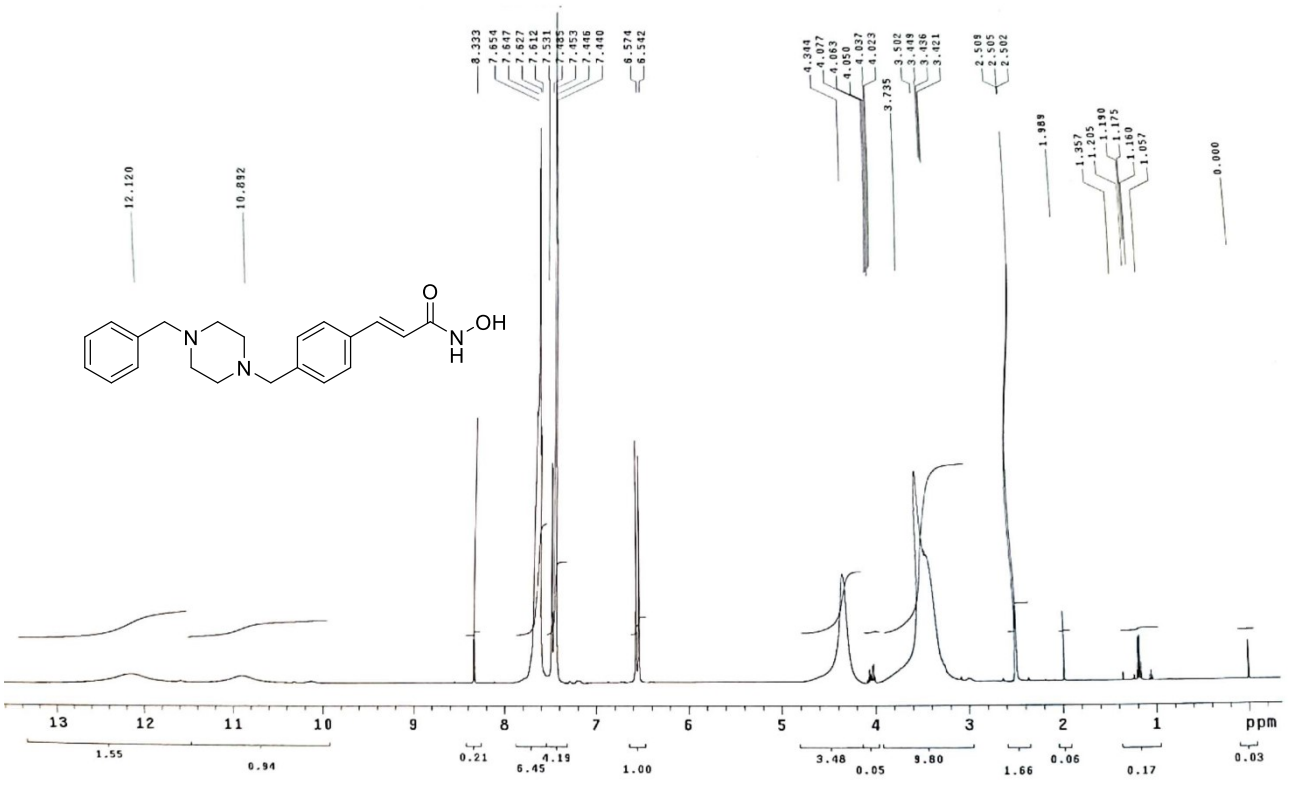

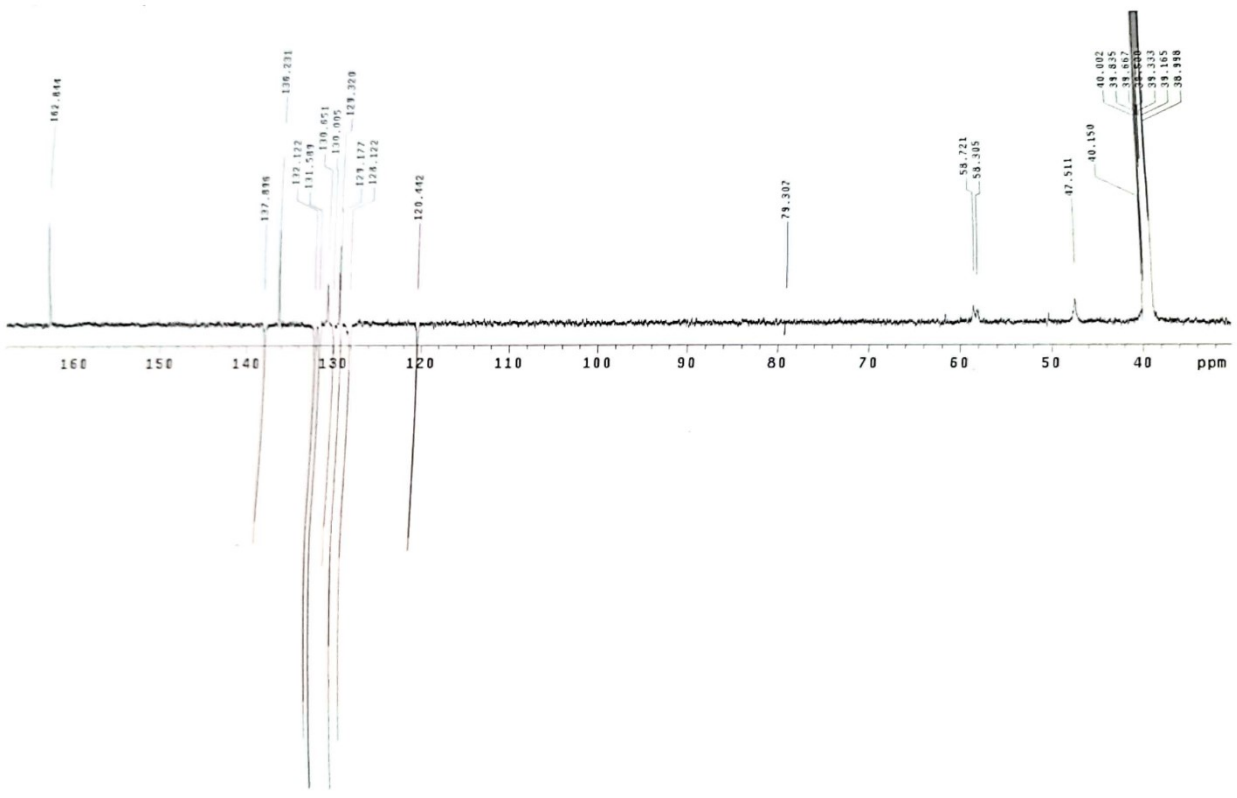

^{1}H (500 MHz, DMSO-d_6) and ^{13}C (125 MHz, $CDCl_3$) for 4-[(4-benzylpiperazin-1-yl)methyl]-N-hydroxybenzamide (9a)

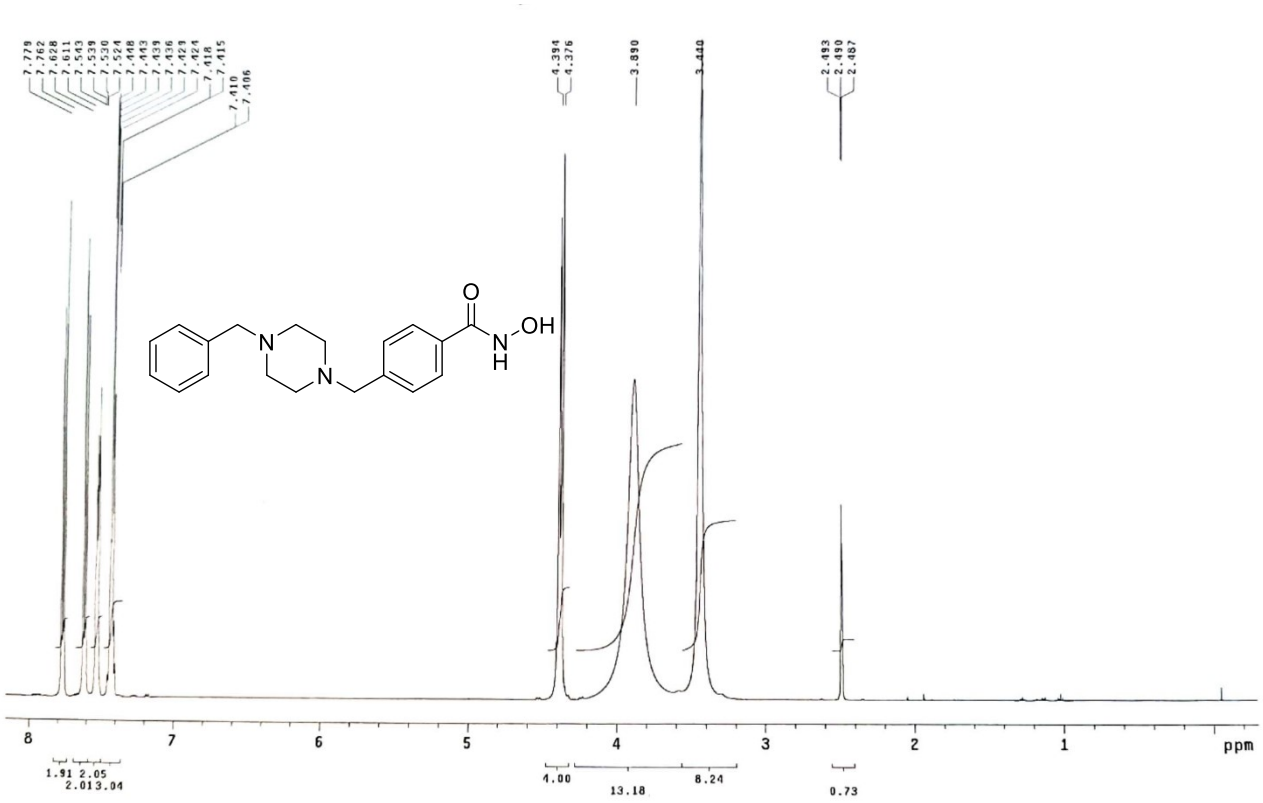

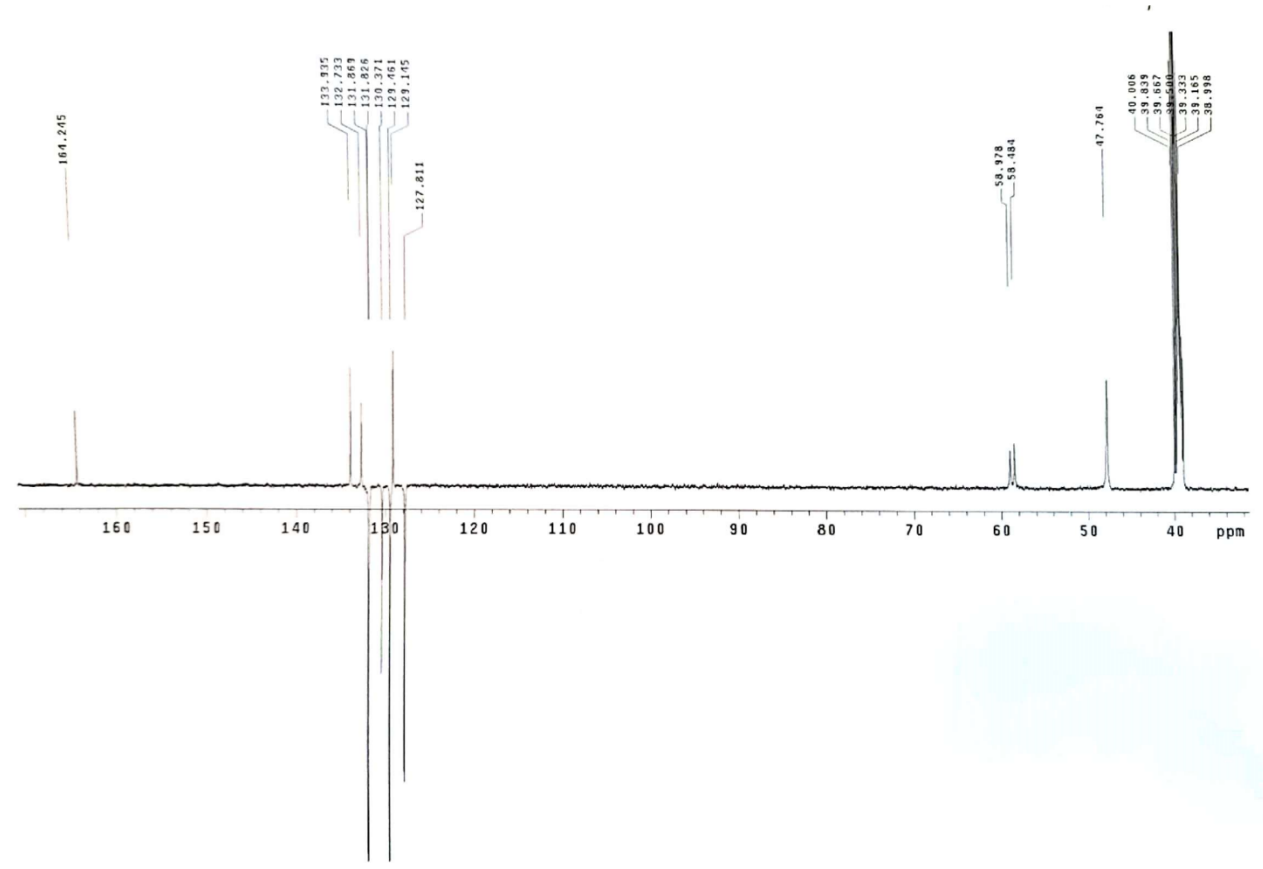

^{1}H (500 MHz, D_2O) and ^{13}C (125 MHz, D_2O) for 4-{[(1-benzylpiperidin-4-yl)(methyl)amino]methyl}-*N*-hydroxybenzamide (9b)

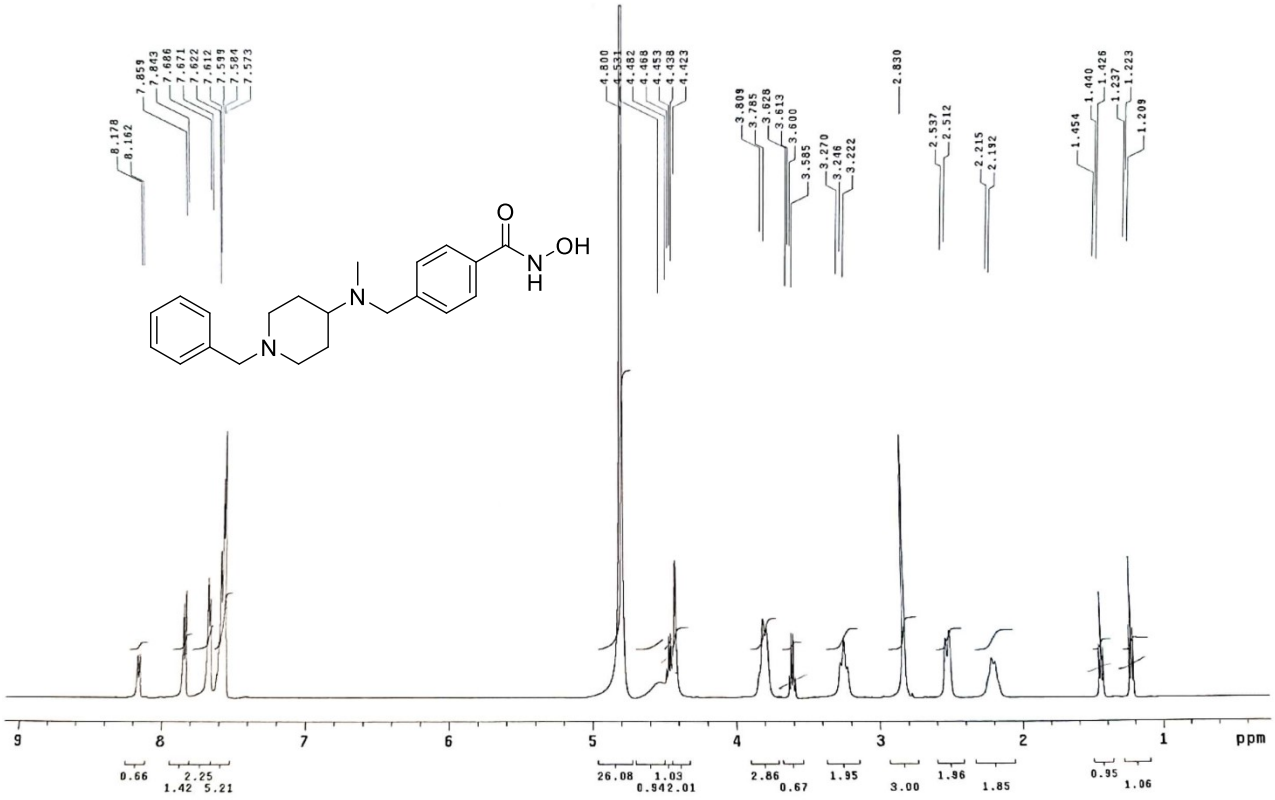

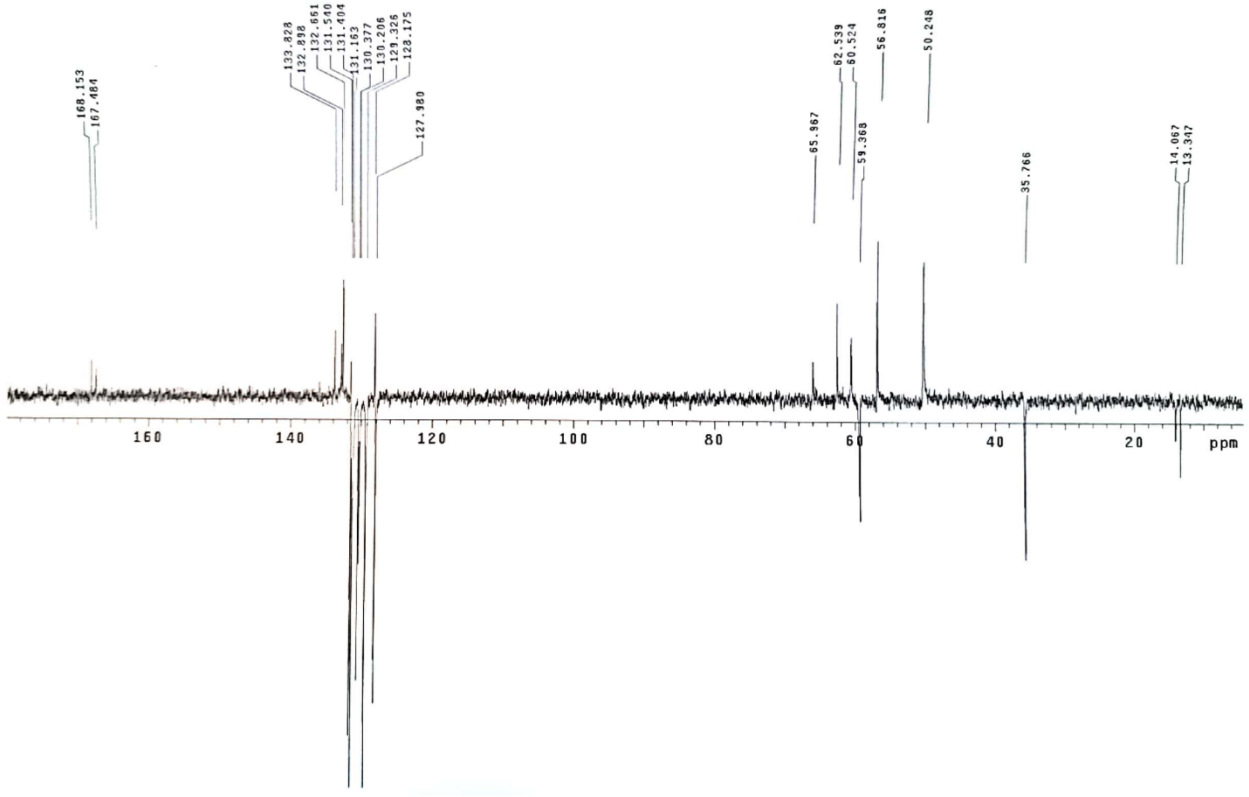

^{1}H (500 MHz, $CDCl_3$) and ^{13}C (125 MHz, $CDCl_3$) for *N*-(2-aminophenyl)-3-chloropropanamide (10a)

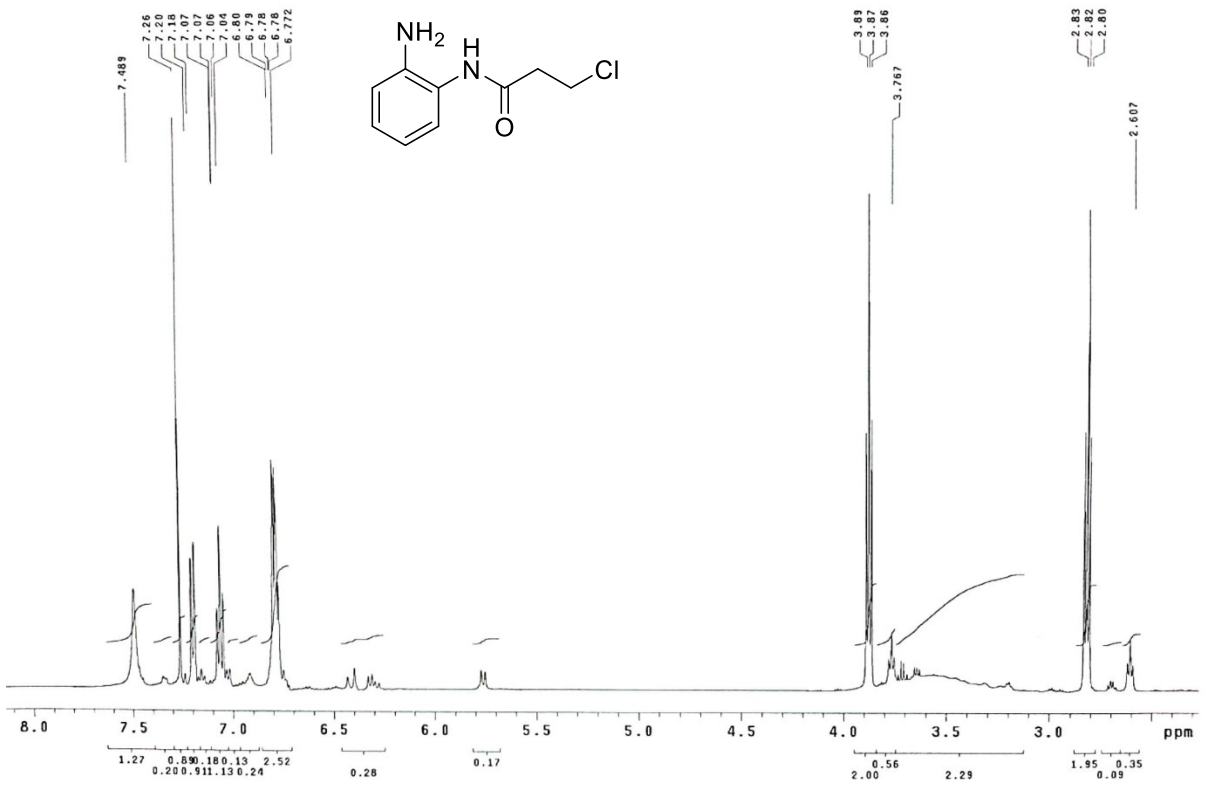

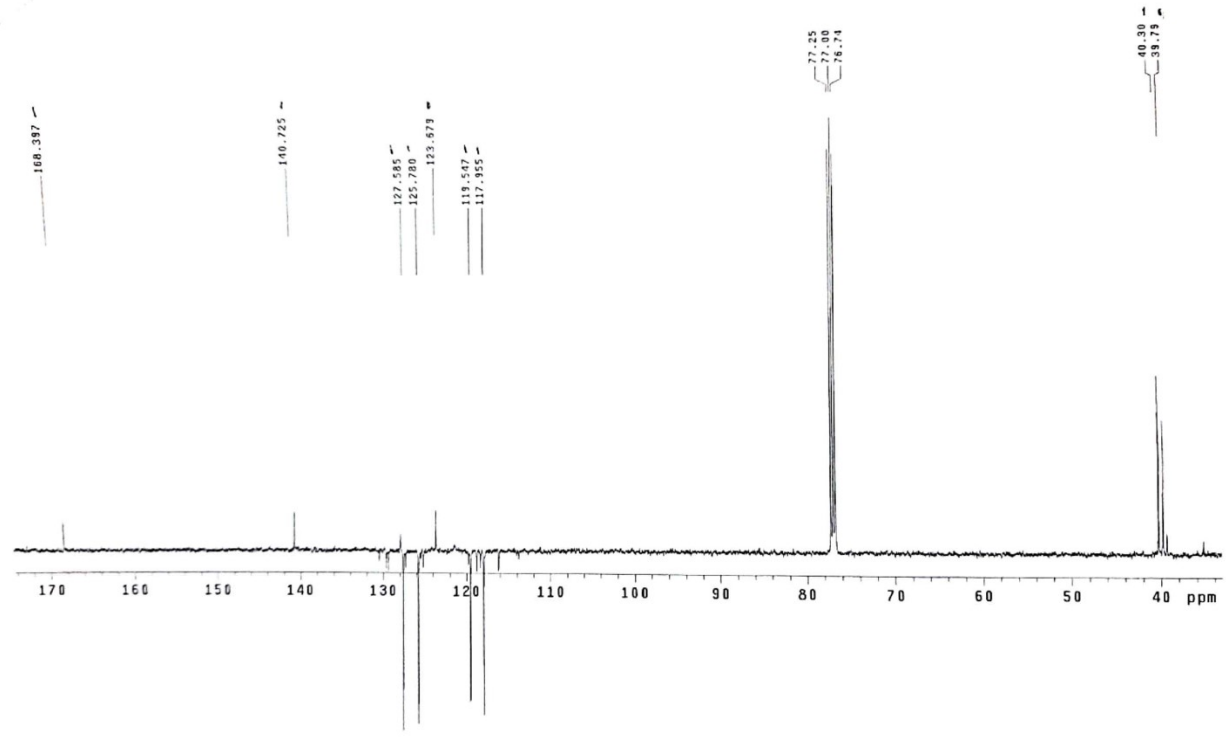

^{1}H (500 MHz, $CDCl_3$) and ^{13}C (125 MHz, $CDCl_3$) for *N*-(2-aminophenyl)-4-chlorobutanamide (10b)

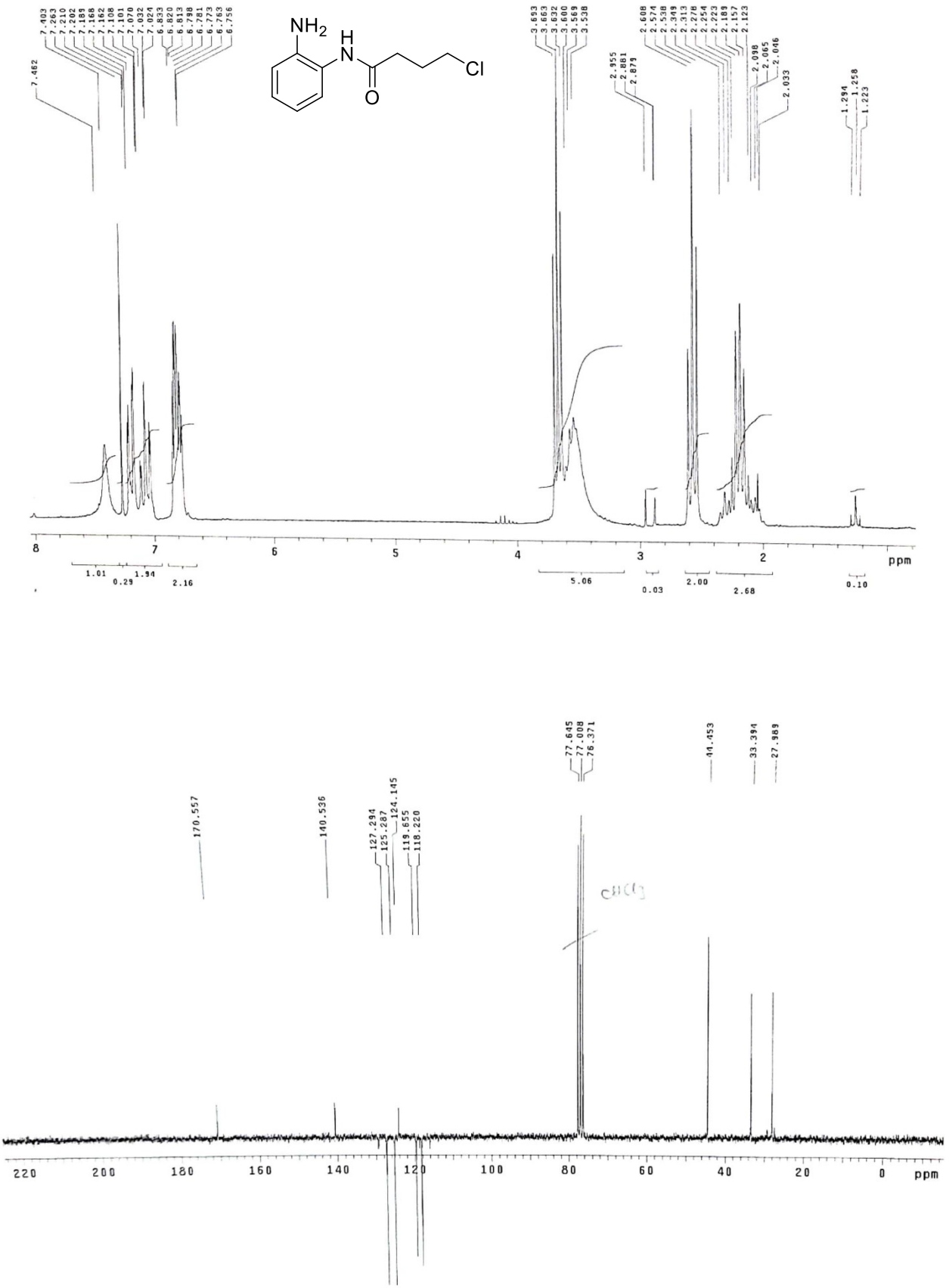

^{1}H (500 MHz, DMSO-d$_6$) and ^{13}C (125 MHz, DMSO-d$_6$) for *N*-(2-aminophenyl)-3-chloropropanamide (10a)

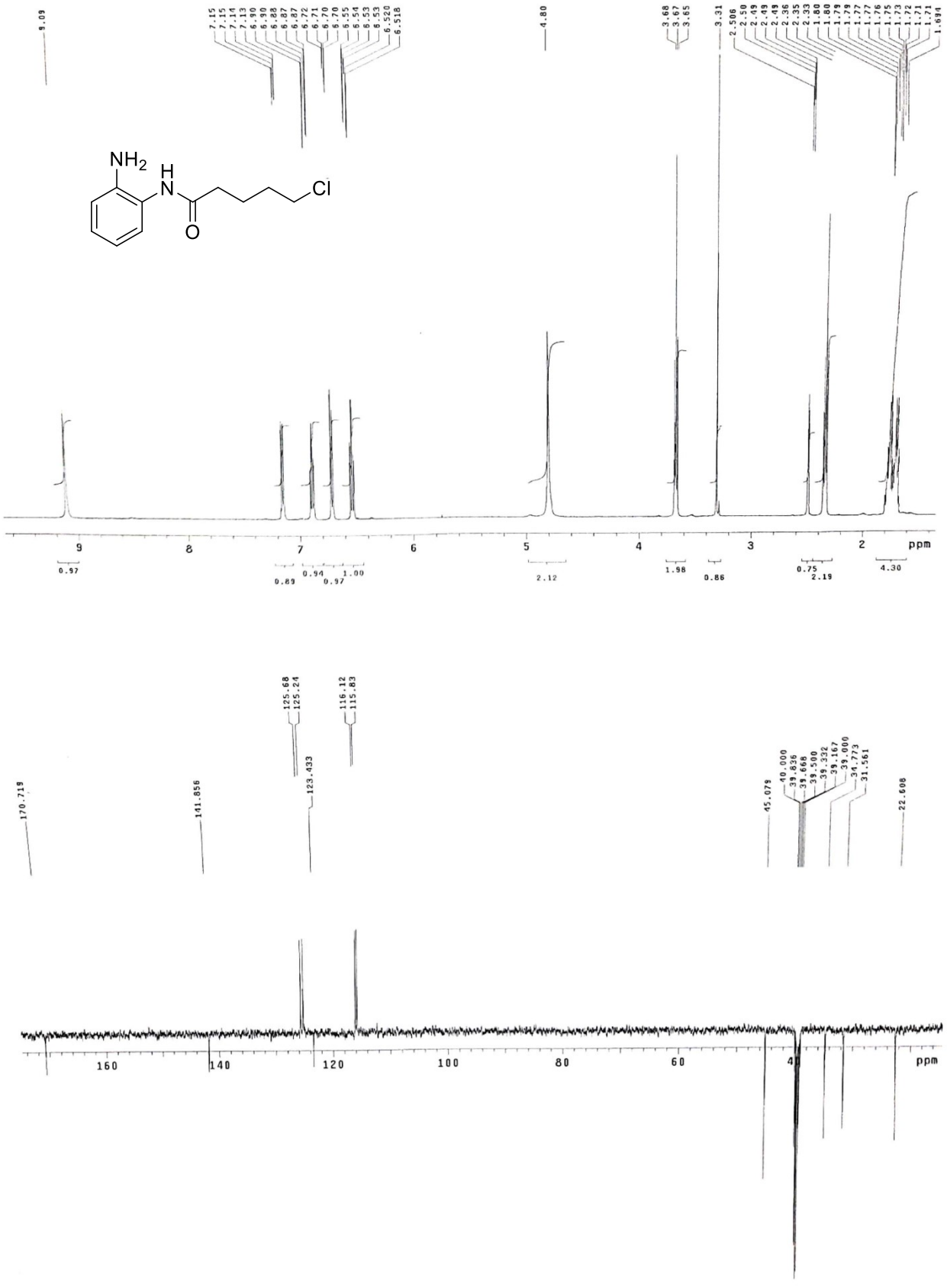

^{1}H (500 MHz, DMSO-d$_6$) and ^{13}C (125 MHz, DMSO-d$_6$) for *N*-(2-aminophenyl)-3-[4-(4-chlorophenyl)-4-hydroxypiperidin-1-yl]propanamide (11a)

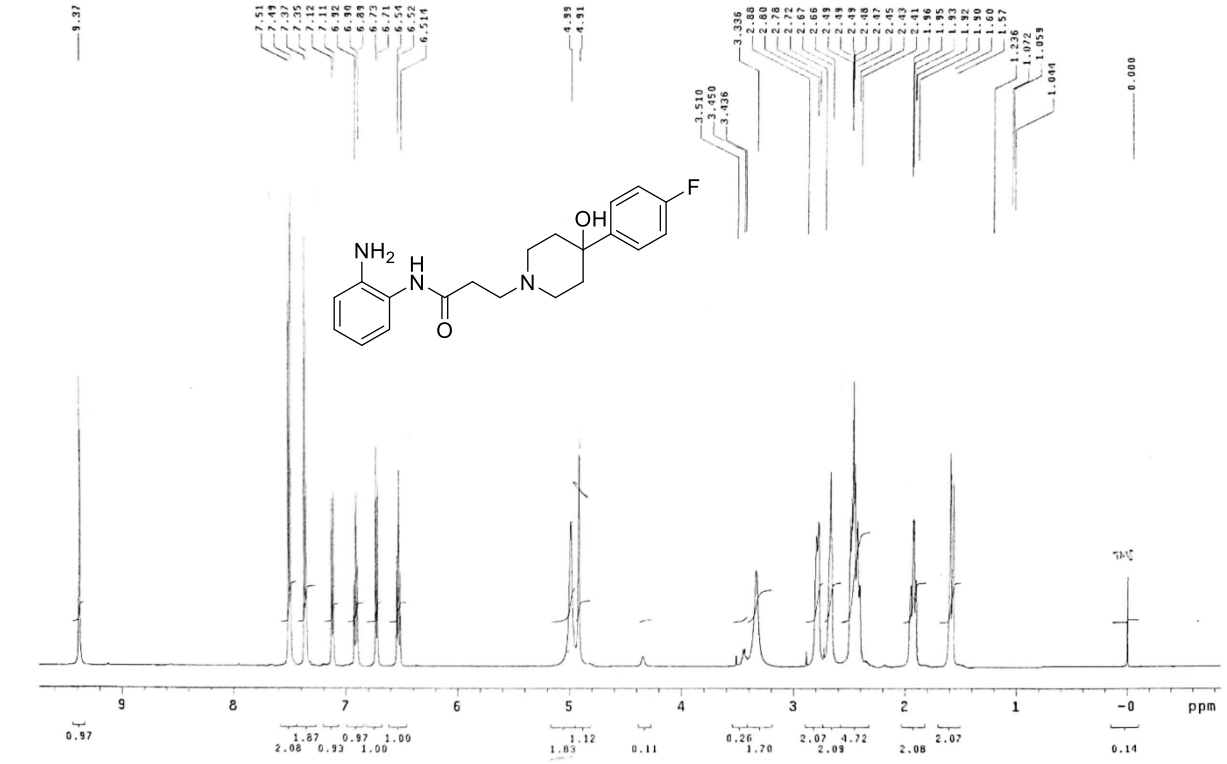

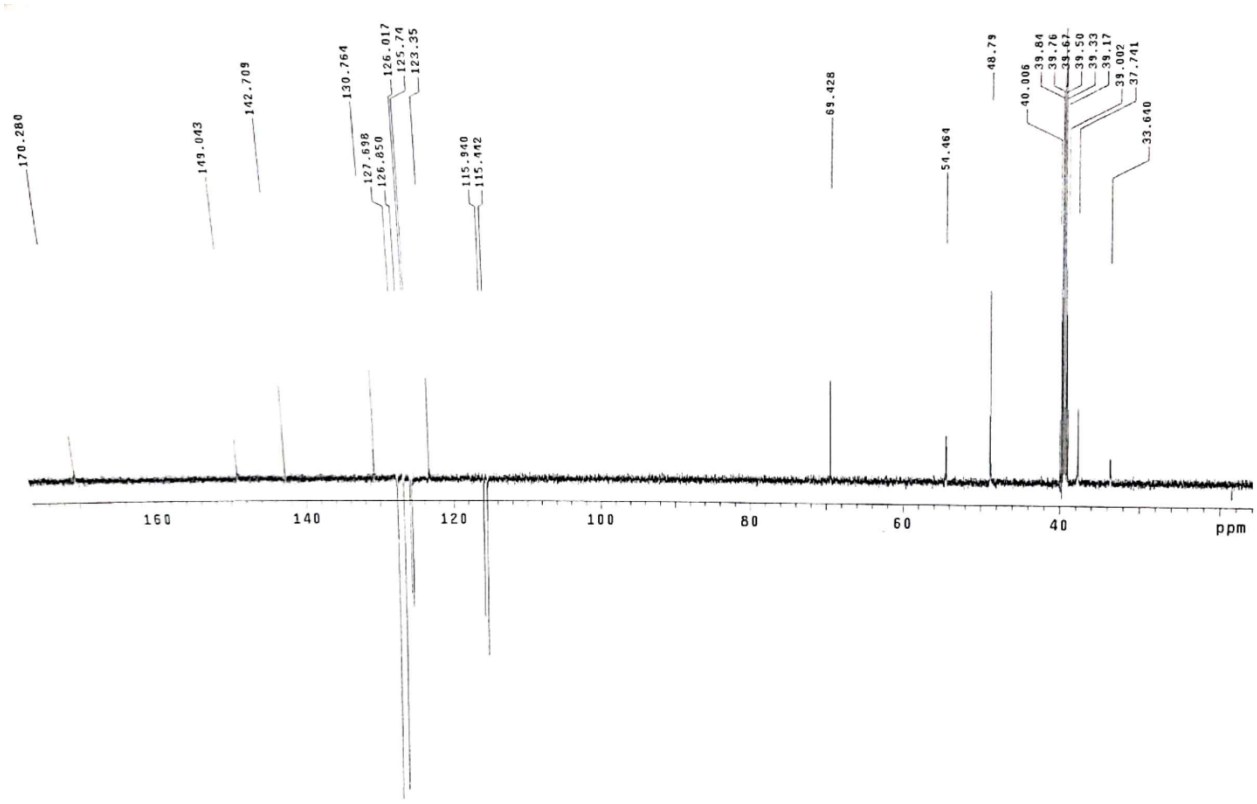

^{1}H (500 MHz, DMSO-d$_6$) and ^{13}C (125 MHz, DMSO-d$_6$) for *N*-(2-aminophenyl)-3-[4-(4-chlorophenyl)-4-hydroxypiperidin-1-yl]butanamide (11b)

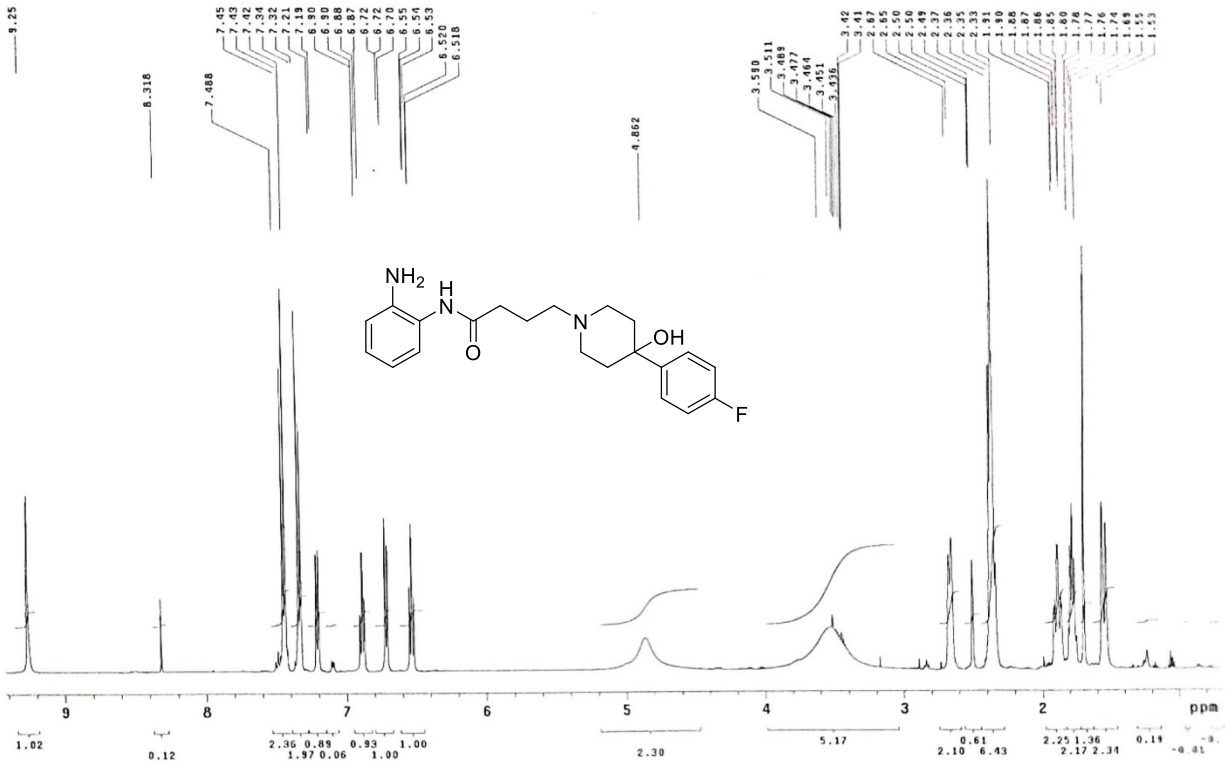

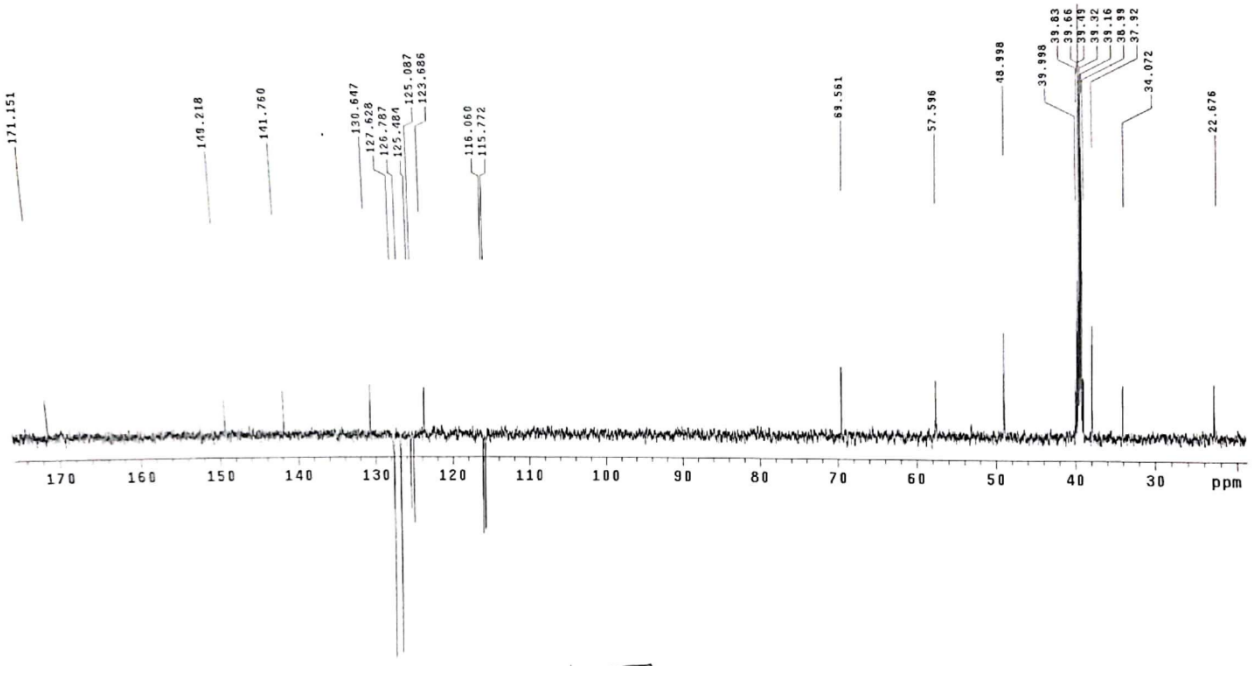

^{1}H (500 MHz, DMSO-d$_6$) and ^{13}C (125 MHz, DMSO-d$_6$) for *N*-(2-aminophenyl)-3-[4-(4-chlorophenyl)-4-hydroxypiperidin-1-yl]pentanamide (11c)

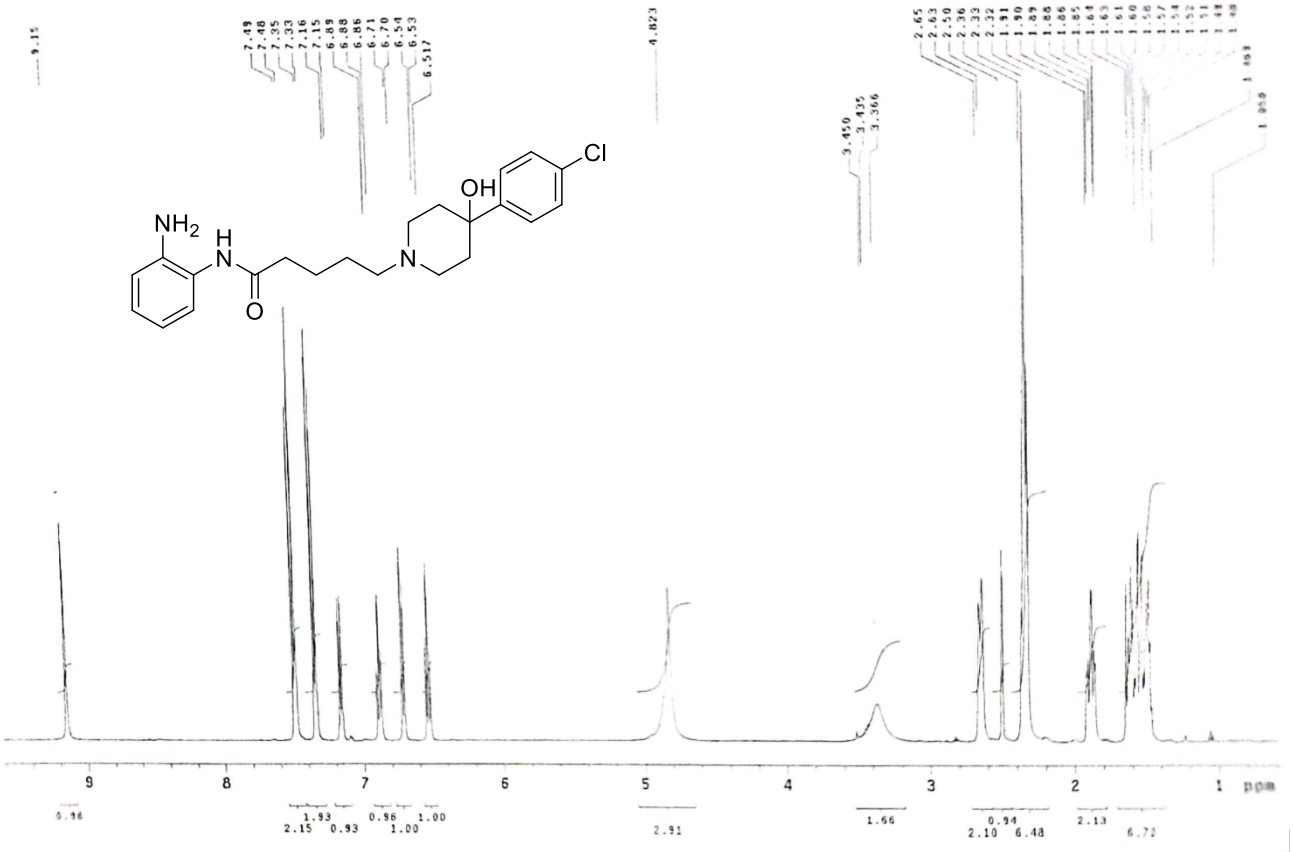

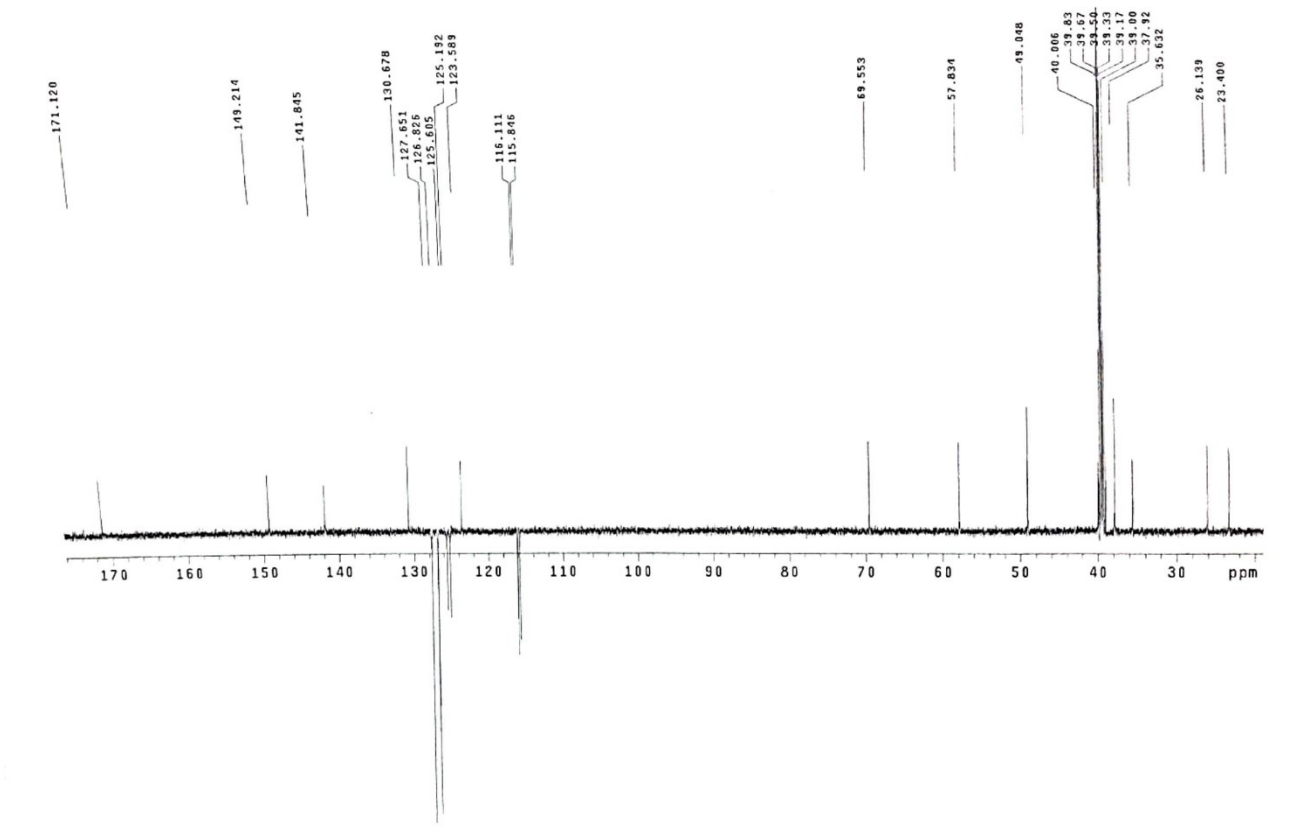

Development of new Sigma/HDAC dual-ligands

Supplemental materials - Experimental section

General details. Reagent grade chemicals were purchased from Sigma-Aldrich (St. Louis, MO, USA) or Fluorochem Derbyshire, United Kingdom) and were used without further purification. All reactions involving air-sensitive reagents were performed under N_2 in oven-dried glassware using the syringe-septum cap technique. All reactions were monitored by thin-layer chromatography (TLC) which was performed on silica gel Merck 60 F254 plates; the spots were visualized by UV light (λ = 254 and 366 nm) and iodine chamber. Melting points were determined on a Büchi B-450 apparatus in glass capillary tubes and are uncorrected. Flash chromatography purification was performed on a Merck silica gel 60, 0.040−0.063 mm (230−400 mesh), stationary phase using glass columns with a diameter between 1 and 4 cm. Nuclear magnetic resonance spectra (^{1}H NMR and ^{13}C NMR recorded at 200 or 500 MHz) were obtained on Varian INOVA spectrometers using $CDCl_3$, CD_3OD and DMSO-d_6 with a 0.03% of TMS as internal standard. Coupling constants (J) are reported in hertz. Signal multiplicities are characterized as s (singlet), d (doublet), t (triplet), q (quartet), m (multiplet), br (broad), ovpl (overlapped). Purities of all compounds was determined by microanalysis (C, H, N) that was performed on a Carlo Erba instrument model E1110; all the results agreed within ±0.4% of the theoretical values. Compound nomenclatures were generated with ChemBioDraw Ultra version 16.0.0.82.

General procedure for *N*-(2-aminophenyl)amide intermediates (1a-b)

To a solution of *o*-phenylenediamine (3 equiv.) in anhydrous CH_2Cl_2 was added dropwise a solution of 3-chloropropyonill or 4-chlorobutiryl chloride (1 equiv.) respectively in anhydrous CH_2Cl_2 at 0 °C and inert atmosphere, then the reaction mixture was stirred 24 hours at room temperature. The reaction was quenched with a saturated solution of $NaHCO_3$ and the aqueous phase extracted with CH_2Cl_2 (3 x 50 ml). The combined organic phases were dried with anhydrous Na_2SO_4, filtered and

evaporated under vacuum. The crude product was purified by flash chromatography with a mixture CH_2Cl_2/EtOAc/EtOH 50-48-2%. to afford the desired products **1a-b**.

***N*-(2-aminophenyl)-3-chloropropanamide (1a)**

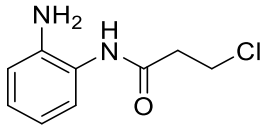

The product has been obtained using *o*-phenylenediamine (1.00g, 9.25 mmol) and 3-chloropropyonill chloride (0.294 ml, 3.08 mmol). Yield 48% (0.297 g), beige solid.

Chemical Formula: $C_9H_{11}ClN_2O$ (198.65 g/mol)

^{1}H NMR (500 MHz, $CDCl_3$) δ 7.50 (s, 1H), 7.20 - 6.76 (m, 4H), 3.87 (t, J = 5.0 Hz, 2H), 3.52 (br. s, 2H), 2.82 (t, J = 5.0 Hz, 2H)

^{13}C NMR (125 MHz, $CDCl_3$) δ 168.39, 140.72, 127.58, 125.78, 123.67, 119.54, 117.95, 40.30, 39.79.

***N*-(2-aminophenyl)-4-chlorobutanamide (1b)**

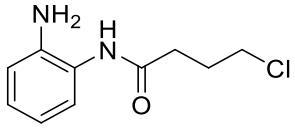

The product has been obtained using *o*-phenylenediamine (0.500g, 4.62mmol) and 4-chlorobutiryl chloride (0.294 ml, 3.08 mmol). Yield 54% (0.177 g), beige solid.

Chemical Formula: $C_{10}H_{13}ClN_2O$ (212.68 g/mol)

^{1}H NMR (500 MHz, $CDCl_3$) δ 7.40 (br. s, 1H), 7.21-7.04 (m, 2H), 6.83-6,75 (m, 2H), 3.66 (t, 2H, J = 16.0 Hz), 3.48 (br s, 2H), 2.57 (t, 2H, J = 17.0 Hz), 2.34-2.03 (m, 2H).

^{13}C NMR (125 MHz, $CDCl_3$) δ 170.55, 140.53, 127.29, 125.28, 124.14, 119.65, 118.22, 44.45, 33.39, 27.98.

General procedure for nucleophilic substitution

The intermediate previously obtained (1 equiv.) or the commercially available methyl 3-bromopropanoate, methyl 4-chlorobutanoate, methyl 5-chloropentanoate, methyl 6-chloroexanoate and methyl 7-chloroheptanoate (1.5 equiv.) were added dropwise (in the first instance, under nitrogen atmosphere) to a solution of piperazine variously substituted (2 or 1 equiv. respectively) and $KHCO_3$ (2 equiv.) in anhydrous ACN or ACN, and the reaction mixture was stirred at 50 °C. The reaction mixture was quenched with a saturated solution of $NaHCO_3$ and extracted with EtOAc (3 x 20 ml). The reunited organic phases were dried with anhydrous Na_2SO_4, filtered and the solvent evaporated under vacuum. The residue was purified by flash chromatography using a gradient elution with EtOAc/MeOH to afford the desired products. According to this procedure, the following products have been obtained.

***N*-(2-aminophenyl)-3-(4-benzylpiperazin-1-yl)propanamide (2a)**

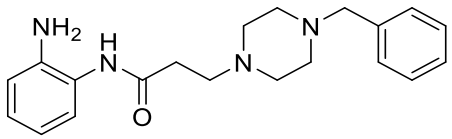

The product has been obtained using **1a** (0.191 g, 0.96 mmol) and 4-benzylpiperazine (0.332 ml, 1.92 mmol) at 50 °C for 48 hours. Yield 98% (0.318 g), beige solid.

Chemical Formula: $C_{20}H_{26}N_4O$ (338.46 g/mol)

m.p: 120 – 122 °C

^{1}H NMR (500 MHz, $CDCl_3$) δ 10.55 (s, 1H), 7.15 (d, *J* = 7.5 Hz, 1H), 7.03 (t, *J* = 7.5 Hz, 1H), 6.79 – 6.76 (m, 2H), 4.00 (br. s, 2H), 2.74 (m, *J* = 6.0 Hz, 2H), 2.62 (br. s, 4H), 2.57 (t, *J* = 6.0 Hz, 2H), 2.47 (br. s, 3H), 2.13 (d, *J* = 7.0 Hz, 2H), 1.77 – 1.66 (m, 6H), 1.51 – 1.42 (m, 1H), 1.27 – 1.12 (m, 3H), 0.90 – 0.83 (m, 2H).

^{13}C NMR (125 MHz, $CDCl_3$) δ 170.96, 140.54, 126.59, 124.92, 124.61, 119.21, 117.96, 65.65, 54.09, 53.79, 52.68, 35.19 , 32.31, 32.00, 26.93, 26.26..

Exact mass Anal. calcd: C, 71.18; H, 8.00; N, 16.45.
Found: C, 70.98; H, 7.74; N, 16.55.

***N*-(2-aminophenyl)-4-(4-benzylpiperazin-1-yl)butanamide (2b)**

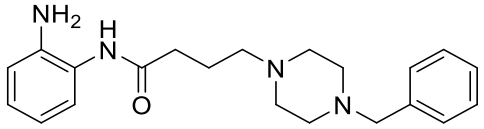

The product has been obtained using **1b** (0.294 g, 1.38mmol) and 4-benzylpiperazine (0.478ml,2.76 mmol) at 50 °C for 48 hours. Yield 34% (0.165 g), beige solid.

Chemical Formula: $C_{21}H_{28}N_4O$ (352.48 g/mol)

m.p: 102 – 104 °C

^{1}H NMR (500 MHz, $CDCl_3$) δ 8.84 (s, 1H), 7.32 – 7.23 (m, 5H), 7.11 (d, *J* = 8.0 Hz, 1H), 7.05 (t, *J* = 8.0 Hz, 1H), 6.77 (app t, 2H), 3.47 (s, 2H), 2.56 – 2.50 (m, 12H), 1.96 – 1.91 (m, 2H).

^{13}C NMR (125 MHz, $CDCl_3$) δ 171.73, 141.29, 137.93, 129.30, 128.38, 127.27, 127.15, 125.51, 124.50, 119.29, 118.15, 63.00, 57.57, 53.15, 52.68, 35.48, 22.22.

Exact mass Anal. calcd: C, 71.76; H, 8.21; N, 15.5.
Found: C, 71.56; H, 8.01; N, 15.90.

***N*-(2-aminophenyl)-3-(4-(cyclohexylmethyl)piperazin-1-yl)propanamide (3a)**

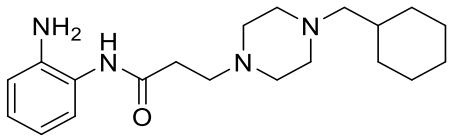

The product has been obtained using **1a** (0.300g. 1.51mmol) and 4-(cyclohexylmethyl)piperazine (0.55g, 3.02mmol) at 50 °C for 48 hours. Yield 95% (0.497 g), beige solid.

Chemical Formula: $C_{20}H_{32}N_4O$ (344.49 g/mol)

m.p: 153 – 156 °C

^{1}H NMR (500 MHz, $CDCl_3$) δ 10.55 (s, 1H), 7.15 (d, J = 10.0 Hz, 1H), 7.03 (t, *J* = 10.0 Hz, 1H), 6.79 – 6.76 (m, 2H), 4.00 (br. s, 2H), 2.74 (m, J = 5.0 Hz, 2H), 2.62 – 2.30 (m + t overlapped, *J* = 10.0 Hz, 10H), 2.13 (d, *J* = 10.0 Hz, 2H), 1.77 – 1.66 (m, 5H), 1.51 – 1.42 (m, 1H), 1.27 – 1.12 (m, 3H), 0.90 – 0.83 (m, 2H).

^{13}C NMR (125 MHz, $CDCl_3$) δ.170.96, 140.54, 126.59, 124.92, 124.61, 119.21, 117.96, 65.65, 54.09, 53.79, 52.68, 35.19 , 32.31, 32.00, 26.93, 26.26.

Exact mass Anal. calcd: C, 70.00; H, 9.46; N, 15.86.
Found: C, 69.73; H, 9.36; N, 16.26.

_N_-(2-aminophenyl)-4-(4-(cyclohexylmethyl)piperazin-1-yl)butanamide (3b)

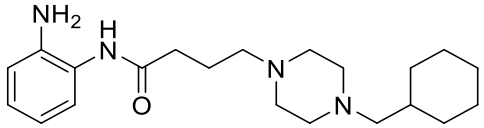

The product has been obtained using **1b** (0.377 g, 1.77 mmol) and 4-(cyclohexylmethyl)piperazine (0.687 ml, 3.54 mmol) at 50 °C for 48 hours. Yield 28% (0.179 g), beige solid.

Chemical Formula: $C_{21}H_{34}N_4O$ (358.53 g/mol)

m.p: 110 – 112 °C

^{1}H NMR (500 MHz, $CDCl_3$) δ 9.04 (s, 1H), 7.06 (dd, *J* = 17.0, 8.0 Hz, 2H), 6.77 (t, *J* = 8.3 Hz, 2H), 3.94 (s, 2H), 2.50, 2.38 (t + m overlapped, 10H), 2.07 (d, *J* = 7.0 Hz, 2H), 1.95 – 1.88 (m, 2H), 1.74 – 1.64 (m, 6H), 1.47 – 1.39 (m, 1H), 1.25 – 1.10 (m, 4H), 0.87 – 0.80 (m, 2H).

^{13}C NMR (125 MHz, $CDCl_3$) δ 171.93, 141.38, 127.18, 125.56, 124.54, 119.31, 118.19, 65.70, 57.71, 53.57, 53.25, 35.78, 35.12, 32.04, 26.92, 26.27, 22.37.

Exact mass Anal. calcd: C, 70.55; H, 9.76; N, 15.33.
Found: C, 70.35; H, 9.56; N, 15.63.

_N_-(2-aminophenyl)-3-(4-cyclohexylpiperazin-1-yl)propanamide (4a)

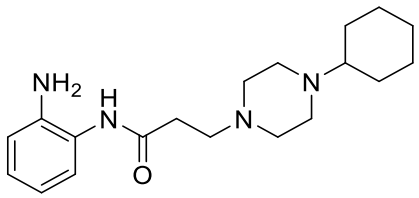

The product has been obtained using **1a** (0.300 g, 1.51 mmol) and 4-cyclohexylpiperazine (0.510 g, 3.02 mmol) at 50 °C for 48 hours. Yield 99% (0.496 g), beige solid.

Chemical Formula: $C_{19}H_{30}N_4O$ (330.48 g/mol)

m.p: 96 – 98 °C

^{1}H NMR (500 MHz, $CDCl_3$) δ 10.48 (s, 1H), 7.18 – 7.14 (d, J = 10.0 Hz 1H), 7.08 – 6.99 (t, J = 10.0 Hz, 1H), 6.82 – 6.75 (m, 2H), 3.95 (br s, 2H), 2.77 – 2.54 (m, 12H), 2.30 – 2.19 (m, 1H), 1.90 – 1.73 (dd, J = 10.0 Hz, J = 35.0 Hz, 4H), 165-160 (d, J = 10.0 Hz, 1H, 1.34 – 0.82 (m, 5H).

^{13}C NMR (125 MHz, $CDCl_3$) δ 170.97, 140.51, 126.56, 124.93, 124.59, 119.23, 117.92, 63.52, 54.11, 53.11, 49.13, 32.32, 29.16, 26.38, 25.90.

Exact mass Anal. calcd: C, 69.255; H, 9.55; N, 16.95.
Found: C, 69.05; H, 9.15; N, 16.95.

***N*-(2-aminophenyl)-4-(4-cyclohexylpiperazin-1-yl)butanamide (4b)**

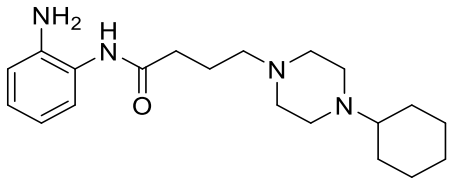

The product has been obtained using **1b** (0.371 g; 1.74 mmol) and 4-cyclohexylpiperazine (0.580 g, 3.48 mmol) at 50 °C for 48 hours. Yield 23% (0.139 g), beige solid.

Chemical Formula: $C_{20}H_{32}N_4O$ (344.50 g/mol)

m.p: 100 – 103 °C

^{1}H NMR (500 MHz, $CDCl_3$) δ 9.14 (s, 1H), 7.12 – 7.02 (m, 2H), 6.81 - 6.74 (m, 2H), 3.97 (br. s, 2H), 2.75 - 2.38 (m, 12H), 2.20 (t, 2H), 1.96 – 1.90 (m, 2H), 1.85 – 1.71 (m, 4H), 1.60 (d, 2H), 1.26 – 1.03 (m, 6H).

^{13}C NMR (125 MHz, $CDCl_3$) δ 171.94, 141.35, 127.15, 125.56, 124.55, 119.33, 118.19, 63.58, 57.84, 53.56, 48.72, 35.87, 28.92, 26.38, 25.96, 22.36.

Exact mass Anal. calcd: C, 70.00; H, 9.56; N, 16.00.
Found: C, 69.73; H, 9.36; N, 16.26.

Methyl 3-(4-benzylpiperazin-1-yl)propanoate (5a)

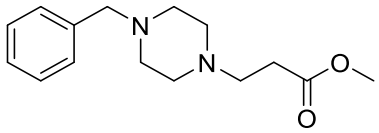

The product has been obtained using 1-benzylpiperazine (0.600 g, 591 µl, 3.404 mmol) and methyl 3-bromopropanoate (0.853 g, 557 µl, 5,106 mmol) at 50 °C overnight. Yield 71% (0.638 g), yellow oil. The pure product was dissolved in EtOAc/Et_2O and added to a solution of HCl in EtOH (1.25 M) dropwise to obtain the desired product as hydrochloride salt (white solid).

Chemical Formula: $C_{15}H_{22}N_2O_2$ (335.27 g/mol)

m.p: 184-186 °C

^{1}H NMR (free base): (200 MHz, $CDCl_3$) δ 6.2-5.88 (m, 5H), 2.42 (s, 3H), 2.25 (s, 2H), 1.45 (t, *J* = 7.2 Hz, 2H), 1.36-1.02 (m, 10H).

^{13}C NMR (free base): (50 MHz, $CDCl_3$) δ 173.08, 138.09, 129.36, 128.33, 127.17, 63.13, 53.60, 53.06, 52.98, 51.79, 32.12.

Exact mass: Anal. calcd: C, 53.74; H, 7.22; N, 8.36.
Found: C, 54.04; H, 7.32; N, 8.26.

Methyl 4-(4-benzylpiperazin-1-yl)butanoate (5b)

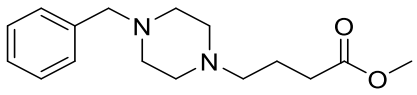

The product has been obtained using 1-benzylpiperazine (0.600 g, 591 µl, 3.404 mmol) and methyl 4-chlorobutanoate (0.697 g, 616 µl, 5.106 mmol) at 50 °C overnight. The crude product was purified by column chromatography on silica gel using a gradient elution with EtOAc/MeOH. Yield 74% (0.696 g), yellow oil. The pure product was dissolved in EtOAc/Et_2O and added to a solution of HCl in EtOH (1.25 M) dropwise to obtain the desired product as hydrochloride salt (white solid).

Chemical Formula: $C_{16}H_{24}N_2O_2 \cdot 2HCl$ (349.30 g/mol)

m.p: 98 - 100 °C

^{1}H NMR (free base)	(500 MHz, $CDCl_3$) δ 7.34-7.21 (m, 5H), 3.66 (s, 3H), 3.50 (s, 2H), 2.65-2.38 (m, 8H), 2.37-2.30 (t-t ovlp., 4H), 1.80 (quint, *J* = 7.5 Hz, 2H).
^{13}C NMR (free base)	(125 MHz, $CDCl_3$) δ 174.12, 138.25, 129.33, 128.48, 128.30, 127.12, 63.21, 57.78, 53.23, 51.63, 32.20, 22.33.
Exact mass	Anal. calcd: C, 55.02; H, 7.50; N, 8.02. Found: C, 55.32; H, 7.70; N, 7.87.

Methyl 3-(4-(cyclohexylmethyl)piperazin-1-yl)propanoate (6a)

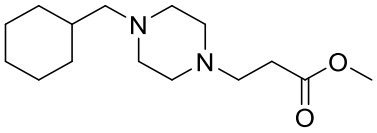

The product has been obtained using 1-(cyclohexylmethyl)piperazine (0.600 g, 639 µl, 3.291 mmol) and methyl 3-bromopropanoate (0.893 g, 583 µl, 5.348 mmol) at 50 °C overnight. The crude product was purified by column chromatography on silica gel using a gradient elution with EtOAc/MeOH. Yield 74 % (0.671 g,), yellow oil. The pure product was dissolved in EtOAc/Et_2O and added to a solution of HCl in EtOH (1.25 M) dropwise to obtain the desired product as hydrochloride salt (white solid).

Chemical Formula: $C_{15}H_{28}N_2O_2 \cdot 2HCl$ (341.32 g/mol)

m.p: 238 - 240 °C

^{1}H NMR (free base)	(200 MHz, $CDCl_3$) δ 3.68 (s, 3H), 2.70 (t, *J* = 6.0 Hz, 2H), 2.60-2.21 (m+t ovlp., *J* = 6.0 Hz, 10H), 2.11 (d, *J* = 8.0 Hz, 2H), 1.85-1.58 (m, 5H), 1.57-1.35 (m, 1H), 1.35-1.03 (m, 3H), 1.01-0.70 (m, 2H).
^{13}C NMR (free base)	(50 MHz, $CDCl_3$) δ 173.14, 65.80, 53.67, 53.07, 51.79, 35.09, 32.14, 32.06, 26.92, 26.28.
Exact mass	Anal. calcd: C, 52.79; H, 8.86; N, 8.21. Found: C, 53.19; H, 9.16; N, 8.11.

Methyl 4-(4-(cyclohexylmethyl)piperazin-1-yl)butanoate (6b)

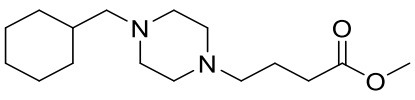

The product has been obtained using 1-(cyclohexylmethyl)piperazine (0.600 g, 639 µl, 3.291 mmol) and methyl 4-chlorobutanoate (0.674 g, 596 µl, 4.936 mmol) at 50 °C overnight. The crude product was purified by column chromatography on silica gel using a gradient elution with EtOAc/MeOH. Yield 74 % (0.696 g), yellow oil. The pure product was dissolved in EtOAc/Et_2O and added to a solution of HCl in EtOH (1.25 M) dropwise to obtain the desired product as hydrochloride salt (white solid).

Chemical Formula: $C_{16}H_{30}N_2O_2 \cdot 2HCl$ (355.34 g/mol)

m.p: 160 - 162 °C

^{1}H NMR (free base) (200 MHz, $CDCl_3$) δ 3.67 (s, 3H), 2.68-2.26 (m-t ovlp., 12H), 2.11 (d, *J* = 7.0 Hz, 2H), 1.95-1.59 (m-quint ovlp., 7H), 1.55-1.37 (m, 1H), 1.34-1.09 (m, 3H), 1.00-0.73 (m, 2H).

^{13}C NMR (free base) (50 MHz, $CDCl_3$) δ 173.98, 65.72, 57.70, 53.61, 53.11, 51.52, 34.94, 31.92, 31.72, 26.78, 26.14, 22.14.

Exact mass Anal. calcd: C, 54.08; H, 9.08; N, 7.88.
Found: C, 54.38; H, 9.28; N, 7.68.

Methyl 3-(4-(cyclohexylpiperazin-1-yl)propanoate (7a)

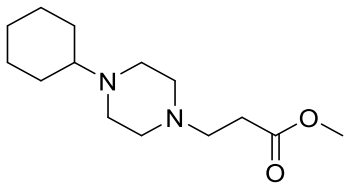

The product has been obtained using 1-cyclohexylpiperazine (0.600 g, 3.565 mmol) and methyl 3-bromopropanoate (0.824 g, 538 µl, 4.936 mmol) at 50 °C overnight. The crude product was purified by column chromatography on silica gel using a gradient elution with EtOAc/MeOH. Yield 70 % (0.621 g), yellow oil. The pure product was dissolved in EtOAc/Et_2O and added to a solution of HCl in EtOH (1.25 M) dropwise to obtain the desired product as hydrochloride salt (white solid).

Chemical Formula: $C_{14}H_{26}N_2O_2 \cdot 2HCl$ (327.29 g/mol)

m.p: 166 - 168 °C

^{1}H NMR (free base) (200 MHz, $CDCl_3$) δ 3.61 (s, 3H), 2.75-2.56 (t, *J* = 8.0 Hz, 2H), 2.58-2.30 (m+t, 10H), 2.29-2.05 (m, 1H), 1.87-1.64 (m, 4H), 1.62-1.45 (m, 1H), 1.28-0.93 (m, 5H).

^{13}C NMR (free base) (50 MHz, $CDCl_3$) δ 173.08, 63.57, 53.65, 53.40, 51.77, 48.87, 32.05, 29.01, 26.38, 25.98.

Exact mass Anal. calcd: C, 51.38; H, 8.62; N, 8.56.
Found: C, 51.68; H, 8.92; N, 8.36.

Methyl 4-(4-cyclohexylpiperazin-1-yl)butanoate (7b)

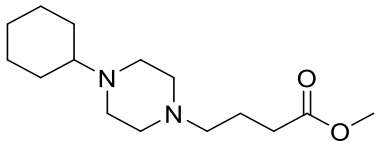

The product has been obtained using 1-cyclohexylpiperazine (0.600 g, 3.565 mmol) and methyl 4-chlorobutanoate (0.730 g, 646 µl, 5.348 mmol) at 50 °C overnight. The crude product was purified by column chromatography on silica gel using a gradient elution with EtOAc/MeOH. Yield 69% (0.660 g), yellow oil. The pure product was dissolved in EtOAc/Et_2O and added to a solution of HCl in EtOH (1.25 M) dropwise to obtain the desired product as hydrochloride salt (white solid).

Chemical Formula: $C_{15}H_{28}N_2O_2 \cdot 2HCl$ (341.32 g/mol)

m.p: 158 - 160 °C

^{1}H NMR (free base) (200 MHz, $CDCl_3$) δ 3.48 (s, 3H), 2.70-1.94 (m-t ovlp., 14H), 1.82-1.36 (m, 7H), 1.19-0.82 (m, 4H).

^{13}C NMR (free base) (50 MHz, $CDCl_3$) δ 173.71, 63.26, 57.53, 53.35, 51.31, 48.67, 31.86, 28.73, 26.11, 25.68, 21.97.

Exact mass Anal. calcd: C, 52.79; H, 8.86; N, 8.21.
Found: C, 52.99; H, 9.06; N, 8.11.

Methyl 3-(4-(4-chlorophenyl)-4-hydroxypiperidin-1-yl)propanoate (8a)

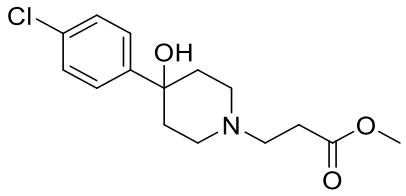

The product has been obtained using 4-(4-chlorophenyl)piperidin-4-ol (0.500 g, 2.36 mmol) and methyl 3-bromopropanoate (0.591 g; 386µL, 3.54 mmol) at 50 °C overnight. The crude product was purified by column chromatography on silica gel using a gradient elution with EtOAc/MeOH. Yield 100 % (0.717 g), white solid.

Chemical Formula: $C_{15}H_{20}ClNO_3$ (297.78 g/mol)

m.p: 166 - 168 °C

^{1}H NMR (free base): (500 MHz, $CDCl_3$) 7.50-7.40 (m, 2H); 7.33-7.28 (m, 2H); 3.69 (s, 3H); 2.81-2.74 (m-t ovlp, *J*=5.0 Hz, 4H); 2.56-2.53 (t, *J*=5.0 Hz, 2H,); 2.51-2.46 (td, *J*=2.5.0, 12.0 Hz, 2H); 2.12-2.06 (td, *J*= 4.5, 13.0 Hz, 2H); 1.75-1.69 (m, 2H).

^{13}C NMR (free base): (125 MHz, $CDCl_3$) δ 173.16, 146.99, 132.97, 128.57, 126.24, 71.12, 53.79, 51.82, 49.31, 38.60, 32.39.

Exact mass: Anal. calcd: C, 60.70; H, 7.07; N, 4.95.
Found: C, 60.50; H, 6.77; N, 4.70.

Methyl 3-(4-(4-chlorophenyl)-4-hydroxypiperidin-1-yl)butanoate (8b)

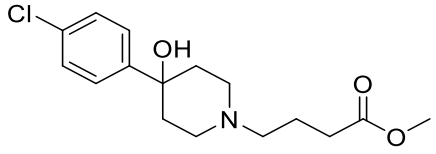

The product has been obtained using 4-(4-chlorophenyl)piperidin-4-ol (0.500 g; 2.36 mmol) and methyl 4-chlorobutanoate (0.392 g; 344µL; 2.83mmol) at 50 °C overnight. The crude product was purified by column chromatography on silica gel using a gradient elution with EtOAc/MeOH. Yield 41.3% (0.304 g), white solid.

Chemical Formula: $C_{16}H_{22}ClNO_3$ (311.81 g/mol)

m.p: 158 - 160 °C

^{1}H NMR (free base) (500 MHz, $CDCl_3$) δ 7.46-7.41 (m, 2H), 7.33-7.28 (m, 2H), 3.68 (s, 3H), 2.85-2.75 (m, 2H), 2.47-2.38 (m-t ovlp, *J*=10.0 Hz, 4H), 2.37 (t, *J*=10.0 Hz, 2H), 2.10 (td, *J*=5.0, 15.0 Hz, 2H), 1.85 (q, *J*=10.0 Hz, 2H), 1.75-1.68 (m, 2H).

^{13}C NMR (free base) (125 MHz, $CDCl_3$) δ 174.16, 147.05, 132.97, 128.55, 126.26, 71.24, 57.90, 51.69, 49.51, 38.63, 32.23, 22.47.

Exact mass Anal. calcd: C, 61.85; H, 7.44; N, 4.61.
Found: C, 61.63; H, 7.11; N, 4.49.

Methyl 5-(4-(4-chlorophenyl)-4-hydroxypiperidin-1-yl)pentanoate (8c)

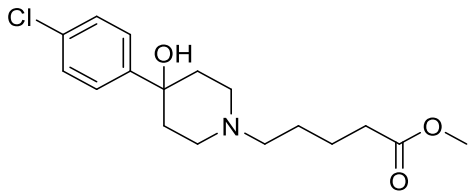

The product has been obtained using 4-(4-chlorophenyl)piperidin-4-ol (0.500 g; 2.36 mmol) and methyl 5-chloropentanoate (0.690 g; 506 µL; 3.54mmol) at 50 °C overnight. The crude product was purified by column chromatography on silica gel using a gradient elution with EtOAc/MeOH. Yield 87.7%. (0.675 g), white solid.

Chemical Formula: $C_{17}H_{24}ClNO_3$ (325.83 g/mol)

m.p: 166 - 168 °C

^{1}H NMR (free base) (500 MHz, $CDCl_3$) δ 7.45-7.41 (m, 2H); 7.32-7.28 (m, 2H); 3.66 (s, 3H); 2.81 (d, *J*= 10.0 Hz, 2H); 2.45-2.35 (m-t ovlp, 4H); 2.34 (t, *J*= 10.0 Hz, 2H); 2.15-2.09 (td, *J*=4.0, 13.0 Hz, 2H); 1.75-1.63 (m-q ovlp, 4H); 1.59-1.53 (m, 2H).

^{13}C NMR (free base) (125 MHz, $CDCl_3$) δ 174.15; 147.02; 132.90; 128.53; 126.25; 71.18; 58.38; 51.65; 49.55; 38.53; 34.05; 26.57; 23.14

Exact mass Anal. calcd: C, 62.92; H, 7.72; N, 4.54.
Found: C, 62.67; H, 7.42; N, 4.30.

Methyl 6-(4-(4-chlorophenyl)-4-hydroxypiperidin-1-yl)hexanoate (8d)

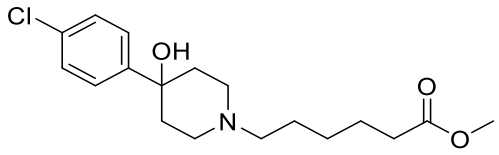

The product has been obtained using 4-(4-chlorophenyl)piperidin-4-ol (0.500 g; 2.36 mmol) and methyl 6-chloroexanoate (0.740 g; 562µL; 3.54mmol) at 50 °C overnight. The crude product was purified by column chromatography on silica gel using a gradient elution with EtOAc/MeOH. Yield 88% (0.696 g), white solid.

Chemical Formula: $C_{18}H_{26}ClNO_3$ (339.86 g/mol)

m.p: 158 - 160 °C

^{1}H NMR (free base): (500 MHz, $CDCl_3$) δ 7.47-7.41 (m, 2H); 7.33-7.28 (m, 2H); 3.66 (s, 3H); 2.90-2.85 (m, 2H); 2.52-2.43 (m, 4H); 2.32 (t, *J*= 10.0 Hz, 2H); 2.20 (t, *J*= 3.5, 13.5 Hz, 2H); 1.73 (dd, *J*= 2.0, 14.0 Hz, 2H); 1.68-1.62 (m, 2H); 1.61-1.57 (m, 2H); 1.35 (q, *J*= 10.0 Hz, 2H).

^{13}C NMR (free base): (125 MHz, $CDCl_3$) δ 174.25; 146.76; 133.01; 128.59; 126.23; 71.10; 58.60; 51.65; 49:54; 38.29; 34.11; 27.26; 26.53; 24.94.

Exact mass: Anal. calcd: C, 63.93; H, 7.86; N, 4.22.
Found: C, 63.61; H, 7.71; N, 4.12.

Methyl 7-(4-(4-chlorophenyl)-4-hydroxypiperidin-1-yl)heptanoate (8e)

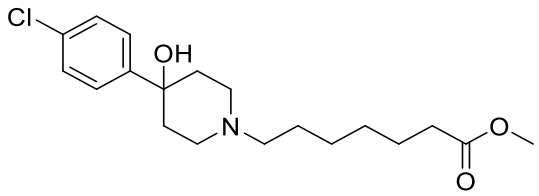

The product has been obtained using 4-(4-chlorophenyl)piperidin-4-ol (0.500 g; 2.36 mmol) and methyl 7-chloroheptanoate (0.790 g; 628µL; 3.54mmol) at 50 °C overnight. The crude product was purified by column chromatography on silica gel using a gradient elution with EtOAc/MeOH. Yield 85% (0.709 g), white solid.

Chemical Formula: $C_{19}H_{28}ClNO_3$ (353.89 g/mol)

m.p: 166 - 168 °C

^{1}H NMR (free base)	(500 MHz, $CDCl_3$) δ 7.45-7.43 (m, 2H); 7.32-7.30 (m, 2H); 3.68 (s, 3H); 2.94-2.91 (d, 2H); 2.57-2.47 (m, t, overlap 4H); 2.32-2.24 (t, m, overlap 4H); 1.76-1.74(d, d, 2H); 1.66-1.58 (m, 4H); 1.35-1.34 (t, 4H).
^{13}C NMR (free base)	(125 MHz, $CDCl_3$) δ 174.33; 146.56; 133.09; 128.62; 126.22; 70.99; 58.67; 51.63; 49.49; 38.05; 34.12; 29.09; 27.32; 26.41; 24.96.
Exact mass	Anal. calcd: C, 64.72; H, 8.28; N, 4.14. Found: C, 64.49; H, 7.98; N, 3.96.

General procedure for preparation of hydroxamic acid

To an ice-cooled solution of hydroxylamine hydrochloride (5 eq) in MeOH (30 ml) was added a solution of NaOH (10 eq) in MeOH (30 ml) dropwise. The resulting mixture was stirred at room temperature for 2 hours. The precipitate was filtered and the filtrate was added to an ice-cooled solution of the esters **5a-b**, **6a-b**, **7a-b** and **8a-e** in MeOH (5 ml) dropwise. An additional amount of NaOH was added and the reaction mixture was stirred overnight at room temperature. The reaction solution was concentrated in vacuo and diluted with DCM. The precipitate was filtered and the filtrate was purified by silica gel filtration with a mixture DCM/MeOH (80-20%) to give the desired final product. After purification, the pure product was dissolved in EtOH/Et_2O and added to a solution of HCl in EtOH (1.25 M) dropwise to obtain the desired product as hydrochloride salt (white solid).

3-(4-benzylpiperazin-1-yl)-*N*-hydroxypropanamide (9a)

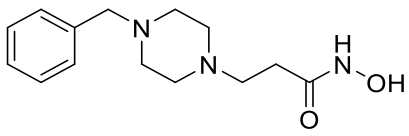

The product has been obtained using **5a** (0.437 g, 1.67 mmol), hydroxylamine hydrochloride (0.579 g, 8.34 mmol) and NaOH (0.667 g, 16.68 mmol). Yield 69% (0.660 g), colorless oil and converted as salt (white solid).

Chemical Formula: $C_{14}H_{21}N_3O_2 \cdot 2HCl$ (336.26 g/mol)

m.p: 175 - 177 °C

^{1}H NMR (hydrochloride)	(500 MHz, CD_3OD) δ 7.64-7.46 (m, 5H), 4.41 (s, 2H), 3.75-3.51 (m, 8H), 3.48 (t, *J* = 7.0 Hz, 2H), 2.89 (t, *J* = 7.0 Hz, 2H).
^{13}C NMR (hydrochloride)	(125 MHz, CD_3OD) δ 173.16, 132.41, 131.31, 130.40, 61.39, 53.56, 50.38, 49.59, 29.80.
Exact mass	Anal. calcd: C, 50.01; H, 6.89; N, 12.50. Found: C, 50.41; H, 7.09; N, 12.24.

4-(4-benzylpiperazin-1-yl)-*N*-hydroxybutanamide (9b)

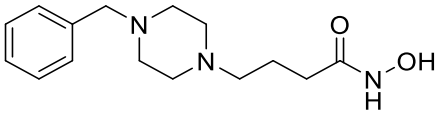

The product has been obtained using **5b** (0.270 g, 0.97mmol), hydroxylamine hydrochloride (0.339 g, 4.88 mmol) and NaOH (0.391 g, 9.76 mmol). Yield 47% (0.128 g), colorless oil and converted as salt (white solid).

Chemical Formula: $C_{15}H_{23}N_3O_2 \cdot 2HCl$ (350.28 g/mol)

m.p: 130 - 132 °C

^{1}H NMR (hydrochloride)	(500 MHz, DMSO-d_6) δ 10.56 (s, 1H), 7.75-7.40 (m, 5H), 4.29 (br. s, 1H), 3.75-2.90 (m-t ovlp., 12H), 2.33 (t, *J* = 7.0 Hz, 1H), 2.06 (t, *J* = 7.0 Hz, 1H), 1.95-1.85 (m, 2H).
^{13}C NMR (hydrochloride)	(125 MHz, DMSO-d_6) δ 173.41, 167.89, 131.17, 129.31, 128.76, 47.83, 47.22, 30.59, 29.14, 19.39, 18.78.
Exact mass	Anal. calcd: C, 51.43; H, 7.19; N, 12.00. Found: C, 51.83; H, 7.59; N, 11.80.

3-(4-(cyclohexylmethyl)piperazin-1-yl)-*N*-hydroxypropanamide (10a)

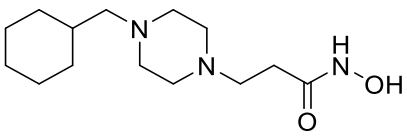

The product has been obtained using **6a** (0.313 g, 1.16 mmol), hydroxylamine hydrochloride (0.405 mg, 5.83 mmol) and NaOH (0.466 mg, 11.66 mmol). Yield 49% (0.156 g), colorless oil and converted as salt (white solid).

Chemical Formula: $C_{14}H_{27}N_3O_2 \cdot 2HCl$ (342.31 g/mol)

m.p: 158 - 160 °C

^{1}H NMR (hydrochloride)	(500 MHz, CD_3OD) δ 3.55-3.10 (m-t ovlp., 10H), 2.99 (d, *J* = 6.0 Hz, 2H), 2.76 (t, *J* = 7.0 Hz, 1H), 2.52 (t, *J* = 7.0 Hz, 1H), 1.91-1.69 (m, 6H), 1.43-1.31 (m, 2H), 1.30-1.17 (m, 1H), 1.13-1.03 (m, 2H).
^{13}C NMR (hydrochloride)	(125 MHz, CD_3OD) δ 169.84, 64.20, 53.96, 52.17, 50.47, 34.15, 31.88, 31.01, 26.98.
Exact mass	Anal. calcd: C, 40.12; H, 8.54; N, 12.28. Found: C, 49.42; H, 8.74; N, 12.18.

4-(4-(cyclohexylmethyl)piperazin-1-yl)-*N*-hydroxybutanamide (10b)

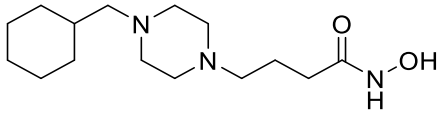

The product has been obtained using **6b** (0.239 g, 0.84 mmol), hydroxylamine hydrochloride (0.293 g, 4.22 mmol) and NaOH (0.337 g, 8.44 mmol). Yield 59% (0.142 g,), colorless oil and converted as salt (white solid).

Chemical Formula: $C_{15}H_{29}N_3O_2 \cdot 2HCl$ (356.33 g/mol)

m.p: 210 - 212 °C

^{1}H NMR (hydrochloride)	(500 MHz, DMSO-d_6) δ 3.92-2.85 (m-t-d ovlp., 12H), 2.35 (t, *J* = 7.5 Hz, 1H), 2.08 (t, *J* = 7.5 Hz, 1H), 1.93-1.84 (m, 4H), 1.82-1.72 (m, 1H), 1.70-1.55 (m, 3H), 1.29-1.06 (m, 3H), 1.00-0.87 (m, 2H).
^{13}C NMR (hydrochloride)	(125 MHz, DMSO-d_6) δ 173.38, 62.00, 55.11, 48.65, 47.61, 32.00, 30.47, 29.10, 25.47, 24.96, 18.65.
Exact mass	Anal. calcd: C, 50.56; H, 8.77; N, 11.79. Found: C, 50.86; H, 8.97; N, 11.69.

3-(4-cyclohexylpiperazin-1-yl)-*N*-hydroxypropanamide (11a)

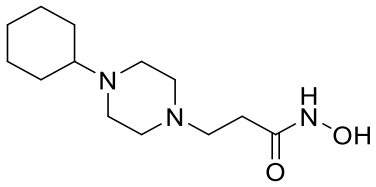

The product has been obtained using **7a** (0.671 g, 2.64 mmol), hydroxylamine hydrochloride (0.916 g, 13.19 mmol) and NaOH (0.667 mg, 16.68 mmol). Yield 47% (0.315 g), colorless oil and converted as salt (white solid).

Chemical Formula: $C_{13}H_{25}N_3O_2 \cdot 2HCl$ (328.28 g/mol)

m.p: 124 - 126 °C

^{1}H NMR (hydrochloride) (500 MHz, DMSO-d_6) δ 10.50 (s, 1H), 9.89 (s, 1H), 3.10–2.64 (m-t ovlp, 10H), 2.17 (t, J = 7.0 Hz, 2H), 2.09-1.95 (m, 2H), 1.81-1.72 (m, 2H), 1.63-1.53 (m, 1H), 1.40-1.15 (m, 5H), 1.13-1.00 (m, 1H).

^{13}C NMR (hydrochloride) (125 MHz, DMSO-d_6) δ 167.54, 63.66, 52.93, 49.78, 47.61, 29.83, 26.56, 24.96, 24.66.

Exact mass Anal. calcd: C, 47.56; H, 8.29; N, 12.80.
Found: C, 47.76; H, 8.49; N, 12.55.

4-(4-cyclohexylpiperazin-1-yl)-*N*-hydroxybutanamide (11b)

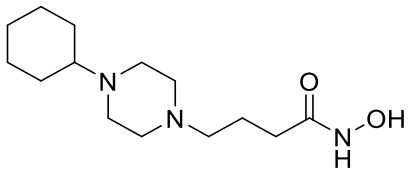

The product has been obtained using **7b** (202 mg, 0.75 mmol), hydroxylamine hydrochloride (261 mg, 3.76 mmol) and NaOH (301 mg, 7.52 mmol). Yield 47% (95 mg,), colorless oil and converted as salt (white solid).

Chemical Formula: $C_{14}H_{27}N_3O_2 \cdot 2HCl$ (342.31 g/mol)

m.p: 241 - 243 °C

^{1}H NMR (hydrochloride) (500 MHz, DMSO-d_6) δ 3.90-3.00 (m-t ovlp., 11H), 2.35 (t, *J* = 7.5 Hz, 2H), 2.14-2.05 (m, 2H), 1.92 (quint, *J* = 7.5 Hz, 2H), 1.86-1.77 (m, 2H), 1.64-1.55 (m, 1H), 1.50-1.36 (m, 2H), 1.34-1.19 (m, 2H), 1.16-1.04 (m, 1H).

^{13}C NMR (hydrochloride)	(125 MHz, DMSO-d_6) δ 173.35, 64.13, 54.91, 47.98, 44.48, 30.52, 25.79, 24.53, 24.30, 18.66.
Exact mass	Anal. calcd: C, 49.12; H, 8.54; N, 12.28. Found: C, 49.42; H, 8.84; N, 12.28.

3-(4-(4-chlorophenyl)-4-hydroxypiperidin-1-yl)-*N*-hydroxypropanamide (12a)

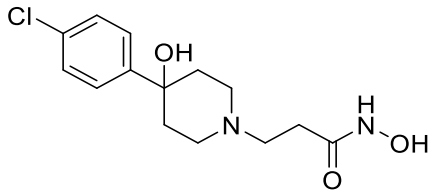

The product has been obtained using **8a** (0.300 g; 1.0 mmol), hydroxylamine hydrochloride (0.350 g; 5.0 mmol) and LiOH (0.240 g; 10 mmol). Yield 33% (0.100 g), colorless oil and converted as salt (white solid).

Chemical Formula: $C_{14}H_{20}Cl_2N_2O_3 \cdot HCl$ (336.26 g/mol)

m.p: 175 - 177 °C

^{1}H NMR (hydrochloride)	(500 MHz, DMSO-d_6) δ 10.44 (br s, 1H); 9.74 (br s, 1H); 7.53-7.43 (m, 2H); 7.40-7.30 (m, 2H); 5.02 (br s, 1H); 2.81 (d, *J*=10.0 Hz, 1H); 2.67 (d, *J*=5.0 Hz, 1H); 2.55 (t, *J*=10.0 Hz, 2H); 2.45-2.25 (m, 3H); 2.04-1.85 (m, 3H); 1.75-1.55 (m, 4H).
^{13}C NMR (hydrochloride)	(125 MHz, DMSO-d_6) δ 174.71; 169.06; 148.57; 130.93; 127.79; 126.79; 69.11; 57.20; 48.60; 37.10; 33.58; 30.33; 21.33.
Exact mass	Anal. calcd: C, 50.42; H, 6.28; N, 8.50. Found: C, 50.16; H, 6.01; N, 8.36.

4-(4-(4-chlorophenyl)-4-hydroxypiperidin-1-yl)-*N*-hydroxybutanamide (12b)

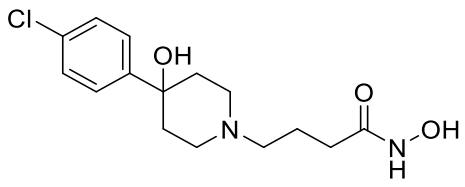

The product has been obtained using **8b** (0.304 g; 0.975 mmol), hydroxylamine hydrochloride (0.339 gr; 4.88 mmol) and LiOH (0.233 g; 9.75 mmol). Yield 49% (0.148 g), colorless oil and converted as salt (white solid).

Chemical Formula: $C_{15}H_{22}Cl_2N_2O_3 \cdot HCl$ (349.25 g/mol)

m.p: 130 - 132 °C

^{1}H NMR (hydrochloride)	(500 MHz, DMSO-d_6) δ 10.44 (br s, 1H); 9.74 (br s, 1H); 7.53-7.43 (m, 2H); 7.40-7.30 (m, 2H); 5.02 (br s, 1H); 2.81 (d, *J*=10.0 Hz, 1H); 2.67 (d, *J*=5.0 Hz, 1H); 2.55 (t, *J*=10.0 Hz, 2H); 2.45-2.25 (m, 3H); 2.04-1.85 (m, 3H); 1.75-1.55 (m, 4H).
^{13}C NMR (hydrochloride)	(125 MHz, DMSO-d_6) δ 174.71; 169.06; 148.57; 130.93; 127.79; 126.79; 69.11; 57.20; 48.60; 37.10; 33.58; 30.33; 21.33.
Exact mass	Anal. calcd: C, 51.87; H, 6.62; N, 8.16. Found: C, 51.59; H, 6.35; N, 8.02.

5-(4-(4-chlorophenyl)-4-hydroxypiperidin-1-yl)-*N*-hydroxypentanamide (12c)

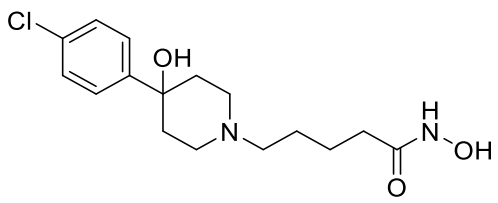

The product has been obtained using **8c** (0.570 g; 1.75 mmol), hydroxylamine hydrochloride (0.609 g; 8.54mmol) and LiOH (0.420 gr; 17.5 mmol). Yield 46% (0.274 g), colorless oil and converted as salt (white solid).

Chemical Formula: $C_{15}H_{22}Cl_2N_2O_3 \cdot HCl$ (363.28 g/mol)

m.p: 130 - 132 °C

^{1}H NMR (hydrochloride)	(500 MHz, DMSO-d_6) δ 10.37 (br s, 1H); 9.73 (br s, 1H); 7.52 - 7.46 (m, 2H); 7.37-7.32 (m, 2H); 4.85 (br s, 1H); 2.62 (d, *J*= 10.0 Hz, 2H); 2.35-2.25 (m, 4H); 1.96 (t, *J*= 10.0 Hz, 2H); 1.82 (td, *J*= 5.0; 15.0 Hz; 2H); 1.58-1.35 (m, 6H).
^{13}C NMR (hydrochloride)	(125 MHz, DMSO-d_6) δ 168.98, 149.18, 130.67, 127.64, 126.60, 69.52, 57.70, 48.99, 37.89, 32.15, 26.01, 23.17.

Exact mass	Anal. calcd: C, 53.22; H, 6.88; N, 7.84.
	Found: C, 52.90; H, 6.66; N, 7.71.

6-(4-(4-chlorophenyl)-4-hydroxypiperidin-1-yl)-N-hydroxyhexanamide (12d)

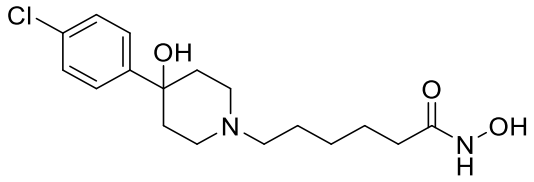

The product has been obtained using **8d** (0.594 g; 1.75 mmol), hydroxylamine hydrochloride (0.609 g; 8.75 mmol) and LiOH (0.420 g; 17.5 mmol). Yield 69% (0.415 g), colorless oil and converted as salt (white solid).

Chemical Formula: $C_{17}H_{26}Cl_2N_2O_3 \cdot HCl$ (377.31 g/mol)

m.p: 130 - 132 °C

^{1}H NMR (hydrochloride)	(500 MHz, DMSO-d_6) δ 10.35 (br s, 1H), 9.72 (br s, 1H), 7.52-7.46 (m, 2H), 7.37-7.32 (m, 2H), 4.88 (br s, 1H), 2.65 (d, *J*= 10.0 Hz, 2H), 2.40-2.25 (t-t ovlp, *J* = 5.0, 10.0 Hz, 4H), 2.06 (t-m ovlp, *J*= 5.0 Hz, 1H), 1.60-1.40 (m, 6H), 1.24 (q, *J* = 5.0 Hz, 2H).
^{13}C NMR (hydrochloride)	(125 MHz, DMSO-d_6) δ 169.05, 149.13, 130.74, 127.69, 126.83, 69.51, 57.98, 40.03, 37.79, 32.25, 26.62, 26.16, 25.10.
Exact mass	Anal. calcd: C, 57.87; H, 6.90; N, 9.10.
	Found: C, 54.12; H, 6.95; N, 7.42.

7-(4-(4-chlorophenyl)-4-hydroxypiperidin-1-yl)-*N*-hydroxyheptanamide (12e)

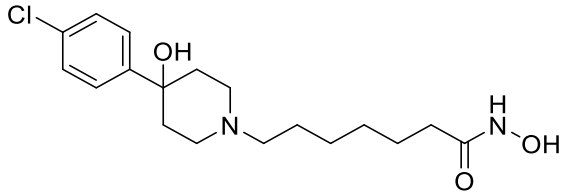

The product has been obtained using **8e** (0.600 g; 1.71 mmol), hydroxylamine hydrochloride (0.609 g; 8.54 mmol) and NaOH (0.410 g; 17.1 mmol). Yield 30 % (0.173 g), colorless oil and converted as salt (white solid).

Chemical Formula: $C_{18}H_{28}Cl_2N_2O_3 \cdot HCl$ (391.33 g/mol)

m.p: 130 - 132 °C

^{1}H NMR (hydrochloride)	(500 MHz, DMSO-d_6) δ 10.34 (br s, 1H); 9.71 (br s, 1H); 7.52-7.46 (m, 2H); 7.37-7.31 (m, 2H); 4.85 (br. s, 1H); 2.62 (d, *J* =10.0 Hz, 2H), 2.36-2.23 (m-t ovlp, *J* = 10.0 Hz, 4H), 1.96-1.83 (t-td, *J* = 10.0, 5.0, 15.0 Hz, 4H); 1.55 (m, 2H); 1.52-1.38 (m, 4H); 1.30-1.21 (m, 2H).
^{13}C NMR (hydrochloride)	(125 MHz, DMSO-d_6) δ 169.00, 149.20, 130.67, 127.65, 126.81, 60.55, 58.13, 49.06, 37.92, 32.22, 28.55, 26.76, 26.46, 25.09.
Exact mass	Anal. calcd: C, 55.53; H, 7.43; N, 7.28. Found: C, 55.25; H, 7.21; N, 7.16.

^{1}H and ^{13}C NMR spectra

^{1}H (500 MHz, $CDCl_3$) for *N*-(2-aminophenyl)-3-chloropropanamide (1a)

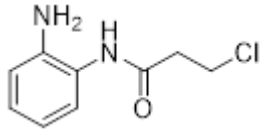

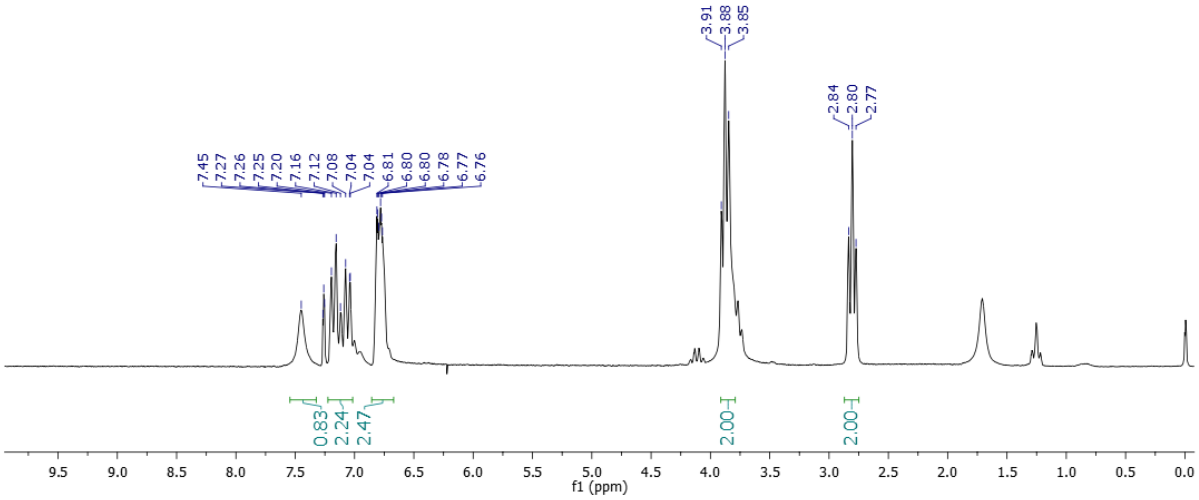

^{1}H (500 MHz, $CDCl_3$) for *N*-(2-aminophenyl)-4-chlorobutanamide (1b)

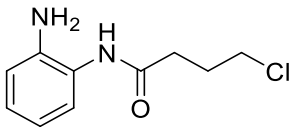

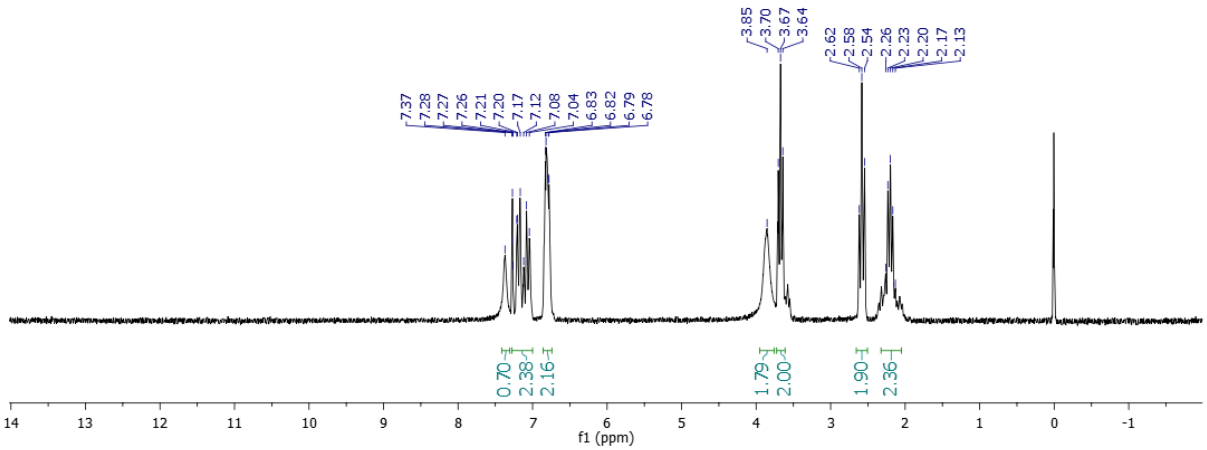

^{1}H (500 MHz, $CDCl_3$) and ^{13}C (125 MHz, $CDCl_3$) for *N*-(2-aminophenyl)-3-(4-(cyclohexylmethyl)piperazin-1-yl)propanamide (2a)

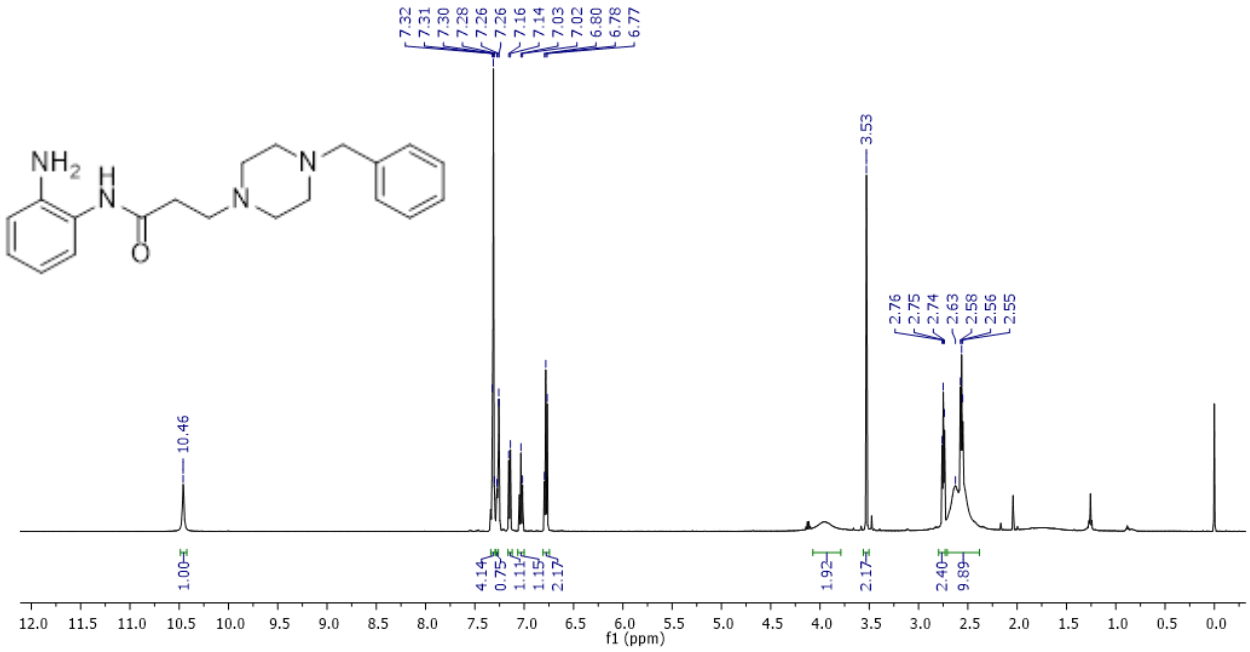

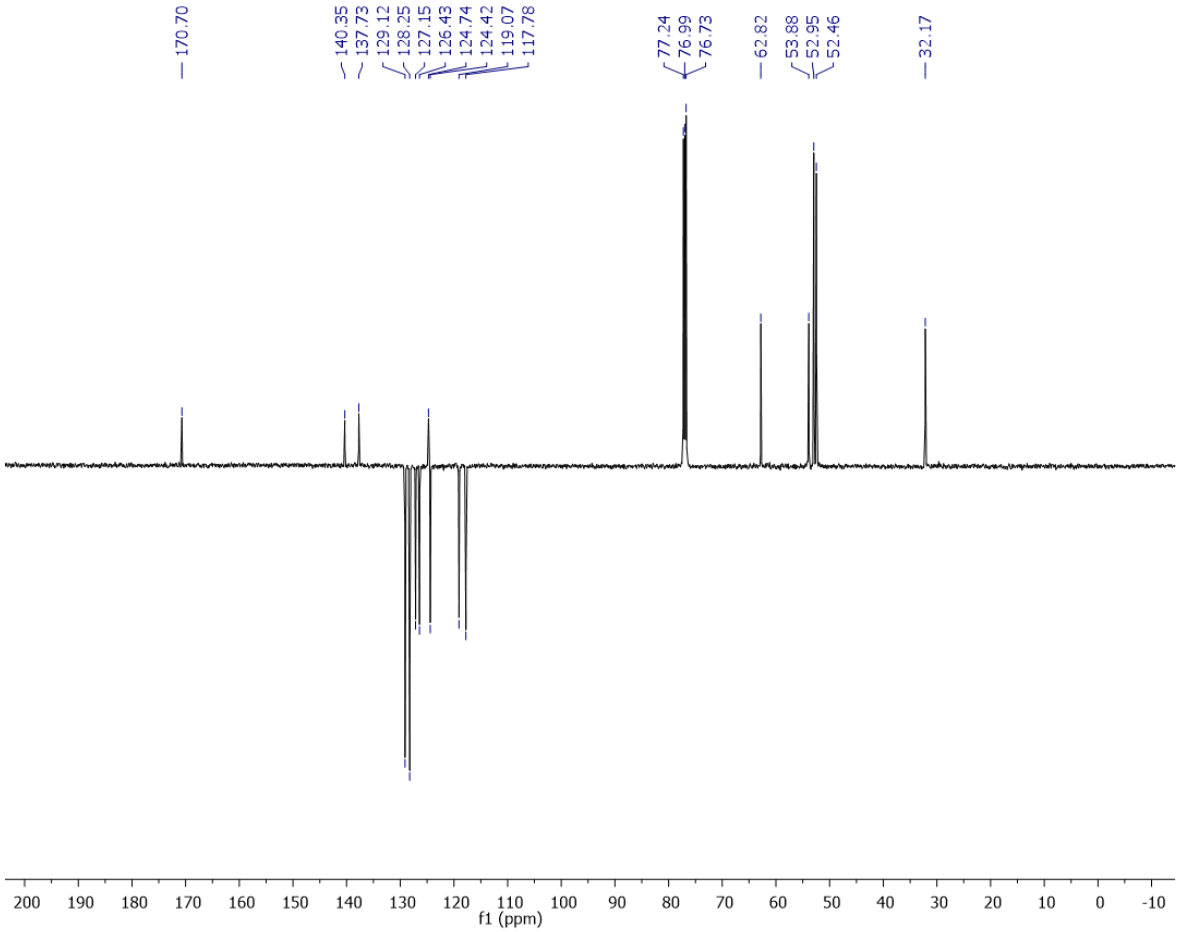

^{1}H (500 MHz, $CDCl_3$) and ^{13}C (125 MHz, $CDCl_3$) for *N*-(2-aminophenyl)-4-(4-(cyclohexylmethyl)piperazin-1-yl)butanamide (2b)

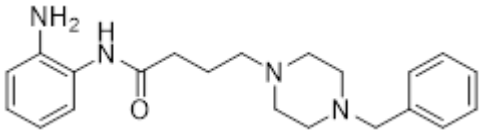

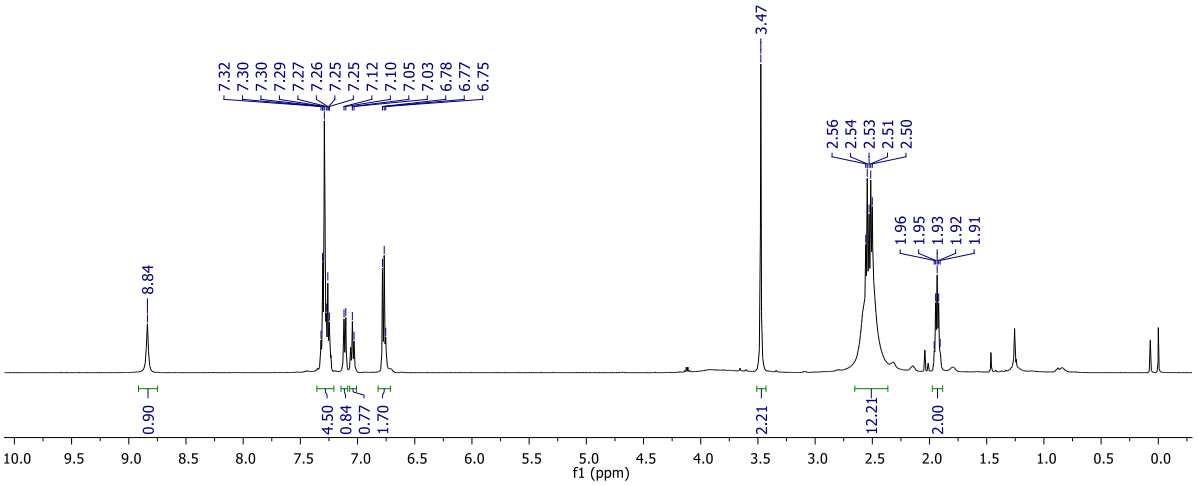

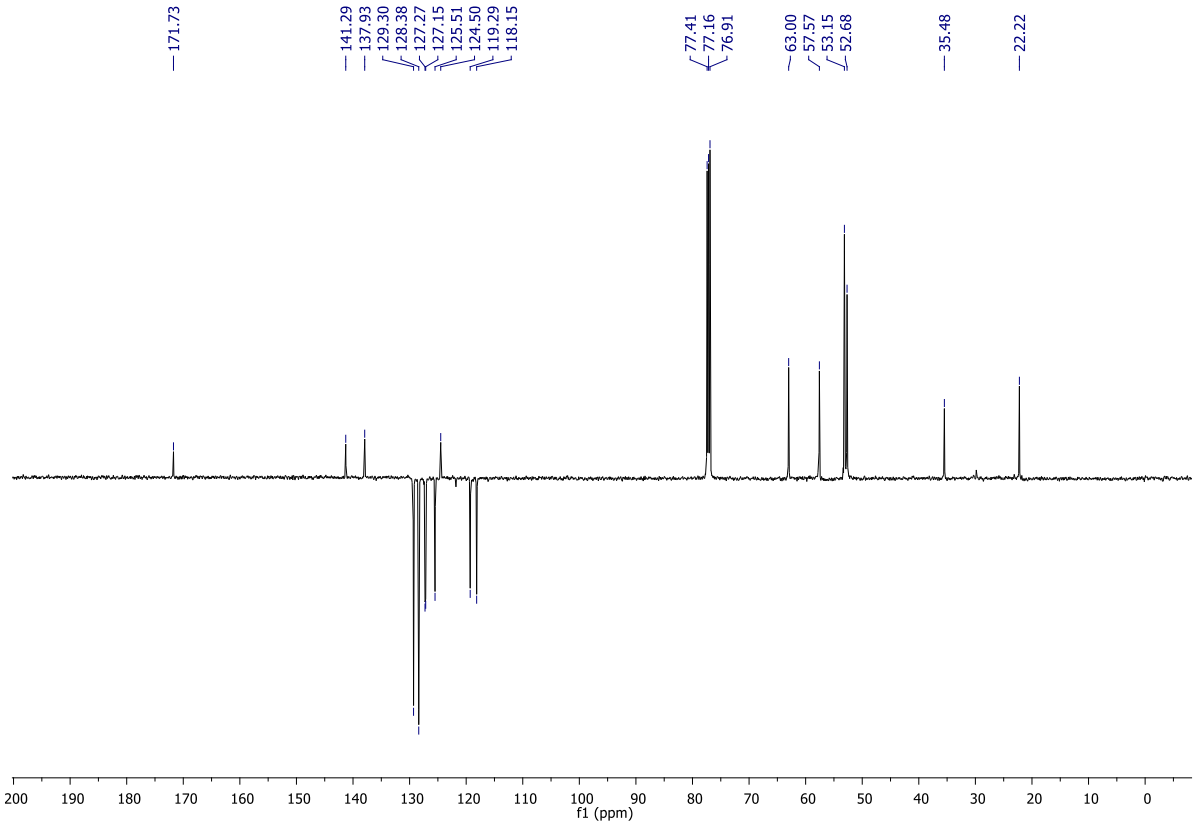

^{1}H (500 MHz, $CDCl_3$) and ^{13}C (125 MHz, $CDCl_3$) for *N*-(2-aminophenyl)-3-(4-(cyclohexylmethyl)piperazin-1-yl)propanamide (3a)

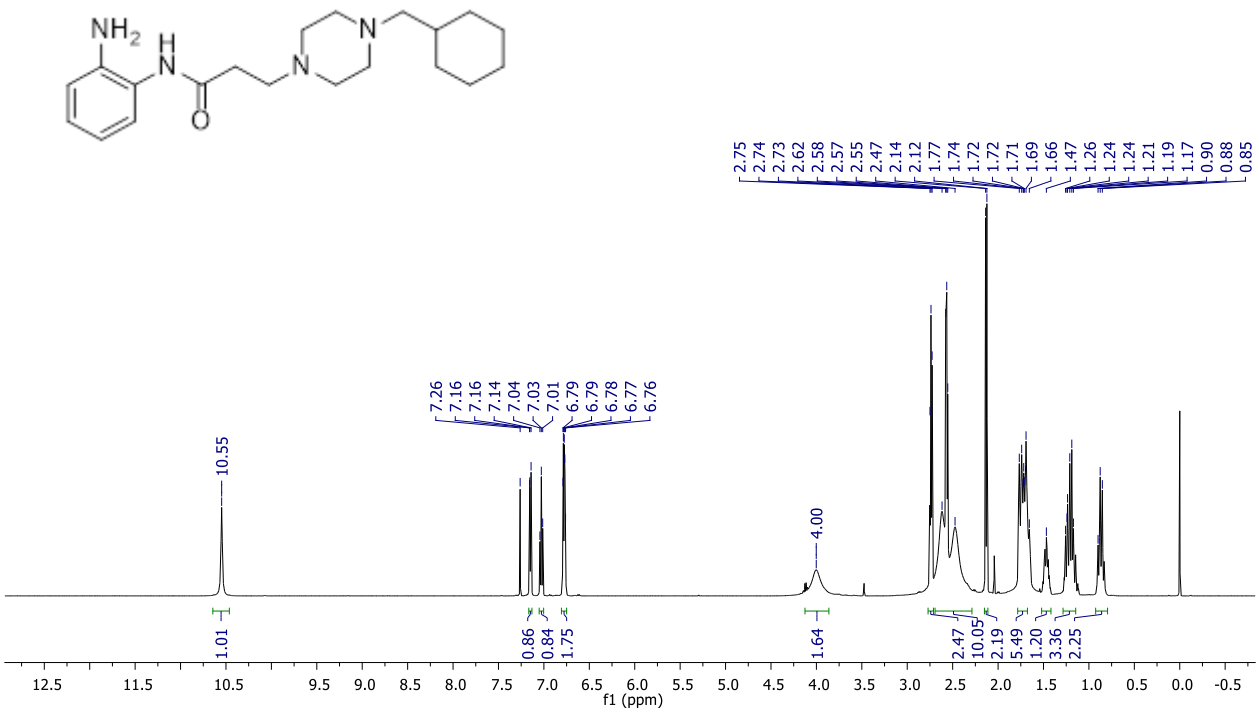

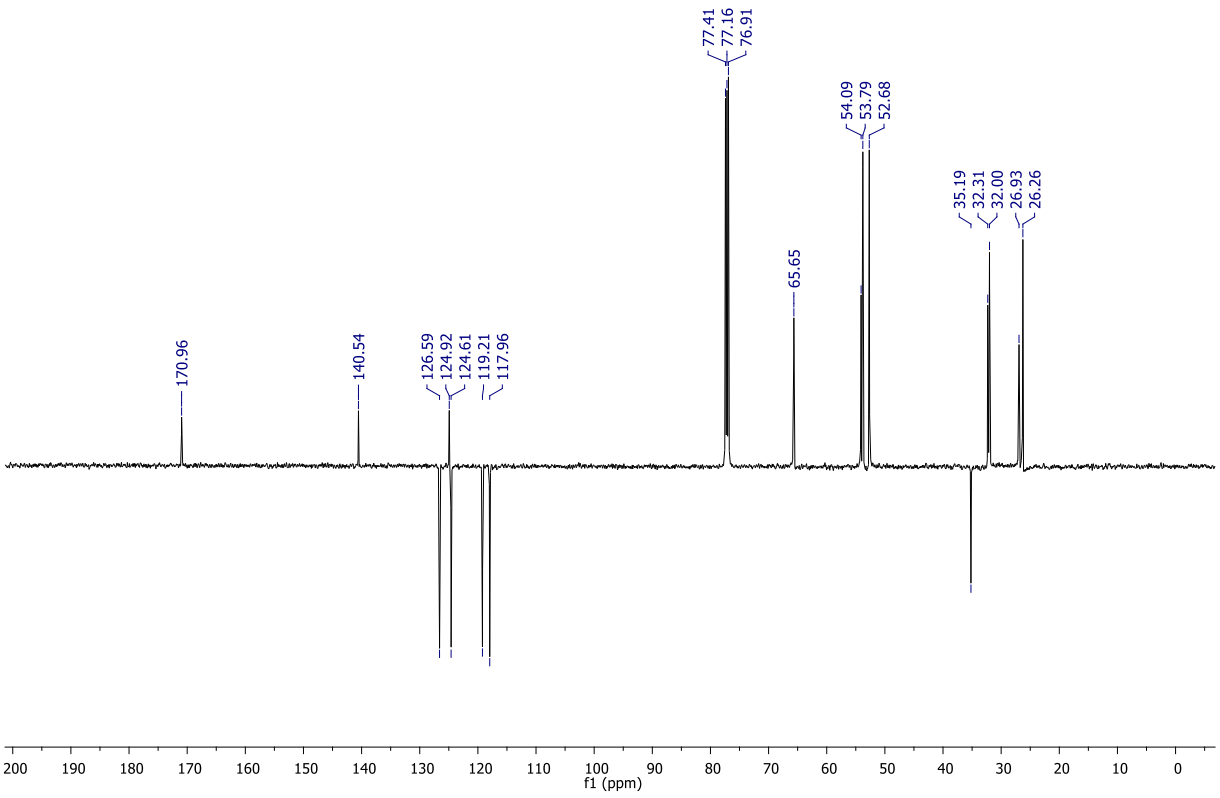

^{1}H (500 MHz, $CDCl_3$) and ^{13}C (125 MHz, $CDCl_3$) for *N*-(2-aminophenyl)-4-(4-(cyclohexylmethyl)piperazin-1-yl)butanamide (3b)

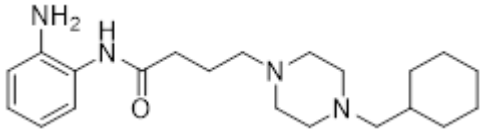

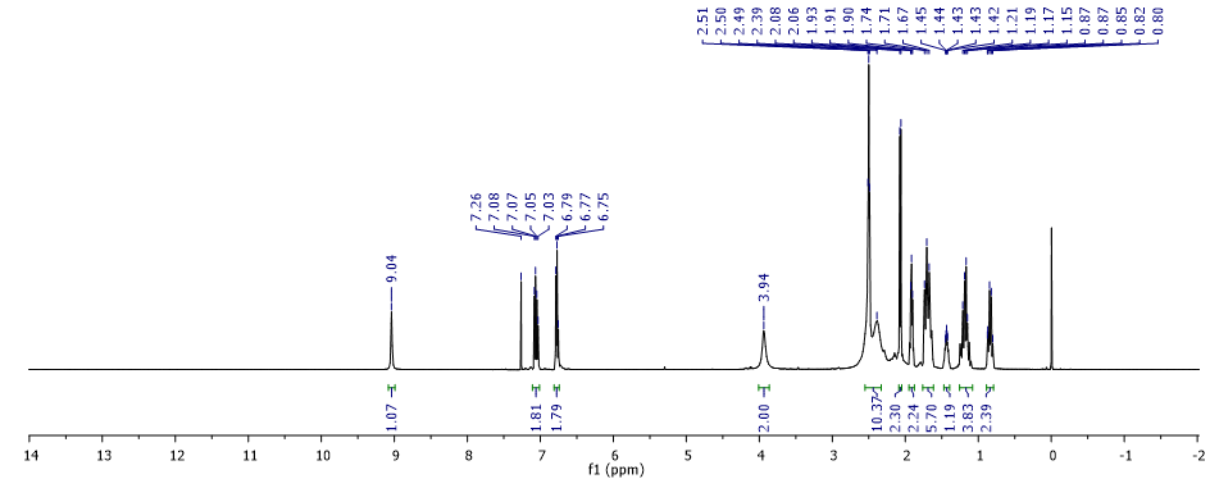

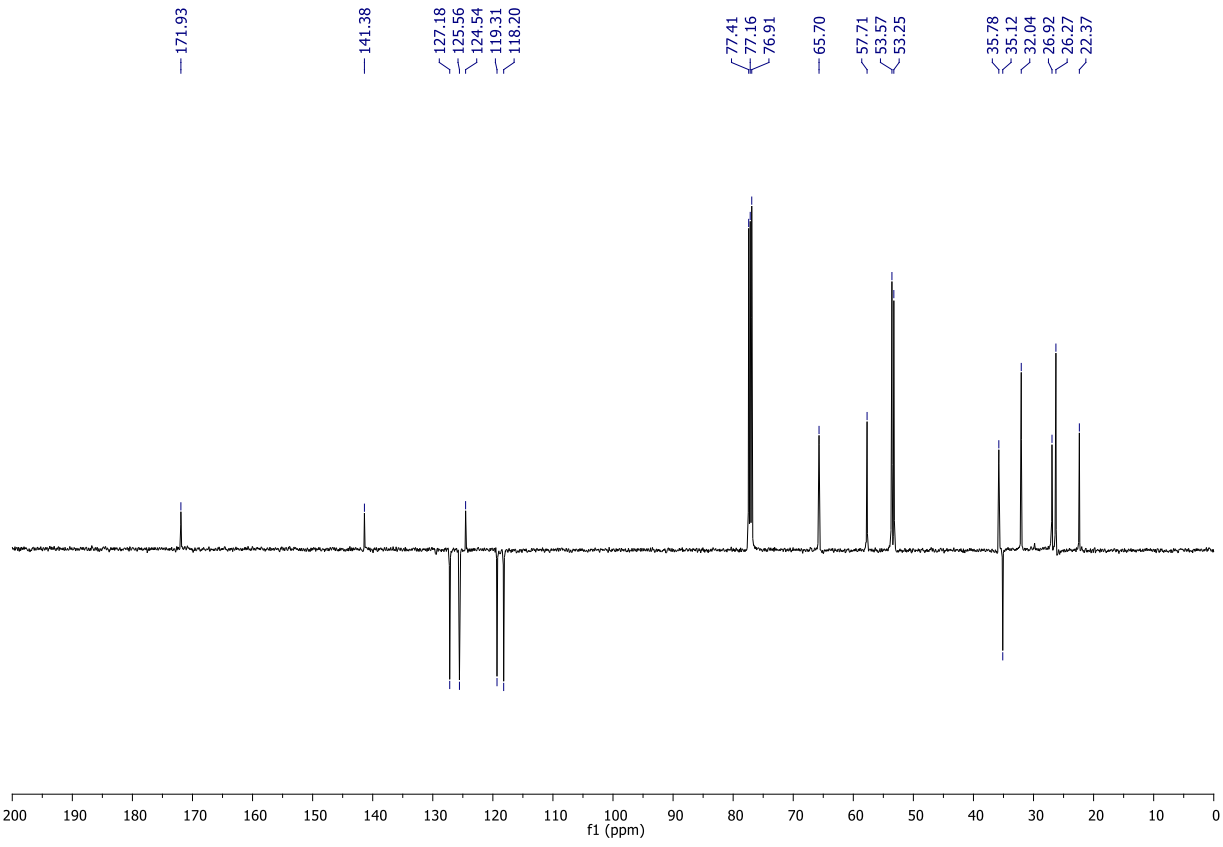

^{1}H (500 MHz, $CDCl_3$) and ^{13}C (125 MHz, $CDCl_3$) for *N*-(2-aminophenyl)-3-(4-(cyclohexylmethyl)piperazin-1-yl)propanamide (4a)

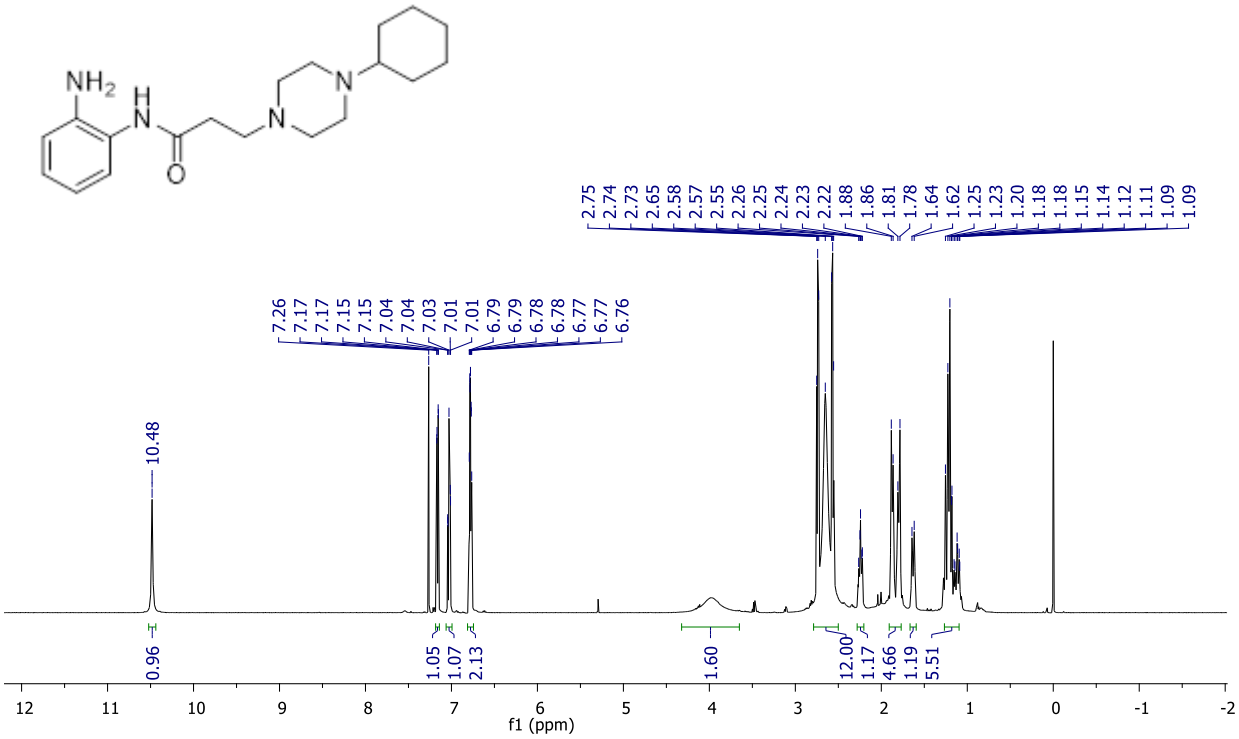

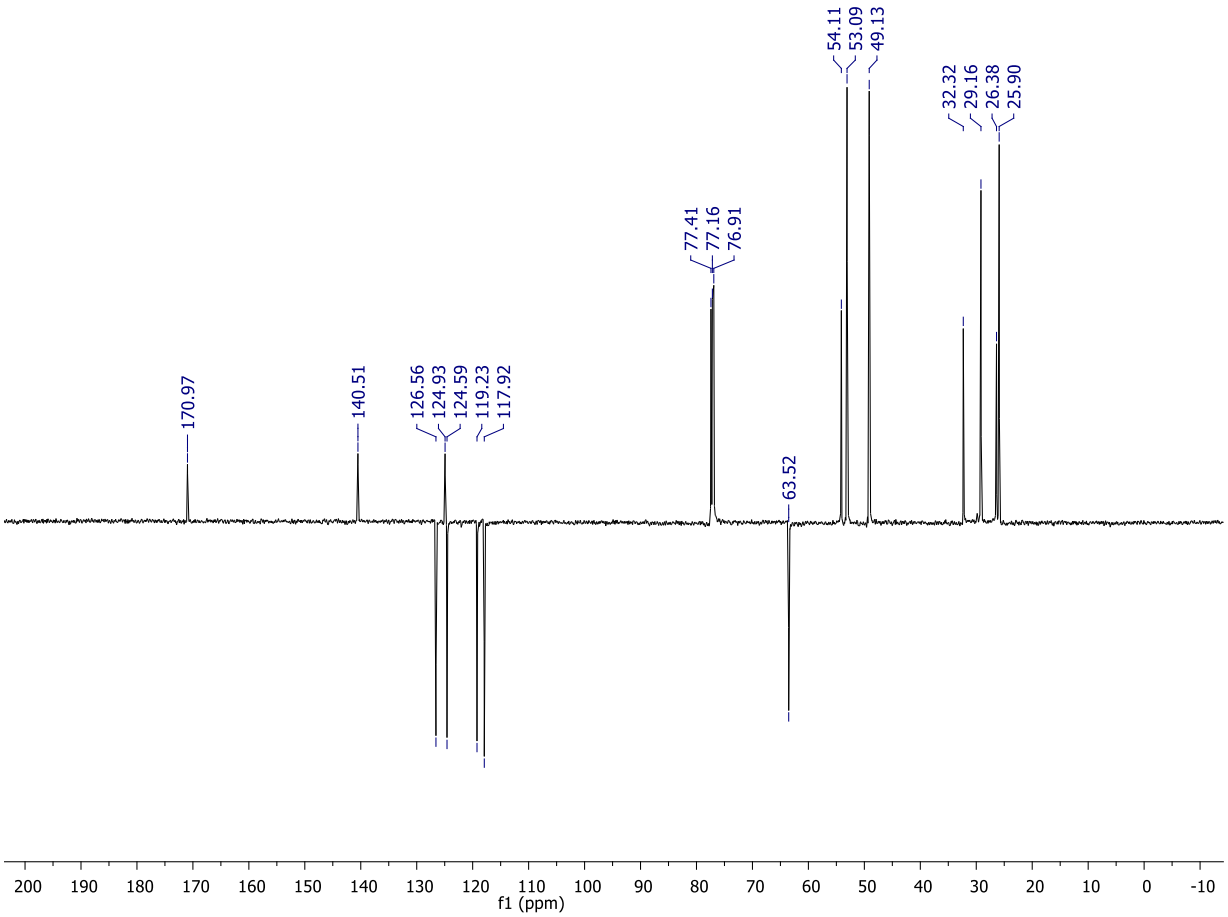

^{1}H (500 MHz, $CDCl_3$) and ^{13}C (125 MHz, $CDCl_3$) for *N*-(2-aminophenyl)-4-(4-cyclohexylpiperazin-1-yl)butanamide (4b)

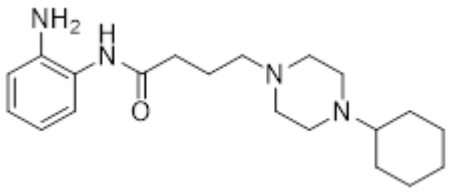

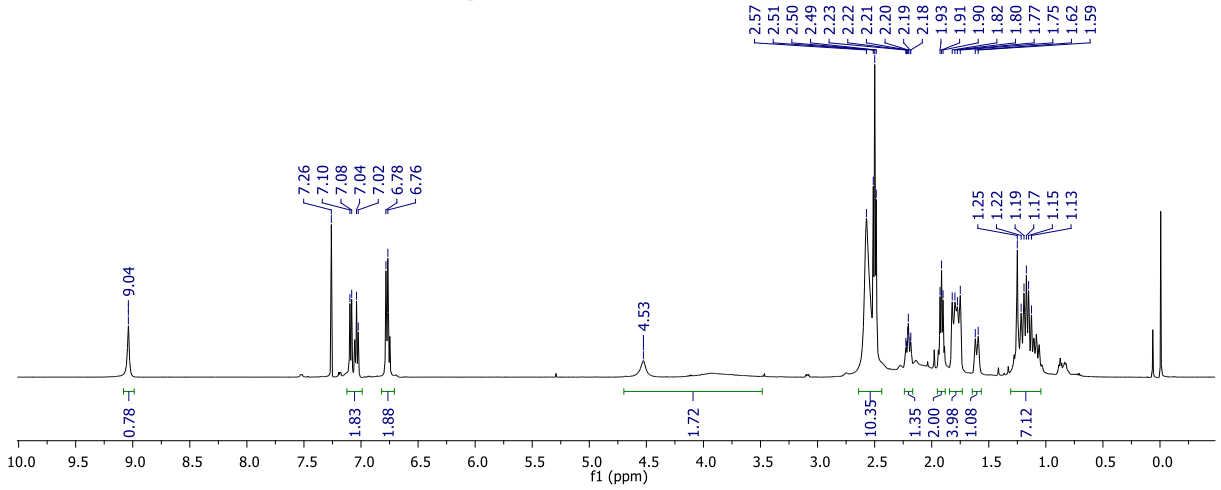

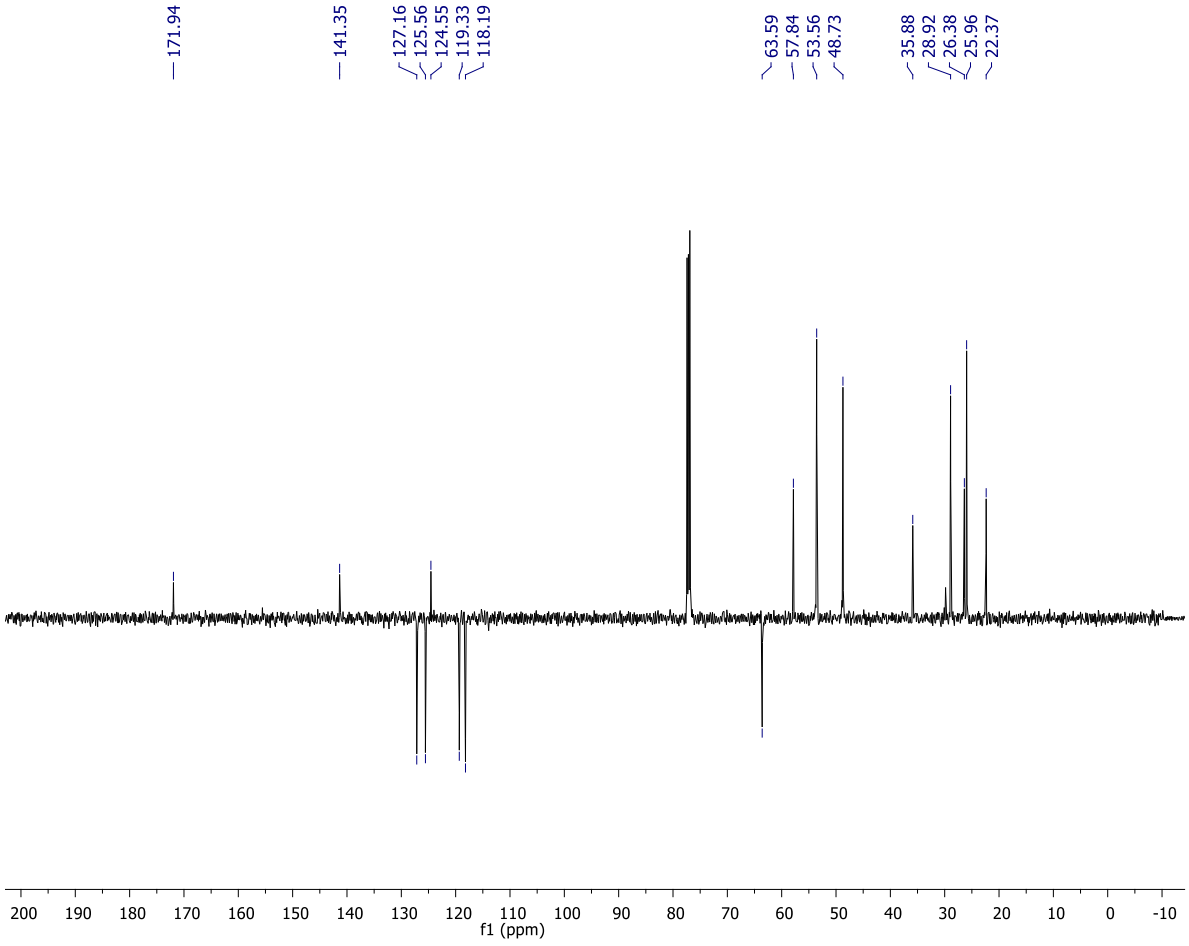

^{1}H (200 MHz, $CDCl_3$) and ^{13}C (50 MHz, $CDCl_3$) for methyl 3-(4-benzylpiperazin-1-yl)propanoate (5a)

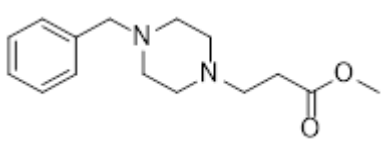

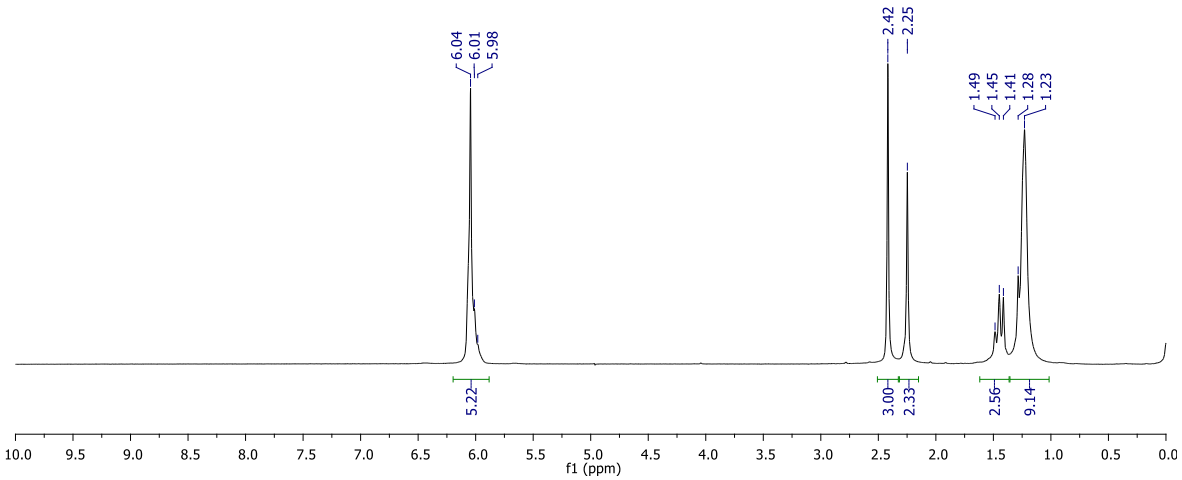

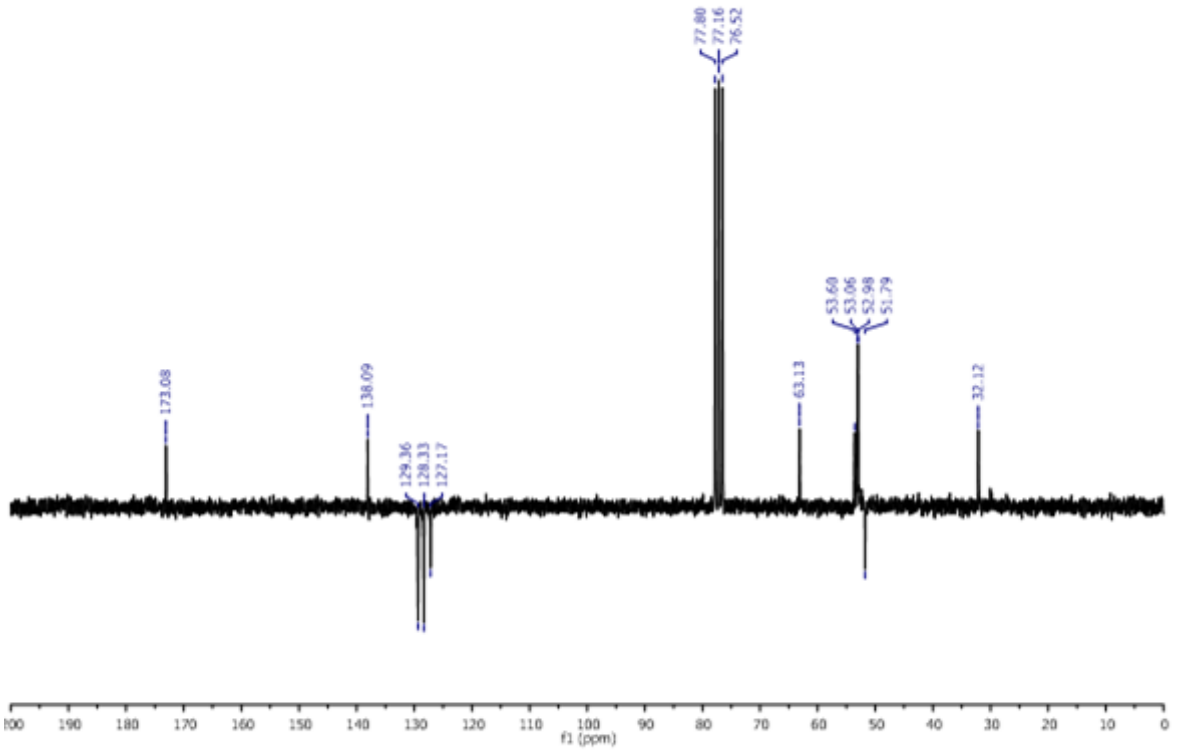

^{1}H (200 MHz, $CDCl_3$) and ^{13}C (50 MHz, $CDCl_3$) for methyl 4-(4-benzylpiperazin-1-yl)butanoate (5b)

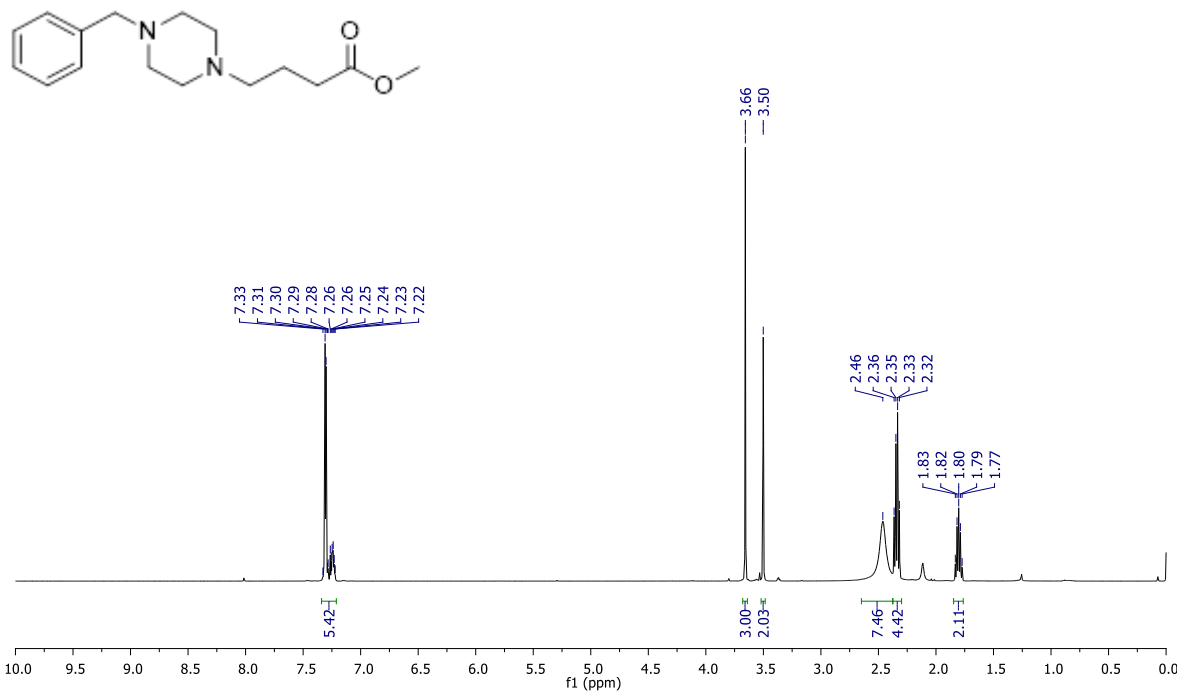

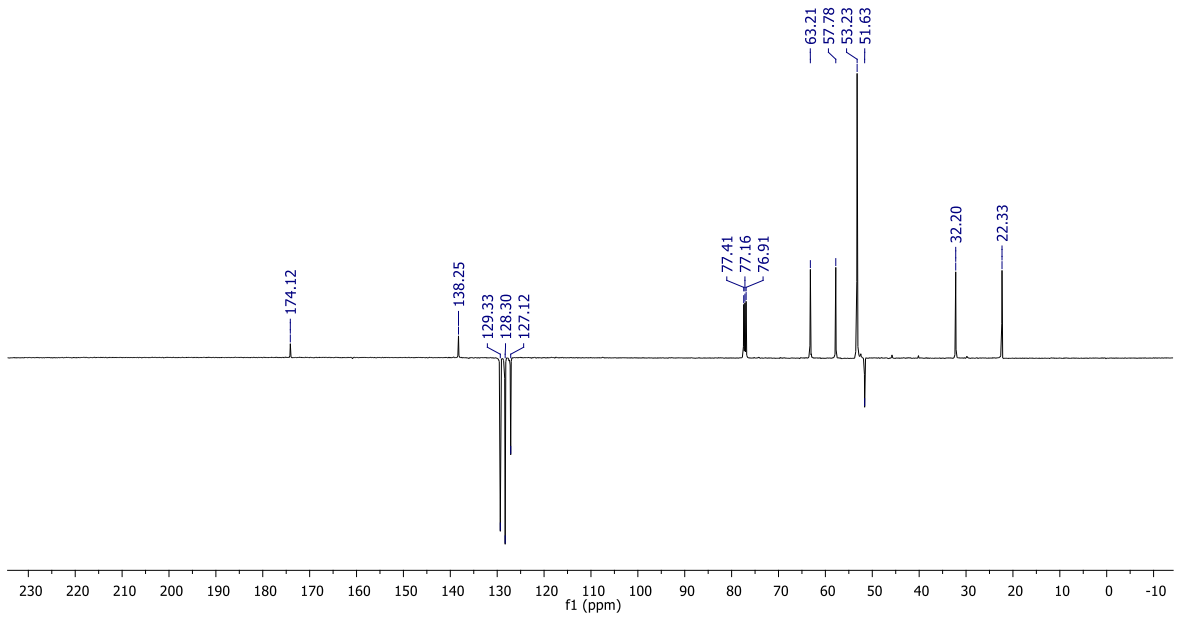

^{1}H (200 MHz, $CDCl_3$) and ^{13}C (50 MHz, $CDCl_3$) for methyl 3-(4-(cyclohexylmethyl)piperazin-1-yl)propanoate (6a)

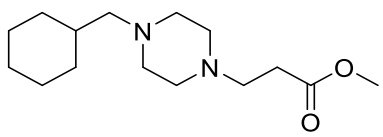

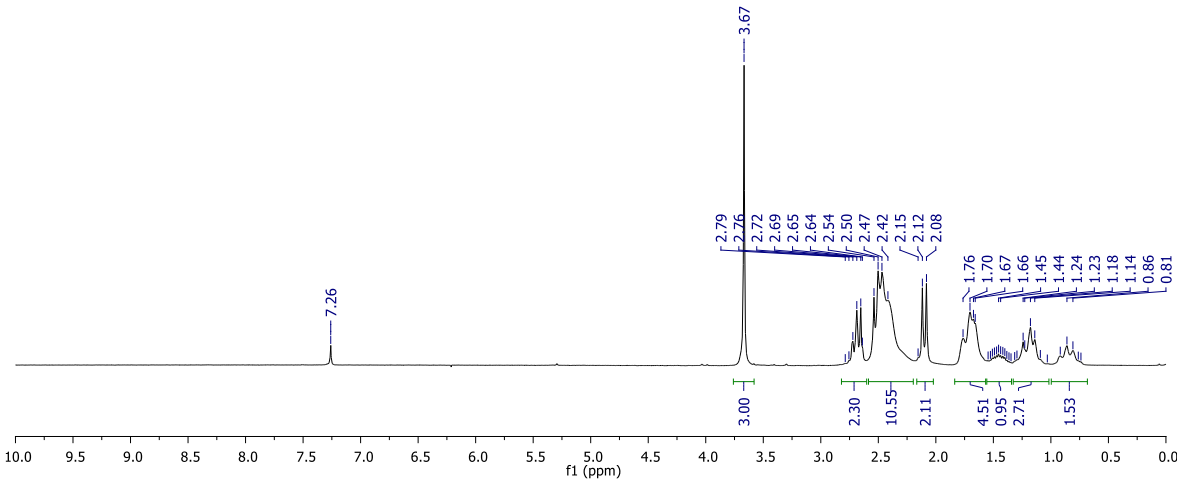

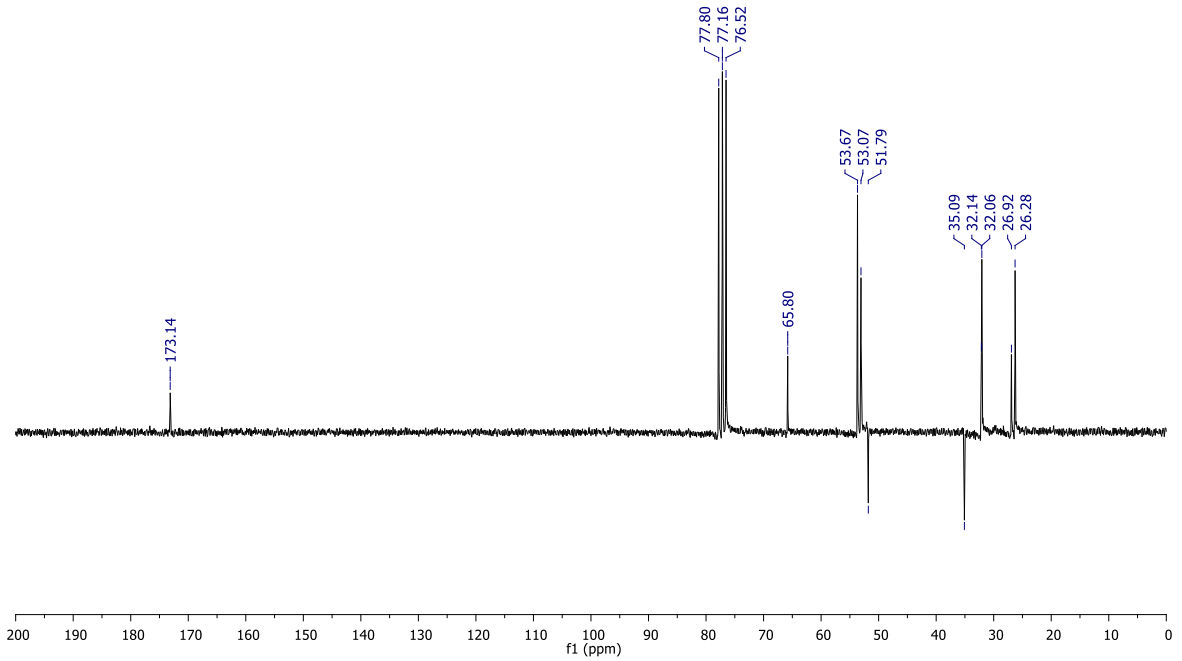

^{1}H (200 MHz, $CDCl_3$) and ^{13}C (50 MHz, $CDCl_3$) for methyl 4-(4-(cyclohexylmethyl)piperazin-1-yl)butanoate (6b)

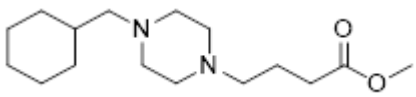

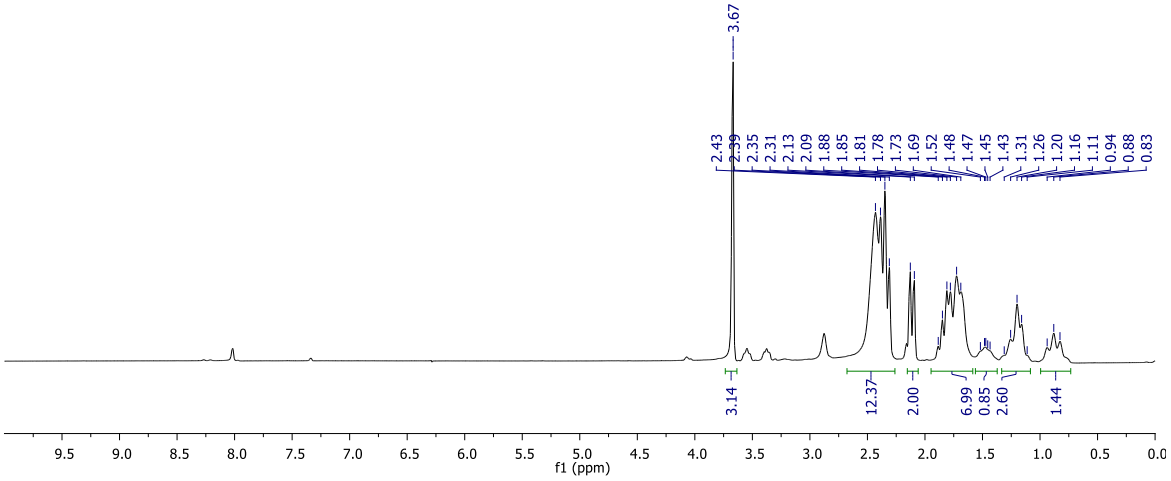

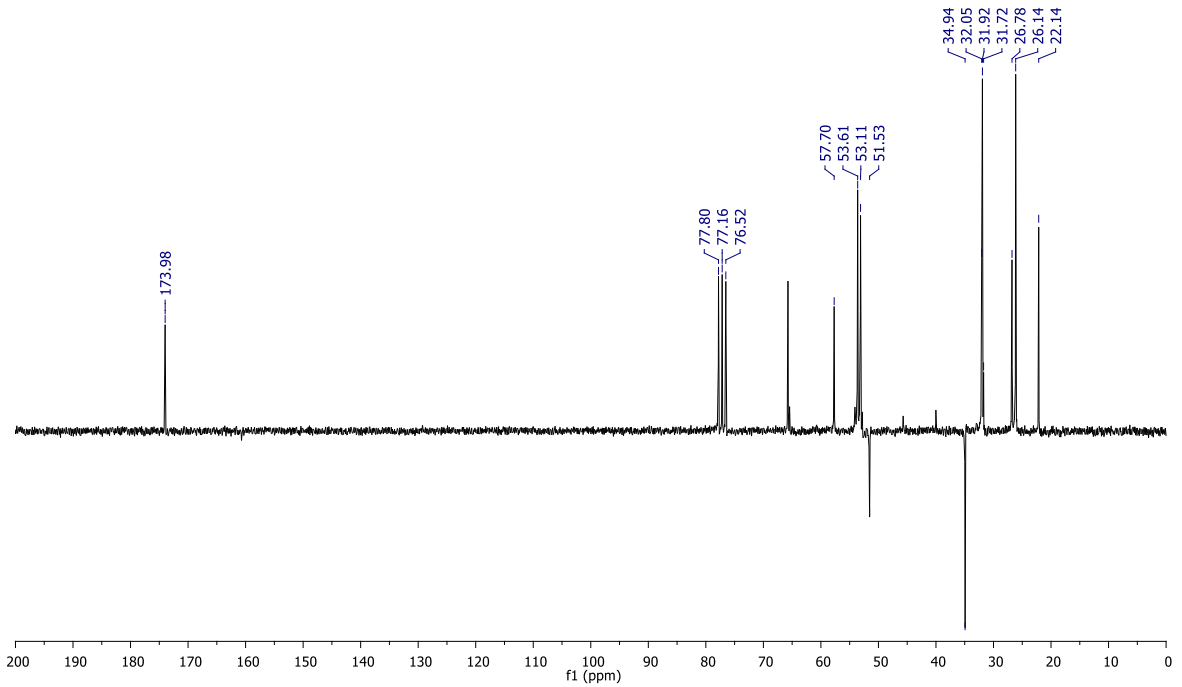

^{1}H (200 MHz, $CDCl_3$) and ^{13}C (50 MHz, $CDCl_3$) for methyl 3-(4-cyclohexylpiperazin-1-yl)propanoate (7a)

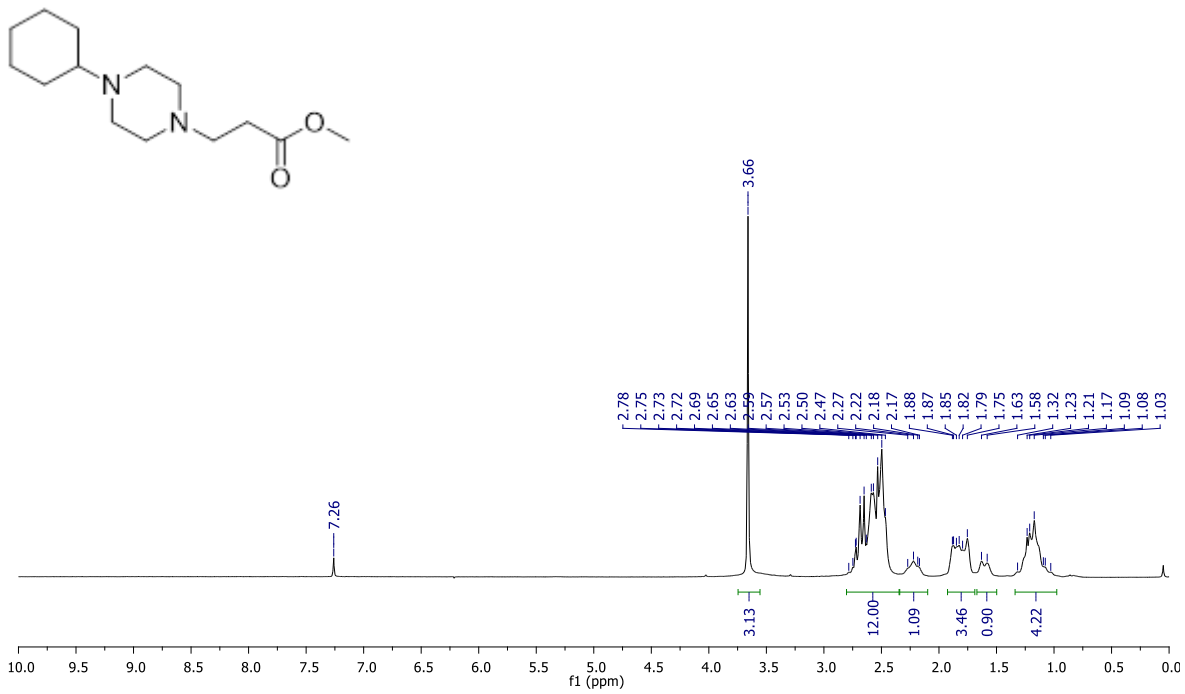

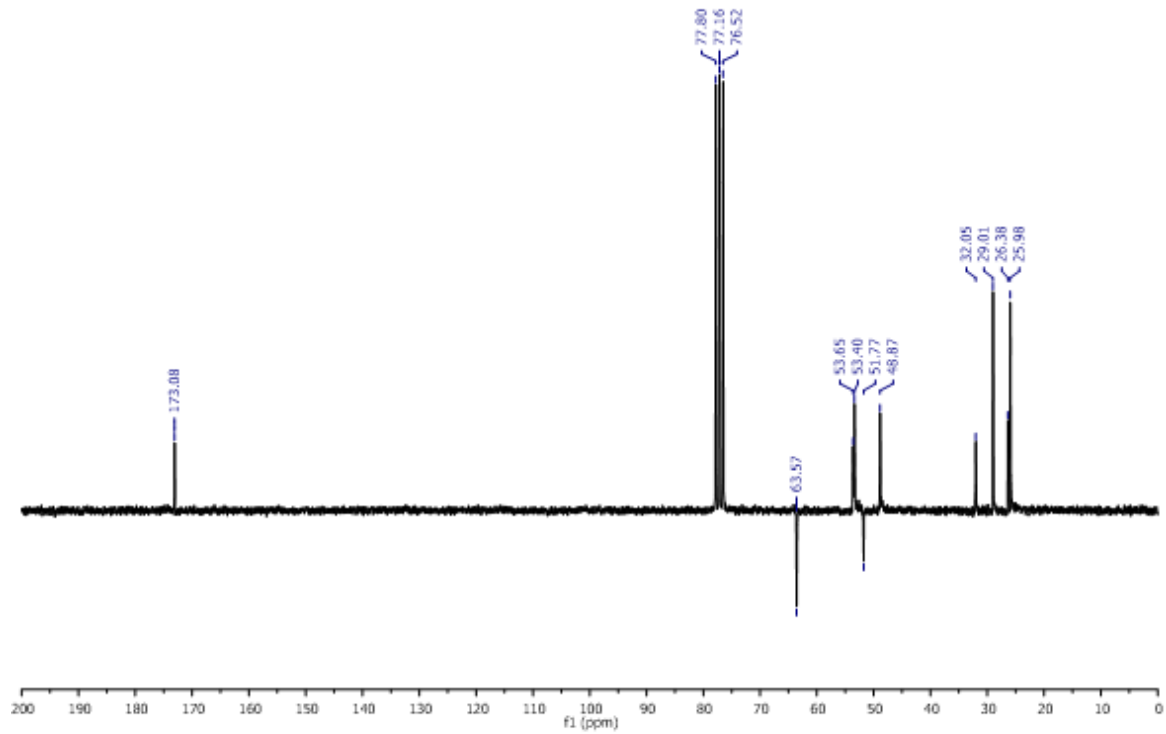

^{1}H (200 MHz, $CDCl_3$) and ^{13}C (50 MHz, $CDCl_3$) for methyl 4-(4-cyclohexylpiperazin-1-yl)butanoate (7b)

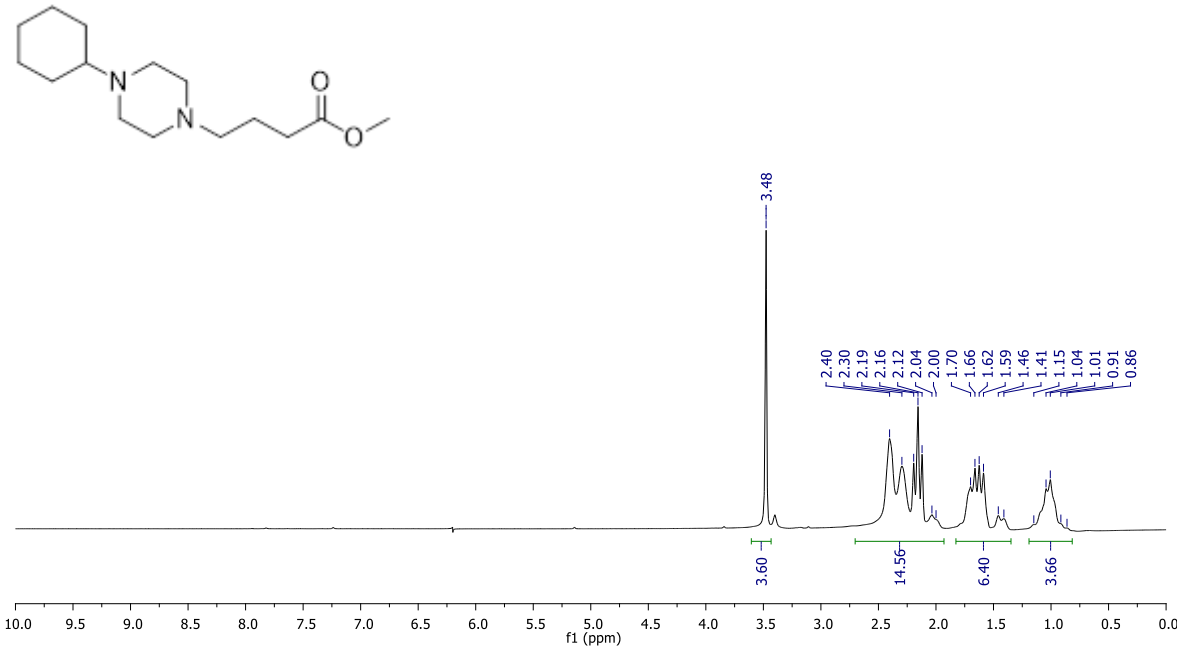

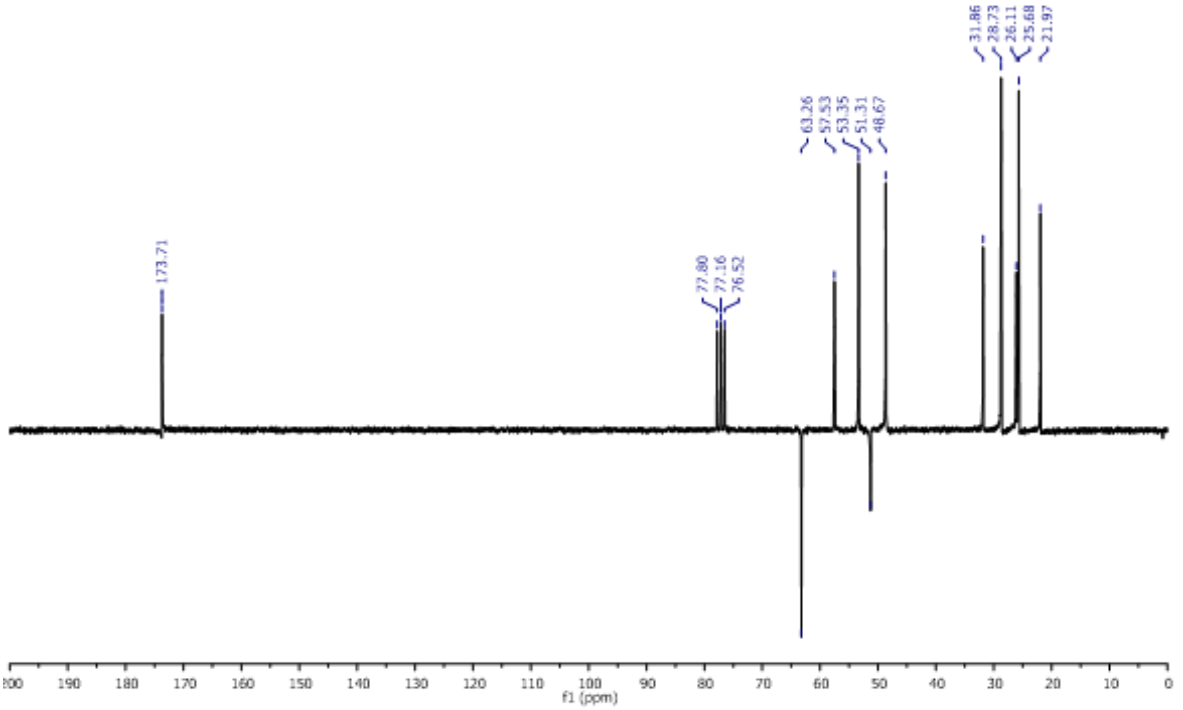

^{1}H (500 MHz, CD_3OD) and ^{13}C (125 MHz, CD_3OD) for methyl 3-(4-(4-chlorophenyl)-4-hydroxypiperidin-1-yl)propanoate (8a)

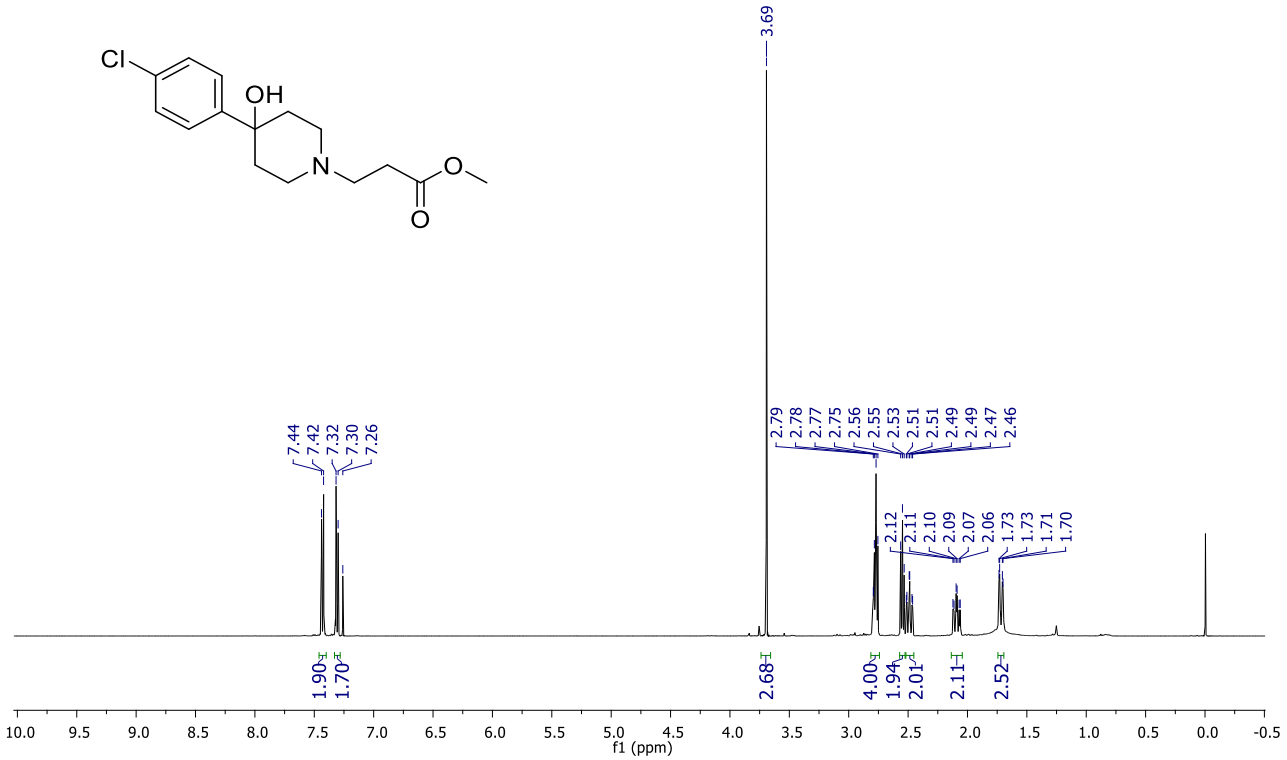

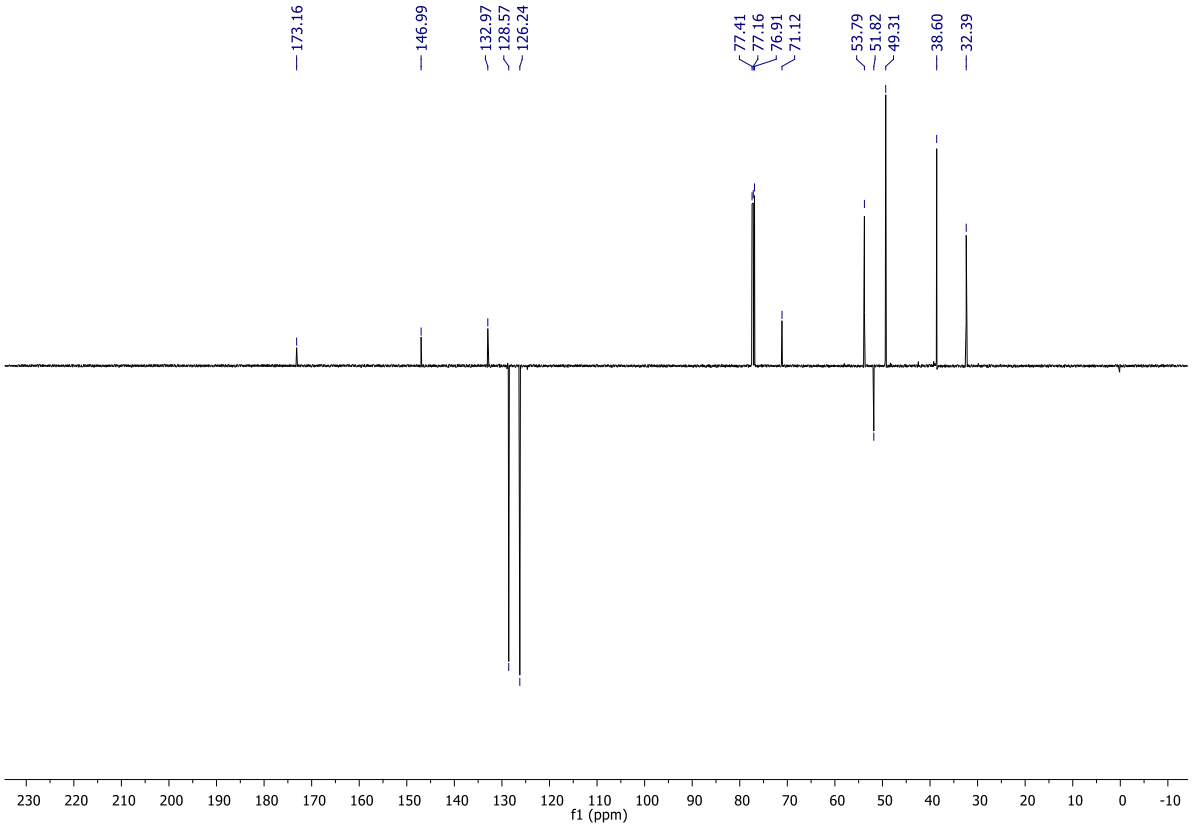

^{1}H (500 MHz, CD_3OD) and ^{13}C (125 MHz, CD_3OD) for methyl 3-(4-(4-chlorophenyl)-4-hydroxypiperidin-1-yl)butanoate (8b)

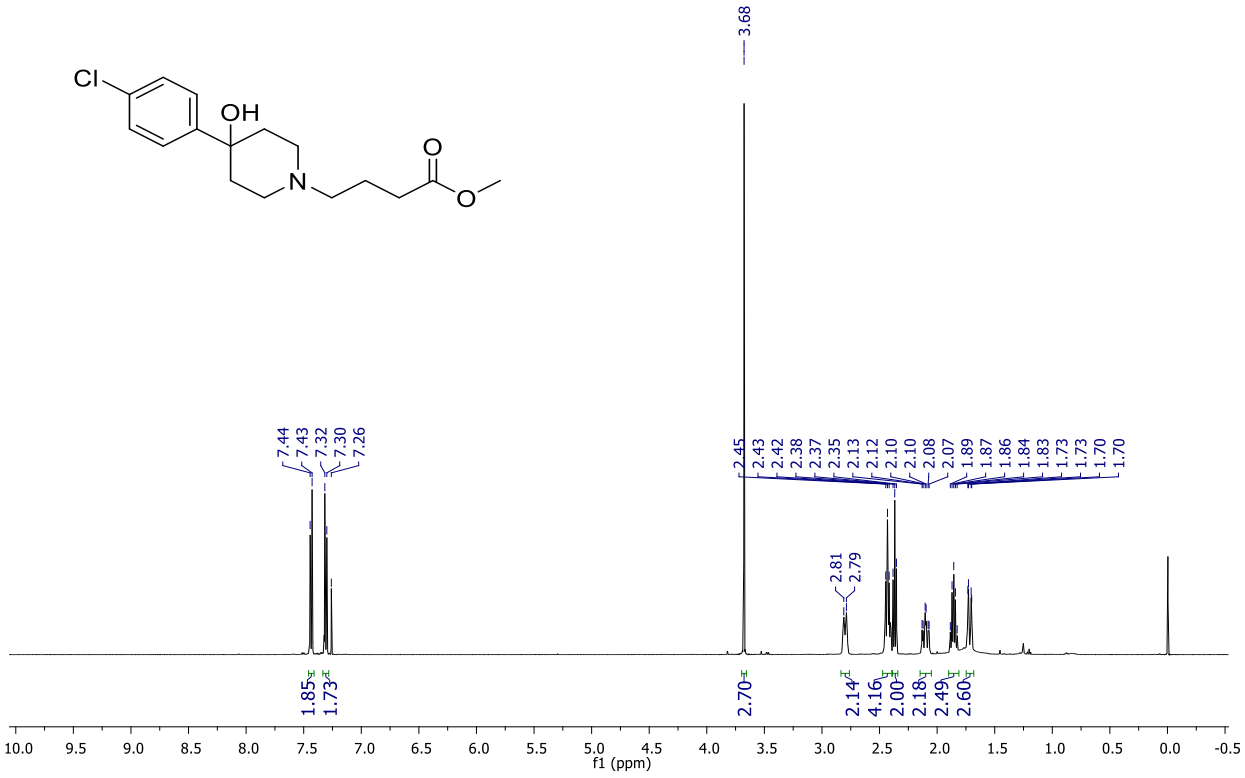

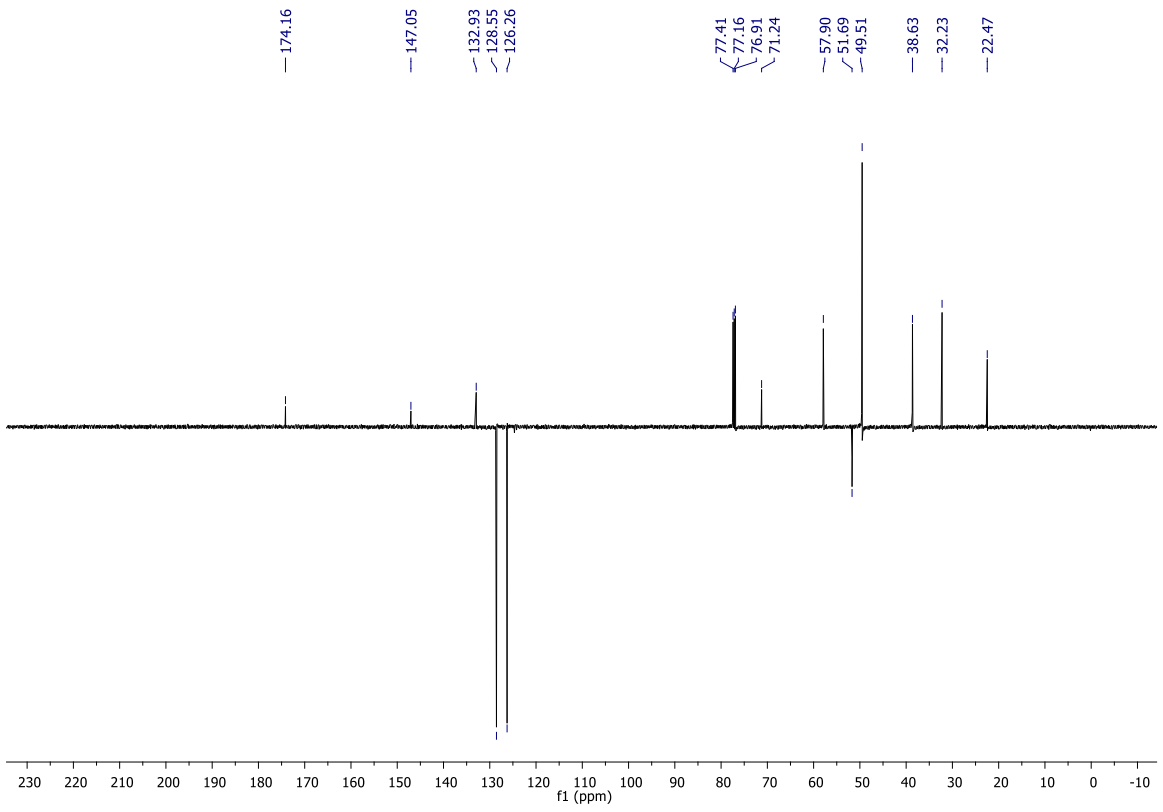

^{1}H (500 MHz, CD_3OD) and ^{13}C (125 MHz, CD_3OD) for methyl 5-(4-(4-chlorophenyl)-4-hydroxypiperidin-1-yl)pentanoate (8c)

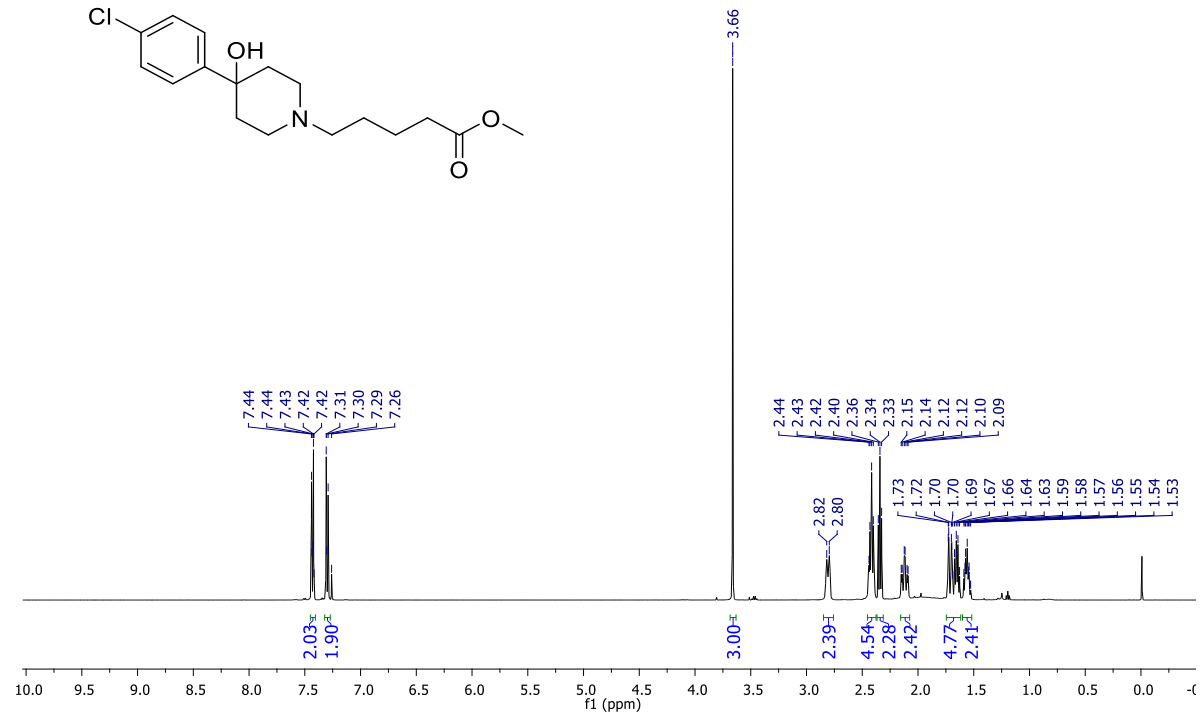

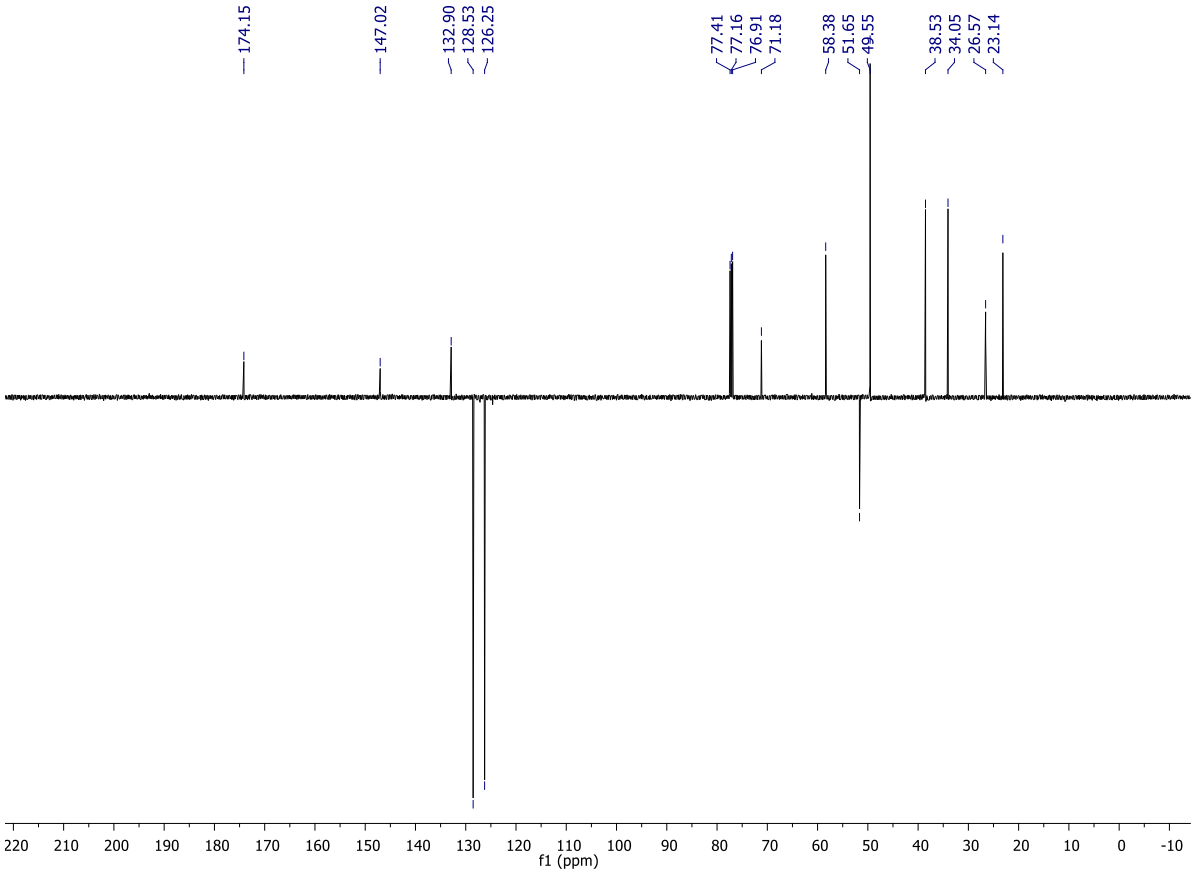

^{1}H (500 MHz, CD_3OD) and ^{13}C (125 MHz, CD_3OD) for methyl 6-(4-(4-chlorophenyl)-4-hydroxypiperidin-1-yl)hexanoate (8d)

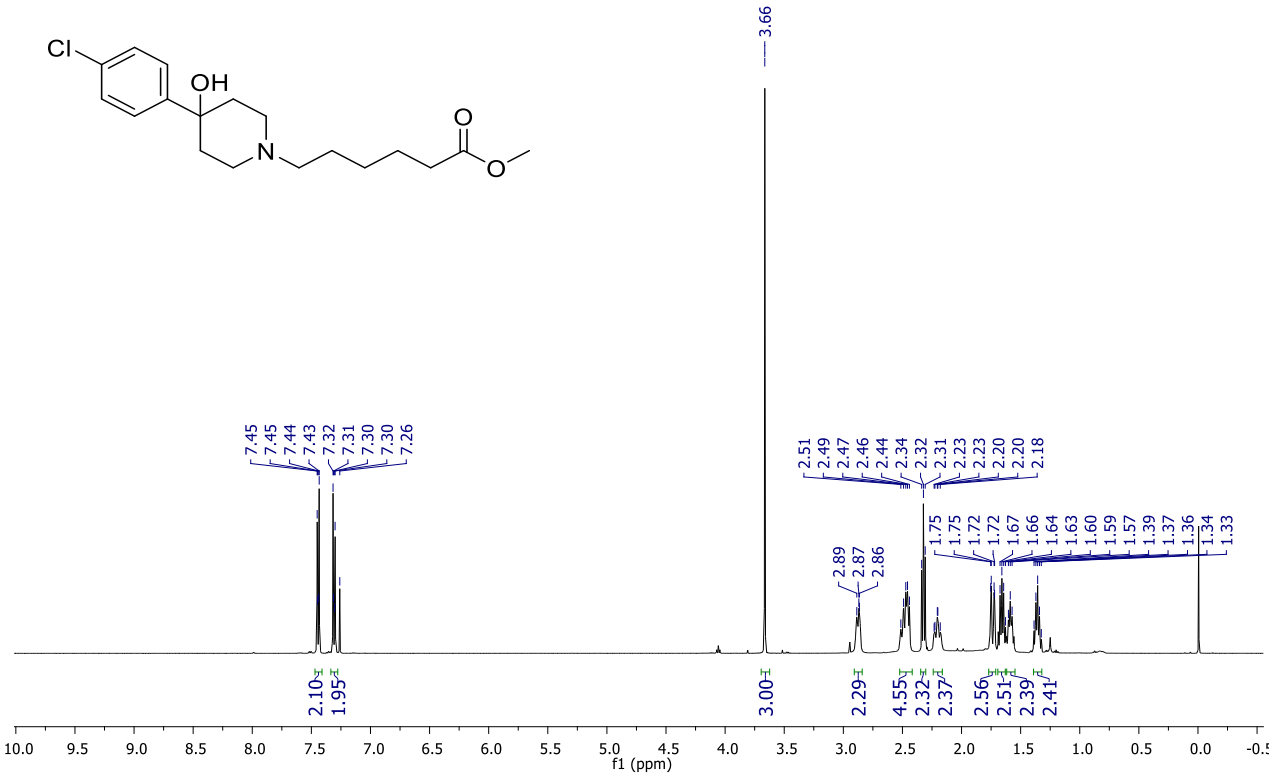

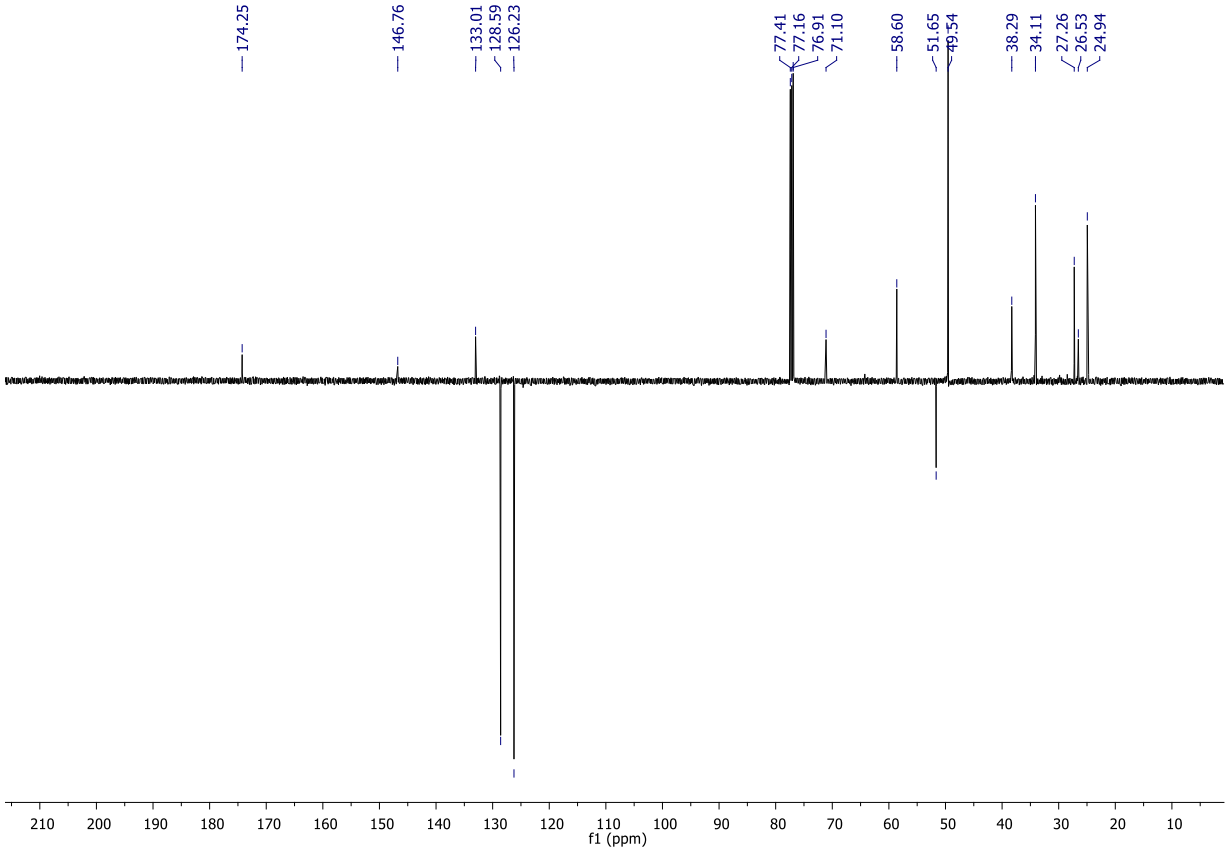

^{1}H (500 MHz, CD_3OD) and ^{13}C (125 MHz, CD_3OD) for methyl 7-(4-(4-chlorophenyl)-4-hydroxypiperidin-1-yl)heptanoate (8e)

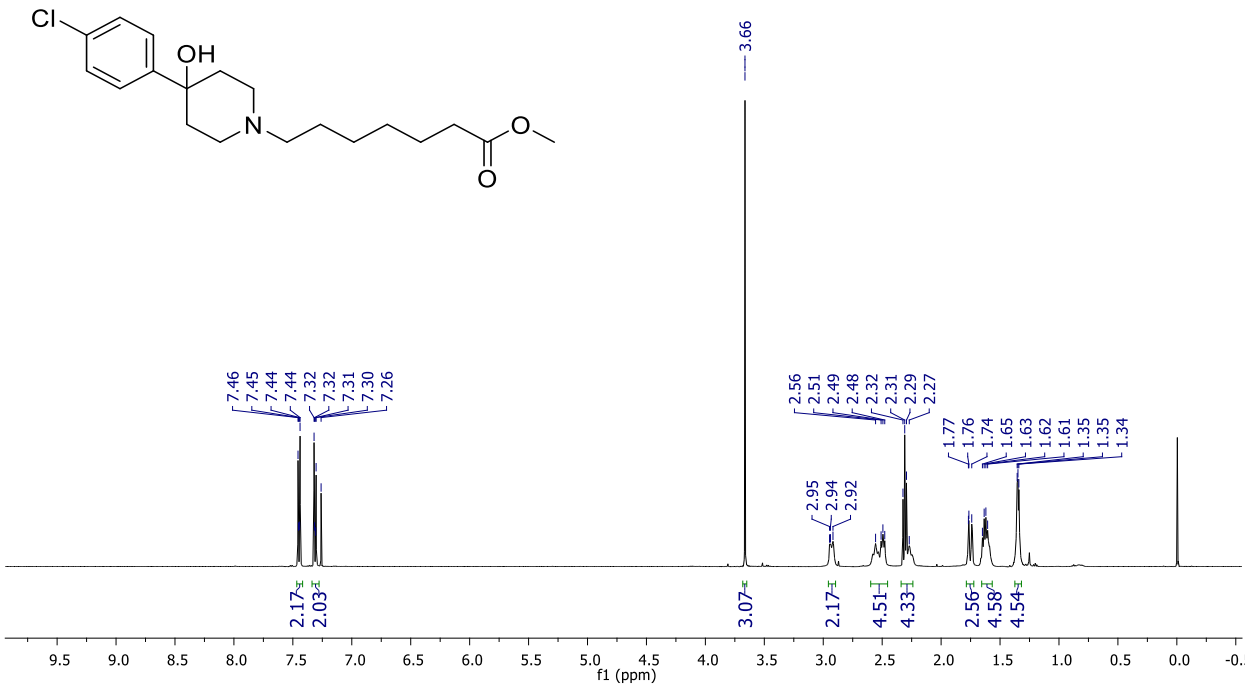

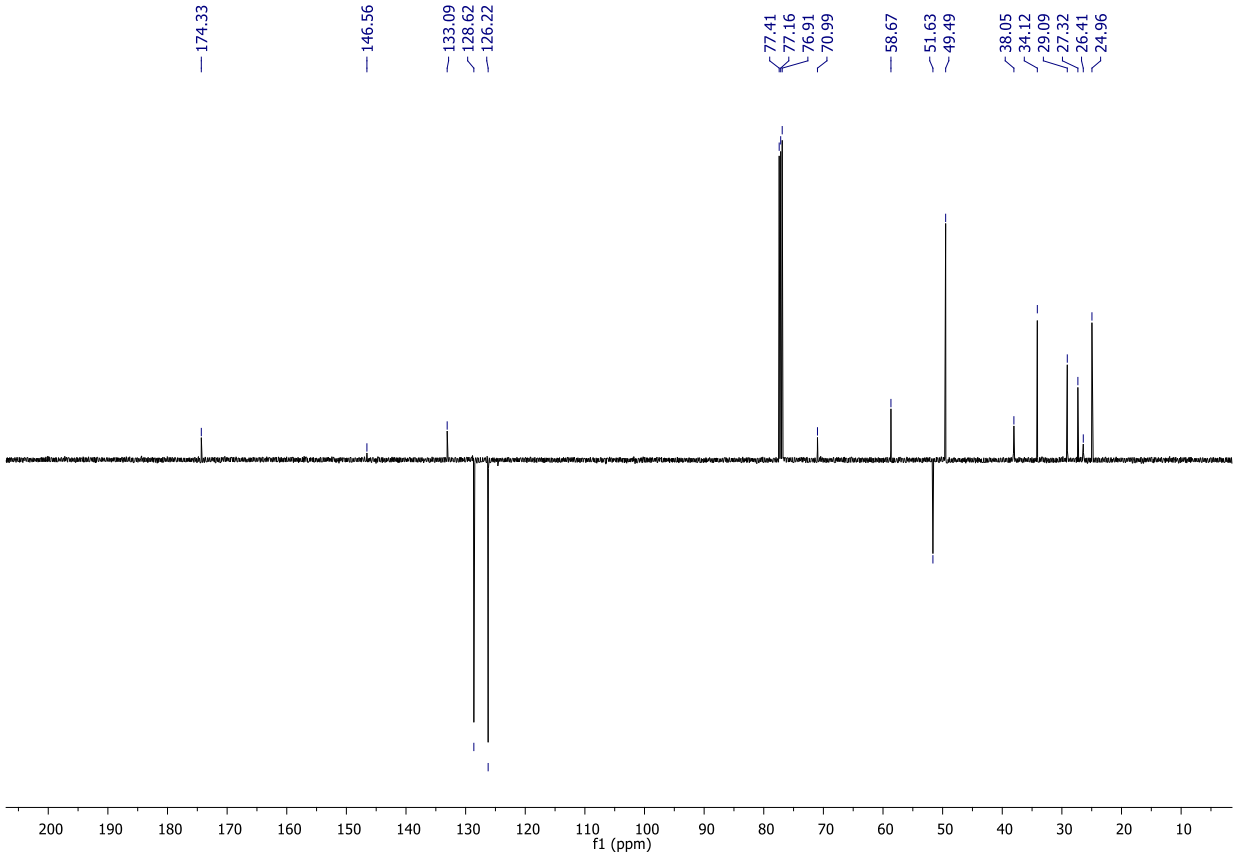

^{1}H (500 MHz, CD_3OD) and ^{13}C (125 MHz, CD_3OD) for 3-(4-benzylpiperazin-1-yl)-*N*-hydroxy propanamide (9a)

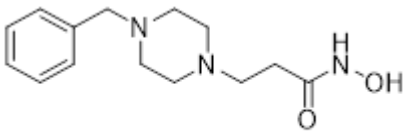

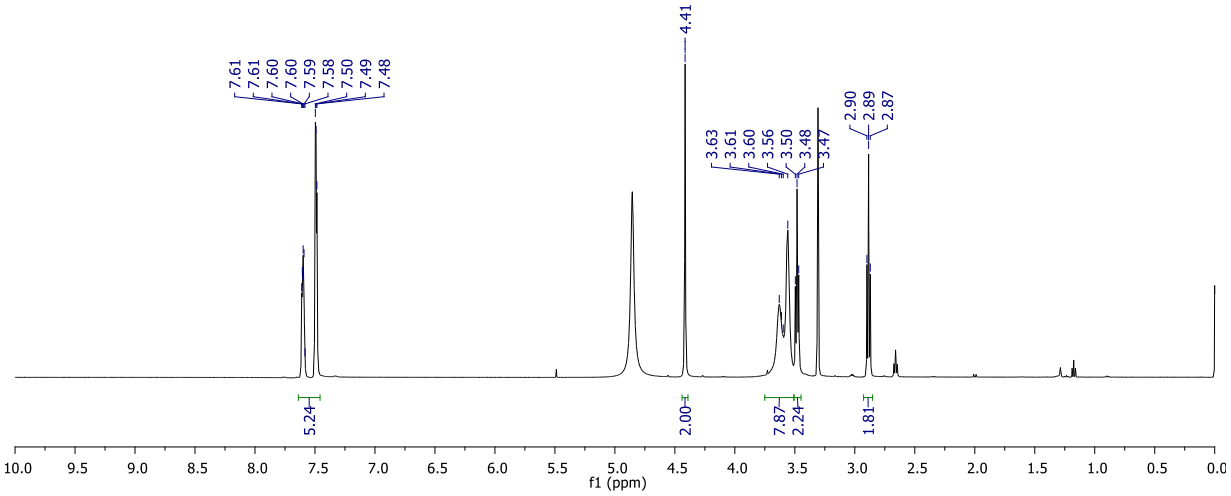

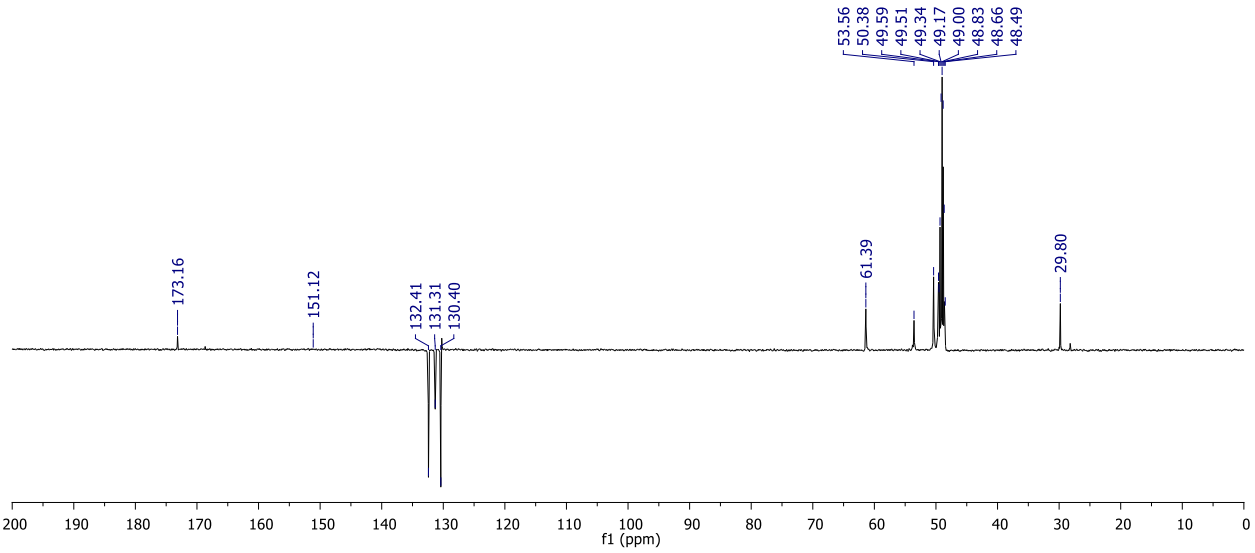

^{1}H (500 MHz, DMSO-d$_6$) and ^{13}C (125 MHz, DMSO-d$_6$) for 4-(4-benzylpiperazin-1-yl)-*N*-hydroxy butanamide (9b)

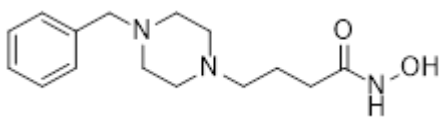

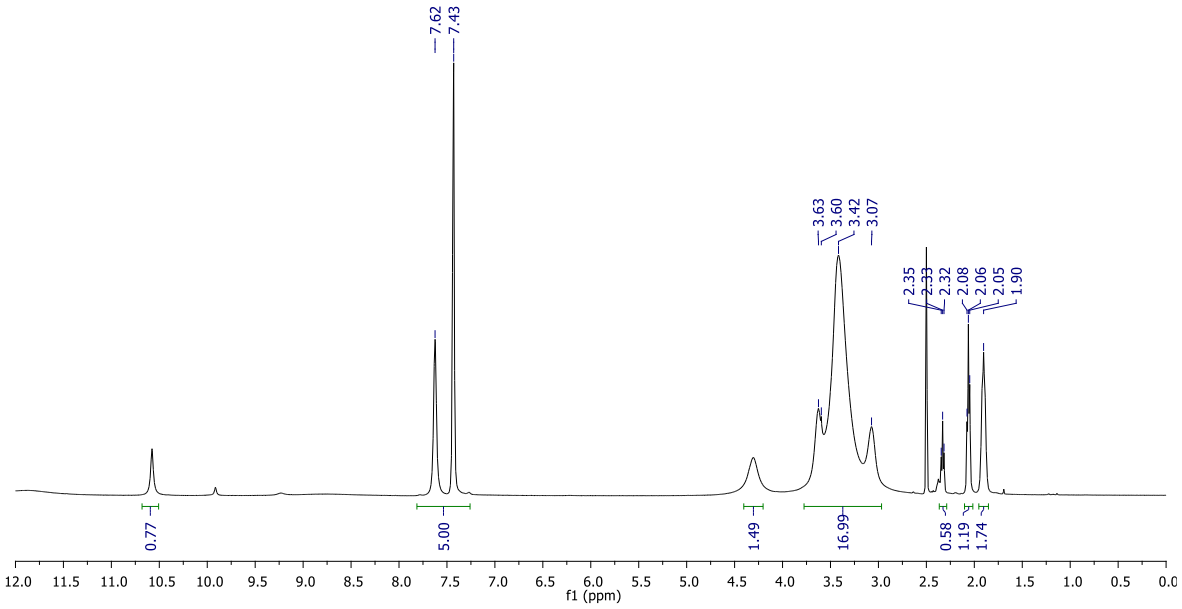

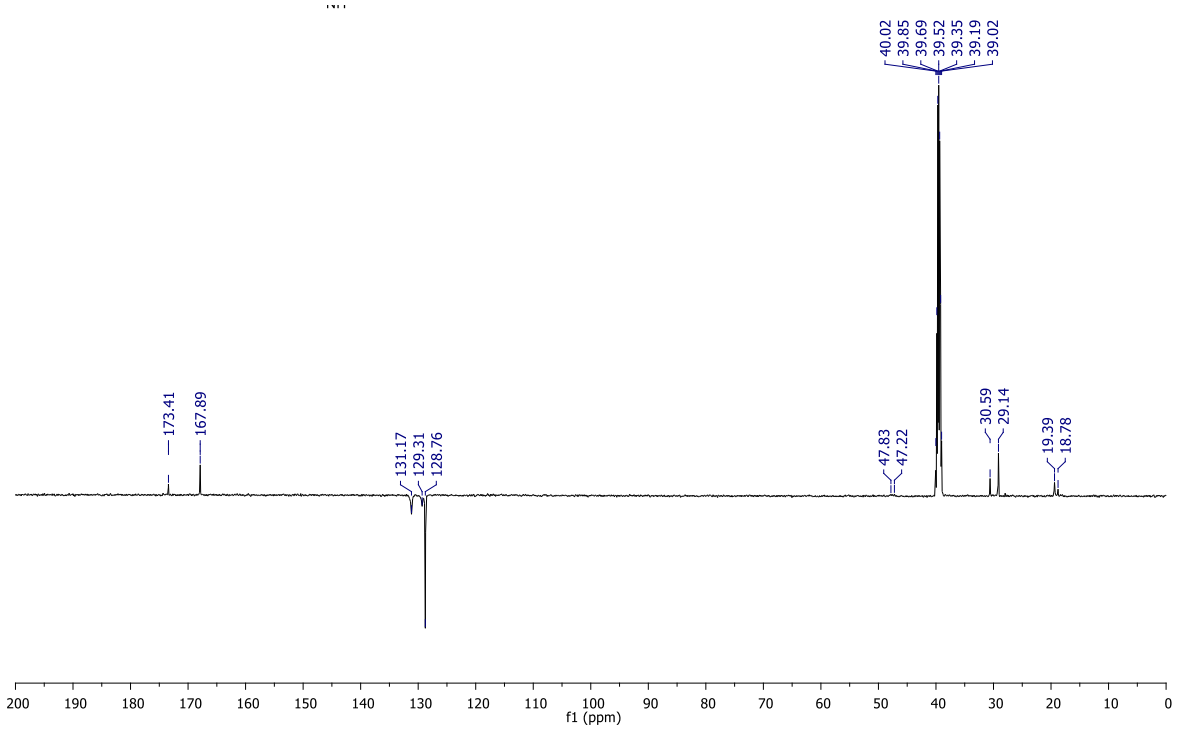

^{1}H (500 MHz, CD_3OD) and ^{13}C (125 MHz, CD_3OD) for 3-(4-(cyclohexylmethyl)piperazin-1-yl)-*N*-hydroxypropanamide (10a)

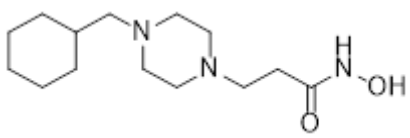

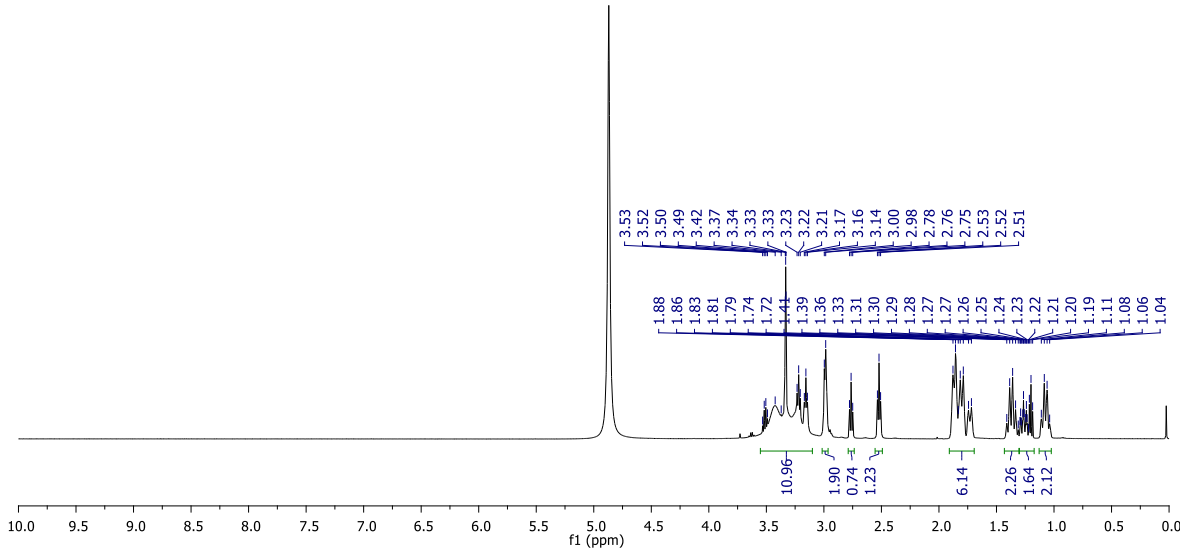

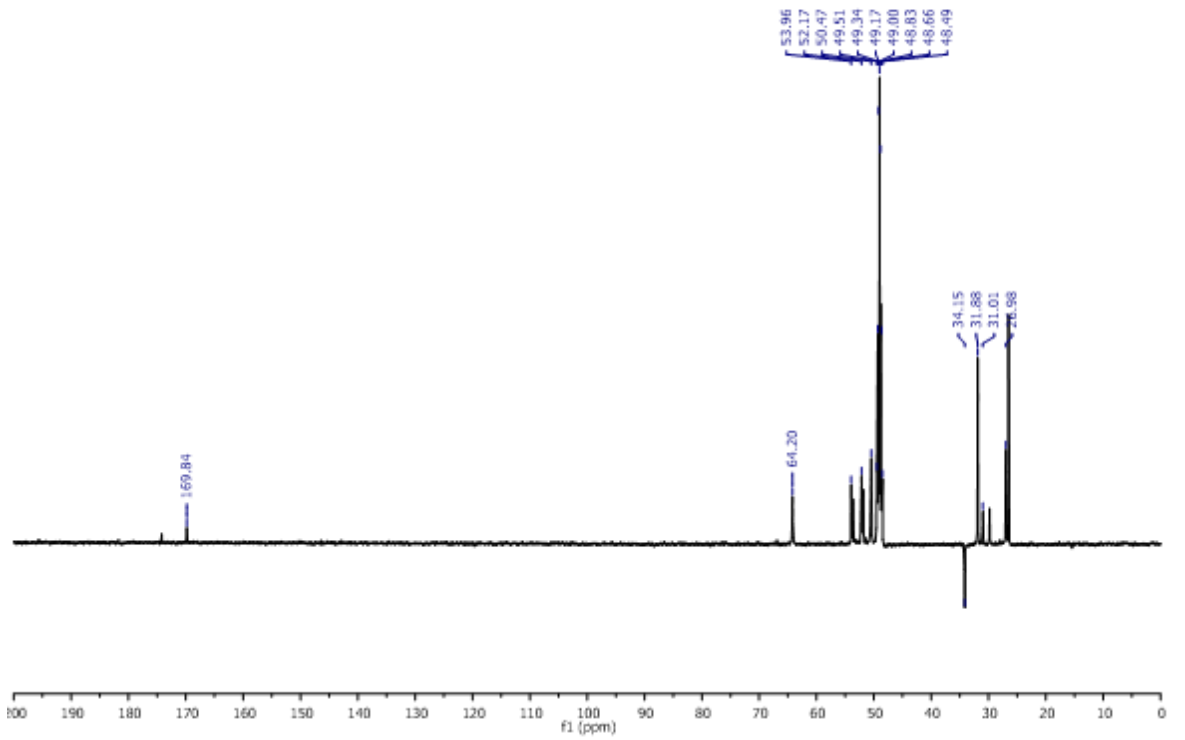

^{1}H (500 MHz, DMSO-d_6) and ^{13}C (125 MHz, DMSO-d_6) for 4-(4-(cyclohexylmethyl)piperazin-1-yl)-*N*-hydroxybutanamide (10b)

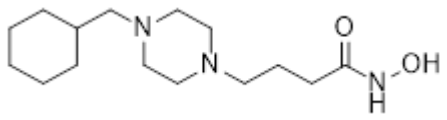

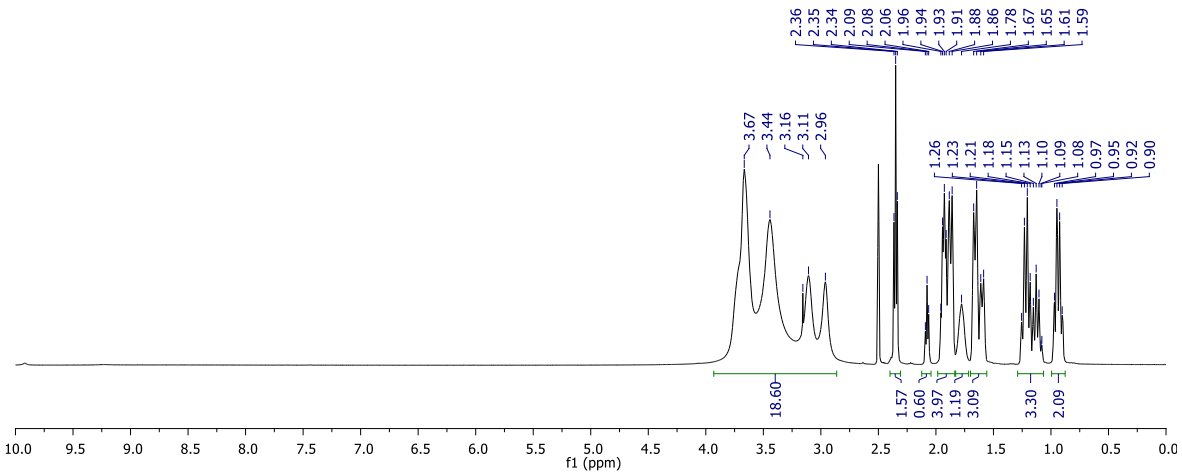

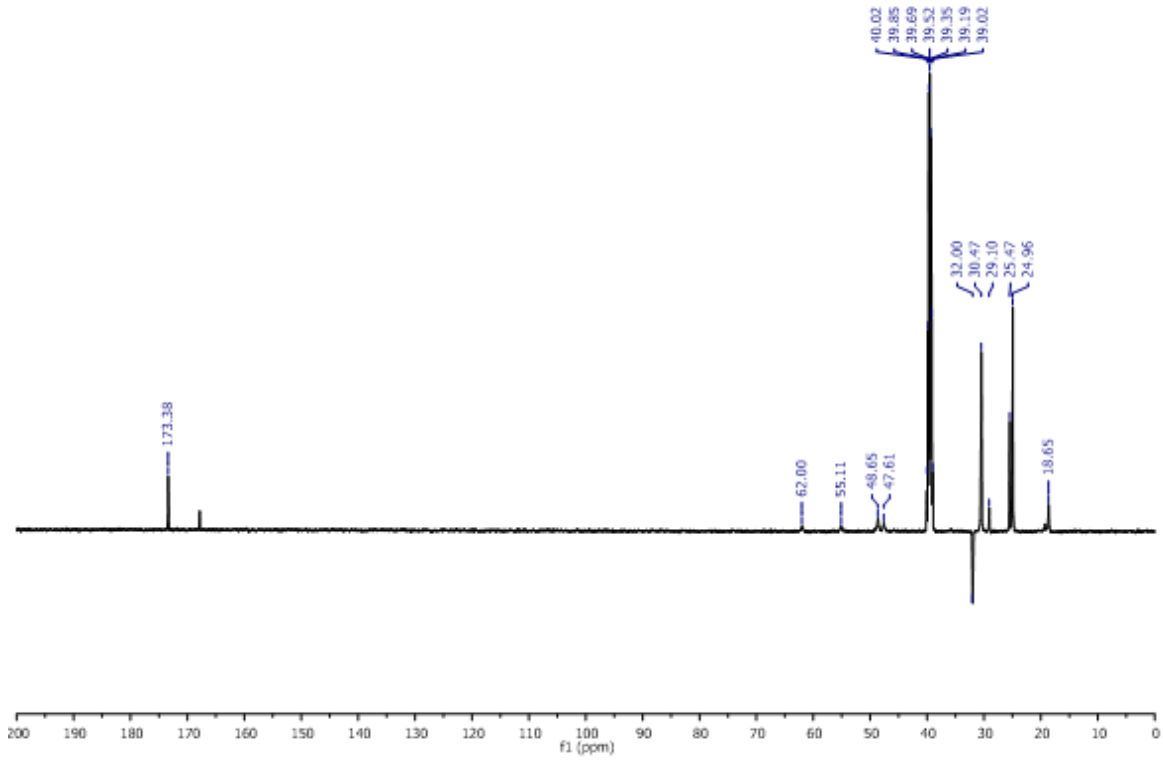

^{1}H (500 MHz, DMSO-d$_6$) and ^{13}C (125 MHz, DMSO-d$_6$) for 3-(4-cyclohexylpiperazin-1-yl)-*N*-hydroxypropanamide (11a)

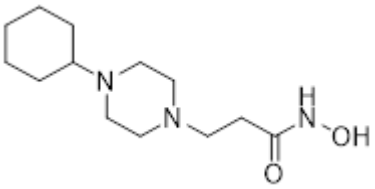

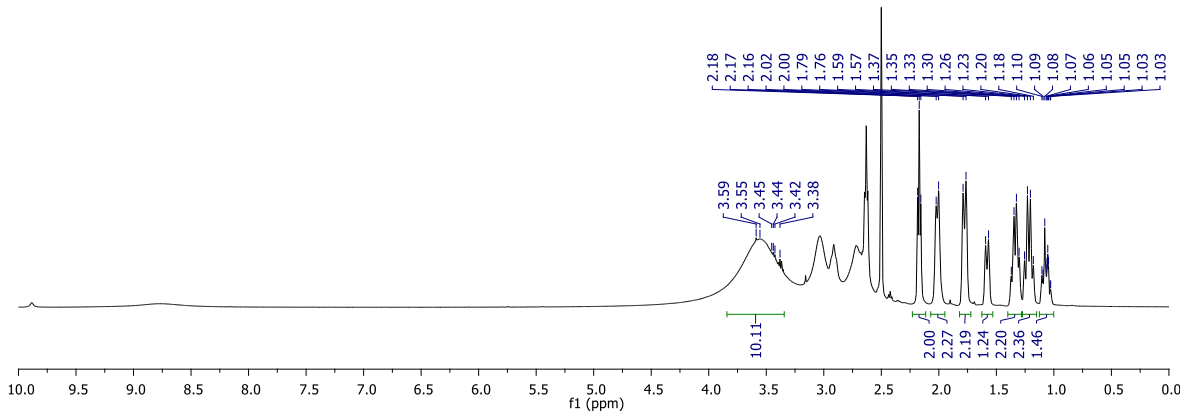

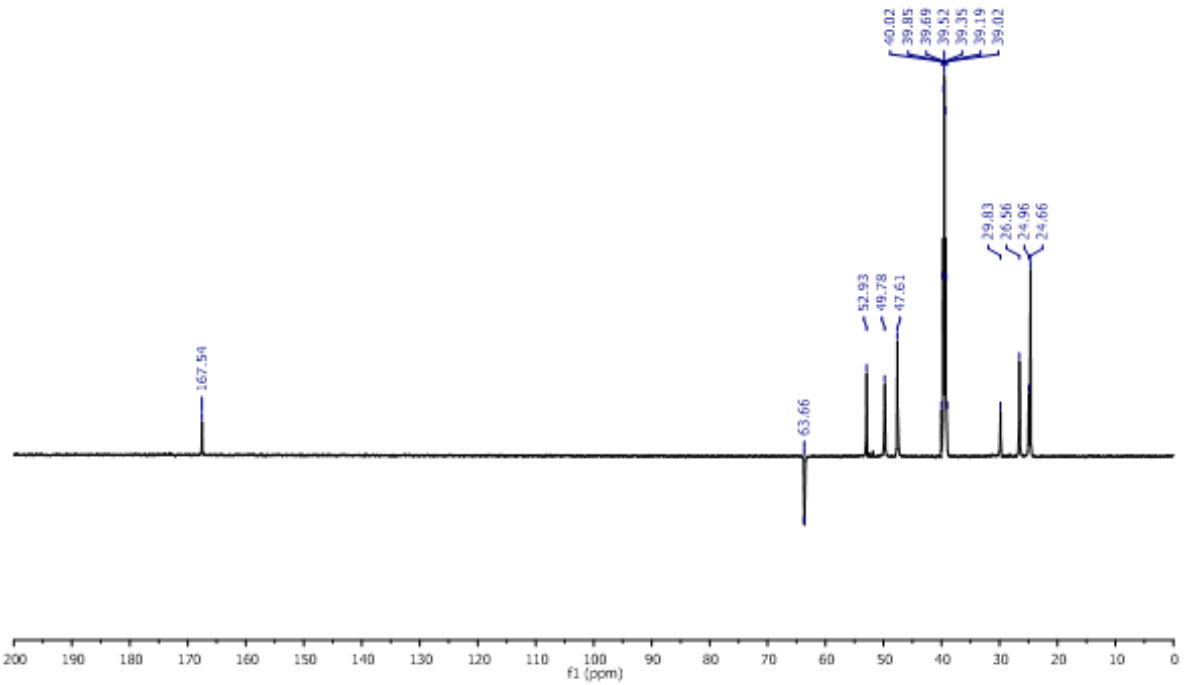

^{1}H (500 MHz, DMSO-d_6) and ^{13}C (125 MHz, DMSO-d_6) for 4-(4-cyclohexylpiperazin-1-yl)-N-hydroxybutanamide (11b)

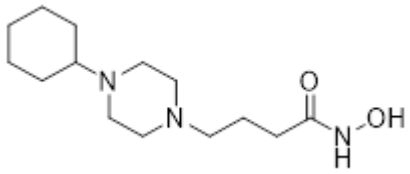

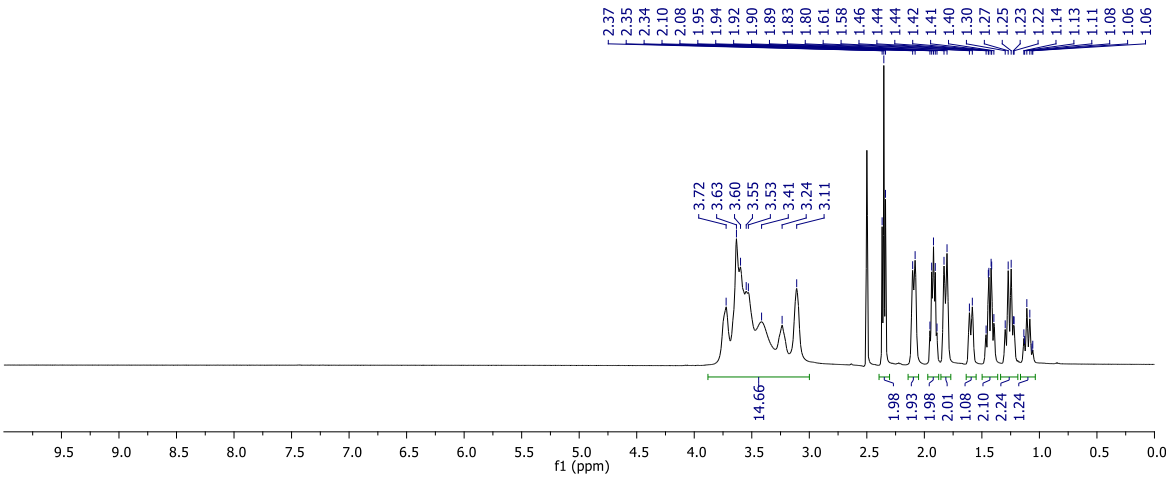

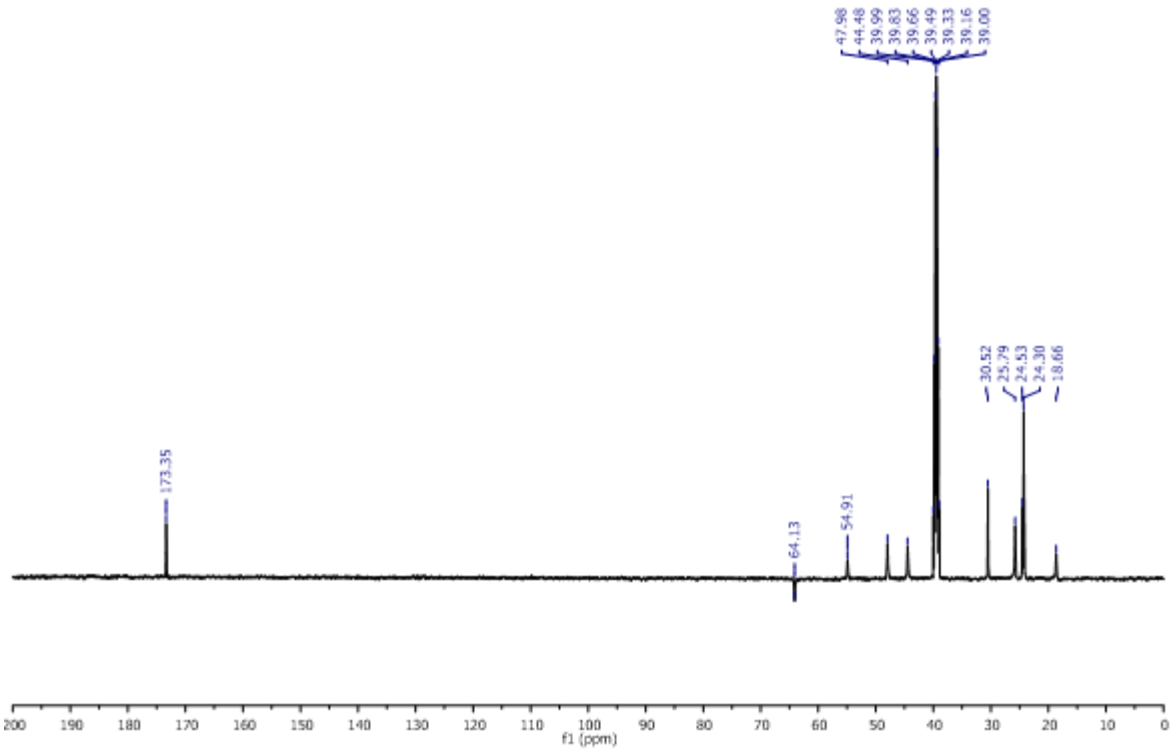

^{1}H (500 MHz, DMSO-d$_6$) and ^{13}C (125 MHz, DMSO-d$_6$) for 3-(4-cyclohexylpiperazin-1-yl)-*N*-hydroxypropanamide (12a)

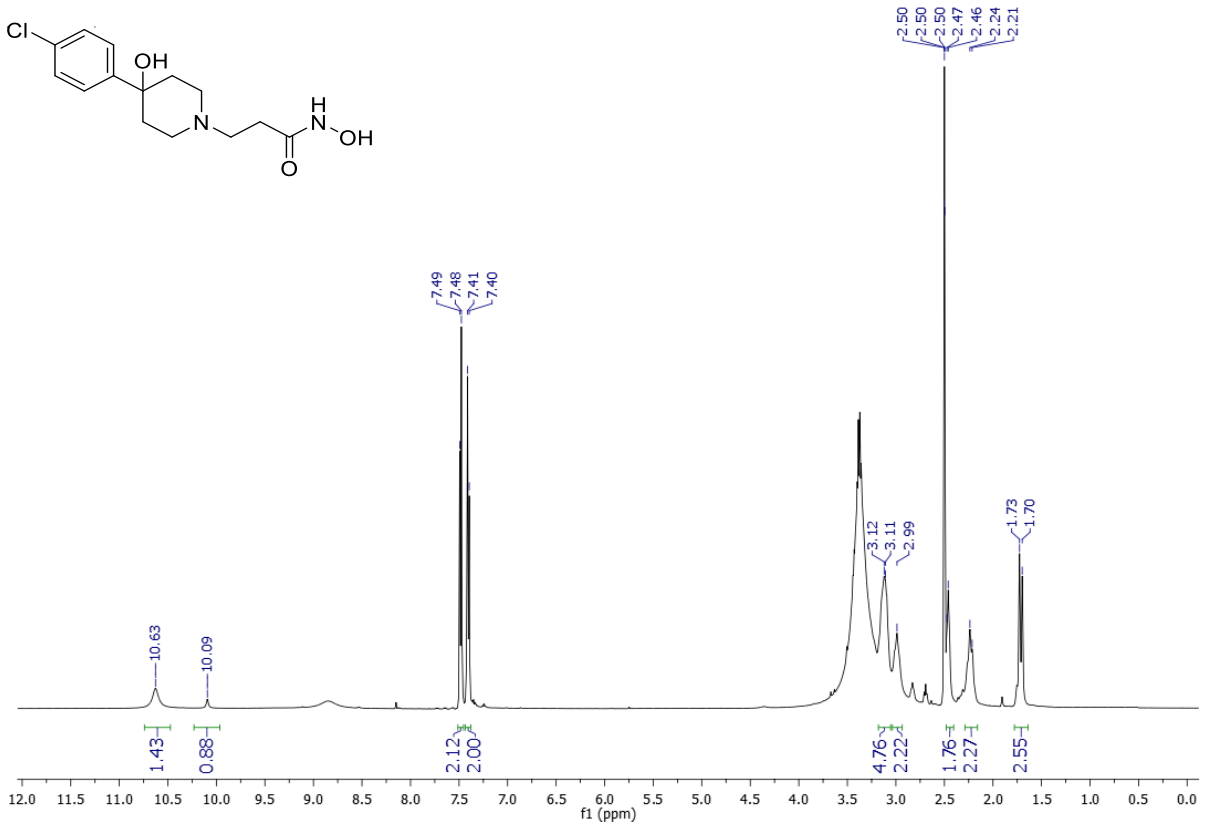

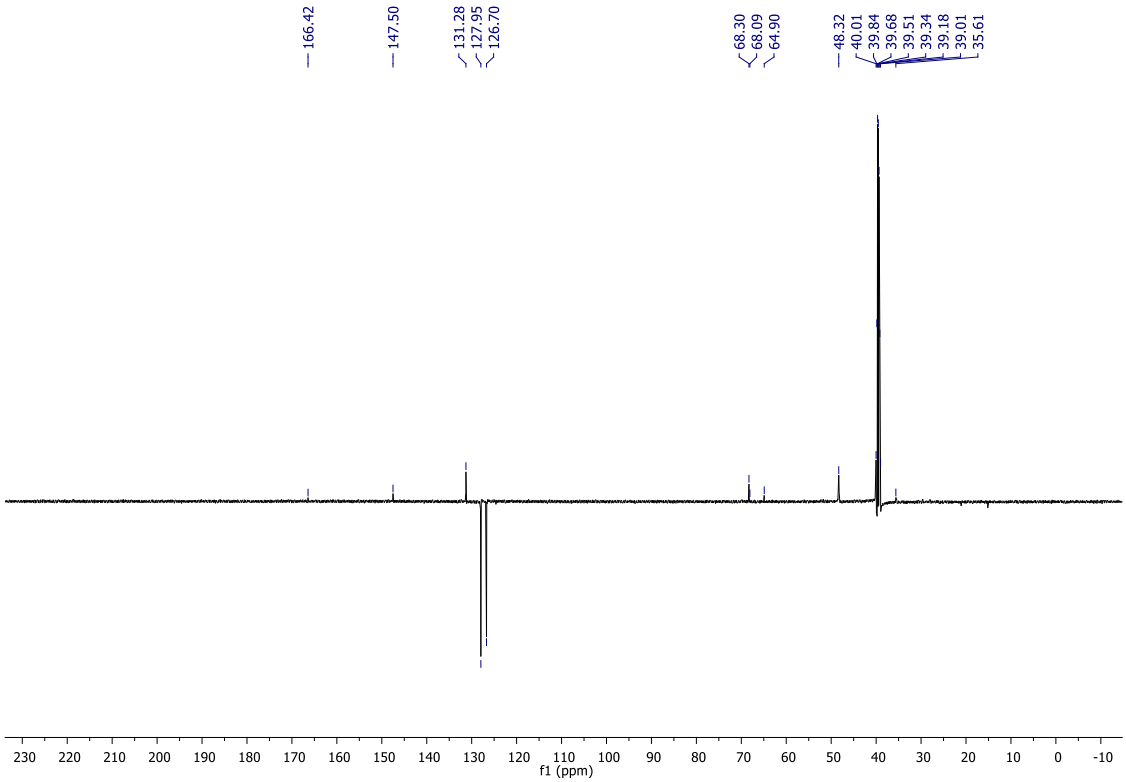

^{1}H (500 MHz, DMSO-d$_6$) and ^{13}C (125 MHz, DMSO-d$_6$) for 4-(4-(4-chlorophenyl)-4-hydroxypiperidin-1-yl)-*N*-hydroxybutanamide (12b).

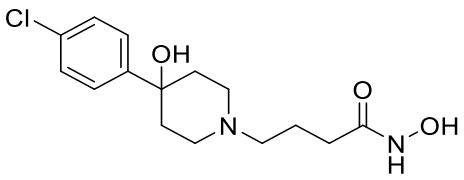

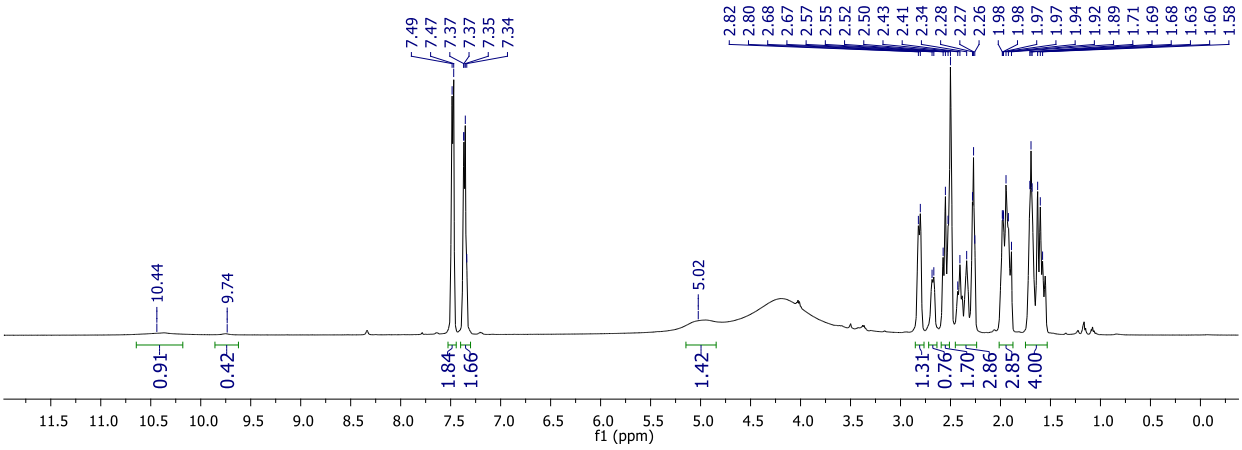

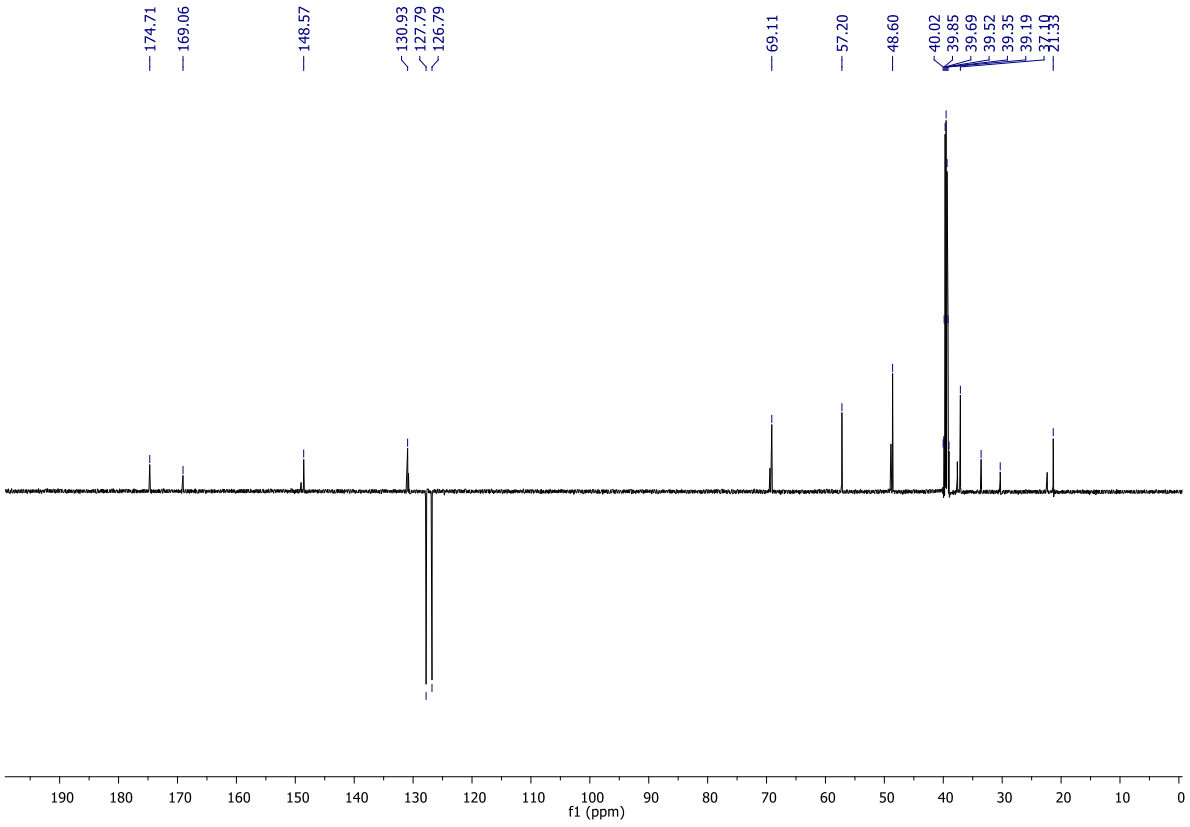

^{1}H (500 MHz, DMSO-d$_6$) and ^{13}C (125 MHz, DMSO-d$_6$) for 5-(4-(4-chlorophenyl)-4-hydroxypiperidin-1-yl)-*N*-hydroxypentanamide (12c).

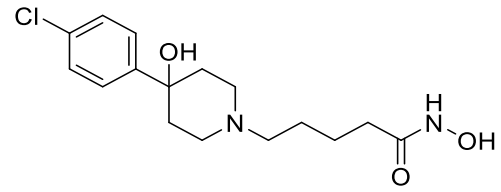

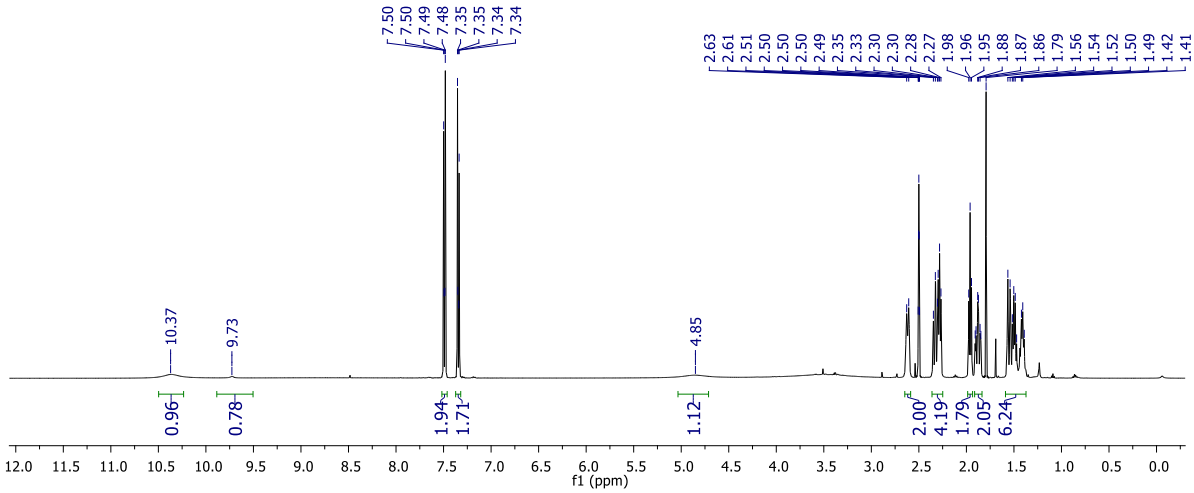

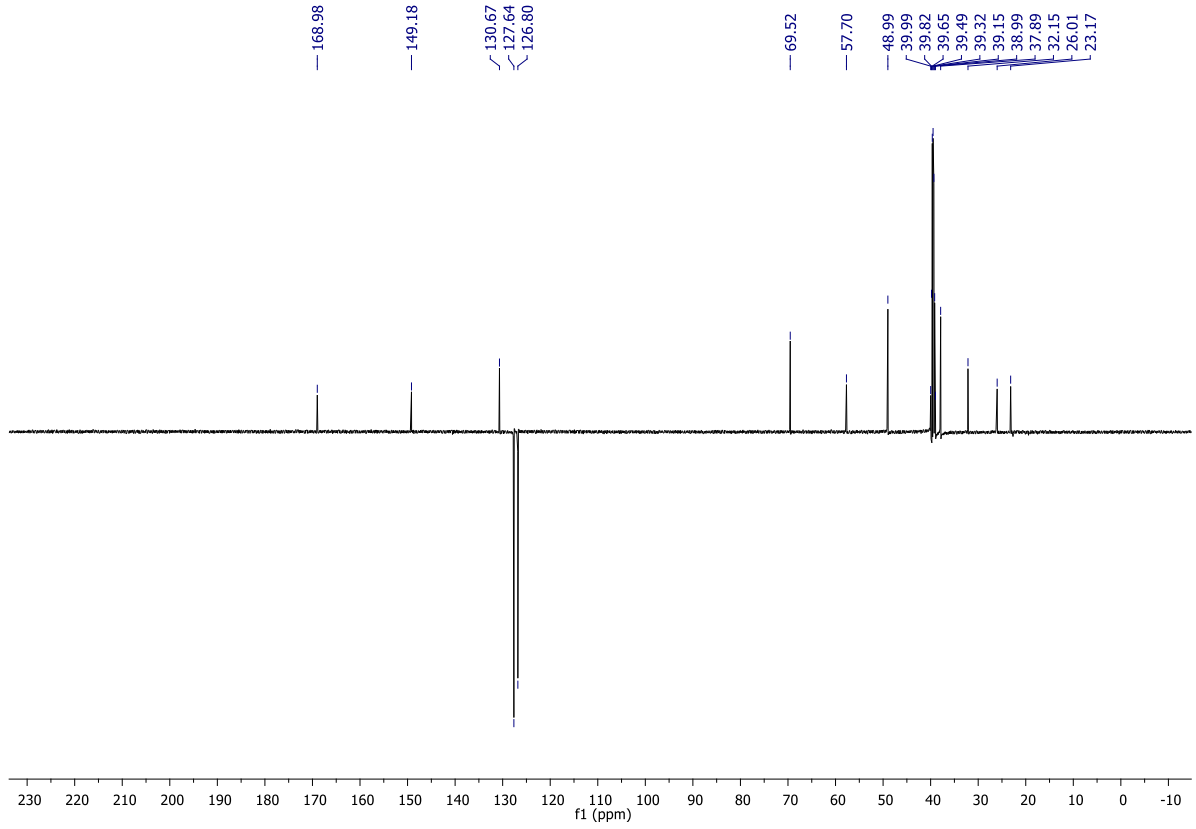

^{1}H (500 MHz, DMSO-d$_6$) and ^{13}C (125 MHz, DMSO-d$_6$) for 6-(4-(4-chlorophenyl)-4-hydroxypiperidin-1-yl)-N-hydroxyhexanamide (12d).

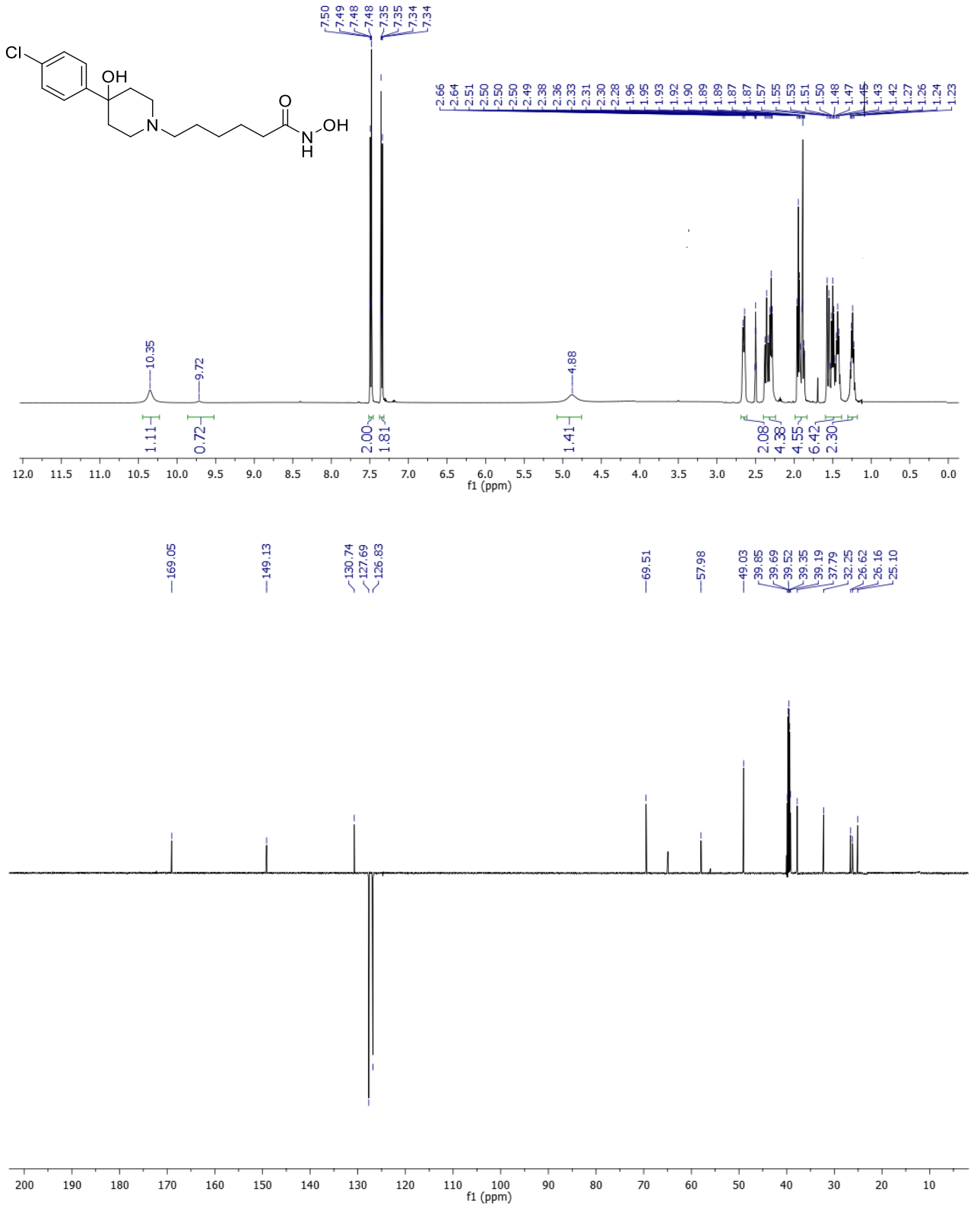

^{1}H (500 MHz, DMSO-d$_6$) and ^{13}C (125 MHz, DMSO-d$_6$) for 7-(4-(4-chlorophenyl)-4-hydroxypiperidin-1-yl)-*N*-hydroxyheptanamide (12e).

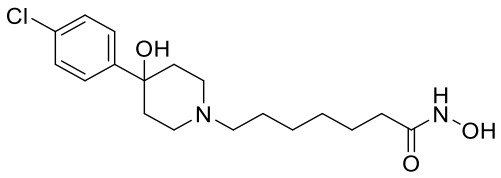

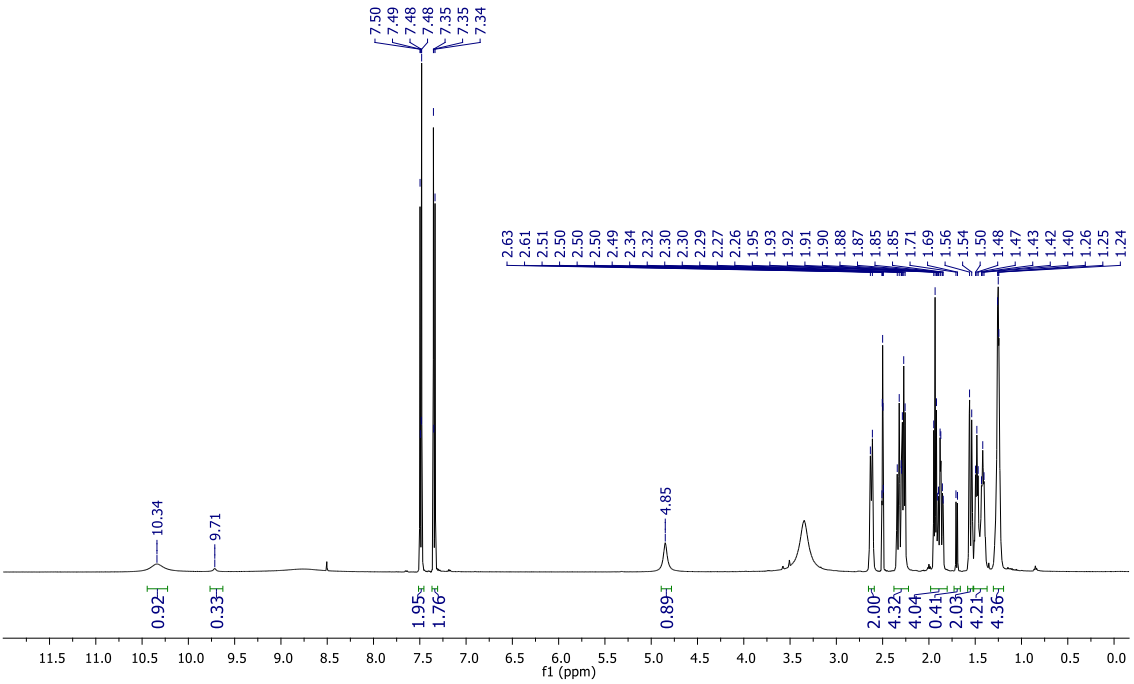

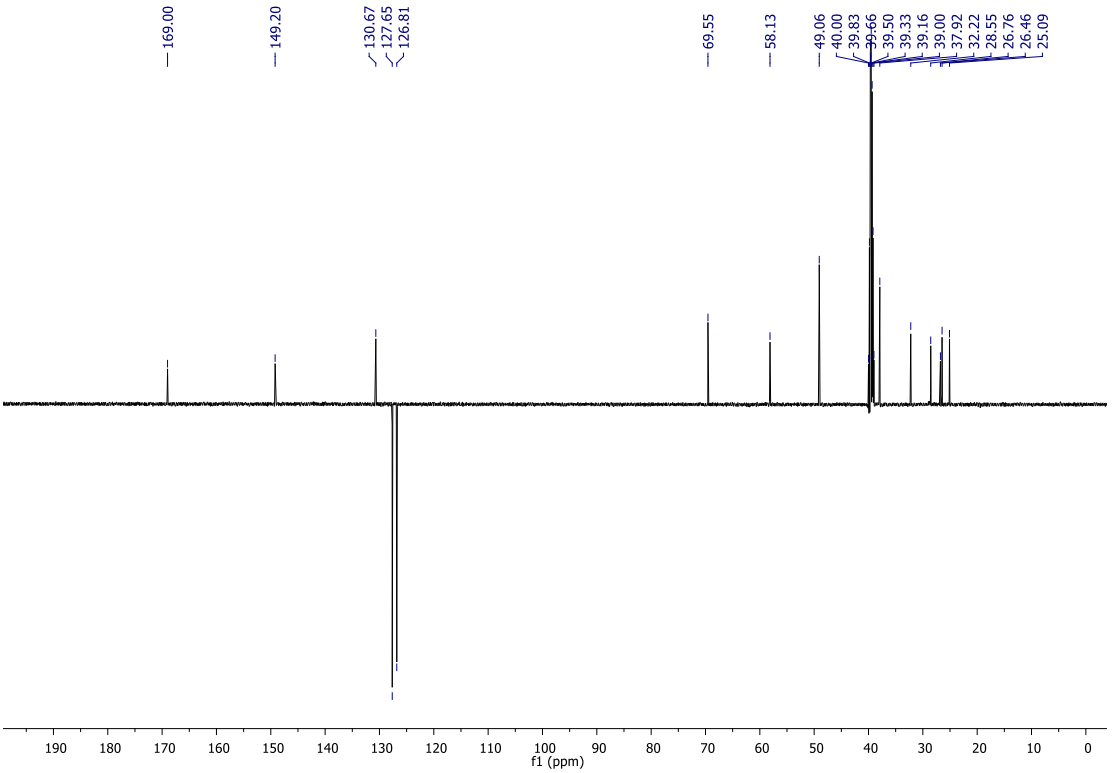

List of paper (2018-2021)

1. Interaction of new sigma ligands with biomembrane models evaluated by differential scanning calorimetry and Langmuir-Blodgett studies.
   Marrazzo A, Torrisi C, Barbaraci C, Amata E, Castelli F, Sarpietro MG.
   Colloids Surf B Biointerfaces. 2021 Feb 18;201:111643. doi: 10.1016/j.colsurfb.2021.111643. Online ahead of print. PMID: 33647709

2. A Structure- and Ligand-Based Virtual Screening of a Database of "Small" Marine Natural Products for the Identification of "Blue" Sigma-2 Receptor Ligands.
   Floresta G, Amata E, Barbaraci C, Gentile D, Turnaturi R, Marrazzo A, Rescifina A.
   Mar Drugs. 2018 Oct 14;16(10):384. doi: 10.3390/md16100384. PMID: 30322188.

3. Generation and Reactions of an Octacyclic Hindered Pyramidalized Alkene.
   Camps P, Lozano D, Barbaraci C, Font-Bardia M, Luque FJ, Estarellas C.
   J Org Chem. 2018 May 18;83(10):5420-5430. doi: 10.1021/acs.joc.8b00212. Epub 2018 Apr 27. PMID: 29652147.

List of conference participations (2018-2021)

1. Barbaraci C., Dichiara M., Fallica A. N., Ciaffaglione V., Intagliata S., Marrazzo A.
   Sigma-HDACi hybrid molecules as potential therapeutic treatment for uveal melanoma: design, synthesis and preliminary results.
   Workshop della Sezione Sicilia della Società Chimica Italiana - WorkshopScisicilia2020, Messina. online conference.
   December 3, 2020
   Oral communication

2. Barbaraci C., Fallica A. N., Marras E., Ignazzitto M. T., Dichiara M., Gariboldi M., Orlandi V., Varchi G., Marrazzo A.
   Shift in activity of ciprofloxacin and norfloxacin "no-light activated" derivatives from antibiotics to anticancer agents: preliminary results.
   Italian Young Medicinal Chemistry virtual meeting – IYMCVMeet, online conference.
   July 22 - 24, 2020.
   Poster presentation

3. Barbaraci C., Dichiara M., Turnaturi R., Fallica A.N., Arena E., Prezzavento O., Amata E., Marrazzo A.
   New selective sigma-1/HDACi prodrugs for neurodegenerative disorders.
   3rd annual meeting - MuTaLig Cost Action, Valletta (Malta).
   October 18 - 19, 2018
   Poster presentation

4. Dichiara M., Barbaraci C., Gentile D., Intagliata S., Pittalà V., Arena E., Fraix A., Farina G., Prezzavento O., Amata E., Marrazzo A.
   Design, synthesis and pharmacological evaluation of NO donor-sigma receptors hybrids for the treatment of cancer.
   Italian-Spanish-Portuguese Joint Meeting in Medicinal Chemistry - MedChemSicily2018, Palermo.
   June 17 - 20, 2018
   Poster presentation

List of course attendance (2018-2021)

1. Radioprotection course - INFN/CNR, Università degli Studi di Catania
   March 19, 2020
2. Basic course on animal experimentation , Capir-Università degli studi di Catania
   October 31, 2019
3. AMBER 18 molecular dynamic basic course (35 hours), Universidad de la Rioja Logroño (Spain).
   July 1 - 5, 2019
4. XIII "Manuel Rico" NMR Summer School (25 hours), Jaca (Spain).
   June 16 - 21, 2019

List of fellowships

- “Manuel Rico” NMR Summer School grant assigned by Real Sociedad Española de Química (RSEQ) to attend XIII "Manuel Rico" NMR Summer School, Jaca (Spain).

La borsa di dottorato è stata cofinanziata con risorse del
Programma Operativo Nazionale Ricerca e Innovazione 2014-2020 (CCI 2014IT16M2OP005),
Fondo Sociale Europeo, Azione I.1 “Dottorati Innovativi con caratterizzazione Industriale”

UNIONE EUROPEA
Fondo Sociale Europeo